Spherically Symmetric Space-times in Effective LQG

by

Jarod Kelly

Bachelor of Science, University of New Brunswick, 2015

A Dissertation Submitted in Partial Fulfilment of
the Requirements for the Degree of

Doctor of Philosophy

In the Graduate Academic Unit of Mathematics and Statistics

Supervisors: Sanjeev Seahra, Ph.D., Mathematics and Statistics
Edward Wilson-Ewing, Ph.D., Mathematics and Statistics

Examining Board: Viqar Husain, Ph.D., Mathematics and Statistics
Branimir Ćaćić, Ph.D., Mathematics and Statistics
Abdelhaq Hamza, Ph.D., Physics

External Examiner: Ivan Booth, Ph.D., Mathematics and Statistics,
Memorial University of Newfoundland

This dissertation is accepted by the
Dean of Graduate Studies

THE UNIVERSITY OF NEW BRUNSWICK

December, 2024

Abstract

Black holes are among the most enigmatic objects in our universe. Although many decades have been dedicated to their study, illuminating several of their key features, there is still very little understood about what happens at their center. At this location general relativity leads to a singularity and it is widely believed that a theory of quantum gravity is necessary to understand the structure of space-time in the vicinity of this point.

In this thesis, we discuss the application of a candidate theory of quantum gravity, namely loop quantum gravity (LQG), to study spherically symmetric black holes. We start in Chapter 2 by developing a framework for an effective LQG description of spherically symmetric black holes in vacuum and analyze the structure of this space-time in depth. In Chapters 3 and 4, we extend this framework by including matter and study black holes that form due to gravitational collapse. We study the dynamics and causal structure of these space-times in depth to uncover new black hole properties that are not captured by the classical theory including: a space-time that is free from strong singularities (although weak singularities in the form of shell-crossings can and do form quite generically) and the formation of shockwaves that will eventually move beyond the outer horizon, marking the "death" of the black hole. Further, we estimate the black hole lifetime to be on the order of M^2, where M is the black hole mass.

Dedication

To my wife Ruixi. Marrying you has been the best decision I have ever made.

Acknowledgements

I would like to express my gratitude to my supervisors Dr. Sanjeev Seahra and Dr. Edward Wilson-Ewing.

Dr. Seahra welcomed me into my journey through theoretical physics and gave me the opportunity to pursue my interests. He was always incredibly approachable and up for a conversation, of which we had many great ones during my time at UNB. He provided invaluable guidance, not only in academia, but also in life, throughout the entirety of my PhD. When I made the decision to transition to industry, he has continually provided support and endless opportunity for collaboration with industrial partners, and for this, I am truly grateful and eternally indebted.

Dr. Wilson-Ewing was a collaborator on nearly all the work done throughout my PhD, including all of the work that embodies this thesis. He perhaps had the more difficult job of my superviors, having to put up with me and my "ideas" (which were not necessarily always based in reality) on a semi-daily basis. He taught me how to continously develop ideas, even when the roadblocks seemed insurmountable, and what it takes to do professional research in theoretical physics. His pedagogical explanations and his tremendously clear understanding of physics was invaluable for a student who often found himself stuck and confused. Without his careful thought, knowledge and patience, this thesis would not have been possible, and for that, I am thankful.

I would also like to thank Dr. Viqar Husain with whom I had the opportunity to

collaborate on several papers. He seemed to be an endless well of knowledge when it came to theoretical physics. I am sure that without his expertise and guidance, the work would not have been nearly as compelling and impactful as it has proven to be.

I would like to thank my parents, Mark and Hope, who have been supportive throughout this endeavor and have never questioned my decision to pursue theoretical physics, even when I, myself, did at times.

Most of all, I would like to thank my wife, Ruixi Zhao, without whose unwavering love and support I could not have made it to the finish line.

I have met many great people during my time at UNB. Although my feelings are mixed about this time in my life ending, I look forward to a new chapter.

Table of Contents

List of Figures

Chapter 1

Introduction

1.1 Why Quantum Gravity?

The 20th century saw quantum mechanics (QM) and general relativity (GR) greatly extend our understanding of the physical universe, but have resulted in a sort of tension that has perplexed physicists for decades. Taken separately, they are two of the most empirically successful theories ever constructed. Indeed, there is currently no evidence of any observed phenomena that contradicts the predictions of either QM or GR.

The reason for their tension is due to the fact that they were developed on contradictory foundations. QM assumes an external time variable and a fixed, non-dynamical background, two assumptions that are incompatible with GR. Additionally, QM is concerned with the evolution of wave functions that are probabilistic in nature. Measurements will "collapse" this wave function into one of its possible eigenstates according to its probability distribution — a very radical development in comparison to the deterministic motion of everyday objects described by classical mechanics.

GR, on the other hand, is formulated in terms of a 4-dimensional Riemannian

geometry[1], specified by a smooth and deterministic dynamical field known as the metric. In this theory, space and time are treated on equal footing, both acting as coordinates on the Riemannian manifold — time is not an external variable. Moreover, and perhaps more importantly, the background geometry itself is the dynamical entity whose evolution is determined by GR, in stark contrast to the evolution of fields on a fixed geometry that QM describes. It is this background independence that has made GR such a revolutionary theory in the history of physics, but also the reason why it has proven so difficult to combine it with QM.

Historically, this type of tension has led to some of the most significant advances in modern physics, with perhaps the preeminent example being that between Newton's mechanics and Maxwell's electrodynamics. In Newtonian mechanics, based on Galilean relativity, the speed of light is dependent on the observers' state of motion — in essence, the faster the observer, the slower the speed of light[2]. At face value this is quite intuitive, this is exactly the behavior we would expect if we were driving alongside another vehicle for example, and so it makes sense why Newton based his mechanics on this type of relativity. Ultimately however, this is not how the universe works. Counter-intuitively to our everyday experience, in Maxwell's theory light always travels at the same speed, regardless of the state of motion of the observer. It was precisely this tension that led Einstein to his revolutionary theory of special relativity, and fame, in 1905 and completely altered our understanding of the universe. Today, we find ourselves at a similar juncture, where two theories at the edge of our current understanding of the universe seem to be at odds. If history is any indication, it may just be that we are in a very exciting time for physics that is ripe for innovation.

The next step in the development of physics, and often considered the holy grail of modern physics, is a theory of quantum gravity, but a logical question to ask at

[1]Named after its inventor, Bernhard Riemann, father of the famous Riemann hypothesis and widely considered one of the greatest mathematicians in history.

[2]This is, of course, assuming the same direction of travel. If the observer and light pulse were travelling in opposite directions, light would appear to move faster according to Galilean relativity.

this point might be "why?". We have these two theories that have never failed an empirical test, despite their contentious relationship. So why exactly do we need a new theory that combines QM and GR into one framework? In other words, why can't we simply use GR where it is applicable and QM where it is applicable and call it a day?

As it turns out, there are regimes where both theories are expected to become applicable simultaneously and in such situations GR and QM by themselves become meaningless. Well known examples of this type of situation, where none of our current theories are able to elucidate the dynamics, include the beginning of our universe — the so-called big bang singularity — and singularities located at the center of black holes. It is precisely in these regimes where one expects the predictions of quantum gravity to become relevant.

Other than this very concrete reason, it can also be argued that some of our biggest insights have come from combining seemingly disparate theories of physics into a single coherent framework, and there is really no reason to believe this wouldn't be the case here as well. In short, quantum gravity represents the next frontier and its discovery could very well lead to a paradigm shift as great as those introduced by GR and QM during the 20th century.

1.1.1 Black Holes and Beyond

It turns out that singularities are ubiquitous in general relativity. One year after GR was introduced by Einstein in 1915, Karl Schwarzschild published the first exact solution to the Einstein field equations, aptly named the Schwarzschild metric. It was quickly realized that this metric exhibited several unusual properties. For example, light or matter that falls within a certain radius cannot escape out to larger radii[3]. Note that when we say "cannot" here, this is not a restriction on the speed of light

[3]This radius is known as the "Schwarzschild radius".

not being fast enough to escape the gravitational field, like the escape velocity on earth for example. It is not physically possible to travel to larger radii once you fall within this radius, just the same way it is not possible to travel to an earlier time. This is rather a consequence of the causal structure of the space-time.

Furthermore, something peculiar happens at the center of this space-time where the radial coordinate is 0. At this point the metric components become undefined, i.e., they blow up to infinity, as does the space-time curvature — GR seems to break down leading to a singularity. Interestingly, not only was this the first exact solution found, this was the first example of a black hole in GR.

At first glance, it might be easy to disregard such solutions as unphysical[4], albeit interesting, peculiarities of the theory that we need not concern ourselves with. However, after their indirect observation in 2015 via gravitational waves [1] and the first image of a black hole in 2017 [2], there is now very strong observational evidence that black holes are indeed real and exist in our current universe.

Although there is very strong evidence for their existence, their dynamics remains something of a mystery. In more familiar space-times, given the initial conditions of a particle, we can predict its dynamics indefinitely in theory. This is not the case however in black hole space-times in GR. Once a particle falls into a black hole, it will inevitably reach the singularity at its center, at which point its dynamics ceases to be well defined. Informally, singularities can simply be thought of as points at which our classical theory of gravity is invalid.

But why are singularities such a staple of solutions in GR? This is directly related to the fact that gravity is always attractive for all forms of matter known to be present in our universe. This is in contrast to a theory such as electromagnetism for example

[4]Although GR is a theory capable of (very accurately) describing our universe, exact solutions of the Einstein equations with unphysical properties do, in fact, exist. For example, the Gödel metric is an exact solution found in 1949 by Kurt Gödel (most famous for his incompleteness theorems) containing closed time-like curves allowing one to time travel in this universe.

where positive and negative charges can exhibit both repulsive and attractive forces. In fact, in the 1960s and 70s, theorems of Geroch, Penrose and Hawking showed that under generic conditions, the space-times of GR will indeed become singular [3–5]. Near such singularities, one usually encounters energy densities that are no longer compatible with a completely classical treatment, since quantum effects should become important.

Aside from their singularity, black holes provide us with one of the starkest examples of the aformentioned incompatibility of QM and GR, and the need for a theory of quantum gravity, known as the "information loss problem". While studying quantum field theory (QFT) in curved space-time, Hawking discovered that black holes are "not so black", but rather emit radiation [6, 7] (see also [8] for a modern review). This implies that black holes will evaporate (shrink) over time as they emit radiation and lose energy. This phenomenon is referred to as "Hawking radiation" and recasts black holes as thermodynamic objects.

The issue with this however is that the disappearance of the black hole threatens our understanding of quantum mechanics, where information is always conserved. Once matter falls into a black hole, there will remain no indication of its information content, save for a few macroscopic properties such as its total mass and angular momentum. Once the evaporation process is complete, the black hole disappears — a non-unitary evolution that contradicts what we expect from quantum mechanics. Many of the difficulties that arise when regarding QM and GR as separate theories — the information loss problem being a prime example — are expected to be resolved once a unified theory of quantum gravity is ultimately discovered.

Although combining QM and GR into a single coherent framework has proven to be a monumental task, this challenge has done little to dissuade the broader physics community from searching for a theory of quantum gravity, and attempts in many directions are currently being explored. Some include modifying the Einstein–Hilbert

action (that leads to GR) given by

$$S_{\text{Einstein–Hilbert}} = \frac{1}{16\pi G}\int \mathrm{d}^4x\sqrt{-g}R, \tag{1.1}$$

where g is the determinant of the gravitational metric and R is the scalar curvature, with terms that are higher order in the curvature scalar R [9]. Others modify some of the metric assumptions of GR, for example adding non-metricity or torsion to the allowable metrics [10–12]. The hope is that such modifications will help solve some of the headaches associated with black holes as well as other problems with the classical theory such as the the dark matter problem [13] or the cosmological constant problem [14], i.e., the discrepancy between its experimentally observed value and that predicted by QFT[5] [17–19].

Aside from simple modifications of GR, many attempts have evolved into their own unique theoretical framework. Since this thesis does not aim to provide a comprehensive review of the literature, we will simply list several approaches that we believe warrant recognition, aside from the main approach that we consider: string theory [20], asymptotic safety [21], group field theory (GFT) [22], causal dynamical triangulations (CDT) [23], non-commutative geometry [24], and generalized uncertainty [25] among others.

One seemingly logical approach to the study of quantum gravity is to quantize metric perturbations on a Minkowski background. This leads to a massless spin-2 particle known as the "graviton" [26]. The perturbative approach has proven very successful in studying the quantum theories of the other three fundamental forces. In the case of gravity however, such a theory is non-renormalizable and therefore we cannot actually extract physical predictions using this approach [27]. The fact that

[5]The discrepancy between these values is between 50 and 120 orders of magnitude [15]; it has been described by some physicists as perhaps "the worst theoretical prediction in the history of physics" [16].

this does not work for gravity is a testament to just how unique GR is in the space of physical theories.

With the shortcomings of the traditional perturbative approach to quantizing GR, many authors have explored the possibility of non-perturbative approaches (several of which we have listed above). A formulation of quantum gravity that does not try to break up the gravitational field into background + perturbations is a background independent (general covariant) QFT. One such theory that is moving along this direction is known as loop quantum gravity (LQG) and it is the focus of this thesis.

1.2 Loop Quantum Gravity

LQG arose in the 1990s as a background independent approach to the problem of quantum gravity [28–30]. Recall that GR describes the dynamics of the space-time geometry itself. This makes background independence one of its key tenets, and hence it is reasonable to expect background independence to be a motivating feature of an ultimate theory of quantum gravity as well.

LQG was originally derived from a reformulation of GR[6] as a dynamical theory of SU(2) connections (and their holonomies), with densitized triads acting as the conjugate variables. The modern starting point is the Holst action [31] given by

$$S_{\text{Holst}} = \frac{1}{16\pi G}\int \mathrm{d}^4x|e|e^\mu_I e^\nu_J \left(F_{\mu\nu}{}^{IJ} + \frac{1}{2\gamma}\epsilon^{IJ}{}_{KL}F_{\mu\nu}{}^{KL}\right), \tag{1.2}$$

where e^μ_I are tetrads, e is their determinant, $F_{\mu\nu}{}^{IJ}$ is the field strength of the $SO(3,1)$ connection $w_\mu{}^{IJ}$ and γ is the Barbero–Immirzi parameter, a free parameter of the theory. In this expression $\mu, \nu, \cdots$ are spacetime indices and $I, J, \cdots$ are Lorentz indices. As we will see below, a Hamiltonian analysis of the Holst action shows that

[6]We use the term "reformulation" here because GR was orginally formulated by Einstein, via the Einstein–Hilbert action (1.1), as a dynamical theory of the metric.

the basic canonically conjugate variables are the connection and densitized triads mentioned earlier. Note that although this starting point differs from the more common Einstein–Hilbert action (1.1), it is well known that they lead to the same dynamics, and hence give the same theory, in the classical setting[7].

1.2.1 A Brief History

The motivation for this "new" starting point is quite simple: to build a quantum theory from the familiar machinery of quantization. Recall that the standard canonical quantization[8] procedure from quantum mechanics is to begin with a Hamiltonian formulation of the theory. We then promote phase space variables (functions on phase space in general) to operators which act on states living in a Hilbert space. Additionally, the Poisson brackets, which allow us to compute trajectories in phase space, are promoted to commutation relations that the operators of our quantum theory satisfy. This is usually straightforward for a theory such as classical mechanics, but has proven to be highly non-trivial in the case of gravity.

The earliest attempts at a Hamiltonian decomposition of GR date back to the late 1950s and early 60s when Richard Arnowitt, Stanley Deser and Charles W. Misner published groudbreaking work on the subject, now known as the "ADM formalism" [33]. This formulation, which starts from the Einstein–Hilbert action (1.1), is a successful Hamiltonian reformulation of GR, with the spatial metric as the canonical variable and conjugate momenta closely related to the extrinsic curvature[9] and has played an important role in canonical quantum gravity. The problem however is that

[7]This, however, is no longer the case after quantization due to the presence of the second term multiplying the Barbero–Immirzi parameter.

[8]There are, of course, other quantization methods as well; for example, path integral quantization starting from a Lagrangian formulation of the theory. Its application in LQG leads to a theory of spin foams [32].

[9]The ADM formalism is based on a foliation of the space-time manifold into 3D spatial slices at each instant of time. The extrinsic curvature essentially describes how these spatial slices evolve in time.

the Hamiltonian of this theory is non-polynomial with respect to the phase space variables, which creates difficulties when we quantize the theory.

As an aside, we note that it is in fact possible to perform a canonical (Schrödinger-type) quantization of the ADM theory, which leads to the Wheeler–DeWitt equation [34]

$$\hat{H}\Psi = 0, \tag{1.3}$$

where $\hat{H}$ is the Hamiltonian operator. This equation is telling us that the physical states of our quantum theory are those that vanish when acted upon by the Hamiltonian.

This is all well and good, but there are many subtle technical issues that remain, making the theory quite formal. For one, solutions are generally difficult to find[10]. There is also the issue of extracting dynamics from a "frozen" formalism since the Hamiltonian operator necessarily vanishes on the physical Hilbert space of the theory. This is referred to as the "problem of time" in quantum gravity. Moreover, even in reduced sectors such as cosmology, where the Wheeler–DeWitt equation is well defined, and we can study the dynamics of states in the quantum theory, it is well known that evolving states that are initially sharply peaked on the classical trajectory, remain sharply peaked all the way to the classical singularity [36]. This implies that there is no singularity resolution in the Wheeler–Dewitt theory, and something else needs to be done.

Luckily, there is another way. The Palatini formulation of GR is an alternative formulation in terms of connections and tetrads. The starting point for this theory is the so-called Hilbert–Palatini action that is related to the Holst action (1.2) by simply removing the second term containing the Barbero-Immirizi parameter

$$S_{\text{Hilbert–Palatini}} = \frac{1}{16\pi G}\int \mathrm{d}^4x|e|e^\mu_I e^\nu_J F_{\mu\nu}{}^{IJ}. \tag{1.4}$$

[10]Although Chern-Simons theory has had something to say about this [35].

In this formulation, the connection becomes the fundamental dynamical field of interest, with tetrads now acting as the conjugate variable. The metric is now a secondary quantity that can be derived from these more fundamental variables.

This has the advantage of casting GR in a form akin to Yang–Mills gauge theory, whose quantization has been well studied and offers several tools for developing a non-perturbative quantization. GR, after all, is a gauge theory[11], with its connection dynamics reformulation possessing similarities to that of Yang–Mills theory, and physicists dating back to Dirac in the late 1950s believed this to be a viable path towards the canonical quantization of gravity. Unfortunately, the 3+1 (Hamiltonian) decomposition of the Hilbert–Palatini action leads to the same issues as ADM — namely a non-polynomial Hamiltonian — making it difficult to study the quantum theory, and it would be decades before this problem was solved.

It wasn't until 1986 that a new set of variables was proposed by Abhay Ashtekar, bypassing the problem that had been troubling the canonical quantization program for decades [37, 38]. This new set of variables — known as the "Ashtekar variables" in honor of their discoverer — still yield a connection based formulation of GR, meaning we have many of the tools of Yang–Mills theory at our disposal, but also simplify the Hamiltonian sufficiently, making canonical quantization viable. It is precisely this formulation that we get from a Hamiltonian decomposition of the Holst action [31, 39].

The Holst action can be thought of as a generalized Hilbert–Palatini action that contains both the ADM formalism and the Ashtekar formalism for different choices of the Barbero-Immirizi parameter. We note here that Ashtekar's original formulation was in terms of a self-dual Hilbert–Palatini action, rather than the full Holst action, where the field strength, $F_{\mu\nu}{}^{IJ}$, in the Hilbert–Palatini action is replaced by its self-dual part. This is equivalent to choosing a purely imaginary Barbero–Immirzi parameter in the Holst action, which, when 3+1 decomposed, leads to Ashtekar's

[11]The gauge transformations of general relativity are coordinate transformations.

original formulation. This formulation has the advantage of greatly simplifying the Hamiltonian at the cost of introducing reality conditions (for metrics with Lorentzian signature) [40–42]. The reality conditions must be imposed to ensure real metrics, but have proven to lead to difficulties in the quantum theory. The Holst action above is the starting point for a generalized version of the original Ashtekar theory, where the Barbero–Immirzi parameter is a free parameter. A real Barbero–Immirzi parameter is typically used in modern research, avoiding the difficulty introduced by reality conditions altogether, but at the cost of a slightly more complicated Hamiltonian [39, 43].

1.2.2 Hamiltonian Picture

Performing the Hamiltonian decomposition of the Holst action (1.2) gives the canonically conjugate gravitational variables: $A_a^i = \epsilon^i{}_{jk} w_a{}^{jk} + \gamma w_a{}^{0i}$ (the Ashtekar–Barbero connection) and $E_i^a = |e| e_i^a$ (the densitized triads) where $a, b, \cdots$ are spatial indices and $i, j, \cdots$ are the spatial components of the Lorentz indices $I, J, \cdots$ in the Holst action [31]. The Ashtekar–Barbero connection and densitized triads thus constitute the dynamical variables of the theory, as promised.

Classically, GR in this form is characterized by 3 constraints[12], the Gauss constraint

$$G_i \equiv \nabla_a E_i^a \approx 0, \tag{1.5}$$

which allow one to arbitrarily rotate the triads with respect to internal indices and represents an SU(2) gauge invariance of the theory, the diffeomorphism constraint

$$\mathcal{H}_a \equiv \frac{1}{8\pi G\gamma} E_k^b F_{ab}{}^k \approx 0, \tag{1.6}$$

[12]Constraints in this context are equations that solutions of the theory must satisfy in addition to the equations of motion.

and the scalar (Hamiltonian) constraint

$$\mathcal{H} \equiv -\frac{E^a_i E^b_j}{16\pi G\gamma^2|e|}\,\epsilon^{ij}{}_k\Big(F_{ab}{}^k - (1+\gamma^2)\Omega_{ab}{}^k\Big) \approx 0. \tag{1.7}$$

Here the field strength is $F_{ab}{}^k = 2\partial_{[a}A^k_{b]} + \epsilon_{ij}{}^k A^i_a A^j_b$, while the spatial curvature is given by $\Omega_{ab}{}^k = 2\partial_{[a}\Gamma^k_{b]} + \epsilon_{ij}{}^k\Gamma^i_a\Gamma^j_b$, with $\Gamma^i_a = \epsilon^i{}_{jk}w_a{}^{jk}$. Note that "$\approx$" in the constraint equations means that these functions must vanish on the solution space. These latter two constraints allow us to choose coordinates — they represent the coordinate independence that underpin general relativity. These are the phase space functions that we will need to properly promote to operators on the Hilbert space of LQG in order to quantize the theory.

It is typical to fix the Gauss constraint by fixing a triad orientation. The total Hamiltonian, which generates the dynamics, is then given by a linear combination of the remaining constraints, $\mathcal{H}_{\text{Tot}} = N\mathcal{H} + N^a\mathcal{H}_a$. Here, N is the lapse and N^a is the shift, which act as Lagrange multipliers imposing the scalar and diffeomorphism constraints, respectively, in the action. Since the total Hamiltonian is a linear combination of constraints, it too must vanish on the solution space. Once this is promoted to an operator in our quantum theory, physical states will be those that vanish when acted on by our Hamiltonian operator — recall that this is exactly what the Wheeler–Dewitt equation (1.3) is saying. Operator evolution will also vanish in the Heisenberg picture, which is an explicit manifestation of the problem of time in quantum gravity that we mentioned in Section 1.2.1. As we will see in Chapters 3 and 4, one way around this problem is to introduce a matter field that will act as a clock, giving a physical Hamiltonian (as opposed to a constraint).

1.2.3 Loop Quantization and the Holonomy

The discussion at the end of the previous section seems to suggest that, using the Ashtekar variables, we are again led to a Wheeler–Dewitt type[13] equation for our quantum states. The difference, as we will see, lies in the selection of canonical variables that will have unambiguous operator analogs in the quantum theory. With this in mind, a key ingredient in the construction of the (loop) quantum theory is the holonomy.

Recall that in Yang–Mills theory, the connection itself is not gauge invariant, but rather it is the trace of the holonomy of the connection around closed loops that gives the gauge invariant variables (and hence observables) of the theory. It turns out that the holonomy is also a convenient choice as one of the fundamental variables in LQG due to the simple way they transform under gauge transformations. The holonomy of the Ashtekar–Barbero connection along a path ℓ is given by

$$h_\ell(A) = \mathcal{P} \exp\left(\int_\ell A_a\right), \tag{1.8}$$

where $A_a = A_a^i \tau_i$, with τ_i a basis of the $\mathfrak{su}(2)$ Lie algebra, and $\mathcal{P}$ denotes path-ordering.

The holonomy of the connection is simply the parallel transport of the connection along the path ℓ — (1.8) is the solution to the parallel transport equation. To see this, following [28], given an edge $\ell : [t_1, t_2] \to M$, where M is some manifold, and a connection A, the parallel transport from $\ell(t_1)$ to $\ell(t)$ along ℓ is defined by

$$\frac{d}{dt} h_\ell(t, t_1; A) = A_a(\ell(t)) \dot{\ell}^a(t) h_\ell(t, t_1; A), \tag{1.9}$$

[13] Since we are working in the Ashtekar variables, the Hamiltonian is different (and quite a bit simpler) than the ADM Hamiltonian that was used to arrive at the Wheeler–Dewitt equation, as is the quantization as discussed in the main text.

with the initial condition

$$h_\ell(t_1, t_1; A) = \mathbb{I}, \tag{1.10}$$

where $\mathbb{I}$ is the identity matrix; below we will omit explicit dependence of the holonomy on the connection A, and assume it is implied. Integrating (1.9) we have

$$h_\ell(t, t_1) = \mathbb{I} + \int_{t1}^{t} ds_1 A_a(\ell(s_1))\dot{\ell}^a(s_1) h_\ell(s_1, t_1), \tag{1.11}$$

where we have changed the dummy integration variable to s_1 and used initial condition (1.10). Although the holonomy h_ℓ is unknown, and appears on both sides of (1.11), this can be solved by repeated substitution of this expression into the right hand side. For example, after the first iteration we have

$$h_\ell(t, t_1) = \mathbb{I} + \int_{t1}^{t} ds_1 A_a(\ell(s_1))\dot{\ell}^a(s_1) \left\{ \mathbb{I} + \int_{t1}^{s_1} ds_2 A_a(\ell(s_2))\dot{\ell}^a(s_2) h_\ell(s_2, t_1) \right\}. \tag{1.12}$$

Continuing this process indefinitely allows us to remove the dependence of the right hand side on the holonomy, thus solving our original equation. Explicitly, this process gives

$$h_\ell(t, t_1) = \mathbb{I} + \sum_{k=0}^{\infty} \int_{t_1}^{t} ds_1 A_a(\ell(s_1))\dot{\ell}^a(s_1) \prod_{n=1}^{k} \int_{t_1}^{s_n} ds_{n+1} A_a(\ell(s_{n+1}))\dot{\ell}^a(s_{n+1}), \tag{1.13}$$

where the product expression goes to 1 in the $k = 0$ case. This final expression is exactly the path ordered exponential defining the holonomy in (1.8) and we have shown explicitly that this indeed solves the parallel transport equation (1.9) with initial condition (1.10). The holonomy, together with the densitized triads, form the basic variables which operators of the quantum theory are defined in terms of. It is the holonomy, being a fundamental variable of the theory, that gives loop quantum gravity its name.

By choosing the holonomy as one of our canonical variables, it is well known that

there is no corresponding operator for the connection in the quantum theory [36]. This becomes an issue when promoting functions on phase space from the classical theory, such as the Hamiltonian and field strength which depend explicitly on the connection variables, to operators on the (kinematic) Hilbert space of LQG, where no operator analog of the connection exists. Nonetheless, these operators can be approximated by holonomy operators that are indeed well defined in the quantum theory. This type of quantization, starting with the holonomy as one of our fundamental variables, is very similar to a procedure known as "polymer quantization". Polymer quantization turns out to be unitarily inequivalent to the more standard Schrödinger quantization. It is here that LQG departs from the original canonical quantization à la Wheeler–Dewitt, leading to a difference equation for the evolution of quantum states rather than the differential equation espoused by Wheeler–DeWitt [36, 44, 45]. This difference equation arises as a result of the non-infinitesimal length of the paths along which the holonomies are evaluated (see Section 1.3.2 for further discussion).

Polymer quantization is not restricted to gravity in the connection variables, but can be applied much more generally. This quantization procedure has been applied to many classical systems, for e.g., point particles and the simple harmonic oscillator [44, 46]. It has also been shown that states of a quantum mechanical particle in the Schrödinger representation can be approximated by states in the polymer representation [47]. In fact, it was even recently shown that polymer quantizing a simple cosmological model starting with the metric (ADM) variables leads to the same modified Friedmann equation that was first derived in LQC, suggesting that it is not the variable selection that is most important to LQG, but rather the polymer quantization itself [48].

We would also like to emphasize here that although we are framing the use of the holonomy as a way to approximate the field strength and connection operators with operators that are well defined in LQG, it is the quantum theory that is ultimately

correct and the classical theory that is an approximation thereof. In other words, the holonomy is the correct object to use and, in the classical limit, the field strength and connection variables will show up in our classical expressions. What we have discussed is rather a way to derive the correct quantum theory starting from the classical theory.

This new quantization gives LQG several properties that make it an attractive candidate for a theory of quantum gravity. It has a well defined Hilbert space that is completely inequivalent to the Wheeler–DeWitt Hilbert space already at the kinematical level. Furthermore, it can be shown that geometric operators corresponding to area and volume (geometric operators in general for that matter) have discrete spectra [49–53]. This latter property is particularly attractive, and quite intuitive, when we ask the question "what exactly should be quantized in a quantum theory of general relativity?". Since GR is really a theory about the geometry of space-time, one would expect that geometry itself is quantized in a quantum version of the theory, and this is explicitly realized in LQG. In particular, it is the minimum (non-zero) eigenvalue of the area operator — referred to as the "area gap" — that leads to singularity resolution in LQG[14] and also in the effective framework that we now introduce.

1.3 Symmetry Reduction and the Effective Framework

The full theory of LQG describes an honest-to-goodness theory of quantum geometry and its dynamics, just as we would intuitively expect of a theory of quantum general relativity. However, the mathematical machinery required to run such a theory is, understandably, quite formidable. As a result, extracting predictions from the

[14]Recall from Section 1.2.1 that cosmological singularities are not resolved in the case of Wheeler–Dewitt quantization [36].

theory is far from practical at this stage in its development in all but the simplest of cases. As a way to study the theory, research has developed an "effective" approach to the problem in order to extract semi-classical dynamics from symmetry reduced sectors. Often, this makes it possible to study the dynamics of this reduced sector in depth. The quintessential example of this is today known as "loop quantum cosmology" (LQC) (see, e.g., [36, 54–56] for reviews), where the reduced sectors of interest are cosmological space-times.

LQC is not "derived" from the full theory in the traditional sense. It rather incorporates elements of the full theory in that it uses a similar selection of phase space variables and follows an LQG motivated quantization procedure. Although in simple cosmological space-times a full quantization can be carried out (and has been studied extensively, see, e.g., [36]), the benefit of the effective theory is that a full quantization need not be carried out in order to study the quantum dynamics (or at least leading order quantum corrections to the classical dynamics) for our sector of interest.

For cosmology, the effective equations derived from this procedure have been shown to give an excellent approximation to the leading order quantum gravity effects for sharply-peaked states [36]. Although it is not certain that the dynamics of the effective theory will continue to closely approximate the full quantum dynamics for such states in more complicated space-times, for e.g. black hole space-times, it is reasonable to assume that the arguments in [57] can be generalized to black holes[15]. This makes it possible to study the quantum dynamics via the effective framework in these sectors as well. With this in mind, in this thesis we will use the effective approach to study the (potential) effects of discrete geometry on the dynamics of black hole space-times.

[15]At least for black holes with a large mass compared to m_{planck}.

1.3.1 Steps to the effective theory

Since the philosophy of LQG is that quantum gravity should really be described as a theory of quantum geometry, the most fundamental question that needs to be answered is "how do we describe gravity in terms of a theory of quantum geometry?". Classically, gravity is described in terms of smooth manifolds and their curvature, so how can we incorporate quantum geometry into such a framework? The basic idea of the effective description answers this question and turns out to be quite intuitive.

Disregarding some technical difficulties in implementing the effective theory for the time being, the steps towards an effective description can roughly be outlined as follows:

1. First, rewrite GR in canonical (Hamiltonian) form — this will facilitate the derivation of our quantum theory — and choose Ashtekar variables as the canonical variables.

2. Next, we select a sector we would like to study and choose the most general metric that satisfies the symmetry of this sector. For example, in Chapter 2 we will select spherical symmetry as the sector of interest and choose the most general spherically symmetric metric as our starting point.

3. With this metric, we compute the classical functions of interest — basically the diffeomorphism constraint (1.6) and Hamiltonian constraint (1.7)[16]. Note that since we are working in a classical theory, these are simply functions on phase space rather than operators — functions that vanish on solutions of the theory since they are constraints in the case of gravity.

4. At this point, as we will see in Chapter 4, it is possible to perform a full quantization of this symmetry reduced sector. Then, taking the expectation

[16]Recall from Section 1.2.2 that it is typical to fix the Gauss constraint by choosing an orientation for the triads, whence the total Hamiltonian is given by a linear combination of these two remaining constraints.

values of operators in sharply peaked (Gaussian) states followed by the continuum limit will give the effective theory we are seeking [58]. Much more straightforward however is to simply take our classical expressions and replace connection components by their holonomy, avoiding the entire quantization procedure altogether. This is a well known shortcut for deriving the effective theory that was developed in LQC and has become a standard method in deriving the effective description. Note that although this is a common shortcut, it was only by understanding the full quantization procedure that the $\bar{\mu}$ scheme (which we discuss below) was understood to be necessary.

1.3.2 Approximating the quantum

At this point, it is useful to try and get a feel for where and how quantum effects are coming into this picture, since we are really working with a modified, but still classical theory. The answer to this lies in the introduction of the holonomy.

Recall from our discussion of the holonomy in Section 1.2.3 that there is no well-defined operator corresponding to the connection on the Hilbert space of LQG as a result of its inherent discreteness. This, in turn, permeates other operators that are important to the quantum theory, notably the field strength operator in the Hamiltonian, which we are forced to approximate by holonomy operators. This should be trivial since, from differential geometry, it is well known how to write the field strength in terms of holonomies of the connection taken around a closed loop that has been shrunk to enclose zero area. Its geometric interpretation is then the curvature of the (classically smooth) manifold at that point. This limit, that is the limit of taking the loop smoothly to zero area, is well defined for Riemannian manifolds to which solutions of GR belong. Recall that in the case of LQG however, since the underlying space is discrete, corresponding geometric operators, such as area, have discrete spectra.

With this in mind, the predicament we find ourselves in should be clear: how exactly are we to shrink our loop to zero area (in order approximate the field strength via holonomies) when areas in LQG should be discrete, i.e., when there is no corresponding limit? The solution: we simply take the limit as far as we can according to the full theory. That is to say, we shrink the loop around which we are computing the holonomy until it encloses an area equal to the area gap[17]. This makes the theory non-local. In a local theory, the field strength (curvature) at a point is a function of that point alone. Now however, due to the non-zero area gap, the curvature depends on the surrounding points.

This non-locality is exactly where the correction to the classical theory is imported into our effective theory. It is also the point at which the Planck length, and hence quantum effects, make their way into our otherwise classical picture. In the literature this type of "quantization" procedure for the effective theory, where connection components are replaced by their holonomy taken around closed loops that enclose areas equal to the area gap, is typically referred to as a "polymerization". We note that although the polymerization function is something of a choice (technically we can choose whatever polymerization we like, so long as the functions are bounded) [59, 60], some choices are more well motivated than others based on LQG considerations where the polymerization function is given by explicit calculation of the holonomy.

In the simplest cases, for e.g. homogeneous space-times of the type studied in LQC, not only does the effective theory fix the big bang singularity that plagues the classical theory, replacing the singularity with a "big bounce", its low energy limit is exactly the GR solution. This low energy limit requirement derives from the fact that GR has proven very accurate at cosmological scales and turns out to be a relatively strict requirement of any theory of quantum gravity. We are not completely out of the

[17]Recall from Section 1.2.3 that the area gap is the minimum non-zero eigenvalue of the area operator in LQG. Also recall that the difference equation governing the quantum dynamics of LQG arises as a result of the non-infinitesimal length of the paths along which the holonomies are evaluated — here we see that the area gap is the reason why these paths are non-infinitesimal.

woods though, there still exist quantization ambiguities in the effective description [61–65] and the question of how well, if at all, does the effective theory capture the quantum dynamics of the full theory in more complicated sectors remains, but this is definitely a good starting point for gaining a fuller understanding of the underlying quantum theory and its consequences.

A bit more technically, the holonomy corrections to the theory turn out to be modifications of the connection variables in the Hamiltonian. Since the modified Hamiltonian generates the dynamics of the effective theory, just as it does classically, this in turn leads to a modification of the equations of motion (EOMs). As we will see, for the black hole framework we present, these equations are modified at high energy, but reduce to classical solutions of GR sufficiently quickly as we move to lower energy regimes, as expected. The solutions of these equations of motion will give the quantum corrected metric(s) of our modified (effective) theory. By studying its properties, we can glean insights about how the quantum corrections affect the properties of the space-time, properties such as curvature scalars, thermodynamics (in the case of black hole space-times), the evolution of matter fields and the causal structure.

There has been a lot of research dedicated to the study of these effective theories, with varying polymerization schemes, the ways holonomies are computed etc., each having been proposed to address particular problems in the effective theory of that sector that existed before it. Many of these issues involve a low energy limit that does not reduce to the predictions of GR in regimes where we wouldn't expect any quantum gravity corrections. The most successful of these attempts has been dubbed the $\bar{\mu}$ scheme (pronounced "mu-bar")[18] where the holonomy length, i.e., the length of the path ℓ in (1.8), is related to the physical Planck length through use of the metric [66].

The earliest polymerization scheme studied in LQC was known as the μ_0 scheme

[18]Also known as the improved dynamics scheme for historical reasons.

where holonomy lengths were taken to be constant. This scheme is successful in resolving cosmological singularities, but it was quickly realized that it could result in bounces at arbitrarily low (non-Planckian) curvatures. The $\bar{\mu}$ scheme was found to resolve these shortcomings and has been shown to be the unique loop quantization scheme[19] if we want our theory to satisfy several physically reasonable requirements [67].

Aside from these choices, and the difficulties that may or may not arise, regardless of the strategy used, each that have been studied in LQC share one common — and monumental — result: the resolution of the big bang singularity. In LQC the big bang is replaced by a so-called "big bounce", where a collapsing universe reaches a minimum volume (maximum density) before it begins to expand again. The big bounce is a direct effect of the boundedness of curvature scalars and energy density that is introduced via the non-local holonomy corrections in the effective theory. In a mathematical sense, this boundedness arises due to the boundedness of the trigonometric functions of the connection that are introduced in the Hamiltonian by explicitly computing the path ordered integral defining the holonomy in equation (1.8). The bounce has implications for early universe physics and the inflation of our universe. In fact, it may even be possible to experimentally observe signatures of this effective dynamics via the CMB, even though current experiments cannot probe the scales at which quantum gravity effects become important due its astonishing smallness [68].

Up to now, these effective techniques have been successfully applied to various space-times and matter configurations including homogeneous and isotropic universes for various curvatures including the flat ($k = 0$) [66, 69, 70], closed ($k = 1$) [71–73] and open ($k = -1$) [74, 75] Friedman-Lemaître-Robertson-Walker (FLRW) models and in the case of a non-zero cosmological constant [76–79]. These methods have also been extended to increasingly complex space-times including to the (anisotropic) Bianchi

[19] At least in isotropic cosmology.

space-times [80–87] and even to inhomogeneous models such as Gowdy models [88–95]. See also [36] for a review of many aspects of these various models. The next logical step in this development is to extend the effective framework to black hole space-times which is the focus of this thesis.

1.3.3 Tackling black hole space-times with effective LQG

Although the techniques of effective LQG have been successfully applied to many simpler space-times to resolve singularities, notably cosmological space-times as discussed in the previous section, it has proven much more difficult to tackle black hole space-times. The main reason for this is due to the inhomogeneity of the metric, where metric components depend on both temporal and spatial coordinates rather than the solely temporal dependence present in, for e.g., homogeneous cosmological space-times. This leads to local degrees of freedom (DOF) and all the difficulties that come when trying to quantize a field theory.

Initial attempts in this direction studied the Kantowski-Sachs metric. This is a cosmological metric that, classically, is isomorphic to the interior of the Schwarschild space-time, the simplest black hole solution in GR. Although this isomorphism holds in GR, it does not necessarily hold in quantum gravity, or even in modified gravity theories for that matter [96], meaning we need to be cautious when implementing such a simplification prior to developing the effective framework.

Nonetheless, this allowed early research to follow exactly the procedure that was successful in resolving cosmological singularities and apply this to a black hole space-time. Although these studies were successful in resolving the singularity at the center of the Schwarzschild black hole [97–99], they are unsatisfactory for several reasons. First, the aforementioned issue of the isometry between Kantowski-Sachs and the Schwarzschild interior, and whether it remains valid in quantum gravity. Secondly, issues begin to arise near the horizon where coordinates become null. Recall from

Section 1.3.2 that the $\bar{\mu}$ scheme requires the use of the metric to relate the coordinate length along which we compute holonomies to the (physical) Planck length. The coordinates used when studying the Kantowski-Sachs space-time become null at the horizon making such a comparison impossible, and it is not known how to properly implement the $\bar{\mu}$ scheme for null coordinates (or for coordinates that become null at a point). As a result, earlier work using this isometry, that naively implementated the $\bar{\mu}$ scheme despite the coordinates becoming null at the horizon, resulted in large quantum corrections near the horizon — a location that we do not expect to find quantum corrections [99]. Finally, and perhaps most importantly, unnaturally studying the interior portion of the space-time in isolation becomes unsatisfactory when we want to study physical black holes which necessarily form due to gravitational collapse.

With this in mind, it becomes necessary to consider both the interior and exterior parts of the space-time simultaneously, since at some point no "interior" exists prior to the formation of the black hole. This requirement, i.e., the inclusion of the exterior, complicates things when trying to implement the $\bar{\mu}$ scheme, due to the aforementioned inhomogeneity. Alternatives to the $\bar{\mu}$ scheme have been proposed that don't have any problems at the horizon, but these necessarily entail a modification of the $\bar{\mu}$ scheme [100–111].

Several early studies have considered the exterior of the space-time as well [112–118] — and notably [119] which played a large role in the early development of our vacuum work that is the subject of Chapter 2 of this thesis. See also [120] for a recent review of black holes in LQG. However, this leads to problems at the horizon and potentially gives the incorrect classical limit, again, if one isn't careful relating holonomy length to the Planck length using the metric via the $\bar{\mu}$ scheme [121–123]. Here, we will deal with these issues by considering the full space-time and choosing coordinates that are nowhere null.

Although reduction to spherical symmetry simplifies the theory quite a bit, in

particular the diffeomorphism constraint, the constraints and equations of motion remain formidable. Add to this the fact that it is not obvious how to analytically compute holonomies in the radial direction in this setting (again, due to the inhomogeneity) and even the effective, symmetry reduced theory becomes intractable. As a workaround, we will further reduce the theory through gauge fixing although other approaches are available [124–126].

In the case of general relativity, a choice of gauge essentially amounts to a choice of coordinates, leaving the physics unaffected. In order to reduce the theory further, we will fix some of the spatial coordinates via gauge fixing. Note that we cannot fix all coordinates in vacuum since this would fully determine our space-time, leaving no room for holonomy corrections and hence no way to study how geometry quantization may affect the space-time in the effective setting. This is related to the question of whether quantization and gauge-fixing commute — if we could quantize first, there would be no problem in a full gauge-fixing.

Since we are not yet at a stage where a full quantization is possible, in Chapters 3 and 4 we will see how to fix coordinates further while maintaining the ability to study how geometry quantization affects space-time dynamics by introducing matter to the system. With the introduction of a matter field, the Hamiltonian will no longer be a constraint as mentioned earlier, yet we will still have DOF from the matter itself.

1.4 Contents of Thesis

As we have alluded to, this thesis contains research towards an effective model of spherically symmetric black holes inspired by the LQC approach that has been tremendously successful in providing insights on the dynamics and causal structure of space-time near cosmological singularities. The goal of this work was to extend previous research on effective models for black hole space-times to properly include the $\bar{\mu}$ scheme

for holonomy corrections without having to resort to the interior isometry with the Kantowski-Sachs cosmological metric. In Chapter 2, we develop a framework for holonomy corrections in vacuum spherically symmetric space-times (the Schwarzschild black hole) that allows us to study the entire space-time — both interior and exterior — and elucidate some of its key features. In Chapter 3, we extend this further by showing how matter can be included in this framework directly and show the connection between this result and previously known results from LQC. We end this chapter by giving a preliminary estimate of what these quantum corrections would mean for the lifetime of a black hole in this framework. Finally, in Chapter 4 we develop the matter collapse picture more fully and show that our previous lifetime estimate is robust across a wide range of initial matter configurations before concluding with a discussion about our key results and potential future research directions in Chapter 5.

1.4.1 Chapter 2: Effective loop quantum gravity framework for vacuum spherically symmetric space-times

Chapter 2 contains the work published in [127]. We start with vacuum spherically symmetric space-times, in particular we show how one can properly incorporate holonomy corrections in this sector. Holonomy corrections have been applied to the study of homogeneous cosmologies to successfully resolve the singularities in these space-times, but up to this point many attempts at a proper way to include holonomy corrections to black-hole space-times using the $\bar{\mu}$ scheme have been elusive.

After reduction to spherical symmetry, in order to facilitate the derivation of the effective theory, we perform a gauge fixing that completely fixes away the diffeomorphism constraint. A very intuitive choice of gauge that is well known in the literature is the areal gauge which geometrically corresponds to choosing a radial coordinate given by the radius of concentric 2-spheres. This is a very simple gauge that can

usually[20] be imposed, regardless of the gravitational dynamics, and this is the gauge we will choose here.

As an aside, there are several other benefits of the areal gauge for this work that we now outline. In order to implement holonomy corrections, we need to compute holonomies according to the path-ordered integral of the connection given by (1.8). Due to the path-ordering, this integral becomes non-trivial when the connection depends on a coordinate we are computing the integral along. In this case, due to the inhomogeneity of general spherically symmetric metrics, it is difficult to compute holonomies in the radial direction since the connection components will depend on the radial coordinate in general. The areal gauge has the property that the gauge fixed Hamiltonian constraint only depends on the angular components of the Ashtekar–Barbero connection, allowing us to avoid this difficulty altogether. It also turns out to be difficult to add holonomy corrections before this gauge fixing since the constraint algebra doesn't close[21], which is an important requirement to ensure consistency of the resulting theory. After gauge fixing using the areal gauge, the algebra generically closes for any polymerization, avoiding this issue as well. It is also worth mentioning here that this gauge fixing forces a relation between the lapse and shift, resulting in the (remaining) connection component making its way into the metric — this will prove important both in vacuum and later when we introduce matter and study black holes that have formed due to gravitational collapse.

After gauge fixing the action, we are left with only the scalar constraint, meaning we still have invariance under arbitrary reparametrizations of the temporal coordinate that has not yet been fixed. The EOMs are easily found by the standard method, i.e., taking the Poisson bracket of the remaining (non-gauge fixed) phase space variables with the scalar constraint, giving the Hamilton's equations for the system. We

[20]In order to impose this gauge, the area of concentric 2-spheres must always change monotonically. Although this is often the case, there are some instances where this does not hold, for example in wormholes.

[21]At least for the simplest attempts at polymerizing the connection components.

show that one solution to our EOMs corresponds to the Schwarzschild solution in Painlevé-Gullstrand (PG) coordinates which sets the stage for the remainder of the paper. These coordinates do not become null at the horizon, nor switch character from time-like to space-like (or vice versa) as we cross the horizon as the standard Schwarzschild coordinates would. This makes the PG coordinates an ideal candidate for this investigation since, as discussed, it is well known that coordinates becoming null along the horizon leads to undesirable physics when attempting to incorporate holonomy corrections in the $\bar{\mu}$ scheme. Finally, we show how holonomy corrections can now be applied to the classical Hamiltonian without affecting the closure of the algebra, thus giving a modified theory of gravity, and calculate the modified EOMs.

The remainder of this first paper is dedicated to analyzing solutions of this theory — mainly one particular solution whose classical limit is the Schwarschild solution in PG coordinates. This analysis shows several interesting features of the modified theory that differ from the classical space-time:

1. curvature scalars are bounded everywhere by the Planck scale[22] and independent of the black hole mass M

2. mass dependent horizon formation — there is now a minimum mass required before horizons in this space-time form and there can be 0, 1 or 2 horizons depending on this mass

3. the solution does not actually reach the center of the black hole, but rather the metric is only well defined for radial coordinates $x \geq x_{\min} \sim (\ell_{\mathrm{Pl}}^2 M)^{1/3}$; inside this radius, metric components become imaginary

4. black hole thermodynamics is also modified in this picture, suggesting that a mass remnant would be left after the black hole evaporation process[23] since the

[22] Everywhere the solution is valid that is; see Chapter 2 for more details.
[23] As opposed to complete evaporation.

horizon disappears for sufficiently small mass black holes

The multi-horizon structure of the space-time we find is a new feature of LQG black holes that is not present when quantizing the interior only. Further, as we will argue in Chapter 2, point 3 above suggests the need to include a matter field in order to understand the entire space-time.

It is interesting to note that there is evidence of the robustness of these results due to a correspondence between the equations we derive and the solution derived in [124], which develops an effective framework from a completely different perspective. In saying this, one more point that is important here, that remains an open question, is the relationship between different solutions of our effective theory. In the modified theory, we still have a closed constraint algebra. This implies we have well defined evolution in the sense that initial conditions satisfying our (modified) constraints will continue to satisfy the constraints at all times. What is not clear, however, is how one solution to our equations can be transformed into another solution in a different gauge. In the classical theory, this can of course be accomplished via diffeomorphisms, but in our modified theory we find that taking diffeomorphisms of a given solution no longer yields valid solutions to our EOMs in general. This could mean one of (at least) two things: either the model is wrong and needs to be corrected, for example perhaps the Hamiltonian we derive only holds in a specific gauge, and modifications are required so it can hold more generally, for recent work in this direction see [126, 128–131], or there is a quantum deformation to diffeomorphism invariance. Since we have a Hamiltonian constraint, we can still generate symmetries (by taking Poisson brackets with the constraints) for our theory, but what exactly the symmetry is will depend on the precise form of the constraint. So if a constraint is modified, it may be that the symmetry (in this case the classical diffeomorphism symmetry) is modified as well. If there is a quantum deformation of this classical symmetry, this means that under a coordinate transformation, tensors will not transform according to the standard tensor

transformation law, but rather a tensor transformation law with quantum corrections of order $\hbar$. Which one of these (or other) possibilities is the case remains an open question and will need to be better understood moving forward.

1.4.2 Chapter 3: Black hole collapse and bounce in effective loop quantum gravity

Chapter 3 contains the work published in [132]. Studying the vacuum space-time leads directly to the need to introduce a matter field in order to understand the entire space-time. In particular, we find that a matter field is necessary to understand the structure of space-time within a radius of $\sim (\ell_{\rm Pl}^2 M)^{1/3}$. In order to understand this region of the vacuum space-time, in Chapter 3 we extend the framework of the previous chapter by including a simple matter field known as "dust". Dust is essentially just an idealized matter field that exerts no pressure meaning that the particles making up the field do not interact with one another as they evolve. Although idealized, it is well known from canonical quantum gravity that this type of matter field can be used as a sort of clock [133, 134], an idea that we use to extend the application of effective LQG in black hole space-times.

We introduce this matter field into the framework developed in Chapter 2 by coupling the dust field to gravity in the action. As before, we gauge fix the diffeomorphism constraint via the areal gauge, but unlike before we can now fix the scalar (Hamiltonian) constraint as well, using the newly introduced matter as a clock. This leaves us with a physical Hamiltonian and no constraints. With the introduction of the matter field, we are left with one physical DOF at each spatial point after this second gauge fixing and are free to study the dynamics of this reduced system.

After this simplification, holonomy corrections are added, as before, in order to derive an effective Hamiltonian that governs the quantum corrected dynamics of

the system. Given this effective Hamiltonian, we are now free to choose an initial matter distribution and study its dynamics. We start this analysis by considering the Oppenheimer-Snyder model, a very simple model of black hole collapse that is well studied in the classical literature [135]. This is an idealized model of a collapsing star, where we assume there is a ball of constant density dust out to some radius, and vacuum outside of this radius. Remarkably, we find the dynamics give precisely the LQC effective Friedmann equation for spatially flat FLRW space-times[24]. Intuitively this makes sense since classically the interior of the Oppenheimer-Snyder model is an FLRW cosmology, but there was no reason a priori to expect this correspondence in the effective model, making this result somewhat surprising and the seeming robustness of the effective theory encouraging.

Studying the dynamics of this model, we find that the dust undergoes an initial collapse, reaches the critical density (the maximum density allowed in LQC) where quantum effects become sufficiently strong to counter the gravitational attraction at which time the ball begins to expand. Eventually the expanding ball of matter reaches the Schwarzschild radius and the apparent horizon disappears leading to the "death" of the black hole. We note that this picture is unlike earlier works describing transition between black and white holes in vacuum [136–138]. We also find that the minimum radius is exactly the radius defining the forbidden region in the vacuum space-time studied in Chapter 2, giving credence to the idea that a matter field is necessary to study the full space-time.

By including edge effects that arise due to a discontinuity in the gravitational field at the boundary of the dust ball (and modify the dynamics), we further show that the dynamics leads to a shockwave after the bounce. Thus, we find that although our model resolves the strong singularity at the center of the black hole, weak singularities that form due to the evolution of the dust field are not resolved. The same is also

[24]In order to derive this result, we make the simplifying assumption to ignore edge effects at the boundary of the star and vacuum where the matter density is discontinuous.

true in LQC [139]. Mathematically, this shockwave arises as a discontinuity of the gravitational metric due to the presence of the shift. Recall that the connection components make their way into the metric (via the shift) through our choice of areal gauge during the simplification process.

The final, and perhaps most intriguing, result outlined in this paper is an estimate of the lifetime of the black hole; that is, the time between the formation of the first apparent horizon (when matter collapses within its Schwarzschild radius) to its disappearence (when matter is ejected from its Schwarzschild radius). Again, after including the previously neglected edge effects, we give an estimate for the lifetime of the black hole which is on the order of M^2 (where M is the black hole mass). This estimate, which has been proposed in previous literature [137, 140], but never derived from the EOMs of an underlying model as we do here, is new in LQG black holes and could have significant implications for black hole physics including the infamous information loss paradox and warrants further investigation. This result forms the basis for the investigation discussed in Chapter 4.

1.4.3 Chapter 4: Fate of quantum black holes

Chapter 4 contains the work published in [141]. Here we revisit the dust collapse scenario developed in Chapter 3 in order to define the quantum theory in full and derive the effective theory (with quantum corrections), again by taking the expectation values of operators in sharply peaked states followed by the continuum limit. In the end, this leads to a set of two coupled PDE's that that are studied both analytically and numerically throughout the remainder of this chapter.

Of particular interest is the family of LTB space-times that describe radially infalling matter starting at rest at infinity, referred to as marginally bound solutions in the classical literature. Classically, these solutions have been studied extensively, and it is well known that shell-crossing singularities may form for general initial conditions

during the collapse. These are points where a certain function becomes non-invertible, leaving us with something that is not a function and hence a smooth solution is no longer well defined beyond such a point. Classically, it can be shown that (under reasonable assumptions) these types of singularities can be avoided with specifically chosen initial matter configurations [142, 143], but are otherwise generic. See, e.g., [144, 145] for further discussion of shell-crossing singularities in classical GR.

In order to solve such systems of equations, i.e., systems where shell-crossing singularities exist, we must rewrite the system in its weak (integral) form. A well known example of these weak solutions — that may not solve the original PDE due to the existence of discontinuities — in GR is the Israel thin shell [142, 146, 147]. Although we are able to solve the quantum corrected (effective) EOMs analytically for some simple initial distributions, like the Oppenheimer-Snyder model, in general we resort to using the well known Gudonov numerical method to study the evolution [148].

Studying this family of space-times, we are able to provide further evidence for a phenomenon alluded to in Chapter 3 — the formation of shockwaves. For all matter configurations studied, we find that after the bounce a shockwave forms in the outgoing phase. Once again, as in Chapter 3, the theory is free from the (strong) curvature singularity at the center of the black hole, but (weak) shell-crossing singularities form quite generically in this framework. Additionally, simulating the gravitational collapse both analytically (for simpler matter configurations) and numerically, we again find the lifetime of the black hole to be on the order of M^2, corroborating our rough estimate from the previous chapter. Finally, using the effective framework developed here, we also sketch the casual structure of spherically symmetric black hole space-times that can be expected from LQG.

The sum of this work provides a complete picture of the life of black holes in the effective theory from initial collapse, to bounce and death as the shockwave exits

the outer horizon. It also successfully extends the use of the $\bar{\mu}$ scheme, not only to inhomogeneous black hole space-times, but also to the matter collapse scenario, both of which were not previously well understood in the literature.

1.5 Personal Contributions

Since this thesis consists of several published papers on which I was a co-author, here I outline my contributions to the research contained in each.

Chapter 2 was developed in collaboration with Robert Santacruz and Edward Wilson-Ewing. I participated in the preliminary work in determining an appropriate initial coordinate selection that became vital to the subsequent research. Once this choice was made I helped deriving the constraints and analyzing the constraint structure in both the classical and effective theories, which were necessary to ensure consistency of the underlying framework. I also played a role in determining an appropriate gauge fixing, allowing us to simplify the model and bypass some of the difficulties outlined above. I then helped derive and solve the EOMs in both the classical and effective theory. In the case of the effective theory, I assisted in analyzing the modified solution(s) to help elucidate some of its key features and produced visualizations for the final manuscript. Finally, I was part of writing, proof reading and editing the final manuscript for publication.

Chapter 3 was also developed in collaboration with Robert Santacruz and Edward Wilson-Ewing. I again helped analyzing the constraint structure of the theory in order to select appropriate matter fields to include in the framework developed in Chapter 2. Once a matter field was selected I helped derive the EOMs and several analytical results in the manuscript. I was again involved in the writing, proof reading and editing of the final manuscript for publication.

Chapter 4 was developed in collaboration with Viqar Husain, Robert Santacruz

and Edward Wilson-Ewing. Here I helped finding appropriate analytical and numerical methods that could be applied to the type of PDEs that were derived in Chapter 3. I helped with deriving some of the analytical results and assisted in developing the code to implement the numerical methods and visualize the dynamics of our model. Finally, I was again involved in writing, proof reading and editing the final manuscript for publication.

Bibliography

[1] B. Abbott & Others, "Observation of Gravitational Waves from a Binary Black Hole Merger," Phys. Rev. Lett. **116** (2016) 061102.

[2] K. Akiyama & Others, "First M87 Event Horizon Telescope Results. I. The Shadow of the Supermassive Black Hole," Astrophys. J. Lett. 875 pp. L1 (2019).

[3] R. P. Geroch, "What is a singularity in general relativity?," Annals Phys. 48, 526-540 (1968).

[4] S. W. Hawking and R. Penrose, "The Singularities of gravitational collapse and cosmology," Proc. Roy. Soc. Lond. A 314, 529-548 (1970).

[5] S. W. Hawking and G. F. R. Ellis, "The large scale structure of space-time," Cambridge University Press, Cambridge (1973).

[6] S. W. Hawking, "Black hole explosions," Nature **248**, 30-31 (1974).

[7] S. W. Hawking, "Particle Creation by Black Holes," Commun. Math. Phys. **43**, 199-220 (1975) [erratum: Commun. Math. Phys. **46**, 206 (1976)].

[8] D. N. Page, "Hawking radiation and black hole thermodynamics," New J. Phys. **7**, 203 (2005), `arXiv:hep-th/0409024`.

[9] T. P. Sotiriou and V. Faraoni, "f(R) Theories Of Gravity," Rev. Mod. Phys. **82**, 451-497 (2010), `arXiv:0805.1726`.

[10] F. W. Hehl, J. D. McCrea, E. W. Mielke and Y. Ne'eman, "Metric affine gauge theory of gravity: Field equations, Noether identities, world spinors, and breaking of dilation invariance," Phys. Rept. **258**, 1-171 (1995), arXiv:gr-qc/9402012.

[11] D. S. Klemm and L. Ravera, "Einstein manifolds with torsion and nonmetricity," Phys. Rev. D **101**, no.4, 044011 (2020), arXiv:1811.11458.

[12] T. P. Sotiriou, "f(R) gravity, torsion and non-metricity," Class. Quant. Grav. **26**, 152001 (2009), arXiv:0904.2774.

[13] A. Arbey and F. Mahmoudi, "Dark matter and the early Universe: a review," Prog. Part. Nucl. Phys. **119**, 103865 (2021), arxiv:2104.11488.

[14] J. Martin, "Everything You Always Wanted To Know About The Cosmological Constant Problem (But Were Afraid To Ask)," Comptes Rendus Physique **13**, 566-665 (2012), arxiv:1205.3365.

[15] G. R. Bengochea, G. León, E. Okon and D. Sudarsky, "Can the quantum vacuum fluctuations really solve the cosmological constant problem?," Eur. Phys. J. C **80**, no.1, 18 (2020), arxiv:1906.05406.

[16] M. P. Hobson, G. P. Efstathiou and A. N. Lasenby, "General relativity: An introduction for physicists".

[17] H. Stefancic, "The Solution of the cosmological constant problem from the inhomogeneous equation of state: A Hint from modified gravity?," Phys. Lett. B **670**, 246-253 (2009), arXiv:0807.3692.

[18] H. Bernardo *et al.* [Foundational Aspects of Dark Energy (FADE)], "Modified Gravity Approaches to the Cosmological Constant Problem," Universe **9**, no.2, 63 (2023), arXiv:2210.06810.

[19] R. Solanki, A. De and P. K. Sahoo, "Complete dark energy scenario in f(Q) gravity," Phys. Dark Univ. **36**, 100996 (2022), arXiv:2203.03370.

[20] S. Mukhi, "String theory: a perspective over the last 25 years," Class. Quant. Grav. **28**, 153001 (2011), arXiv:1110.2569.

[21] A. Eichhorn, "An asymptotically safe guide to quantum gravity and matter," Front. Astron. Space Sci. **5**, 47 (2019), arXiv:1810.07615.

[22] D. Oriti, "The Group field theory approach to quantum gravity," arXiv:gr-qc/0607032.

[23] R. Loll, "Quantum Gravity from Causal Dynamical Triangulations: A Review," Class. Quant. Grav. **37**, 013002 (2020), arXiv:1905.08669.

[24] J. Aastrup, J. M. Grimstrup and R. Nest, "Holonomy Loops, Spectral Triples & Quantum Gravity," Class. Quant. Grav. **26**, 165001 (2009), arXiv:0902.4191.

[25] A. N. Tawfik and A. M. Diab, "Review on Generalized Uncertainty Principle," Rept. Prog. Phys. **78**, 126001 (2015), arXiv:1509.02436.

[26] B. R. Holstein, "Graviton Physics," Am. J. Phys. **74**, 1002-1011 (2006), arXiv:gr-qc/0607045.

[27] M. H. Goroff and A. Sagnotti, "The Ultraviolet Behavior of Einstein Gravity," Nucl. Phys. B **266**, 709-736 (1986).

[28] A. Ashtekar and J. Lewandowski, "Background independent quantum gravity: A Status report," Class. Quant. Grav. **21**, R53 (2004), arXiv:gr-qc/0404018.

[29] C. Rovelli, *Quantum Gravity.* Cambridge University Press, 2004.

[30] T. Thiemann, *Modern Canonical Quantum General Relativity.* Cambridge University Press, 2007.

[31] S. Holst, "Barbero's Hamiltonian derived from a generalized Hilbert–Palatini action," Phys. Rev. D **53**, 5966-5969 (1996), arXiv:gr-qc/9511026.

[32] A. Perez, "The Spin Foam Approach to Quantum Gravity," Living Rev. Rel. **16**, 3 (2013), arXiv:1205.2019.

[33] R. L. Arnowitt, S. Deser and C. W. Misner, "The Dynamics of general relativity," Gen. Rel. Grav. 40, 1997-2027 (2008), arXiv:gr-qc/0405109.

[34] B. S. DeWitt, "Quantum Theory of Gravity. 1. The Canonical Theory," Phys. Rev. **160**, 1113-1148 (1967).

[35] S. Alexander, T. Daniel, M. Howard and M. Konig, "Exact fermionic Chern-Simons-Kodama state in quantum gravity," Phys. Rev. D **106**, 106012 (2022), arXiv:2207.11856.

[36] A. Ashtekar and P. Singh, "Loop Quantum Cosmology: A Status Report," Class. Quant. Grav. **28**, 213001 (2011), arXiv:1108.0893.

[37] A. Ashtekar, "New Variables for Classical and Quantum Gravity," Phys. Rev. Lett. **57**, 2244-2247 (1986).

[38] A. Ashtekar, "New Hamiltonian Formulation of General Relativity," Phys. Rev. D **36**, 1587-1602 (1987).

[39] J. F. Barbero G., "Real Ashtekar variables for Lorentzian signature space times," Phys. Rev. D **51**, 5507-5510 (1995), arXiv:gr-qc/9410014.

[40] A. Ashtekar, J. D. Romano and R. S. Tate, "New Variables for Gravity: Inclusion of Matter," Phys. Rev. D **40**, 2572 (1989).

[41] A. Ashtekar, "Lectures on nonperturbative canonical gravity," Adv. Ser. Astrophys. Cosmol. **6**, 1-334 (1991).

[42] G. A. Mena Marugan, "Reality conditions for Lorentzian and Euclidean gravity in the Ashtekar formulation," Int. J. Mod. Phys. D **3**, 513-528 (1994), arXiv:gr-qc/9311020.

[43] G. Immirzi, "Real and complex connections for canonical gravity," Class. Quant. Grav. **14**, L177-L181 (1997), arXiv:gr-qc/9612030.

[44] A. Ashtekar, S. Fairhurst and J. L. Willis, "Quantum gravity, shadow states, and quantum mechanics," Class. Quant. Grav. **20**, 1031-1062 (2003), arXiv:gr-qc/0207106.

[45] A. Ashtekar, M. Bojowald and J. Lewandowski, "Mathematical structure of loop quantum cosmology," Adv. Theor. Math. Phys. **7**, no.2, 233-268 (2003), arXiv:gr-qc/0304074.

[46] A. Corichi, T. Vukasinac and J. A. Zapata, "Polymer Quantum Mechanics and its Continuum Limit," Phys. Rev. D **76**, 044016 (2007), arXiv:0704.0007.

[47] K. Fredenhagen and F. Reszewski, "Polymer state approximations of Schrödinger wave functions," Class. Quant. Grav. **23**, 6577-6584 (2006), arXiv:gr-qc/0606090.

[48] M. Saeed and V. Husain, "Quantum cosmology as a lattice in a box," arXiv:2407.08117.

[49] C. Rovelli and L. Smolin, "Discreteness of area and volume in quantum gravity," Nucl. Phys. B **442**, 593-622 (1995) [erratum: Nucl. Phys. B **456**, 753-754 (1995)], arXiv:gr-qc/9411005.

[50] A. Ashtekar and J. Lewandowski, "Quantum theory of geometry. 1: Area operators," Class. Quant. Grav. **14**, A55-A82 (1997), arXiv:gr-qc/9602046.

[51] A. Ashtekar and J. Lewandowski, "Quantum theory of geometry. 2. Volume operators," Adv. Theor. Math. Phys. **1**, 388-429 (1998), arXiv:gr-qc/9711031.

[52] A. Ashtekar, A. Corichi and J. A. Zapata, "Quantum theory of geometry III: Noncommutativity of Riemannian structures," Class. Quant. Grav. **15**, 2955-2972 (1998), arXiv:gr-qc/9806041.

[53] T. Thiemann, "A Length operator for canonical quantum gravity," J. Math. Phys. **39**, 3372-3392 (1998), arXiv:gr-qc/9606092.

[54] M. Bojowald, "Loop quantum cosmology," Living Rev. Rel. **8**, 11 (2005), arXiv:gr-qc/0601085.

[55] A. Ashtekar, "Loop Quantum Cosmology: An Overview," Gen. Rel. Grav. **41**, 707-741 (2009), arXiv:0812.0177.

[56] I. Agullo and P. Singh, "Loop Quantum Cosmology," arXiv:1612.01236.

[57] C. Rovelli and E. Wilson-Ewing, "Why are the effective equations of loop quantum cosmology so accurate?," Phys. Rev. D **90**, 023538 (2014), arXiv:1310.8654.

[58] V. Husain and O. Winkler, "Semiclassical states for quantum cosmology," Phys. Rev. D **75**, 024014 (2007), arXiv:gr-qc/060709.

[59] J. Ben Achour, S. Brahma and M. Geiller, "New Hamiltonians for loop quantum cosmology with arbitrary spin representations," Phys. Rev. D **95**, 086015 (2017), arXiv:1612.07615.

[60] J. Münch, A. Perez, S. Speziale and S. Viollet, "Generic features of a polymer quantum black hole," Class. Quant. Grav. **40**, 135003 (2023), arXiv:2212.06708.

[61] M. Gaul and C. Rovelli, "A Generalized Hamiltonian constraint operator in loop quantum gravity and its simplest Euclidean matrix elements," Class. Quant. Grav. **18**, 1593-1624 (2001), arXiv:gr-qc/0011106.

[62] M. Bojowald, "Quantization ambiguities in isotropic quantum geometry," Class. Quant. Grav. **19**, 5113-5230 (2002), arXiv:gr-qc/0206053.

[63] A. Perez, "On the regularization ambiguities in loop quantum gravity," Phys. Rev. D **73**, 044007 (2006), arXiv:gr-qc/0509118.

[64] P. Singh and E. Wilson-Ewing, "Quantization ambiguities and bounds on geometric scalars in anisotropic loop quantum cosmology," Class. Quant. Grav. **31**, 035010 (2014), arXiv:1310.6728.

[65] L. Amadei, A. Perez and S. Ribisi, "Landscape of polymer quantum cosmology," Phys. Rev. D **107**, 086007 (2023), arXiv:2203.07044.

[66] A. Ashtekar, T. Pawlowski and P. Singh, "Quantum Nature of the Big Bang: Improved dynamics," Phys. Rev. D **74**, 084003 (2006), arXiv:gr-qc/0607039.

[67] A. Corichi and P. Singh, "Is loop quantization in cosmology unique?," Phys. Rev. D **78**, 024034 (2008), arXiv:0805.0136.

[68] I. Agulló, A. Wang and E. Wilson-Ewing, "Loop quantum cosmology: relation between theory and observations," arXiv:2301.10215.

[69] A. Ashtekar, T. Pawlowski and P. Singh, "Quantum nature of the big bang," Phys. Rev. Lett. **96**, 141301 (2006), arXiv:gr-qc/0602086.

[70] A. Ashtekar, T. Pawlowski and P. Singh, "Quantum Nature of the Big Bang: An Analytical and Numerical Investigation. I.," Phys. Rev. D **73**, 124038 (2006), arXiv:gr-qc/0604013.

[71] A. Ashtekar, T. Pawlowski, P. Singh and K. Vandersloot, "Loop quantum cosmology of k=1 FRW models," Phys. Rev. D **75**, 024035 (2007), arXiv:gr-qc/0612104.

[72] L. Szulc, W. Kaminski and J. Lewandowski, "Closed FRW model in Loop Quantum Cosmology," Class. Quant. Grav. **24**, 2621-2636 (2007), arXiv:gr-qc/0612101.

[73] A. Corichi and A. Karami, "Loop quantum cosmology of k=1 FRW: A tale of two bounces," Phys. Rev. D **84**, 044003 (2011), arXiv:1105.3724.

[74] K. Vandersloot, "Loop quantum cosmology and the k = - 1 RW model," Phys. Rev. D **75**, 023523 (2007), arXiv:gr-qc/0612070.

[75] L. Szulc, "Open FRW model in Loop Quantum Cosmology," Class. Quant. Grav. **24**, 6191-6200 (2007), arXiv:0707.1816.

[76] E. Bentivegna and T. Pawlowski, "Anti-deSitter universe dynamics in LQC," Phys. Rev. D **77**, 124025 (2008), arXiv:0803.4446.

[77] W. Kaminski and T. Pawlowski, "The LQC evolution operator of FRW universe with positive cosmological constant," Phys. Rev. D **81**, 024014 (2010), arXiv:0912.0162.

[78] T. Pawlowski and A. Ashtekar, "Positive cosmological constant in loop quantum cosmology," Phys. Rev. D **85**, 064001 (2012), arXiv:1112.0360.

[79] M. Dupuis and F. Girelli, "Observables in Loop Quantum Gravity with a cosmological constant," Phys. Rev. D **90**, 104037 (2014), arXiv:1311.6841.

[80] M. Bojowald, G. Date and G. M. Hossain,"The Bianchi IX model in loop quantum cosmology," Class. Quant. Grav. **21**, 3541-3570 (2004), arXiv:gr-qc/0404039.

[81] A. Ashtekar and E. Wilson-Ewing,"Loop quantum cosmology of Bianchi I models," Phys. Rev. D **79**, 083535 (2009), arXiv:0903.3397.

[82] A. Ashtekar and E. Wilson-Ewing, "Loop quantum cosmology of Bianchi type II models," Phys. Rev. D **80**, 123532 (2009), arXiv:0910.1278.

[83] A. Corichi, A. Karami and E. Montoya,"Effective Vacuum Bianchi IX in Loop Quantum Cosmology," Springer Proc. Phys. **157**, 573-577 (2014)

[84] A. Corichi and E. Montoya,"Loop quantum cosmology of Bianchi IX: Effective dynamics," Class. Quant. Grav. **34**, 054001 (2017), arXiv:1502.02342.

[85] A. Corichi and A. Karami,"Loop quantum cosmology of Bianchi IX: Inclusion of inverse triad corrections," Int. J. Mod. Phys. D **25**, no.08, 1642011 (2016), arXiv:1605.01383.

[86] E. Wilson-Ewing,"A quantum gravity extension to the Mixmaster dynamics," Class. Quant. Grav. **36**, 195002 (2019), arXiv:1809.09659.

[87] T. Blackmore and E. Wilson-Ewing, "Numerics of Bianchi type II and type IX spacetimes in effective loop quantum cosmology," Class. Quant. Grav. **40**, 215010 (2023), arXiv:2303.16747.

[88] G. A. Mena Marugan and M. Martin-Benito,"Hybrid Quantum Cosmology: Combining Loop and Fock Quantizations," Int. J. Mod. Phys. A **24**, 2820-2838 (2009), arXiv:0907.3797.

[89] L. J. Garay, M. Martin-Benito and G. A. Mena Marugan,"Inhomogeneous Loop Quantum Cosmology: Hybrid Quantization of the Gowdy Model," Phys. Rev. D **82**, 044048 (2010), arXiv:1005.5654.

[90] M. Martin-Benito, L. J. Garay and G. A. Mena Marugan,"Quantum Gowdy model within the new loop quantum cosmology improved dynamics," J. Phys. Conf. Ser. **314**, 012047 (2011), arXiv:1012.3713.

[91] M. Martin-Benito, D. Martin-de Blas and G. A. Mena Marugan,"Matter in inhomogeneous loop quantum cosmology: the Gowdy T^3 model," Phys. Rev. D **83**, 084050 (2011), arXiv:1012.2324.

[92] D. Brizuela, G. A. Mena Marugan and T. Pawlowski,"Effective dynamics of the hybrid quantization of the Gowdy T^3 universe," Phys. Rev. D **84**, 124017 (2011), arXiv:1106.3793.

[93] M. Martín-Benito, D. Martín-de Blas and G. A. Mena Marugán,"Approximation methods in loop quantum cosmology: from Gowdy cosmologies to inhomogeneous models in Friedmann–Robertson–Walker geometries," Class. Quant. Grav. **31**, 075022 (2014), arXiv:1307.1420.

[94] P. Tarrío, M. F. Méndez and G. A. M. Marugán,"Singularity avoidance in the hybrid quantization of the Gowdy model," Phys. Rev. D **88**, 084050 (2013), arXiv:1310.1290.

[95] B. Elizaga Navascués, M. Martín-Benito and G. A. Mena Marugán,"Hybrid models in loop quantum cosmology," Int. J. Mod. Phys. D **25**, no.08, 1642007 (2016), arXiv:1608.05947.

[96] M. de Cesare, S. S. Seahra and E. Wilson-Ewing, "The singularity in mimetic Kantowski-Sachs cosmology," JCAP **07**, 018 (2020), arXiv:2002.11658.

[97] L. Modesto, "Disappearance of black hole singularity in quantum gravity," Phys. Rev. D **70**, 124009 (2004), arXiv:gr-qc/0407097.

[98] A. Ashtekar and M. Bojowald, "Quantum geometry and the Schwarzschild singularity," Class. Quant. Grav. **23**, 391-411 (2006), arXiv:gr-qc/0509075.

[99] C. G. Boehmer and K. Vandersloot, "Loop Quantum Dynamics of the Schwarzschild Interior," Phys. Rev. D **76**, 104030 (2007), arXiv:0709.2129.

[100] M. Campiglia, R. Gambini, and J. Pullin, "Loop quantization of spherically symmetric midi-superspaces : The Interior problem," AIP Conf. Proc. **977** (2008) 52–63, arXiv:0712.0817.

[101] D.-W. Chiou, "Phenomenological loop quantum geometry of the Schwarzschild black hole," Phys. Rev. D **78**, 064040 (2008), arXiv:0807.0665.

[102] J. Brannlund, S. Kloster, and A. DeBenedictis, "The Evolution of Lambda Black Holes in the Mini-Superspace Approximation of Loop Quantum Gravity," Phys. Rev. D **79**, 084023 (2009), arXiv:0901.0010.

[103] A. Joe and P. Singh, "Kantowski-Sachs spacetime in loop quantum cosmology: bounds on expansion and shear scalars and the viability of quantization prescriptions," Class. Quant. Grav. **32**, 015009 (2015), arXiv:1407.2428

[104] A. Corichi and P. Singh, "Loop quantization of the Schwarzschild interior revisited," Class. Quant. Grav. **33**, 055006 (2016), arXiv:1506.08015.

[105] J. Cortez, W. Cuervo, H. A. Morales-Tecotl, and J. C. Ruelas, "Effective loop quantum geometry of Schwarzschild interior," Phys. Rev. D **95**, 064041 (2017), arXiv:1704.03362.

[106] J. Olmedo, S. Saini, and P. Singh, "From black holes to white holes: a quantum gravitational, symmetric bounce," Class. Quant. Grav. **34**, 225011 (2017), arXiv:1707.07333.

[107] J. Ben Achour, F. Lamy, H. Liu, and K. Noui, "Polymer Schwarzschild black hole: An effective metric," EPL **123**, 20006 (2018), arXiv:1803.01152.

[108] A. Ashtekar, J. Olmedo, and P. Singh, "Quantum extension of the Kruskal spacetime," Phys. Rev. **D98**, 126003 (2018), arXiv:1806.02406.

[109] N. Bodendorfer, F. M. Mele, and J. Münch, "Effective Quantum Extended Spacetime of Polymer Schwarzschild Black Hole," Class. Quant. Grav. **36**, 195015 (2019), arXiv:1902.04542.

[110] E. Alesci, S. Bahrami, and D. Pranzetti, "Quantum gravity predictions for black hole interior geometry," Phys. Lett. **B797**, 134908 (2019), arXiv:1904.12412.

[111] M. Assanioussi, A. Dapor, and K. Liegener, "Perspectives on the dynamics in a loop quantum gravity effective description of black hole interiors," Phys. Rev. D **101**, 026002 (2020), arXiv:1908.05756.

[112] M. Bojowald and R. Swiderski, "Spherically symmetric quantum geometry: Hamiltonian constraint," Class. Quant. Grav. **23**, 2129–2154 (2006), arXiv:gr-qc/0511108.

[113] R. Gambini and J. Pullin, "Black holes in loop quantum gravity: The Complete space-time," Phys. Rev. Lett. **101**, 161301 (2008), arXiv:0805.1187.

[114] R. Gambini, J. Olmedo, and J. Pullin, "Quantum black holes in Loop Quantum Gravity," Class. Quant. Grav. **31**, 095009 (2014), arXiv:1310.5996.

[115] J. Ben Achour, S. Brahma, and A. Marciano, "Spherically symmetric sector of self dual Ashtekar gravity coupled to matter: Anomaly-free algebra of constraints with holonomy corrections," Phys. Rev. D **96**, 026002 (2017), arXiv:1608.07314.

[116] M. Bojowald, S. Brahma, and D.-h. Yeom, "Effective line elements and black-hole models in canonical loop quantum gravity," Phys. Rev. D **98**, 046015 (2018), arXiv:1803.01119.

[117] J. D. Reyes, "Spherically Symmetric Loop Quantum Gravity: Connection to Two-Dimensional Models and Applications to Gravitational Collapse,". PhD thesis, The Pennsylvania State University, 2009. Available online at https://etda.libraries.psu.edu/catalog/10349.

[118] R. Gambini and J. Pullin, "Loop quantization of the Schwarzschild black hole," Phys. Rev. Lett. **110**, 211301 (2013), arXiv:1302.5265.

[119] A. Ashtekar, J. Olmedo and P. Singh,"Quantum extension of the Kruskal spacetime," Phys. Rev. D **98**, 126003 (2018), arXiv:1806.02406

[120] A. Ashtekar, J. Olmedo and P. Singh,"Regular black holes from Loop Quantum Gravity," arXiv:2301.01309.

[121] M. Bouhmadi-López, S. Brahma, C. Y. Chen, P. Chen and D. h. Yeom, "Asymptotic non-flatness of an effective black hole model based on loop quantum gravity," Phys. Dark Univ. **30**, 100701 (2020), arXiv:1902.07874.

[122] M. Bojowald, "Comment (2) on "Quantum Transfiguration of Kruskal Black Holes", arXiv:1906.04650.

[123] A. Ashtekar and J. Olmedo, "Properties of a recent quantum extension of the Kruskal geometry," Int. J. Mod. Phys. D **29**, no.10, 2050076 (2020), arXiv:2005.02309.

[124] R. Gambini, J. Olmedo, and J. Pullin, "Spherically symmetric loop quantum gravity: analysis of improved dynamics," Class. Quant. Grav. **37**, 205012 (2020), arXiv:2006.01513.

[125] R. Gambini, J. Olmedo and J. Pullin,"Quantum Geometry and Black Holes," arXiv:2211.05621.

[126] K. Giesel, H. Liu, P. Singh and S. A. Weigl,"Generalized analysis of a dust collapse in effective loop quantum gravity: fate of shocks and covariance," arXiv:2308.10953.

[127] J. G. Kelly, R. Santacruz, and E. Wilson-Ewing, "Effective loop quantum gravity framework for vacuum spherically symmetric spacetimes," Phys. Rev. D **102** (2020) 106024, arXiv:2006.09302.

[128] A. Alonso-Bardaji, D. Brizuela and R. Vera, "An effective model for the quantum Schwarzschild black hole," Phys. Lett. B **829**, 137075 (2022), arXiv:2112.12110.

[129] M. Bojowald and E. I. Duque, "Emergent modified gravity: Covariance regained," Phys. Rev. D **108**, 084066 (2023), arXiv:2310.06798.

[130] C. Zhang, J. Lewandowski, Y. Ma and J. Yang, "Black Holes and Covariance in Effective Quantum Gravity," arXiv:2407.10168.

[131] I. H. Belfaqih, M. Bojowald, S. Brahma and E. I. Duque, "Black holes in effective loop quantum gravity: Covariant holonomy modifications," arXiv:2407.12087.

[132] J. G. Kelly, R. Santacruz and E. Wilson-Ewing, "Black hole collapse and bounce in effective loop quantum gravity," Class. Quant. Grav. **38**, 04LT01 (2021), arXiv:2006.09325.

[133] V. Husain and T. Pawlowski, "Time and a physical Hamiltonian for quantum gravity," Phys. Rev. Lett. **108**, 141301 (2012), arXiv:1108.1145.

[134] V. Husain and T. Pawlowski,"Dust reference frame in quantum cosmology," Class. Quant. Grav. **28**, 225014 (2011), arXiv:1108.1147.

[135] J. R. Oppenheimer and H. Snyder, "On Continued gravitational contraction," Phys. Rev. **56**, 455-459 (1939).

[136] C. Rovelli and F. Vidotto, "Planck stars," Int. J. Mod. Phys. D **23**, 1442026 (2014), arXiv:1401.6562.

[137] H. M. Haggard and C. Rovelli, "Quantum-gravity effects outside the horizon spark black to white hole tunneling," Phys. Rev. D **92**, 104020 (2015), arXiv:1407.0989.

[138] C. Barcelo, R. Carballo-Rubio, L. J. Garay and G. Jannes, "The lifetime problem of evaporating black holes: mutiny or resignation," Class. Quant. Grav. **32**, 035012 (2015), arXiv:1409.1501.

[139] P. Singh, "Are loop quantum cosmos never singular?," Class. Quant. Grav. **26**, 125005 (2009), arXiv:0901.2750.

[140] M. Christodoulou, C. Rovelli, S. Speziale and I. Vilensky, "Planck star tunneling time: An astrophysically relevant observable from background-free quantum gravity," Phys. Rev. D **94**, 084035 (2016), arXiv:1605.05268.

[141] V. Husain, J. G. Kelly, R. Santacruz and E. Wilson-Ewing, "Fate of quantum black holes," Phys. Rev. D **106**, 024014 (2022), arXiv:2203.04238.

[142] C. Hellaby and K. Lake, "Shell crossings and the Tolman model," Astrophys. J. **290**, 381 (1985).

[143] P. S. Joshi and R. V. Saraykar, "Shell-crossings in Gravitational Collapse," Int. J. Mod. Phys. D **22**, 1350027 (2013), arXiv:1205.3263.

[144] S. M. C. V. Goncalves, "Shell crossing in generalized Tolman-Bondi space-times," Phys. Rev. D **63**, 124017 (2001), arXiv:gr-qc/0107087.

[145] B. K. Tippett and I. Booth, "Closest Safe Approach to an Accreting Black Hole," Phys. Rev. D **90**, 084027 (2014), arXiv:1406.4039.

[146] P. D. Lasky, A. W. C. Lun and R. B. Burston,"Initial value formalism for dust collapse," arXiv:gr-qc/0606003.

[147] S. P. Tegai,"On a weak solution of Einstein equations for expanding dust," J. Sib. Fed. U. **4**, 43-49 (2011), arXiv:1104.1664.

[148] R. J. LeVeque, *Finite Volume Methods for Hyperbolic Problems.* Cambridge University Press, 2002.

Chapter 2

Effective loop quantum gravity framework for vacuum spherically symmetric space-times

2.1 Introduction

It is widely expected that the singularity at the center of a black hole, predicted by classical general relativity, signals the breakdown of the classical theory and indicates the need to include quantum gravity effects. In addition, the black hole information loss problem further underlines the importance of understanding the role of quantum gravity effects in black hole space-times, with modifications to the causal structure of the quantum-corrected space-time being especially relevant.

One approach to explore how quantum gravity could affect black hole space-times is by modifying the metric of the Schwarzschild space-time, often by hand, to provide concrete examples of non-singular space-times [1–11], that can then be classed according to their geometry [12, 13]. However, in principle the best would be to start from a specific theory of quantum gravity, to determine the states that correspond

to spherically symmetric space-times, and to extract physical predictions from these states. While this so far remains an outstanding challenge for all candidate theories of quantum gravity, it is nonetheless possible to include certain effects—predicted by particular theories—and study their impact on black hole space-times. There has been considerable work in this direction in a number of quantum gravity theories (see, e.g., [14–16]), and in particular in loop quantum gravity (LQG), a background-independent and non-perturbative theory of quantum gravity [17–19].

The work in LQG has built on earlier research that studied LQG effects in cosmological space-times following the loop quantum cosmology (LQC) procedure: first, the symmetries of the space-time of interest are imposed at the classical level, and second, the symmetry-reduced classical theory is quantized using LQG methods—notably, the fundamental operators are holonomies of the connection and areas. For a review on LQC, see, e.g., [20]; this same procedure has since been applied to black hole space-times as well.

There has been a considerable focus on the Schwarzschild interior, using the isometry between the interior and the Kantowski-Sachs space-time to more easily import techniques from LQC [21–23]. Despite this effort, as shall be discussed in Sec. 2.2 in more detail, it has turned out to be difficult to handle holonomy corrections properly in this framework. To ensure that the edges along which the holonomies are evaluated have a physical length $\sim \ell_{\mathrm{Pl}}$, it is necessary to relate the physical length to a coordinate length by the metric; this is called the '$\bar{\mu}$ scheme'. However, it is not clear how to properly take into account the $\bar{\mu}$ scheme near the horizon when using a set of coordinates where a spatial coordinate becomes null at the horizon and the physical length along that coordinate tends to 0, as is the case for the Schwarzschild interior in Kantowski-Sachs coordinates [23]. There exist various proposals in the literature to address this difficulty [24–35], but here we suggest instead that the $\bar{\mu}$ scheme simply cannot be implemented in terms of a particular set of (spatial) coordinates if one of

these coordinates becomes null, for example at a horizon.

There has also been significant work studying the dynamics of the full space-time—interior and exterior together—with LQG-inspired corrections, whether holonomy effects [36–42] or inverse triad effects [43–47], and there has also been some more recent work in this setting where it has been shown how to implement the $\bar{\mu}$ scheme [48, 49], which raises the hope that by considering the whole space-time at once it may be possible to avoid the difficulties that arise when considering the Schwarzschild interior only.

In this paper, we will further study the $\bar{\mu}$ scheme for holonomy corrections in vacuum spherically symmetric space-times and also extend earlier results in a manner so that the extension to include matter fields will be quite direct; in particular, it is straightforward to include pressureless dust [50]. For previous work on including matter in spherically symmetric space-times (although not in the $\bar{\mu}$ scheme), see [41, 51–54].

By including matter, it is possible to study how quantum gravity effects may arise during black hole collapse, and how they could modify the resulting space-time. LQG effects on black hole collapse have previously been explored in a number of settings [55–64], and extending these studies to include the $\bar{\mu}$ treatment of the holonomies in a way that provides a general framework that determines the dynamics for both the interior and exterior regions will set the stage for more detailed investigations into the role of quantum gravity effects on gravitational collapse.

In particular, one possibility that has been suggested is that when the energy density of the matter composing the collapsing star reaches the Planck scale, quantum gravity effects could generate a non-singular transition to a slowly expanding white hole solution [65–68], with potential observational implications [69–71]. It turns out that this general picture is explicitly realized in this framework when a pressureless dust field is coupled to gravity; for details see [50].

We begin the paper with a general discussion on holonomy corrections and some specific comments on the difficulties that arise in black hole space-times in Sec. 2.2, then present the classical Hamiltonian framework and impose the areal gauge in Sec. 2.3, and finally construct the effective theory with LQG holonomy corrections and study its solutions in Sec. 2.4. Although the effective theory is obtained by following a different path, the results are in perfect agreement with [49], showing the robustness of the results. We end with a discussion in Sec. 2.5

Our conventions are the following: space-time indices are denoted by $\mu, \nu, \rho, \sigma, \ldots$; spatial indices are denoted by $a, b, c, \ldots$; and internal indices are denoted by $i, j, k, \ldots$ We use units where $c = 1$, but leave G and $\hbar$ explicit to clarify the interplay of gravitational and quantum effects.

2.2 Holonomy Corrections

To develop an effective framework for vacuum spherically symmetric black holes following the standard LQC procedure, it is necessary to incorporate holonomy corrections in an appropriate fashion. In this section, we will briefly review the main steps, offer an explanation on why it has been found to be difficult to properly implement the $\bar{\mu}$ scheme for holonomy corrections in the Schwarzschild interior, and explain the procedure we will follow in this paper to avoid these difficulties.

2.2.1 Holonomies

The holonomy of the Ashtekar-Barbero connection $A_a = A_a^i \tau_i$ along a path ℓ is given by

$$h_\ell(A) = \mathcal{P} \exp\left(\int_\ell A_a\right), \tag{2.1}$$

where $\mathcal{P}$ denotes path-ordering, while the τ_i are a basis of the $\mathfrak{su}(2)$ Lie algebra. There are two points here that are important to understand for what follows.

First, the connection is usually expressed in terms of some coordinates, in which case the length of the edge as calculated in terms of these coordinates will necessarily be a coordinate length L_c. So to calculate the holonomy along a path that has a specific physical length L_p, it will be necessary to use the space-time metric $g_{\mu\nu}$ to relate the coordinate and physical lengths to calculate the required coordinate length L_c.

Second, the path-ordered exponential of an integral is defined by a series of nested integrals which, in general, are typically difficult to evaluate. In the simple case when the connection is independent of a particular coordinate, then the path-ordering trivializes for holonomies in that direction and (2.1) can be evaluated much more directly. This is relevant for spherically symmetric space-times: holonomies in the radial direction will be difficult to evaluate, while holonomies along paths where only the angular coordinates vary will be much easier to calculate.

2.2.2 Black Holes and the Near-Horizon Region

In LQC, the holonomies are taken along paths of physical length $\sqrt{\Delta}$, where the area gap Δ is the minimum non-zero area eigenvalue in LQG [72]. As explained in the first point above, it is necessary to use the metric to relate this physical length to a coordinate length, and the result of doing this gives what is called the $\bar{\mu}$ scheme. If the coordinate and physical lengths are not related properly, it is well known in cosmological space-times that the resulting theory is not physically viable and does not have a good classical limit [20].

To avoid the difficulty of evaluating holonomies in the inhomogeneous radial direction (as described in the second point above), it is possible to consider the

Schwarzschild interior only, whose geometry can be expressed in terms of the Kantowski-Sachs cosmological metric

$$ds^2 = -\left(\frac{R_S}{T} - 1\right)^{-1} dT^2 + \left(\frac{R_S}{T} - 1\right) dR^2 + T^2 d\Omega^2, \tag{2.2}$$

where $R_S = 2GM$ is the Schwarzschild radius, $d\Omega^2 = d\theta^2 + \sin^2\theta d\phi^2$, and T is the radial coordinate that becomes time-like inside the horizon; this coordinate system is valid for $T \in [0, R_S)$.

For this choice of coordinates, the metric (and the connection) are independent of any spatial coordinate, and therefore holonomies in all spatial directions can be evaluated rather directly [21, 22]. Despite this advantage, close to the horizon it is difficult to relate the coordinate length of a radial path in the R direction with the physical length—as required by the $\bar{\mu}$ scheme—because R becomes null at the horizon and $ds \to 0$. Requiring that the physical length nonetheless be finite leads to unacceptably large quantum gravity effects near the horizon [23].

Due to this problem, several alternate forms of holonomy corrections have been proposed [28, 30, 32, 33], but what this discussion suggests is that the problem lies in the choice of coordinates that become null and that, to avoid these issues, it is necessary to use coordinates where there is a clean separation between time-like and space-like coordinates everywhere in the space-time.

As an aside, note also that the isometry between the Schwarzschild interior and the Kantowski-Sachs space-time depends on the dynamics of the space-time and is not guaranteed to hold once quantum gravity effects are included. Among other possibilities, if there is an inner horizon in the LQG-corrected space-time then the Kantowski-Sachs metric could not describe the innermost region of the black hole lying within the inner horizon. For an example of a modified gravity theory where Kantowski-Sachs is not isometric to the Schwarzschild interior see [73].

Therefore, in the following we will only consider choices of coordinates where the spatial coordinates always remain space-like, whether inside the horizon or out; the Painlevé-Gullstrand coordinates are one such example that we will use here. The results in this paper can be adapted to several different coordinate choices, but the coordinates should always have the property that the spatial coordinates remain space-like everywhere. Then, we will follow the general prescription for the $\bar{\mu}$ scheme that was first laid out in [23], except here we will use coordinates that are everywhere space-like.

This approach has also been considered in some previous works [48, 49]. In this case, when considering coordinate choices such that the radial coordinate is always space-like, the challenge is to either evaluate holonomies in the radial direction (a difficult problem, in general) or to find a viable way to avoid doing so. In the first work [48], the holonomies in the radial direction were evaluated in a 'point-wise' fashion, this is an approximation where the path-ordering is dropped. However, the constraints of the resulting theory did not close, showing that this approximation is not viable. More recently, this problem was reconsidered using an Abelianized version of the constraints (see [42]) in which case only holonomies in the angular directions are needed to construct the Hamiltonian constraint operator [49]; this resulting theory is well-defined.

Here we will consider a complementary approach, where we will fix a gauge in the classical theory before introducing holonomy corrections, instead of using the Abelianized set of constraints as in [42, 49]. Although the procedure that is followed here is slightly different, the end result is the same. Specifically, we will gauge-fix the diffeomorphism constraint by imposing the areal gauge (which imposes that the prefactor to $d\Omega^2$ in the metric be x^2, with x the radial coordinate). This is a very simple gauge choice, which can always be chosen in spherical symmetry no matter the gravitational dynamics. The areal gauge also has the additional property that

the gauge-fixed Hamiltonian constraint only depends on the angular components of the Ashtekar-Barbero connection: as a result, the only holonomies that need to be evaluated are holonomies along paths that lie on spheres of constant radius—this avoids the difficulty of needing to evaluate holonomies in the radial direction and makes it possible to include holonomy corrections in a rather straightforward manner. In Sec. 2.3, we will go through this gauge-fixing procedure in detail, before continuing to the effective theory with LQG holonomy corrections in Sec. 2.4.

2.3 Classical Theory

The metric of any spherically symmetric space-time can be expressed in the form

$$ds^2 = -N^2 dt^2 + f^2(dx + N^x dt)^2 + g^2 d\Omega^2, \tag{2.3}$$

where the lapse $N(x,t)$, shift vector $N^x(x,t)$ and the functions $f(x,t), g(x,t)$ all depend on time t and the radial coordinate x, while $d\Omega^2 = d\theta^2 + \sin^2\theta\, d\phi^2$. Note that we denote the radial coordinate by x, since it is not necessarily equal to the area radial coordinate r that satisfies $A_r = 4\pi r^2$, with A_r being the surface area of the sphere at radius r.

2.3.1 Basic Variables

The spatial metric q_{ab} can be rewritten in terms of the co-triads

$$e^1_x = f(x,t), \qquad e^2_\theta = g(x,t), \qquad e^3_\phi = g(x,t)\,\sin\theta, \tag{2.4}$$

with $q_{ab} = e^i_a e^j_b \delta_{ij}$. The densitized triads are then given by $E^a_i = \sqrt{q}\, e^a_i$, with the triads e^a_i satisfying $e^i_a e^b_i = \delta^b_a$ and $e^i_a e^a_j = \delta^i_j$, so

$$E^x_1 = g^2 \sin\theta = E^a \sin\theta, \qquad E^\theta_2 = fg\, \sin\theta = E^b \sin\theta, \qquad E^\phi_3 = fg = E^b, \tag{2.5}$$

with $E^a(x,t)$ and $E^b(x,t)$ capturing the degrees of freedom of the densitized triads. The metric can now be rewritten as

$$ds^2 = -N^2 dt^2 + \frac{(E^b)^2}{E^a}\big(dx + N^x dt\big)^2 + E^a d\Omega^2. \tag{2.6}$$

The Ashtekar-Barbero connnection $A^i_a = \Gamma^i_a + \gamma K^i_a$ is the conjugate variable to the densitized triad, with the spin-connection given by

$$\Gamma^i_a = \frac{1}{2}\, \epsilon^i{}_{jk}\, e^{bk} \left(\partial_a e^j_b - \partial_b e^j_a + e^{cj} e_{am} \partial_c e^m_b\right), \tag{2.7}$$

while the extrinsic curvature is $K^i_a = K_{ab} e^{bi}$, with $K_{ab} = \frac{1}{2}\mathcal{L}_t q_{ab}$, and γ is the Barbero-Immirzi parameter. Since the spatial metric is diagonal, so is K_{ab} and we parametrize it by $a(x,t)$ and $b(x,t)$,

$$\gamma K^1_x = a, \qquad \gamma K^2_\theta = b, \qquad \gamma K^3_\phi = b \sin\theta, \tag{2.8}$$

while a short calculation gives

$$\Gamma^3_\theta = \frac{\partial_x E^a}{2E^b}, \qquad \Gamma^1_\phi = \cos\theta, \qquad \Gamma^2_\phi = -\frac{\partial_x E^a}{2E^b} \sin\theta, \tag{2.9}$$

all other components of the spin-connection are 0.

2.3.2 Constraints and Dynamics

The dynamics follow from the gravitational action [17–19],

$$S = \int dt \int_\Sigma \left[\frac{\dot{A}^i_a E^a_i}{8\pi G\gamma} - N\mathcal{H} - N^a \mathcal{H}_a \right], \tag{2.10}$$

where dots denote derivatives with respect to t, the scalar constraint is

$$\mathcal{H} = -\frac{E^a_i E^b_j}{16\pi G\gamma^2\sqrt{q}}\, \epsilon^{ij}{}_k \Big(F_{ab}{}^k - (1+\gamma^2)\Omega_{ab}{}^k \Big), \tag{2.11}$$

and the diffeomorphism constraint is

$$\mathcal{H}_a = \frac{1}{8\pi G\gamma}\, E^b_k F_{ab}{}^k. \tag{2.12}$$

Here the field strength is $F_{ab}{}^k = 2\partial_{[a}A^k_{b]} + \epsilon_{ij}{}^k A^i_a A^j_b$, while the spatial curvature is given by $\Omega_{ab}{}^k = 2\partial_{[a}\Gamma^k_{b]} + \epsilon_{ij}{}^k \Gamma^i_a \Gamma^j_b$.

Using the coordinate choices for spherical symmetry described in Sec. 2.3.1 and integrating over $d\Omega$ gives the symmetry-reduced action

$$S = \int dt \int dx \, \left[\frac{\dot{a}E^a + 2\dot{b}E^b}{2G\gamma} - N\mathcal{H} - N^x \mathcal{H}_x \right], \tag{2.13}$$

with the scalar constraint

$$\mathcal{H} = -\frac{1}{2G\gamma}\left[\frac{2ab\sqrt{E^a}}{\gamma} + \frac{E^b}{\gamma\sqrt{E^a}}(b^2+\gamma^2) - \frac{\gamma(\partial_x E^a)^2}{4E^b\sqrt{E^a}} - \gamma\sqrt{E^a}\partial_x\left(\frac{\partial_x E^a}{E^b}\right)\right], \tag{2.14}$$

and the diffeomorphism constraint

$$\mathcal{H}_x = \frac{1}{2G\gamma}\left(2E^b\partial_x b - a\partial_x E^a\right). \tag{2.15}$$

Note that only the radial component of the diffeomorphism constraint is non-trivial

once coordinates that are explicitly spherically symmetric have been chosen, as is the case here.

The action also shows that the symplectic structure of the symmetry-reduced theory is given by

$$\{a(x_1), E^a(x_2)\} = 2G\gamma\,\delta(x_1 - x_2), \tag{2.16}$$

$$\{b(x_1), E^b(x_2)\} = G\gamma\,\delta(x_1 - x_2). \tag{2.17}$$

Denoting $\mathcal{C}[N] = \int dx\, N\mathcal{H}$ and $\mathcal{D}[N^x] = \int dx\, N^x\mathcal{H}_x$, it is a straightforward, although long, calculation to verify that the constraint algebra (for the symmetry-reduced theory) is

$$\{\mathcal{C}[N_1], \mathcal{C}[N_2]\} = \mathcal{D}\left[\frac{E^a}{(E^b)^2}\left(N_1\partial_x N_2 - N_2\partial_x N_1\right)\right], \tag{2.18}$$

$$\{\mathcal{D}[N_1^x], \mathcal{D}[N_2^x]\} = \mathcal{D}[(N_2^x\partial_x N_1^x - N_1^x\partial_x N_2^x)], \tag{2.19}$$

$$\{\mathcal{C}[N], \mathcal{D}[N^x]\} = -\mathcal{C}[N^x\partial_x N]. \tag{2.20}$$

The equations of motion, determined by $\dot{f} = \{f, \mathcal{C}[N] + \mathcal{D}[N^x]\}$, are given by:

$$\dot{E}^a = \frac{2Nb}{\gamma}\sqrt{E^a} + N^x\partial_x E^a, \tag{2.21}$$

$$\dot{E}^b = \frac{N}{\gamma\sqrt{E^a}}(aE^a + bE^b) + \partial_x(N^x E^b), \tag{2.22}$$

$$\begin{aligned}\dot{a} = &\frac{N}{2\gamma\sqrt{E^a}}\left[\frac{E^b}{E^a}(b^2+\gamma^2) - 2ab\right] + \frac{N\gamma}{2\sqrt{E^a}}\left[\partial_x\left(\frac{\partial_x E^a}{E^b}\right) - \frac{(\partial_x E^a)^2}{4E^a E^b}\right] \\ &+ \gamma\,\partial_x\left(\frac{\partial_x(N\sqrt{E^a})}{E^b}\right) - \frac{\gamma}{2}\partial_x\left(N\frac{\partial_x E^a}{E^b\sqrt{E^a}}\right) + \partial_x(N^x a),\end{aligned} \tag{2.23}$$

$$\dot{b} = -\frac{N}{2\gamma\sqrt{E^a}}\left(b^2+\gamma^2\right) - \frac{\gamma}{2}\left[\frac{N}{\sqrt{E^a}}\left(\frac{\partial_x E^a}{2E^b}\right)^2 - \partial_x\left(N\sqrt{E^a}\right)\frac{\partial_x E^a}{(E^b)^2}\right] + N^x\partial_x b. \quad (2.24)$$

After choosing a lapse and a shift, solutions to these equations of motion and the constraints $\mathcal{H} = 0$ and $\mathcal{H}_x = 0$ will give a metric (2.6) that satisfies the vacuum Einstein equations.

One example that will be relevant here is the Schwarzschild space-time for a black hole of mass M, expressed in Painlevé-Gullstrand coordinates for which

$$N_{PG} = 1, \qquad N^x_{PG} = \sqrt{\frac{R_S}{x}}, \quad (2.25)$$

where $R_S = 2GM$ is the usual Schwarzschild radius. Unsurprisingly, the solution is

$$\begin{aligned} a_{PG} &= \gamma\sqrt{\frac{R_S}{4x^3}}, \qquad E^a_{PG} = x^2, \\ b_{PG} &= -\gamma\sqrt{\frac{R_S}{x}}, \qquad E^b_{PG} = x, \end{aligned} \quad (2.26)$$

corresponding exactly to the Painlevé-Gullstrand metric.

2.3.3 The Areal Gauge

In order to simplify the passage to the effective Hamiltonian, and to avoid evaluating non-trivial path-ordered exponentials to calculate holonomies in the radial direction, we will perform a partial gauge-fixing known as the areal gauge. This corresponds to setting $E^a = x^2$ (or, in the original metric (2.3), $g(x,t) = x$). Importantly, this choice can be imposed without any reference to the equations of motion (indeed, this is typically done in textbook treatments of the Schwarzschild solution before even deriving the Einstein equations), so long as the surface area of spheres of constant x increases monotonically with x, which can easily be checked once the solution is known.

The gauge-fixing condition $\chi = E^a - x^2 = 0$ is clearly second-class with the diffeomorphism constraint $\mathcal{H}_x$, and so can be used to gauge fix $\mathcal{H}_x$, giving

$$E^a = x^2, \qquad a = \frac{E^b}{x}\,\partial_x b. \tag{2.27}$$

Then, requiring that this gauge be preserved by the equations of motion, i.e., $\dot{\chi} = 0$, imposes the condition that $\dot{E}^a = 0$ and therefore

$$N^x = -\frac{Nb}{\gamma}. \tag{2.28}$$

Note that this implies that, after imposing the areal gauge-fixing condition, b now appears in the metric through the shift vector N^x which is no longer a Lagrange multiplier that can be freely chosen, but is fully determined once the lapse N has been chosen. On the other hand, the lapse remains a Lagrange multiplier that can be freely chosen and imposes the scalar constraint $\mathcal{H} = 0$.

This gauge significantly simplifies the action, which becomes

$$S_{GF} = \int dt \int dx \left[\frac{\dot{b}E^b}{G\gamma} - N\mathcal{H}\right], \tag{2.29}$$

with

$$\mathcal{H} = \frac{1}{2G\gamma}\left[\frac{3\gamma x}{E^b} - \frac{2\gamma x^2}{(E^b)^2}\partial_x E^b - \frac{E^b}{\gamma x}\partial_x\left[x(b^2+\gamma^2)\right]\right]. \tag{2.30}$$

Note that the symplectic term $\dot{a}E^a$ in (2.13) becomes a total time derivative $(aE^a)^{\cdot}$ since E^a is independent of time, and so this term can be dropped.

The remaining Poisson bracket is

$$\{b(x_1), E^b(x_2)\} = G\gamma\,\delta(x_1 - x_2), \tag{2.31}$$

and the constraint algebra also simplifies, becoming

$$\begin{aligned}\{\mathcal{C}[N_1],\mathcal{C}[N_2]\} &= \mathcal{C}\left[-\frac{1}{\gamma}\left(N_1\partial_x N_2 - N_2\partial_x N_1\right)b\right]\\ &= \mathcal{C}\Big[N_1^x\partial_x N_2 - N_2^x\partial_x N_1\Big],\end{aligned} \tag{2.32}$$

using (2.28) to obtain the second relation. The second form of the constraint algebra in the areal gauge will give some insight into what the correct form for the shift vector N^x should be in the effective theory once LQG effects are included.

Finally, the equations of motion are

$$\dot{E}^b = \frac{b}{\gamma x}\Big(NE^b - x\partial_x(NE^b)\Big), \tag{2.33}$$

$$\dot{b} = \frac{\gamma N x}{2(E^b)^2} + \frac{\gamma x^2}{(E^b)^2}\partial_x N - \frac{N}{2x\gamma}\partial_x(xb^2+\gamma^2 x). \tag{2.34}$$

These equations can be obtained either by imposing the conditions (2.27) on the original equations of motion (2.21)–(2.24), or by deriving them directly from the simplified scalar constraint (2.30) via $\dot{f} = \{f, \int dx\, N\mathcal{H}\}$. As expected, the solution for $N = 1$ is exactly the Painlevé-Gullstrand metric.

2.4 LQG Effective Dynamics

The procedure to obtain the LQG effective dynamics for vacuum spherically symmetric space-times is to take the classical theory, described in Sec. 2.3, then (i) replace the components of the Ashtekar-Barbero connection by holonomies, and (ii) include correction functions multiplying inverse powers of the densitized triad. The first step is necessary since the basic operators in LQG are holonomies and areas (there is no operator corresponding to the connection itself), and it gives rise to 'holonomy corrections'. The second step arises because 0 is a discrete eigenvalue of the area

operator in LQG, so there is no well-defined operator corresponding to, e.g., $1/E^b$; introducing well-defined operators corresponding to inverse powers of E^a_i gives 'inverse triad corrections'.

Here we will focus on holonomy corrections for two reasons. First, in LQC the dominant quantum gravity effects comes from holonomy corrections: these are the source of the non-singular bounce, and it seems reasonable to expect that holonomy corrections will be dominant compared to inverse triad corrections in spherical symmetry as well. Second, there is considerable ambiguity in the choice of inverse triad corrections, and in fact some choices of inverse triad operators in LQC do not generate any inverse triad corrections in the effective theory [74]. Therefore, in the following we will assume that the inverse triad operator in the underlying quantum theory has an action such that there are no inverse triad corrections in the effective theory, and only consider holonomy corrections.

In LQC, the effective dynamics are known to provide an excellent approximation to the full quantum dynamics for states that are sharply peaked, and for which the expectation value for the spatial volume is always much larger than $\ell^3_{\rm Pl}$ [75, 76]. While it is not yet clear whether the effective dynamics will also provide a good approximation to the full quantum dynamics for black hole space-times, it seems likely that the arguments in [76] can be generalized. If this turns out to be the case, then the effective dynamics could be used to approximate the quantum dynamics of semi-classical states, at least for observables whose relevant physical length scale is much larger than $\ell_{\rm Pl}$. Based on this expectation, we will focus on the effective theory here, but we note that it is possible to construct the quantum theory following an analogous procedure to the one given in [49].

2.4.1 Effective Hamiltonian

To include holonomy corrections, it is necessary to replace in $\mathcal{H}$ the connection by holonomies. This is, in the simplest cases, done by expressing the field strength $F_{ab}{}^k$ in terms of the holonomy of the Ashtekar-Barbero connection around a loop of minimal area Δ, where the area gap $\Delta \sim \ell_{\rm Pl}^2$ is the smallest non-zero eigenvalue of the area operator in LQG [72].

However, this procedure is not always viable in LQC when the spatial curvature is non-vanishing (as is the general case in spherical symmetry). This is because the holonomy of A_a^i, evaluated around a loop of physical area Δ, cannot be expressed as an operator on the LQC Hilbert space (to be specific, the holonomy cannot be written in terms of almost-periodic functions of the connection). For the case of spherical symmetry, using the Cayley-Hamilton theorem it is possible to check that the holonomy of A_a^i around a loop of minimal area is not almost periodic in b, and therefore a different approach is necessary.

This is a difficulty that has already been addressed in cosmological space-times with non-vanishing spatial curvature, and in this case what is known as the 'K' loop quantization is preferred [74, 77]. For the case of spherical symmetry (and after imposing the areal gauge), this means replacing b by holonomies of the extrinsic curvature 1-form γK_a^i, evaluated in the $d\theta$ direction[1],

$$h_\theta(\delta_b) = \exp\left(\int_0^{\delta_b} \gamma K_\theta^i \tau_i \, d\theta\right) = \cos\left(\frac{\delta_b b}{2}\right)\mathbb{I} + 2\sin\left(\frac{\delta_b b}{2}\right)\tau_2. \tag{2.35}$$

where the τ^i are a basis in the (fundamental representation of the) $\mathfrak{su}(2)$ Lie algebra satisfying $\tau^i\tau^j = \frac{1}{2}\epsilon^{ij}{}_k\tau^k - \frac{1}{4}\delta^{ij}\mathbb{I}$, and $\mathbb{I}$ is the 2×2 identity matrix.

Then, to extract a scalar quantity from the $SU(2)$-valued expression (2.35), we

[1]We could equally well choose any path that follows a great circle, we choose $\phi =$ constant for simplicity.

replace

$$b \to -2\,\frac{\mathrm{Tr}(h_\theta(2\delta_b)\cdot\tau_2)}{2\delta_b}. \tag{2.36}$$

Here the factor of 2 in $2\delta_b$ is to ensure consistency between the 'K' loop quantization and the loop quantization based on expressing the field strength in terms of holonomies [78].

The remaining task is to determine the appropriate value for δ_b. The key heuristic argument from LQG, which guides the choice of δ_b, is that the physical length of this edge should be given by $\sqrt{\Delta}$. Since the holonomy was integrated along the edge with respect to the coordinate θ, δ_b gives the coordinate length of the path, not the physical length. The coordinate and physical lengths are simply related by the metric; for a path with constant x and ϕ (and constant t, of course) the relation is just $ds = x\,d\theta$. So, for the physical length to be $\sqrt{\Delta}$, the coordinate length must be taken to be

$$\delta_b = \frac{\sqrt{\Delta}}{x}. \tag{2.37}$$

(In general, if the areal gauge is not imposed then $ds = \sqrt{E^a}\,d\theta$ and $\delta_b = \sqrt{\Delta/E^a}$.) This result is in agreement with what has earlier been argued in [23, 48, 49] (up to an overall factor of 4π in some cases, which essentially implies a slightly different choice for Δ). Then, (2.36) becomes

$$b \to \frac{x}{\sqrt{\Delta}}\sin\left(\frac{\sqrt{\Delta}}{x}b\right). \tag{2.38}$$

It is now possible to construct the effective Hamiltonian by replacing all instances of b in (2.30) using (2.38), with the result

$$\mathcal{H}^{(LQG)} = -\frac{1}{2G\gamma}\left[\frac{E^b}{\gamma x}\partial_x\left(\frac{x^3}{\Delta}\sin^2\frac{\sqrt{\Delta}\,b}{x}+\gamma^2 x\right)-\frac{3\gamma x}{E^b}+\frac{2\gamma x^2}{(E^b)^2}\,\partial_x E^b\right]. \tag{2.39}$$

A direct calculation of the Poisson bracket of the effective scalar constraint with itself gives the following constraint algebra,

$$\{\mathcal{C}^{(LQG)}[N_1], \mathcal{C}^{(LQG)}[N_2]\} = \mathcal{C}^{(LQG)}\left[-\frac{x}{\gamma\sqrt{\Delta}}\sin\frac{\sqrt{\Delta}\,b}{x}\cos\frac{\sqrt{\Delta}\,b}{x}\left(N_1\partial_x N_2 - N_2\partial_x N_1\right)\right]. \tag{2.40}$$

Note that although the constraint algebra has changed compared to the classical form (2.32), the constraint algebra for the effective scalar constraint is closed: there are no anomalies.

Next, it is necessary to update the areal gauge relation between the lapse and the shift, which is classically given by (2.28), by replacing b by an appropriate expression in terms of holonomies. A simple way to do this is in fact suggested by comparing the classical constraint algebra (2.32) and the constraint algebra in the effective theory (2.40): the choice

$$N^x = -\frac{Nx}{\gamma\sqrt{\Delta}}\sin\frac{\sqrt{\Delta}\,b}{x}\cos\frac{\sqrt{\Delta}\,b}{x} \tag{2.41}$$

ensures that the constraint algebra for the effective theory will have exactly the classical form

$$\{\mathcal{C}^{(LQG)}[N_1], \mathcal{C}^{(LQG)}[N_2]\} = C^{(LQG)}\left[N_1^x\partial_x N_2 - N_2^x\partial_x N_1\right]. \tag{2.42}$$

This choice for the shift vector, although based on different arguments, is the same as in [49].

As an aside, we mention that if a different modification for b is preferred for the effective Hamiltonian, say $b \to f(x,b)$, then the constraint algebra will be $\{\mathcal{C}_f[N_1], \mathcal{C}_f[N_2]\} = C_f[-\gamma^{-1}(N_1\partial_x N_2 - N_2\partial_x N_1)(f\partial_b f)]$, and by redefining the lapse-shift relation to be $N^x = -N(f\partial_b f)/\gamma$, the constraint algebra becomes identical with the classical case (And for a more general analysis of modified constraint algebras in spherical symmetry for the case of the diffeomorphism constraint not being gauge-fixed,

see [79]).

For the choice (2.41) for the shift vector, the effective metric will be

$$ds^2 = -N^2 dt^2 + \frac{(E^b)^2}{x^2}\big(dx + N^x dt\big)^2 + x^2 d\Omega^2. \tag{2.43}$$

Finally, from the scalar constraint and the basic Poisson bracket relation (2.31), the equations of motion for E^b and b are derived in the usual manner, giving

$$\dot{E}^b = -\frac{x^2}{\gamma\sqrt{\Delta}}\,\partial_x\left(\frac{NE^b}{x}\right)\sin\frac{\sqrt{\Delta}\,b}{x}\cos\frac{\sqrt{\Delta}\,b}{x}, \tag{2.44}$$

$$\dot{b} = \frac{\gamma N x}{2(E^b)^2}\left(1 + 2x\frac{\partial_x N}{N}\right) - \frac{\gamma N}{2x} - \frac{N}{2\gamma\Delta x}\partial_x\left(x^3\sin^2\frac{\sqrt{\Delta}\,b}{x}\right). \tag{2.45}$$

2.4.2 Solution in Painlevé-Gullstrand Coordinates

A stationary solution to the equations of motion and to the scalar constraint $\mathcal{H}^{(LQG)} = 0$ can easily be found in terms of Painlevé-Gullstrand-like coordinates for $N = 1$. For $N = 1$, then $\dot{E}^b = 0$ implies that[2]

$$E^b = x, \tag{2.46}$$

while $\dot{b} = 0$ gives

$$b = \frac{x}{\sqrt{\Delta}}\arcsin\frac{C}{x^{3/2}}, \tag{2.47}$$

where C is a constant of integration.

It is immediately clear that $C = 0$ gives Minkowski space, $ds^2 = -dt^2 + dx^2 + x^2 d\Omega^2$. Note that there are no quantum gravity effects in this case, which is not surprising

[2]If $\dot{E}^b = 0$, then either $E_b = x$, or $\sin\frac{\sqrt{\Delta}\,b}{x} = 0$, or $\cos\frac{\sqrt{\Delta}\,b}{x} = 0$. In the second case, $\dot{b} = 0$ implies $E_b = x$ in agreement with the first case, while in the third case $\sin\frac{\sqrt{\Delta}\,b}{x} = \pm 1$ and $\dot{b} = 0$ gives $E_b^2 = \gamma^2\Delta x^2/(3x^2 + \gamma^2\Delta)$, which does not satisfy the scalar constraint. Therefore, only the first two cases are viable and both imply $E^b = x$.

since the curvature is zero.

The black hole solutions are obtained for $C = -\sqrt{\gamma^2 \Delta R_S}$, where $R_S = 2GM$ is the Schwarzschild radius and M is the mass of the black hole. This is easily verified by considering the solution at large x, in which case $\arcsin(C/x^{3/2}) \approx C/x^{3/2}$ and the usual Painlevé-Gullstrand solution (2.26) is recovered.

An important point, as already pointed out in [49], is that this solution is only well-defined for

$$x \geq x_{\min} = (\gamma^2 \Delta R_S)^{1/3}. \tag{2.48}$$

This lower bound on x in vacuum space-times is not surprising given the following argument. First, in spherically symmetric space-times there are no local gravitational degrees of freedom (gravitational waves), so a matter source is needed to generate any space-time curvature. Second, studies in LQC show that quantum gravity effects due to holonomy corrections generate an upper bound on the possible energy density of any matter field. Therefore, to generate a gravitational field corresponding to mass M, a matter field with density $\rho \sim M/R^3$ is needed, and if $\rho \leq \rho_{\max} \sim \rho_{\rm Pl}$, then the matter field must extend to at least a radius of $\sim (M/\rho_{\rm Pl})^{1/3} \sim x_{\min}$. This argument can be made precise, and shown to be exact, in the case that the matter field is pressureless dust field [50]. So to describe the solution for $x < x_{\min}$, it is necessary to include matter fields.

For the vacuum part of the space-time, the shift vector is

$$N^x = \sqrt{\frac{R_S}{x}\left(1 - \frac{\gamma^2 \Delta R_S}{x^3}\right)}, \tag{2.49}$$

which gives the effective metric

$$ds^2 = -\left(1 - \frac{R_S}{x} + \frac{\gamma^2 \Delta R_S^2}{x^4}\right) dt^2 + 2\sqrt{\frac{R_S}{x}\left(1 - \frac{\gamma^2 \Delta R_S}{x^3}\right)}\, dt\, dx + dx^2 + x^2 d\Omega^2. \tag{2.50}$$

Note that in the limit $\Delta \to 0$, the effective metric tends to the classical Schwarzschild metric in Painlevé-Gullstrand coordinates, as expected. Also, the condition $x \geq x_{\min}$ ensures that the shift (2.49) is well-defined for all $x \geq x_{\min}$. Another interesting point is that in the limit $x \to x_{\min}$, the effective line element tends to the Minkowski metric. As we shall see, this is because the repulsive quantum gravity effects exactly balance out the attractive classical gravitational force at $x = x_{\min}$.

2.4.3 Curvature Scalars and Killing Horizons

To understand the geometry underlying the effective metric (2.50), it is useful to examine curvature scalars and look for horizons, with Killing horizons being particularly easy to find in stationary space-times.

In the following, to simplify the notation we will express the metric as $ds^2 = -Fdt^2 + 2N^x dtdx + dx^2 + x^2 d\Omega^2$, with

$$F(x) \equiv 1 - \frac{R_S}{x} + \frac{\gamma^2 \Delta R_S^2}{x^4}, \tag{2.51}$$

and N^x given by (2.49), note that $F + (N^x)^2 = N^2 = 1$.

It is straightforward to calculate some simple curvature scalars for (2.50), with the results

$$R = -\frac{6\gamma^2 \Delta R_S^2}{x^6}, \qquad R_{\mu\nu}R^{\mu\nu} = \frac{90\gamma^4 \Delta^2 R_S^4}{x^{12}}, \tag{2.52}$$

$$R_{\mu\nu\rho\sigma}R^{\mu\nu\rho\sigma} = \frac{12R_S^2}{x^6}\left(1 - \frac{10\gamma^2 \Delta R_S}{x^3} + \frac{39\gamma^4 \Delta^2 R_S^2}{x^6}\right). \tag{2.53}$$

Note that these expressions for the curvature scalars are exact. Also, setting $\Delta = 0$ in these equations gives the expected classical expressions, in particular $R_{\mu\nu} = 0$. Further, as the lower bound $x_{\min}$ is approached, all of these curvature scalars approach a critical value that is independent of their mass, and which provides an upper bound

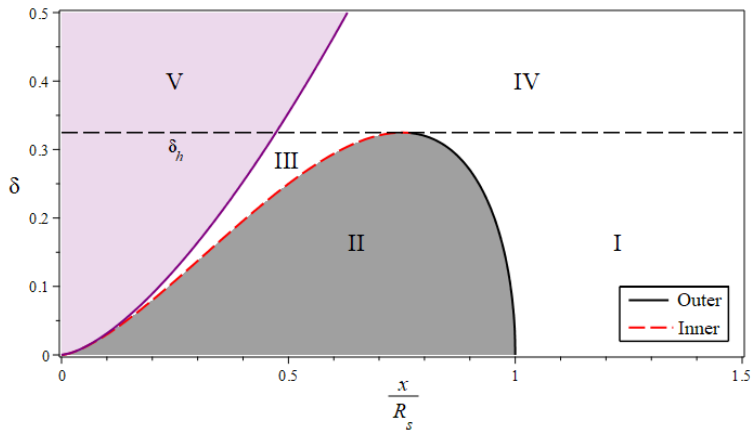

Figure 2.1: This figure shows the location of $x_{\rm min}$ (solid purple line), $x_{\rm inner}$ (dashed red line) and $x_{\rm outer}$ (solid black line) as a function of $\delta = \gamma\sqrt{\Delta}/R_S$; the scale on the x-axis is in units of x/R_S. Region I corresponds to $x > x_{\rm outer}$, in Region II $x_{\rm inner} < x < x_{\rm outer}$, and in Region III $x_{\rm min} < x < x_{\rm inner}$. For a black hole mass of $M < M_\star$ there are no horizons, this corresponds to Region IV with $\delta > \delta_h$. Finally, the effective solution is only valid for $x > x_{\rm min}$; in Region V the vacuum solution is not well-defined and it is necessary to include matter fields. Note that in the limit of a large mass ($\delta \to 0$), $x_{\rm inner} \to x_{\rm min}$ while $x_{\rm outer} \to R_S$.

to the amplitude of each curvature scalar in the vacuum region,

$$\lim_{x\to x_{\rm min}} R = -\frac{6}{\gamma^2\Delta}, \qquad \lim_{x\to x_{\rm min}} R_{\mu\nu}R^{\mu\nu} = \frac{90}{\gamma^4\Delta^2}, \qquad \lim_{x\to x_{\rm min}} R_{\mu\nu\rho\sigma}R^{\mu\nu\rho\sigma} = \frac{360}{\gamma^4\Delta^2}. \tag{2.54}$$

These upper bounds agree with the results obtained in [49] (up to overall factors of 4π due to what amounts to a different choice by [49] for Δ in (2.37)).

Next, in an explicitly stationary space-time like this one, $\xi^\mu = (1,0,0,0)$ is necessarily a Killing vector field and the Killing horizons are located where $\xi^\mu\xi_\mu = 0$, which corresponds to $F = 0$. What is interesting here is that (for $M \gg m_{\rm Pl}$) there are two Killing horizons[3]: an outer Killing horizon near $x = R_S$, and an inner Killing horizon just outside $x_{\rm min}$.

[3] $F = 0$ gives a fourth-order polynomial in x; two roots are always complex and for $M \gg m_{\rm Pl}$ the other two roots are real and distinct. As will be explored next, there is a limiting case $M = M_\star$ where there is one repeated real root, and for $M < M_\star$ all four roots are complex, in which case there is no Killing horizon.

Specifically, to leading order in Δ/R_S^2 the outer Killing horizon is located at

$$x_{\rm outer} = R_S - \frac{\gamma^2\Delta}{R_S} + O\left(\frac{\Delta^{4/3}}{R_S^{5/3}}\right), \tag{2.55}$$

while the inner horizon is located at

$$x_{\rm inner} = (\gamma^2\Delta R_S)^{1/3} + \frac{1}{3}\left(\frac{\gamma^4\Delta^2}{R_S}\right)^{1/3} + O\left(\frac{\Delta^{4/3}}{R_S^{5/3}}\right), \tag{2.56}$$

note that the first term is exactly $x_{\rm min}$. The location of the Killing horizons as a function of the black hole mass is shown in Fig. 2.1.

This shows that the outer Killing horizon is located (up to small quantum corrections) at the classical horizon R_S, while the interior horizon is a new feature of the quantum geometry that lies within the region where the space-time curvature is Planckian. As depicted in Fig. 2.2, this shows that there is a thin region inside the black hole where the lightcone flips again and outgoing null rays begin to expand (with respect to the coordinate x) once again. Note that the presence of an interior horizon is analogous to what occurs in Reissner-Nordström black holes, although the new term in the Reissner-Nordström metric with charge Q goes as GQ^2/x^2 while here the quantum gravity correction in the effective metric is proportional to $\Delta R_S^2/x^4$.

This result also emphasizes the importance of studying the full space-time rather than using the classical isometry between the Schwarzschild interior and the Kantowski-Sachs space-time, which implicitly assumes that there is no interior horizon. Also, note the existence of an interior horizon is a necessary condition for a transition to occur from a black hole collapse to an expanding white hole solution [64]; for details in how such a transition is realized in this effective framework for the case that the matter field is pressureless dust, see [50].

The above results for the locations of the two horizons assumes $M \gg m_{\rm Pl}$, but if M is sufficiently small there may be only 1 or 0 Killing horizons. The limiting

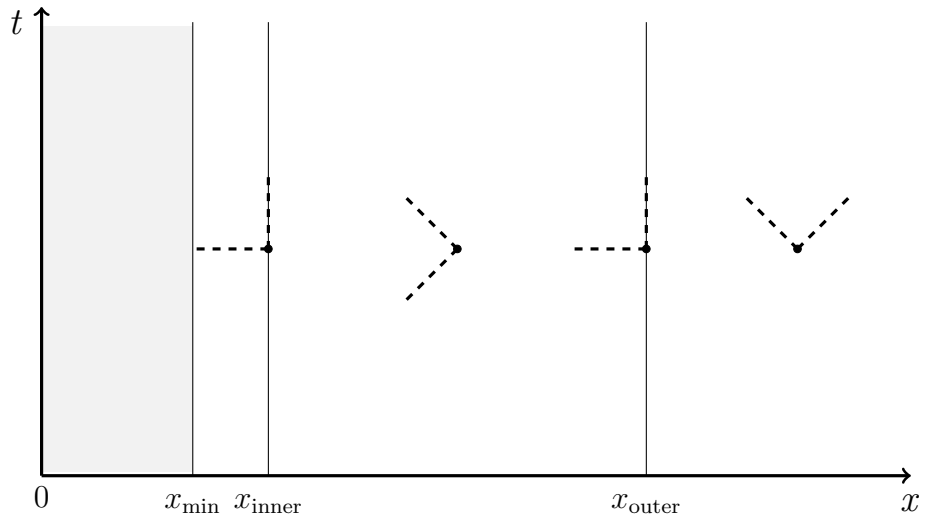

Figure 2.2: Schematic diagram for $M \gg m_{\text{Pl}}$ showing the behaviour of the lightcone in the presence of multiple horizons. The shaded area is outside the domain of our solution and the innermost region between $x_{\min}$ and x_{inner} is a shell of thickness $\sim (\gamma^4\Delta^2/R_S)^{1/3}$.

case occurs for $M_\star = 8\gamma\sqrt{\Delta}/\sqrt{27}G$, when there is exactly one Killing horizon, while if $M < M_\star$ then there are no Killing horizons at all. Although it is likely that the effective description fails for small $x < R_S$ in a space-time with such a small mass, the absence of Killing horizons in this case is nonetheless interesting as it suggests that a minimal mass is required to form a black hole, with a (Killing) horizon—if $M < M_\star$, the space-time is indeed curved by the mass but not sufficiently for a horizon to form. This is very different from the situation in classical general relativity, where there is always a horizon surrounding a sufficiently compact matter source. Note that this also suggests that elementary particles with $m < m_{\text{Pl}}$ (like electrons, say) cannot form a black hole alone; rather, many elementary particles must be packed in a sufficiently small region for a black hole to form.

2.4.4 Geodesics and Apparent Horizons

Further insight into the effective geometry of the LQG-corrected black hole can be obtained by studying geodesics. For the sake of simplicity we will consider radial

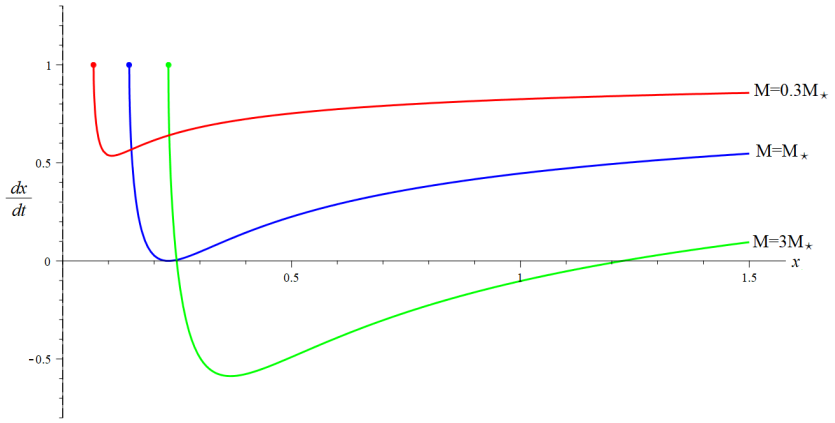

Figure 2.3: Behaviour of outgoing radial null geodesics, $dx/dt = 1 - N^x$, for the effective metric with shift (2.49) for black holes of different mass. These three curves are characteristic of the different possible behaviours that the outgoing null rays may exhibit depending on the mass of the black hole compared to $M_\star$. Here the red curve corresponds to $M = 0.3M_\star$, the blue curve to $M = M_\star$, and the green to $M = 3M_\star$. The abrupt end to each curve corresponds to $x = x_{\rm min}$ for each of the three black hole masses. In these plots we set $\gamma = G = 1$ and $\Delta = 10^{-2}$.

motion only, but it is straightforward to extend these results to include rotational motion as well.

Radial geodesics satisfy

$$-\epsilon = -F(x)\dot{t}^2 + 2N^x\dot{t}\dot{x} + \dot{x}^2\,; \tag{2.57}$$

for time-like geodesics, $\epsilon = 1$ and the dots denote derivatives with respect to proper time τ, while for null geodesics $\epsilon = 0$ and dots denote derivatives with respect to an affine parameter λ.

For time-like geodesics, it is convenient to use the conserved energy associated with the time-like Killing vector $\xi^\mu = (1, 0, 0, 0)$ to isolate $\dot{x}$; specifically,

$$E \equiv \xi_\mu \dot{x}^\mu = -F(x)\dot{t} + N^x\dot{x}. \tag{2.58}$$

Combining this with $\epsilon = 1$, the geodesic equation (2.57) simplifies to

$$-F(x) = -(N^x\dot{x} - E)^2 + 2N^x(N^x\dot{x} - E)\dot{x} + F\dot{x}^2, \tag{2.59}$$

giving

$$\frac{dx}{d\tau} = \pm\sqrt{E^2 - 1 + \frac{R_S}{x}\left(1 - \frac{\gamma^2\Delta R_S}{x^3}\right)}. \tag{2.60}$$

Note that in the case $E = 1$, corresponding to a particle that starts at rest at infinity, this particle will again have $\dot{x} = 0$ at $x = x_{\min}$. This is another way to see that $x = x_{\min}$ is the location where the quantum gravity repulsive effects cancel out the classical gravitational attraction.

For null geodesics the calculation is even simpler. Since $\epsilon = 0$, dividing (2.57) by $\dot{t}^2$ gives

$$0 = -F(x) + 2N^x\frac{dx}{dt} + \left(\frac{dx}{dt}\right)^2, \tag{2.61}$$

which has the solution

$$\frac{dx}{dt} = -N^x \pm 1. \tag{2.62}$$

For $dx/dt = -N^x - 1$, the ingoing null rays always have decreasing x, but the situation is a little more complicated for the outgoing rays with $dx/dt = 1 - N^x$ which will depend on the location of the zeros of $1 - N^x$; unsurprisingly these correspond exactly to the Killing horizons found in Sec. 2.4.3.

For $M \gg m_{\rm Pl}$, the x position of the outgoing rays will increase for $x > x_{\rm outer}$ and $x < x_{\rm inner}$, but decrease for $x_{\rm inner} < x < x_{\rm outer}$. On the other hand, if $M < M_\star$, then the outgoing null rays will satisfy $dx/dt > 0$ everywhere. This is depicted in Fig. 2.3; once again the behaviour is analogous with that of a Reissner-Nordström black hole.

Next, it is possible to determine whether there are any apparent horizons by considering congruences of null geodesics. Due to spherical symmetry, it is sufficient to consider congruences that are orthogonal to the surface of concentric 2-spheres

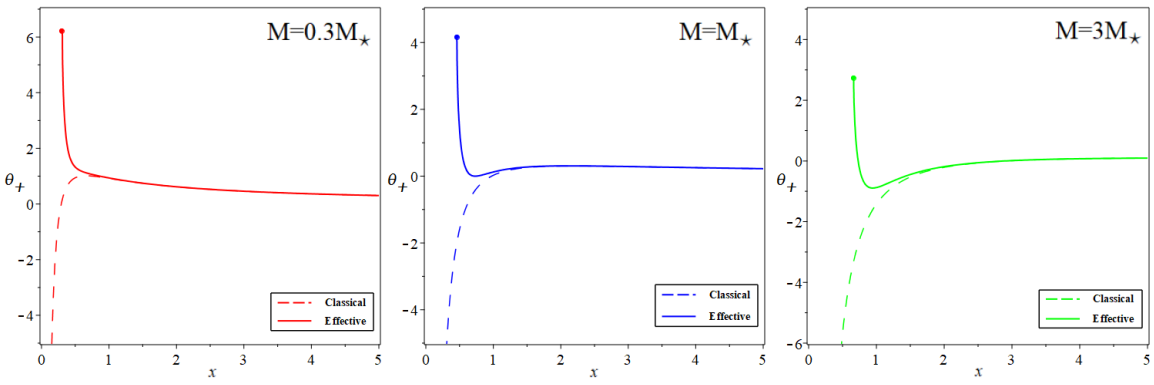

Figure 2.4: Comparison of the outgoing null expansion $\theta_+ = 2x^{-1}(1 - N^x)$ for the effective metric (2.50) (solid line) compared to the classical limit $\Delta \to 0$ (dashed line). The three cases, from left to right, correspond to: (i) a space-time with no apparent horizon (left), (ii) a space-time with one sphere S that is marginally trapped sphere (where $\theta_+ = 0$) but no region with $\theta_+ < 0$ (middle), and (iii) a space-time with two apparent horizons (right). In the first two cases, $\theta_+ \geq 0$ throughout the entire space-time while in the large mass case of $M > M_\star$, θ_+ is negative for $x_{\rm inner} < x < x_{\rm outer}$. Each of these examples are qualitatively different from the classical case where, in all examples, at $x = R_S$ the expansion θ_+ becomes negative and diverges to $-\infty$ as $x \to 0$. Note that θ_+ for the effective metric stops at $x = x_{\rm min}$. In the plots we set $\gamma = G = 1$ and $\Delta = 10^{-2}$.

S defined by constant x and t. Denoting the tangent vector to the outgoing null geodesics by $\ell^\mu = (1, 1 - N^x, 0, 0)$, then the other linearly independent null vector that is also orthogonal to S is $k^\mu = (1, -1 - N^x, 0, 0)$, which is the tangent vector to ingoing null geodesics. Here the overall normalization of these two vectors fields is such that $\ell^\mu k_\mu = -2$, so the hypersurface metric for S is given by

$$h_{\mu\nu} = g_{\mu\nu} + \frac{1}{2}\Big(\ell_\mu k_\nu + k_\mu \ell_\nu\Big). \tag{2.63}$$

The outgoing and ingoing expansions are respectively

$$\theta_+ = h^{\mu\nu}\nabla_\mu \ell_\nu, \qquad \theta_- = h^{\mu\nu}\nabla_\mu k_\nu, \tag{2.64}$$

and a short calculation gives

$$\theta_+ = \frac{2}{x}(1 - N^x), \qquad \theta_- = -\frac{2}{x}(1 + N^x). \tag{2.65}$$

The standard definition of a trapped surface S is one where both expansions $\theta_\pm$ are negative, and the boundary of the total trapped region is called the apparent horizon—in this case, since $\theta_- < 0$ for all x, the apparent horizon corresponds to the surfaces where $\theta_+ = 0$. Interestingly, for $M \gg m_{\rm Pl}$, in addition to the usual outer boundary to the trapped region, there is also an interior boundary and there are therefore two apparent horizons. As expected, these apparent horizons are located at precisely the same location as the Killing horizons, $x_{\rm inner}$ and $x_{\rm outer}$. The expansion θ_+ is plotted in Fig. 2.4 for different M and compared to the classical result.

It is straightforward to calculate the surface gravity at the outer horizon,

$$\kappa = \frac{R_S}{2x_{\rm outer}^2} - \frac{2\gamma^2 \Delta R_S^2}{x_{\rm outer}^5}. \tag{2.66}$$

In the case that $M \gg m_{\rm Pl}$, then the outer horizon is given by (2.55) and the surface

gravity, to leading order in Δ, is given by

$$\kappa = \frac{1}{2R_S} - \frac{\gamma^2\Delta}{R_S^3} + O\left(\frac{\Delta^{4/3}}{R_S^{11/3}}\right). \tag{2.67}$$

It is also interesting to examing the surface gravity for smaller masses which is shown in Fig. 2.5; of course, since there is no horizon for $M < M_\star$, a surface gravity can be associated to a horizon only for $M \geq M_\star$. It is interesting to note that the slope of $\kappa(M)$ is positive for small M, so the specific heat of black holes becomes positive for sufficiently small mass (assuming the black hole thermodynamics correspondence between surface gravity and temperature continues to hold in this setting).

Finally, for large M and keeping only the leading order LQG correction, the black hole thermodynamics relation for these effective (non-rotating, zero charge) black holes is slightly modified to

$$\kappa\,\delta A_{\text{outer}} = 8\pi G\left(1 - \frac{2\gamma^2\Delta}{R_S}\right)\delta M, \tag{2.68}$$

suggesting that, not too surprisingly, quantum gravity effects will generate some departures from semi-classical expectations based on quantum field theory on a classical background. A more detailed exploration of this topic is left for future work.

2.4.5 Other Coordinate Systems

While we have so far used the Painlevé-Gullstrand coordinate system, it is also possible to express the stationary solution in terms of other coordinate systems.

Leaving N free in (2.44) and (2.45), requiring $\dot{E}^b = 0$ gives

$$N = \frac{x}{E^b} \tag{2.69}$$

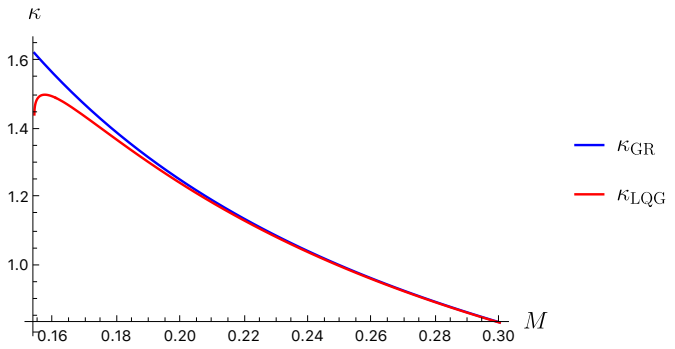

Figure 2.5: This plot shows the (outer) horizon surface gravity κ as a function of the black hole mass M for small M; the smallest mass shown here is $M = M_\star$, as there are no horizons for $M < M_\star$. Note that the slope of the curve is positive for small M close to $M_\star$, but κ rapidly tends to the classical result $\kappa = 1/2R_S$. In this plot we set $\gamma = G = 1$ and $\Delta = 10^{-2}$.

which can then be substituted into $\dot{b} = 0$, with the result

$$\frac{x^2}{\Delta}\sin^2\frac{\sqrt{\Delta}\,b}{x} = \gamma^2\left(\frac{x^2}{(E^b)^2} - 1 + \frac{R_S}{x}\right), \tag{2.70}$$

where the constant of integration has been chosen to obtain the correct classical limit at large x.

To make contact with [49], we will now consider the specific example

$$N = \frac{1}{\sqrt{1 + R_S/x}}, \tag{2.71}$$

for which it follows that

$$E^b = x\sqrt{1 + R_S/x}, \qquad \frac{x^2}{\Delta}\sin^2\frac{\sqrt{\Delta}\,b}{x} = \frac{\gamma^2 R_S^2}{x^2(1 + R_S/x)}, \tag{2.72}$$

and so the resulting effective line element is

$$ds^2 = -\left(1 - \frac{R_S}{x} + \frac{\gamma^2 \Delta R_S^4}{x^6(1+R_S/x)^2}\right) dt^2 + \left(1 + \frac{R_S}{x}\right) dx^2 + 2\,\frac{R_S}{x(1+R_S/x)}\sqrt{1 - \frac{\gamma^2 \Delta R_S^2}{x^4(1+R_S/x)}}\; dx\, dt + x^2 d\Omega^2. \tag{2.73}$$

This is precisely the effective metric found in [49], up to some small discretization effects which are not included in the analysis here. This shows that the different approaches followed here and in [49] give the same effective metric, and are consistent with each other.

While the effective line elements (2.50) and (2.73) are both solutions of the effective equations of motion (2.44) and (2.45), these two effective metrics are not related by coordinate transformations, as would be the case in classical general relativity. Rather, there is a quantum deformation to this classical symmetry; we leave a determination of the precise properties of this deformation for future work. We emphasize that although the classical symmetry is deformed due a modification of the structure function in the effective algebra (2.40), the modified constraint algebra does close, thus ensuring the covariance of the effective model considered here.

One way to verify that the two metrics are not related by a coordinate transformation is to compare curvature scalars. While R, $R_{\mu\nu}R^{\mu\nu}$ and $R_{\mu\nu\rho\sigma}R^{\mu\nu\rho\sigma}$ are all slightly different for the effective line elements (2.50) and (2.73), nonetheless these curvature scalars have a nearly identical behaviour (especially for large M, with differences only becoming apparent near $x_{\min}$ for small M) and in fact have exactly the same upper bound that in both cases is reached at $x = x_{\min}$.

The fact that the space-time geometry depends on the coordinates—or, in other words, is observer-dependent—is (at least in hindsight) not surprising. It is well known in the context of quantum field theory on curved space-times that different observers see different states: one may observe the quantum vacuum, while another (at the

same location but with a relative acceleration) sees a thermal state. Something similar appears to occur here: the quantum gravity corrections to the classical metric are observer-dependent (although some quantum gravity effects, like the presence of a Planck-scale bound on curvature scalars, appear to be observer-independent). An in-depth study of this effect is left for future work.

2.5 Summary and Discussion

In this paper we constructed an effective framework to study quantum gravity holonomy effects in vacuum spherically symmetric space-times, and studied the stationary solutions to the effective theory. By imposing the areal gauge, it was possible to implement the $\bar{\mu}$ loop quantization scheme; in an important sign of the robustness of these results, this gives results in perfect agreement with the $\bar{\mu}$ loop quantization based on the Abelianized version of the constraints [49].

We explored the geometry of the solution mostly in terms of the effective line element expressed in Painlevé-Gullstrand-like coordinates, and found that quantum gravity effects: (i) slightly shift the location of the outer horizon from $x = R_S$ by a term of the order Δ/R_S, (ii) showed that the vacuum solution only holds for $x \geq x_{\rm min} = (\gamma\Delta R_S)^{1/3}$, with the implication that the presence of matter is necessary at smaller x to curve the space-time, and (iii) there is now an inner horizon located just outside $x_{\rm min}$ where the outgoing expansion of radial null geodesics becomes positive again. (In this effective space-time, Killing horizons and apparent horizons are the same, so we simply refer to 'horizons'.) Note that the presence of an outer and inner horizon occurs in many models of non-singular black holes, including the well-known Bardeen model [1]. Further, in agreement with [49], the curvature scalars R, $R^{\mu\nu}R_{\mu\nu}$ and $R^{\mu\nu\rho\sigma}R_{\mu\nu\rho\sigma}$ are all bounded by quantum gravity effects, with each bound depending only on $\gamma^2\Delta \sim \ell_{\rm Pl}^2$ and independent of M.

Also, while this may lie outside the regime of validity of the effective description, it is nonetheless interesting to point out that the effective theory predicts that for sufficiently small $M \lesssim m_{\rm Pl}$ there will not be any horizon at all: although the mass will curve the space-time in the usual way far from the source, the gravitational field will never be strong enough to generate a trapped region, even for $x \leq R_S$; this provides a quantum gravitational counterexample to the hoop conjecture for sufficiently low mass objects.

The static space-time solution that we derived as a solution to the effective scalar constraint corresponds to an eternal (vacuum) black hole. To describe physical black holes, it will be important to extend these results to include matter fields and to study the process of the formation of a black hole. In addition, by including dynamical effects, it will be possible to study the problem of mass inflation, which appears to indicate that inner horizons in an eternal black hole are unstable [80–82] (although this conclusion has recently been challenged, see [83]). More generally, to properly understand the properties of astrophysically relevant black holes, it will be essential to include matter and allow for fully dynamical space-times.

Importantly, the effective framework developed here can be extended to include matter fields, and in particular it is quite straightforward to include a pressureless dust field [50]. Then, it is possible to study black hole collapse; for example, it can be shown that in the Oppenheimer-Snyder collapse model the dynamics of the interior of the 'star' are given by exactly the LQC effective Friedman equation, and therefore the star bounces at the LQC critical density $\rho_c \sim \rho_{\rm Pl}$ and then starts to expand, much like a white hole [50]. This model is a first step towards a more complete analysis of quantum gravity effects in a dynamical black hole space-time, starting from the collapse of an in-falling matter field. Interestingly, it provides an explicit realization, derived from an effective LQG description of the full black hole space-time, that shows how quantum gravity effects can generate a transition from a collapsing black hole to

an expanding 'white hole', as suggested in [65].

There also remain several other important open questions, in addition to the inclusion of matter and the study of the dynamics of evolving black hole space-times starting from their initial formation. In particular, it is important to explore the relation of the effective metric expressed in terms of different coordinates, and to understand precisely how quantum gravity effects will differ depending on the observer. While these questions are by now quite well understood for quantum field theory on curved space-times, this is not the case for quantum gravity effects, even in relatively simple effective theories like the one considered here. Finally, it will also be important to go beyond the effective description in order to study other quantum gravity effects in black holes, most notably Hawking radiation and the black hole information loss problem.

Bibliography

[1] J. Bardeen, "Non-singular general-relativistic gravitational collapse," Proc. Int. Conf. GR5, Tbilisi (1968) p. 174.

[2] V. P. Frolov and G. Vilkovisky, "Spherically Symmetric Collapse in Quantum Gravity," Phys. Lett. B **106** (1981) 307–313.

[3] T. A. Roman and P. G. Bergmann, "Stellar collapse without singularities?," Phys. Rev. D **28** (1983) 1265–1277.

[4] I. Dymnikova, "Vacuum nonsingular black hole," Gen. Rel. Grav. **24** (1992) 235–242.

[5] A. Borde, "Regular black holes and topology change," Phys. Rev. D **55** (1997) 7615–7617, `arXiv:gr-qc/9612057`.

[6] E. Ayon-Beato and A. Garcia, "Regular black hole in general relativity coupled to nonlinear electrodynamics," Phys. Rev. Lett. **80** (1998) 5056–5059, `arXiv:gr-qc/9911046`.

[7] I. Dymnikova, "Spherically symmetric space-time with the regular de Sitter center," Int. J. Mod. Phys. D **12** (2003) 1015–1034, `arXiv:gr-qc/0304110`.

[8] S. A. Hayward, "Formation and evaporation of regular black holes," Phys. Rev. Lett. **96** (2006) 031103, `arXiv:gr-qc/0506126`.

[9] T. De Lorenzo, C. Pacilio, C. Rovelli, and S. Speziale, "On the Effective Metric of a Planck Star," Gen. Rel. Grav. **47** (2015) 41, arXiv:1412.6015.

[10] V. P. Frolov, "Notes on nonsingular models of black holes," Phys. Rev. D **94** (2016) 104056, arXiv:1609.01758.

[11] A. Simpson and M. Visser, "Regular black holes with asymptotically Minkowski cores," Universe **6** (2019) 8, arXiv:1911.01020.

[12] R. Carballo Rubio, F. Di Filippo, S. Liberati, and M. Visser, "Phenomenological aspects of black holes beyond general relativity," Phys. Rev. D **98** (2018) 124009, arXiv:1809.08238.

[13] R. Carballo Rubio, F. Di Filippo, S. Liberati, and M. Visser, "Geodesically complete black holes," Phys. Rev. D **101** (2020) 084047, arXiv:1911.11200.

[14] S. D. Mathur, "The Fuzzball proposal for black holes: An Elementary review," Fortsch. Phys. **53** (2005) 793–827, arXiv:hep-th/0502050.

[15] P. Nicolini, A. Smailagic, and E. Spallucci, "Noncommutative geometry inspired Schwarzschild black hole," Phys. Lett. B **632** (2006) 547–551, arXiv:gr-qc/0510112.

[16] K. Falls, D. F. Litim, and A. Raghuraman, "Black Holes and Asymptotically Safe Gravity," Int. J. Mod. Phys. A **27** (2012) 1250019, arXiv:1002.0260.

[17] A. Ashtekar and J. Lewandowski, "Background independent quantum gravity: A Status report," Class. Quant. Grav. **21** (2004) R53, arXiv:gr-qc/0404018.

[18] C. Rovelli, *Quantum Gravity*. Cambridge University Press, 2004.

[19] T. Thiemann, *Modern Canonical Quantum General Relativity*. Cambridge University Press, 2007.

[20] A. Ashtekar and P. Singh, "Loop Quantum Cosmology: A Status Report," Class. Quant. Grav. **28** (2011) 213001, arXiv:1108.0893.

[21] L. Modesto, "Disappearance of black hole singularity in quantum gravity," Phys. Rev. D **70** (2004) 124009, arXiv:gr-qc/0407097.

[22] A. Ashtekar and M. Bojowald, "Quantum geometry and the Schwarzschild singularity," Class. Quant. Grav. **23** (2006) 391–411, arXiv:gr-qc/0509075.

[23] C. G. Boehmer and K. Vandersloot, "Loop Quantum Dynamics of the Schwarzschild Interior," Phys. Rev. D **76** (2007) 104030, arXiv:0709.2129.

[24] M. Campiglia, R. Gambini, and J. Pullin, "Loop quantization of spherically symmetric midi-superspaces : The Interior problem," AIP Conf. Proc. **977** (2008) 52–63, arXiv:0712.0817.

[25] D.-W. Chiou, "Phenomenological loop quantum geometry of the Schwarzschild black hole," Phys. Rev. D **78** (2008) 064040, arXiv:0807.0665.

[26] J. Brannlund, S. Kloster, and A. DeBenedictis, "The Evolution of Lambda Black Holes in the Mini-Superspace Approximation of Loop Quantum Gravity," Phys. Rev. D **79** (2009) 084023, arXiv:0901.0010.

[27] A. Joe and P. Singh, "Kantowski-Sachs spacetime in loop quantum cosmology: bounds on expansion and shear scalars and the viability of quantization prescriptions," Class. Quant. Grav. **32** (2015) 015009, arXiv:1407.2428.

[28] A. Corichi and P. Singh, "Loop quantization of the Schwarzschild interior revisited," Class. Quant. Grav. **33** (2016) 055006, arXiv:1506.08015.

[29] J. Cortez, W. Cuervo, H. A. Morales-Tecotl, and J. C. Ruelas, "Effective loop quantum geometry of Schwarzschild interior," Phys. Rev. D **95** (2017) 064041, arXiv:1704.03362.

[30] J. Olmedo, S. Saini, and P. Singh, "From black holes to white holes: a quantum gravitational, symmetric bounce," Class. Quant. Grav. **34** (2017) 225011, arXiv:1707.07333.

[31] J. Ben Achour, F. Lamy, H. Liu, and K. Noui, "Polymer Schwarzschild black hole: An effective metric," EPL **123** (2018) 20006, arXiv:1803.01152.

[32] A. Ashtekar, J. Olmedo, and P. Singh, "Quantum extension of the Kruskal spacetime," Phys. Rev. D **98** (2018) 126003, arXiv:1806.02406.

[33] N. Bodendorfer, F. M. Mele, and J. Münch, "Effective Quantum Extended Spacetime of Polymer Schwarzschild Black Hole," Class. Quant. Grav. **36** (2019) 195015, arXiv:1902.04542.

[34] E. Alesci, S. Bahrami, and D. Pranzetti, "Quantum gravity predictions for black hole interior geometry," Phys. Lett. B **797** (2019) 134908, arXiv:1904.12412.

[35] M. Assanioussi, A. Dapor, and K. Liegener, "Perspectives on the dynamics in a loop quantum gravity effective description of black hole interiors," Phys. Rev. D **101** (2020) 026002, arXiv:1908.05756.

[36] M. Bojowald and R. Swiderski, "Spherically symmetric quantum geometry: Hamiltonian constraint," Class. Quant. Grav. **23** (2006) 2129–2154, arXiv:gr-qc/0511108.

[37] R. Gambini and J. Pullin, "Black holes in loop quantum gravity: The Complete space-time," Phys. Rev. Lett. **101** (2008) 161301, arXiv:0805.1187.

[38] R. Gambini, J. Olmedo, and J. Pullin, "Quantum black holes in Loop Quantum Gravity," Class. Quant. Grav. **31** (2014) 095009, arXiv:1310.5996.

[39] J. Ben Achour, S. Brahma, and A. Marciano, "Spherically symmetric sector of

self dual Ashtekar gravity coupled to matter: Anomaly-free algebra of constraints with holonomy corrections," Phys. Rev. D **96** (2017) 026002, arXiv:1608.07314.

[40] M. Bojowald, S. Brahma, and D.-h. Yeom, "Effective line elements and black-hole models in canonical loop quantum gravity," Phys. Rev. **D98** (2018) 046015, arXiv:1803.01119.

[41] J. D. Reyes, "Spherically Symmetric Loop Quantum Gravity: Connection to Two-Dimensional Models and Applications to Gravitational Collapse,". PhD thesis, The Pennsylvania State University, 2009. Available online at https://etda.libraries.psu.edu/catalog/10349.

[42] R. Gambini and J. Pullin, "Loop quantization of the Schwarzschild black hole," Phys. Rev. Lett. **110** (2013) 211301, arXiv:1302.5265.

[43] V. Husain and O. Winkler, "Quantum resolution of black hole singularities," Class. Quant. Grav. **22** (2005) L127–L134, arXiv:gr-qc/0410125.

[44] J. Ziprick and G. Kunstatter, "Dynamical Singularity Resolution in Spherically Symmetric Black Hole Formation," Phys. Rev. D **80** (2009) 024032, arXiv:0902.3224.

[45] M. Bojowald, J. D. Reyes, and R. Tibrewala, "Non-marginal LTB-like models with inverse triad corrections from loop quantum gravity," Phys. Rev. D **80** (2009) 084002, arXiv:0906.4767.

[46] A. Kreienbuehl, V. Husain, and S. S. Seahra, "Modified general relativity as a model for quantum gravitational collapse," Class. Quant. Grav. **29** (2012) 095008, arXiv:1011.2381.

[47] M. Bojowald, G. M. Paily, J. D. Reyes, and R. Tibrewala, "Black-hole horizons in modified space-time structures arising from canonical quantum gravity," Class. Quant. Grav. **28** (2011) 185006, arXiv:1105.1340.

[48] D.-W. Chiou, W.-T. Ni, and A. Tang, "Loop quantization of spherically symmetric midisuperspaces and loop quantum geometry of the maximally extended Schwarzschild spacetime," arXiv:1212.1265.

[49] R. Gambini, J. Olmedo and J. Pullin, "Spherically symmetric loop quantum gravity: analysis of improved dynamics," Class. Quant. Grav. **37** (2020) 205012, arXiv:2006.01513.

[50] J. G. Kelly, R. Santacruz and E. Wilson-Ewing, "Black hole collapse and bounce in effective loop quantum gravity," Class. Quant. Grav. **38** (2021) 04LT01, arXiv:2006.09325.

[51] R. Gambini, J. Pullin, and S. Rastgoo, "Quantum scalar field in quantum gravity: The vacuum in the spherically symmetric case," Class. Quant. Grav. **26** (2009) 215011, arXiv:0906.1774.

[52] R. Gambini, E. M. Capurro, and J. Pullin, "Quantum spacetime of a charged black hole," Phys. Rev. D **91** (2015) 084006, arXiv:1412.6055.

[53] M. Bojowald, S. Brahma, and J. D. Reyes, "Covariance in models of loop quantum gravity: Spherical symmetry," Phys. Rev. D **92** (2015) 045043, arXiv:1507.00329.

[54] M. Campiglia, R. Gambini, J. Olmedo, and J. Pullin, "Quantum self-gravitating collapsing matter in a quantum geometry," Class. Quant. Grav. **33** (2016) 18LT01, arXiv:1601.05688.

[55] V. Husain and O. Winkler, "Quantum Hamiltonian for gravitational collapse," Phys. Rev. D **73** (2006) 124007, arXiv:gr-qc/0601082.

[56] V. Husain, "Critical behaviour in quantum gravitational collapse," Adv. Sci. Lett. **2**, 214 (2009), arXiv:0808.0949.

[57] A. Ashtekar, V. Taveras, and M. Varadarajan, "Information is Not Lost in the Evaporation of 2-dimensional Black Holes," Phys. Rev. Lett. **100** (2008) 211302, arXiv:0801.1811.

[58] S. Hossenfelder, L. Modesto, and I. Premont-Schwarz, "A Model for non-singular black hole collapse and evaporation," Phys. Rev. D **81** (2010) 044036, arXiv:0912.1823.

[59] A. Ashtekar, F. Pretorius, and F. M. Ramazanoglu, "Evaporation of 2-Dimensional Black Holes," Phys. Rev. D **83** (2011) 044040, arXiv:1012.0077.

[60] Y. Tavakoli, J. Marto, and A. Dapor, "Semiclassical dynamics of horizons in spherically symmetric collapse," Int. J. Mod. Phys. D **23** (2014) 1450061, arXiv:1303.6157.

[61] M. Christodoulou, C. Rovelli, S. Speziale, and I. Vilensky, "Planck star tunneling time: An astrophysically relevant observable from background-free quantum gravity," Phys. Rev. D **94** (2016) 084035, arXiv:1605.05268.

[62] M. Christodoulou and F. D'Ambrosio, "Characteristic Time Scales for the Geometry Transition of a Black Hole to a White Hole from Spinfoams," arXiv:1801.03027.

[63] F. Benitez, R. Gambini, L. Lehner, S. Liebling, and J. Pullin, "Critical collapse of a scalar field in semiclassical loop quantum gravity," Phys. Rev. Lett. **124** (2020) 071301, arXiv:2002.04044.

[64] J. Ben Achour, S. Brahma, S. Mukohyama and J. P. Uzan, "Towards consistent black-to-white hole bounces from matter collapse," JCAP **09**, 020 (2020), arXiv:2004.12977.

[65] C. Rovelli and F. Vidotto, "Planck stars," Int. J. Mod. Phys. D **23** (2014) 1442026, arXiv:1401.6562.

[66] H. M. Haggard and C. Rovelli, "Quantum-gravity effects outside the horizon spark black to white hole tunneling," Phys. Rev. D **92** (2015) 104020, arXiv:1407.0989.

[67] C. Barcelo, R. Carballo-Rubio, L. J. Garay and G. Jannes, "The lifetime problem of evaporating black holes: mutiny or resignation," Class. Quant. Grav. **32** (2015) 035012, arXiv:1409.1501.

[68] E. Bianchi, M. Christodoulou, F. D'Ambrosio, H. M. Haggard, and C. Rovelli, "White Holes as Remnants: A Surprising Scenario for the End of a Black Hole," Class. Quant. Grav. **35** (2018) 225003, arXiv:1802.04264.

[69] A. Barrau and C. Rovelli, "Planck star phenomenology," Phys. Lett. B **739** (2014) 405–409, arXiv:1404.5821.

[70] A. Barrau, C. Rovelli, and F. Vidotto, "Fast Radio Bursts and White Hole Signals," Phys. Rev. D **90** (2014) 127503, arXiv:1409.4031.

[71] A. Barrau, B. Bolliet, F. Vidotto, and C. Weimer, "Phenomenology of bouncing black holes in quantum gravity: a closer look," JCAP **02** (2016) 022, arXiv:1507.05424.

[72] A. Ashtekar, T. Pawlowski, and P. Singh, "Quantum Nature of the Big Bang: Improved dynamics," Phys. Rev. D **74** (2006) 084003, arXiv:gr-qc/0607039.

[73] M. de Cesare, S. S. Seahra and E. Wilson-Ewing, "The singularity in mimetic Kantowski-Sachs cosmology," JCAP **07**, 018 (2020), arXiv:2002.11658.

[74] P. Singh and E. Wilson-Ewing, "Quantization ambiguities and bounds on geometric scalars in anisotropic loop quantum cosmology," Class. Quant. Grav. **31** (2014) 035010, arXiv:1310.6728.

[75] V. Taveras, "Corrections to the Friedmann Equations from LQG for a Universe with a Free Scalar Field," Phys. Rev. D **78** (2008) 064072, arXiv:0807.3325.

[76] C. Rovelli and E. Wilson-Ewing, "Why are the effective equations of loop quantum cosmology so accurate?," Phys. Rev. D **90** (2014) 023538, arXiv:1310.8654.

[77] K. Vandersloot, "Loop quantum cosmology and the k = - 1 RW model," Phys. Rev. D **75** (2007) 023523, arXiv:gr-qc/0612070.

[78] A. Ashtekar and E. Wilson-Ewing, "Loop quantum cosmology of Bianchi type II models," Phys. Rev. D **80** (2009) 123532, arXiv:0910.1278.

[79] D. Arruga, J. Ben Achour and K. Noui, "Deformed General Relativity and Quantum Black Holes Interior," Universe **6** (2020) 39, arXiv:1912.02459.

[80] E. Alesci and L. Modesto, "Particle Creation by Loop Black Holes," Gen. Rel. Grav. **46** (2014) 1656, arXiv:1101.5792.

[81] E. G. Brown, R. B. Mann and L. Modesto, "Mass Inflation in the Loop Black Hole," Phys. Rev. D **84** (2011) 104041, arXiv:1104.3126.

[82] R. Carballo-Rubio, F. Di Filippo, S. Liberati, C. Pacilio and M. Visser, "On the viability of regular black holes," JHEP **07** (2018) 023, arXiv:1805.02675.

[83] A. Bonanno, A. P. Khosravi and F. Saueressig, "Regular black holes with stable cores," Phys. Rev. D **103**, 124027 (2021), arXiv:2010.04226.

Chapter 3

Black hole collapse and bounce in effective loop quantum gravity

3.1 Introduction

General relativity is typically expected to break down when the curvature reaches the Planck scale, at which point a theory of quantum gravity becomes necessary. One important example is a black hole of mass M: in the simplest case of the Schwarzschild vacuum spherically symmetric space-time, the Kretschmann scalar $R_{\mu\nu\rho\sigma}R^{\mu\nu\rho\sigma} \sim (2GM)^2/r^6$ reaches the Planck scale at the radius $r \sim (2GM\ell_{\rm Pl}^2)^{1/3}$, suggesting that quantum gravity effects may become important not only close to the singularity at $r = 0$, but as far away from the black hole center as $(2GM\ell_{\rm Pl}^2)^{1/3}$.

In addition to quantum gravity effects being presumably important in vacuum black hole solutions, quantum gravity is also expected to play an important role during black hole collapse. While the matter forming the star is classically predicted to reach the central singularity, quantum gravity effects could resolve the singularity and modify the dynamics of infalling matter.

In spherically symmetric space-times, there are no gravitational waves and therefore

to study black hole collapse a matter field is needed. A simple choice is pressureless dust; spherically symmetric space-times minimally coupled to dust are known as the Lemaître-Tolman-Bondi (LTB) solutions [1–3].

To explore how quantum gravity effects may modify black hole collapse, we will consider the effect of expressing the (classical) Hamiltonian in terms of area and holonomy variables, as suggested by loop quantum gravity (LQG) [4]. (For the quantization of LTB space-times in other contexts, see [5–7].) In this approach, the Hamiltonian depends on holonomies of the Ashtekar-Barbero connection along paths of physical length $\sim \ell_{\rm Pl}$, rather than the connection itself. The resulting 'effective' equations of motion include quantum gravity effects due to the presence of these Planck-length holonomies in the Hamiltonian. For cosmology, the effective equations derived in this manner have been shown to give an excellent approximation to the leading order quantum gravity effects for sharply-peaked states in loop quantum cosmology (LQC) [8]. Note that to ensure the physical length of the holonomy paths is $\sim \ell_{\rm Pl}$, the coordinate length has to be related to the physical length through the metric; this step is essential to obtain physical results (otherwise an unphysical coordinate length is related to the physical Planck scale, resulting in inconsistencies) and this procedure is called, for historical reasons, the 'improved dynamics' or '$\bar{\mu}$-scheme' [9].

There has been considerable work studying various LQG effects in spherically symmetric space-times. For vacuum space-times, most studies are based on the isometry between the classical Schwarzschild interior and the Kantowski-Sachs space-time [10–24], but this isometry is based on results in classical general relativity and may not hold in LQG (it is also unclear how to properly carry out the $\bar{\mu}$ scheme when a spatial coordinate becomes null at a horizon). The full vacuum space-time (interior and exterior) was first studied without using the $\bar{\mu}$ scheme [25–31], and more recent work has shown how to include that missing step and implement the $\bar{\mu}$ scheme in vacuum spherically symmetric space-times [32–34].

To study black hole collapse, it is necessary to include a matter field. For previous work on the inclusion of matter fields in spherical symmetry in the context of LQG, see [27, 35–38], and for studies of black hole collapse based on this approach, see [38–42]. (And for other LQG/LQC-based studies of black hole collapse, see [43–51]). Although these studies provide interesting insights into potential quantum gravity effects in black hole collapse—in particular, many predict that the black hole singularity is resolved and that the black hole bounces into a white-hole-like solution—none use the $\bar{\mu}$ scheme throughout the entire space-time. (Some of these studies do not use the $\bar{\mu}$ scheme at all, while others use it only for the interior of the star and use the equations of general relativity for the vacuum region outside the star.) Finally, there have also been some studies of LQG-motivated inverse triad effects in spherical symmetry, for details see [52–56].

In this paper we will show how to implement the $\bar{\mu}$ scheme for the full family of LTB space-times and then use this framework to derive effective equations of motion. These equations will hold both in the presence and absence of matter, as well as inside and outside a horizon. We then use the resulting effective equations to study LQG effects in the Oppenheimer-Snyder black hole collapse model. Note that we will refer to a black hole being present if there is, at that instant of (coordinate) time, an apparent horizon; we do not require an event horizon to exist since we do not necessarily expect an event horizon to be present in a non-singular black hole space-time.

3.2 Classical Theory

The line element for a spherically symmetric space-time can be put in the form

$$ds^2 = -N^2 dt^2 + \frac{(E^b)^2}{E^a}(dx + N^x dt)^2 + E^a d\Omega^2, \tag{3.1}$$

where $N(x,t)$ and $N^x(x,t)$ are the lapse and the radial component of the shift vector, $E^a(x,t)$ and $E^b(x,t)$ are the densitized triad in the radial and angular directions, and $d\Omega^2 = d\theta^2 + \sin^2\theta\ d\phi^2$.

The densitized triads are conjugate to the Ashtekar-Barbero connection whose components are [34]

$$\begin{aligned} A_a^i \tau_i dx^a = a\,\tau_1\,dx + \left(b\,\tau_2 + \frac{\partial_x E^a}{2E^b}\,\tau_3\right) d\theta \\ + \left(\cot\theta\,\tau_1 - \frac{\partial_x E^a}{2E^b}\tau_2 + b\,\tau_3\right)\sin\theta\,d\phi. \end{aligned} \tag{3.2}$$

Here $a(x,t)$ and $b(x,t)$ capture the extrinsic curvature in the radial and angular directions respectively, while $\tau^j = -i\sigma^j/2$, with σ^j the Pauli matrices.

For the Lemaître-Tolman-Bondi (LTB) space-times the matter content is a pressureless dust field and, after integrating over $d\Omega$, the action is [57]

$$\begin{aligned} S = \int dt \int dx \Bigg[\frac{\dot{a}E^a + 2\dot{b}E^b}{2G\gamma} + 4\pi \dot{T} p_T - N\left(\mathcal{H}^{(g)} + \mathcal{H}^{(d)}\right) \\ - N^x\left(\mathcal{H}_x^{(g)} - 4\pi p_T \partial_x T\right)\Bigg]. \end{aligned} \tag{3.3}$$

Here T denotes the dust field and p_T is its conjugate momentum, while the dots denote derivatives with respect to t. The contributions to the scalar constraint from the gravitational and dust sectors are

$$\begin{aligned} \mathcal{H}^{(g)} =& -\frac{1}{2G\gamma^2}\left(2ab\sqrt{E^a} + \frac{E^b}{\sqrt{E^a}}(b^2+\gamma^2)\right) \\ &+ \frac{1}{8G}\frac{(\partial_x E^a)^2}{E^b\sqrt{E^a}} + \frac{\sqrt{E^a}}{2G}\partial_x\left(\frac{\partial_x E^a}{E^b}\right), \end{aligned} \tag{3.4}$$

$$\mathcal{H}^{(d)} = 4\pi\sqrt{p_T^2 + \frac{E^a}{(E^b)^2}p_T^2(\partial_x T)^2}, \tag{3.5}$$

and the gravitational term in the diffeomorphism constraint is $\mathcal{H}_x^{(g)} = (2G\gamma)^{-1}\cdot$

$(2E^b\partial_x b - a\partial_x E^a)$.

The Hamiltonian framework can be simplified by using the dust-time gauge to fix the scalar constraint [57] and the areal gauge to fix the diffeomorphism constraint [13, 34]. After this gauge-fixing there will remain a true Hamiltonian, with no constraints left. Note that due to this gauge-fixing procedure, the resulting effective theory does not fall within the class of (vacuum) models studied in [58].

The benefit of the dust-time gauge $T = t$ is clear, as then $\partial_x T = 0$. The gauge-fixing condition $\chi_1 = T - t = 0$ is second-class with the scalar constraint, so χ_1 can be used to gauge-fix it. Solving the scalar constraint gives $4\pi p_T = -\mathcal{H}^{(g)}$, while requiring that the gauge-fixing condition be preserved by the dynamics imposes $N = 1$. Further, the symplectic term in the action $4\pi p_T \dot{T}$ simplifies to $4\pi p_T = -\mathcal{H}^{(g)}$, which becomes a true physical Hamiltonian $\mathcal{H}_{\rm phys} = \mathcal{H}^{(g)}$ [57].

The next simplification is to impose the areal gauge through the condition $\chi_2 = E^a - x^2 = 0$, which imposes that a sphere at radius x has surface area $4\pi x^2$. The condition χ_2 is second-class with the diffeomorphism constraint, which can be solved giving $a = E^b(\partial_x b)/x$, and requiring that χ_2 be preserved dynamically gives $N^x = -b/\gamma$ [34]. Since E^a is independent of time, the $\dot{a}E^a$ term is a total time derivative and can be dropped from the action, while $\mathcal{H}_{\rm phys}$ simplifies considerably after substituting for E^a and a:

$$S_{GF} = \int dt \int dx \left(\frac{\dot{b}E^b}{G\gamma} - \mathcal{H}_{\rm phys} \right), \tag{3.6}$$

$$\mathcal{H}_{\rm phys} = -\frac{1}{2G\gamma}\left[\frac{E^b}{\gamma x}\left(b^2 + x\partial_x b^2\right) + \frac{\gamma E^b}{x} + \frac{2\gamma x^2}{(E^b)^2}\partial_x E^b - \frac{3\gamma x}{E^b} \right]. \tag{3.7}$$

After fixing these two gauges, the metric reduces to

$$ds^2 = -dt^2 + \frac{(E^b)^2}{x^2}\,(dx + N^x\,dt)^2 + x^2 d\Omega^2, \tag{3.8}$$

with $N^x = -b/\gamma$ for classical general relativity, and it is clear that there is one physical degree of freedom at each point due to the dust field (there are no gravitational waves in spherically symmetric space-times). The energy density $\rho(x,t)$ of the dust field, related to the dust contribution to the scalar constraint by $\mathcal{H}^{(d)} = \int d\Omega\,\sqrt{q}\rho$, where $\sqrt{q}$ is the determinant of the spatial metric, is

$$\rho = \frac{p_T}{\sqrt{E^a}\,E^b} = -\,\frac{\mathcal{H}_{\rm phys}}{4\pi x\,E^b}, \tag{3.9}$$

and the remaining non-trivial Poisson bracket is

$$\{b(x_1,t), E^b(x_2,t)\} = G\gamma\,\delta(x_1 - x_2). \tag{3.10}$$

The dynamics follow from $\dot{f} = \{f, \int dx\ \mathcal{H}_{\rm phys}\}$, giving

$$\dot{E}^b = \frac{bE^b}{\gamma x} - \frac{b}{\gamma}\,\partial_x E^b, \tag{3.11}$$

$$\dot{b} = \frac{\gamma x}{2(E^b)^2} - \frac{1}{2\gamma x}\Big(2xb\partial_x b + b^2 + \gamma^2\Big). \tag{3.12}$$

These are the usual equations of motion for the LTB family of metrics, for the Painlevé-Gullstrand coordinates (3.8) of the metric [59, 60], and in a form convenient to include holonomy corrections as motivated by LQG.

3.3 LTB Effective Equations

One of the main features of LQG is that the fundamental operators, out of which all other operators are constructed, are holonomies of A_a and the areas E^a. In LQC, it has

been shown that there exist 'effective equations' that provide a good approximation to the dynamics of expectation values of observables, at least for wave functions that are sharply peaked and whose expectation value for the spatial volume satisfies $\langle V\rangle \gg \ell_{\rm Pl}^3$ [61, 62]. These effective equations can be derived as the Hamilton equations of an effective Hamiltonian that includes modifications proportional to $\hbar$ which ensure the resulting dynamics track sharply-peaked wave functions in the full quantum theory.

To derive an effective Hamiltonian for (gauge-fixed) LTB space-times, the main step is to replace the connection component b by minimal length holonomies of b in the classical gauge-fixed Hamiltonian. (Recall that after the gauge-fixing imposed in Sec. 3.2, the system is described by a single true Hamiltonian—there are no constraints left.) It is necessary that these holonomies give trigonometric functions of b (without b-dependent prefactors) for it to be possible to promote the holonomies to operators in LQC. This condition is satisfied by holonomies of the extrinsic curvature 1-form in the θ direction,

$$\begin{aligned} h_\theta(2\delta_b) &= \exp\left(\int_0^{2\delta_b} b\tau_2\, d\theta\right) \\ &= \cos(\delta_b b)\,\mathbb{I} + 2\sin(\delta_b b)\,\tau_2. \end{aligned} \tag{3.13}$$

This is known as the 'K' loop quantization, for details see [63, 64]. (The path could be a portion of any great circle on the sphere, for simplicity we took $\phi = \text{const.}$)

Still following [63, 64], the coordinate length $2\delta_b$ must be chosen so that the physical length of the path is $\sqrt{\Delta}$, where $\Delta \sim \ell_{\rm Pl}^2$ is the smallest non-zero eigenvalue of the area operator in LQG. (The factor of 2 is to ensure consistency with expressions of the curvature in terms of holonomies [65].) For this path, x and ϕ are constant, so the metric (3.8) implies $ds = x\, d\theta$. Integrating and requiring that the physical length be $\sqrt{\Delta}$ gives $\int_0^{\sqrt{\Delta}} ds = \int_0^{2\delta_b} x\, d\theta$, so $2\delta_b = \sqrt{\Delta}/x$, see also [32–34].

Finally, b must be replaced in $\mathcal{H}_{\rm phys}$ by an appropriate expression in terms of

$h_\theta(2\delta_b)$ [63, 64],

$$b \to \frac{-2\,\mathrm{Tr}(h_\theta(2\delta_b)\cdot\tau_2)}{2\delta_b} = \frac{x}{\sqrt{\Delta}}\sin\left(\frac{\sqrt{\Delta}}{x}b\right). \tag{3.14}$$

This substitution gives the effective physical Hamiltonian for LTB space-times,

$$\mathcal{H}^{LQG}_{\mathrm{phys}} = -\frac{1}{2G\gamma}\left[\frac{E^b}{\gamma x}\partial_x\left(\frac{x^3}{\Delta}\,\sin^2\frac{\sqrt{\Delta}\,b}{x}\right) - \frac{3\gamma x}{E^b} + \frac{2\gamma x^2}{(E^b)^2}\partial_x E^b + \frac{\gamma E^b}{x}\right]. \tag{3.15}$$

To reconstruct the space-time metric from the phase space variables it is necessary to find the shift N^x, and this requires rewriting the relation between N^x and b in terms of holonomies (as before, this step is required since there is no operator corresponding to b in the quantum theory). Following earlier work in vacuum spherically symmetric space-times gives [33, 34]

$$N^x = -\frac{x}{\gamma\sqrt{\Delta}}\sin\frac{\sqrt{\Delta}\,b}{x}\cos\frac{\sqrt{\Delta}\,b}{x}. \tag{3.16}$$

Note that the form of the metric (3.8) remains unchanged.

The effective dynamics for general LTB space-times follow directly from $\mathcal{H}^{LQG}_{\mathrm{phys}}$ and the (unchanged) Poisson bracket (3.10),

$$\dot{E}^b = -\frac{x^2}{\gamma\sqrt{\Delta}}\partial_x\left(\frac{E^b}{x}\right)\sin\frac{\sqrt{\Delta}\,b}{x}\cos\frac{\sqrt{\Delta}\,b}{x}, \tag{3.17}$$

$$\dot{b} = \frac{\gamma}{2}\left(\frac{x}{(E^b)^2} - \frac{1}{x}\right) - \frac{1}{2\gamma\Delta x}\partial_x\left(x^3\sin^2\frac{\sqrt{\Delta}\,b}{x}\right). \tag{3.18}$$

These effective equations can be used to study LQG effects in LTB space-times, and in particular in black hole collapse models.

The vacuum solutions $\rho = 0$ correspond to $\mathcal{H}^{LQG}_{\mathrm{phys}} = 0$ and have already been studied [33, 34]. In Painlevé-Gullstrand coordinates, the metric for the vacuum solution has

the form

$$ds^2 = -\left(1 - \frac{R_S}{x} + \frac{\gamma^2 \Delta R_S^2}{x^4}\right) dt^2 + dx^2 + 2\sqrt{\frac{R_S}{x}\left(1 - \frac{\gamma^2 \Delta R_S}{x^3}\right)}\, dt\, dx + x^2 d\Omega^2, \tag{3.19}$$

where $R_S = 2GM$ is the Schwarzschild radius, and the quantum gravity corrections are proportional to Δ. Note that for the vacuum case $M = 0$, the result is the classical Minkowski solution without any quantum gravity corrections. Interestingly, this metric is only valid for $x \geq x_{\rm min} = (\gamma^2 \Delta R_S)^{1/3}$ [33, 34]. This is not surprising, since in spherical symmetry there are no gravitational waves and therefore a central potential must be generated by some distribution of matter. Since LQC effects are known to bound $\rho \lesssim \rho_{\rm Pl}$ by the Planck scale, this suggests that to have a source of mass M, there must be some matter content out to (assuming maximal density) $x \sim (M/\rho_{\rm Pl})^{1/3}$, in qualitative agreement with the bound $x \geq x_{\rm min}$ for the vacuum solution. In the simple model for black hole collapse considered next, this expectation will be shown to be precisely correct.

This vacuum solution has an outer apparent horizon located at $x_{\rm outer} \sim R_S - \gamma^2 \Delta / R_S$ and an inner apparent horizon at $x_{\rm inner} \sim x_{\rm min} + (\gamma^4 \Delta^2 / 27 R_S)^{1/3}$ [34]; matter that lies inside the inner horizon can remain at rest, or bounce and start to expand as required for a transition from a black hole to a white hole [50]. In the Planck regime, quantum gravity repulsive effects counteract the classical gravitational attractive force, and the outgoing expansion becomes positive again for $x < x_{\rm inner}$.

3.4 Black Hole Collapse and Bounce

A simple model for black hole collapse is the Oppenheimer-Snyder model [66]. This space-time belongs to the family of LTB solutions, and corresponds to a 'star' of

radius $L(t)$, with vacuum outside. The star is composed of pressureless dust, and it is further assumed that the star has a spatially constant density ρ within its interior: $\rho(x,t) = \rho(t)$ if $x \leq L(t)$ and $\rho(x,t) = 0$ for $x > L(t)$. As the star collapses, $L(t)$ will decrease and $\rho(t)$ will increase. To simplify the analysis, for now we neglect edge effects due to the discontinuity in ρ at the surface L of the star. Note that the interior of the Oppenheimer-Snyder model is a Friedman-Lemaître-Robertson-Walker (FLRW) cosmology, while the exterior is vacuum.

For a spatially flat interior, we set $E^b = x$ which is clearly a solution of (3.17). Then (3.18) and (3.9) simplify to

$$\dot{b} = -\frac{1}{2\gamma\Delta x}\,\partial_x\left(x^3 \sin^2\frac{\sqrt{\Delta}\,b}{x}\right), \tag{3.20}$$

$$\rho = \frac{1}{8\pi G\gamma^2\Delta\, x^2}\,\partial_x\left(x^3\, \sin^2\frac{\sqrt{\Delta}\,b}{x}\right), \tag{3.21}$$

and conservation of energy implies that $M = 4\pi\rho L^3/3$ is constant. The relation (3.21) is easily inverted, and for the collapsing Oppenheimer-Snyder model this gives

$$\sin\frac{\sqrt{\Delta}b}{x} = \begin{cases} -\sqrt{\rho(t)/\rho_c} & \text{if } x \leq L(t), \\ -\sqrt{3M/4\pi\rho_c x^3} & \text{if } x > L(t), \end{cases} \tag{3.22}$$

where the critical energy density is $\rho_c = 3/(8\pi G\gamma^2\Delta)$. Note that the overall minus sign is chosen so $N^x > 0$ and the star collapses (for $\cos(\sqrt{\Delta}b/x) \geq 0$).

Combining (3.20) and the interior solution (3.22) gives an equation for $\dot{\rho}$, and using $\rho = 3M/4\pi L^3$ this becomes

$$\left(\frac{\dot{L}}{L}\right)^2 = \frac{8\pi G}{3}\rho\left(1 - \frac{\rho}{\rho_c}\right), \tag{3.23}$$

exactly the LQC effective Friedmann equation for spatially flat FLRW space-times

with scale factor L [9]. This is easily solved, with the result

$$L(t) = \left[\gamma^2 \Delta R_S \left(\frac{9t^2}{4\gamma^2\Delta} + 1\right)\right]^{1/3}, \tag{3.24}$$

and $\rho = 3M/4\pi L^3$.

This solution shows that the star contracts until it reaches $L = x_{\min} = (\gamma^2 \Delta R_S)^{1/3}$ $\sim (\ell_{\rm Pl}^2 R_S)^{1/3}$ at $t = 0$, when there is a bounce, and after this the radius L of the star begins to expand: quantum gravity effects generate a non-singular transition from a black hole to something similar to a white hole, as has previously been suggested [67–69]. The difference between the white hole solution proposed in these works and the post-bounce $t > 0$ solution derived here is subtle, but important. In the white hole solution for vacuum general relativity, the whole interior of the white hole is anti-trapped. For this solution, it is only part of the region inside $x < L(t)$ that is anti-trapped, while on the other hand the region $L(t) < x < R_S$ is trapped, like for a black hole; see Fig. 1. L will move outwards, and once L reaches a value $L(t) > x_{\rm outer} \sim R_S$, the apparent horizon will go away and so at this time there is no longer a black hole—this Oppenheimer-Snyder space-time only contains a black hole for the time interval between when $L = x_{\rm outer}$ during the contracting phase and when $L = x_{\rm outer}$ after the bounce.

Importantly, the minimal value of the radius of the star is $L = x_{\min}$. This fits exactly with the constraint that the vacuum solution is only valid for $x \geq x_{\min}$: the curvature of the space-time (in the absence of gravitational waves) must be generated by a matter field, and since ρ is bounded in LQC, matter must extend out at least to the minimal radius $x_{\min}$ (that depends on M).

The metric describing this collapse and bounce of a black hole is (3.8), with $E^b = x$

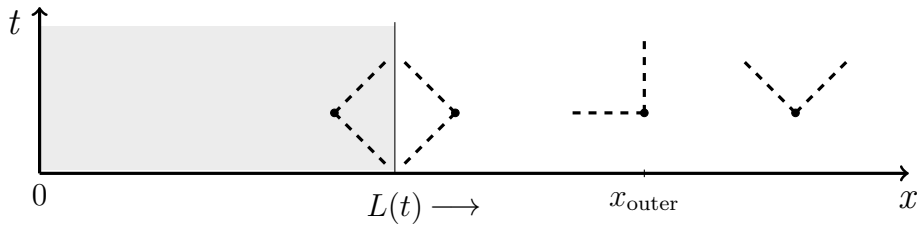

Figure 3.1: This shows a snapshot of the lightcones on a spatial slice of the effective Oppenheimer-Snyder space-time at an instant of time, after the bounce has occurred and L is moving outwards. The dust field is shown in gray, and the energy density of the dust field will be larger near L than in the interior. The dust field is coupled to gravity, and will act on the space-time geometry of the outer neighbourhood of L with the ultimate effect of rotating the lightcone in that neighbourhood upwards. This in turn will allow the dust to move outwards, little by little, as the outer neighbourhood of L stops being trapped. An estimate of the rate of expansion of L is given in Sec. 3.5.

and the shift vector

$$N^x = \begin{cases} -\dfrac{6xt}{9t^2 + 4\gamma^2\Delta} & \text{if } x \leq L(t), \\ \sqrt{\dfrac{R_S}{x}\left(1 - \dfrac{\gamma^2\Delta R_S}{x^3}\right)} & \text{if } x > L(t). \end{cases} \tag{3.25}$$

For the interior, the coordinate transformation $x = L(t)\chi$ gives the flat FLRW metric

$$ds^2 = -dt^2 + L^2(t)\left(d\chi^2 + \chi^2 d\Omega^2\right). \tag{3.26}$$

It is easy to verify that N^x is continuous at $x = L$ when the star is contracting, but these terms differ by a sign after the bounce: for $t > 0$, there will be a shock wave in the gravitational field with a discontinuity at $x = L$ in $b(x)$ and in the effective metric.

The presence of a discontinuity in the gravitational field variable b (and also in the space-time metric) shows that the assumption that edge effects can be neglected (which the calculations giving (3.22)–(3.25) rely upon) fails after the bounce at $t = 0$, and therefore the solution (3.22)–(3.25) cannot be expected to be correct for the expanding post-bounce phase. To correctly describe the expanding phase and the effect of the shock wave that appears then, it is necessary to include the edge effects

which have been ignored so far. Note that this shock wave, i.e., the discontinuity in b, will persist when edge effects are included—so the importance of including edge effects is not to remove the shock wave (which is predicted to form whether edge effects are included in the analysis or not), but rather to be able to accurately calculate the rate at which the shock wave moves outwards after the bounce.

3.5 The White Hole Shock Wave

Since $E^b = x$, as assumed at the onset of the Oppenheimer-Snyder collapse, the dynamics of the shock wave are given by $\dot{E}^b = 0$, due to (3.17), and

$$\dot{b} = -4\pi G\gamma x\rho, \tag{3.27}$$

$$\dot{\rho} = \frac{1}{3\gamma\Delta x^2}\partial_x\left(x^4 N^x \rho\right), \tag{3.28}$$

which follow from (3.9), (3.15), (3.16), and (3.18). Note that these equations hold even if ρ is not (piecewise) spatially homogeneous.

The first equation clearly shows that b is monotonically decreasing, and constant outside the star where $\rho = 0$ (this is why N^x remains constant for $x > L$). Away from the edge $x = L$, the second equation shows that ρ increases for $N^x > 0$ (a collapsing star) while ρ decreases for $N^x < 0$ (the post-bounce expanding white hole).

One way to explore the edge dynamics near $x = L$ is to do a simple discretization of (3.28) on a lattice with spacing δx, replacing $\partial_x f(x_i) \to [f(x_{i+1}) - f(x_{i-1})]/2\delta x$. During collapse, $N^x > 0$ everywhere and at the edge $x_i = L$, the discretized derivative is negative since $\rho(x_{i+1}) = 0$ and $\rho(x_{i-1}) > 0$, so $\dot{\rho}(x_i) < 0$. As expected, in a collapse the density increases inside the star, and decreases at x_i precisely as the edge L becomes smaller than x_i. This agrees with (3.25), which can be trusted for the collapse phase as there is no shock wave then.

On the other hand, after the bounce $N^x < 0$ inside the expanding star, but $N^x > 0$ in the surrounding vacuum region. If the edge is at $x_i = L$ (assuming $N^x < 0$ for $x_j \leq x_i$ and $N^x > 0$ for $x_j \geq x_{i+1}$), it is easy to see that $\dot{\rho}(x_{i+1}) > 0$ since $\rho(x_{i+2}) = 0$ and $N^x(x_i) < 0$. However, at the next time step the dust field cannot (yet) go beyond x_{i+1}: this is because $\dot{\rho}(x_{i+2}) < 0$ due to $N^x(x_{i+1}) > 0$, even though now $\rho(x_{i+1}) > 0$. (Of course, ρ cannot decrease below 0, $\dot{\rho} < 0$ occuring in this context is an artefact of the simple discretization.) Instead, the white hole cannot expand further until $N^x(x_{i+1})$ becomes negative, i.e., when $\sin(\sqrt{\Delta}b(x_{i+1})/x_{i+1}) = -1$. So the discontinuity in N^x will cause the white hole to expand at a much slower rate than it collapsed. Also, the dust field will accumulate near the edge $x = L$ (since $\dot{\rho}(x_i),\ \dot{\rho}(x_{i+1}) > 0$ as long as L does not move), so ρ will become greater at the wave front than inside the star. Results obtained neglecting edge effects can be trusted far from the white hole edge, but the wave front location L will move outwards at a slowed rate and ρ will be greater near L than for $x \ll L$.

From a physical perspective, the dust field in the vicinity of $x = L$ is caught between an outside trapped region and an inside anti-trapped region, as shown in Fig. 3.1. Although the matter field located at L initially cannot move, it is of course coupled to gravity and changes the geometry of the space-time in its neighbourhood. In particular, in the outer neighbourhood of L, the orientation of the lightcones will change so that this region is no longer trapped, and then the dust field will be able to move outwards into this region. This slow process will end once L reaches the outer horizon, at which point the matter fields will be able to freely move outwards. In the following, we estimate the time required for L to reach x_{outer}.

This calculation can be used to obtain an estimate for the lifetime T of a black hole (as measured by a distant observer detecting light signals emitted from the surface of the star), which is given by the coordinate time t elapsed between the instants when $L = x_{\text{outer}} \sim R_S$ before and after the bounce, as shown in Appendix A.

From (3.24), the duration of the contracting portion (from $L = x_{\rm outer}$ to $L = x_{\rm min}$) is $\sim R_S$, so the last step to find T is to calculate the duration of the expanding phase, from $L = x_{\rm min}$ to when $L = x_{\rm outer}$ once more. A precise determination of the white hole's lifetime T will require a considerably more detailed analysis, likely including high-resolution numerics, but it is possible to obtain a simple estimate for T by using (3.27) to calculate the time δt_i, for each location of the shock-wave front L, it takes for N^x to change sign, and then sum over all x from $x_{\rm min}$ to R_S, assuming $\delta x \sim \ell_{\rm Pl}$.

It is enough to start the calculation at, say, $x_i \sim \sqrt{\ell_{\rm Pl} R_S} \gg x_{\rm min}$. (The following calculation can also be used to estimate the contribution to T for the time elapsed while $x_{\rm min} < L(t) < x_i$, which shows that it is subleading compared to the contribution from $x_i < L < x_{\rm outer}$ and so can safely be ignored for an estimate of the leading contribution to T.) When the front L of the shock wave first reaches the radius x, then $|\sin(\sqrt{\Delta} b/x)| \ll 1$ for $x \geq x_i$ and therefore, for N^x to change signs, b must change by $\sim -\pi x/2\sqrt{\Delta}$. Then, from (3.27) it follows that (dropping numerical prefactors of order 1) $\delta t_i \sim 1/(G\sqrt{\Delta}\rho(x_i))$.

At the bounce, $\rho = \rho_c$ but ρ will decrease as the shock wave expands. The leading edge of the shock wave will have a greater ρ than the center (where ρ evolves in a symmetric fashion around the bounce) since the dust field will be pushed towards the edge where it will accumulate due to the slow expansion of the front of the shock wave. After some time, it can be expected that a significant fraction of the dust field will lie within a short distance w of the leading front, in which case the energy density at the edge ρ_e will scale as $\rho_e \sim M/(x^2 w)$. Evaluating ρ at the bounce gives $\rho_c \sim M/x_{\rm min}^3$ so $M \sim \Delta \rho_c R_S$ and $\rho_e \sim \Delta \rho_c R_s/x^2 w$. Then, $\delta t_i \sim w x^2/(G\Delta^{3/2} R_S \rho_c)$ and, since the pre-bounce phase is much shorter than the post-bounce expansion,

$$T \sim \sum_i \delta t_i \sim \int_{x_i}^{R_S} \frac{\delta t_i}{\ell_{\rm Pl}} dx \sim \frac{w R_S^2}{\ell_{\rm Pl}^2}, \tag{3.29}$$

similar what is suggested in [48]. If w is independent of R_S, then $w/\ell_{\rm Pl}$ is a (potentially large) dimensionless constant and the black hole lifetime $T \sim R_S^2/\ell_{\rm Pl}$ is significantly shorter than the Page time [70] in which case the standard black hole information loss problem is avoided.

3.6 Discussion

The LTB space-times are spherically symmetric space-times coupled to pressureless dust. After imposing some convenient gauges, we constructed an effective Hamiltonian following the standard LQC procedure of replacing components of the Ashtekar-Barbero connection by holonomies using the $\bar{\mu}$ scheme, and derived the effective equations for LTB space-times. A particularly interesting case is the Oppenheimer-Snyder model for black hole collapse, which can be solved exactly if edge effects are neglected; the result is that the star contracts until the density reaches the LQC critical density $\rho_c \sim \rho_{\rm Pl}$ and then bounces; for the post-bounce phase it is necessary to include edge effects which become important. Although the post-bounce phase does not exactly correspond to a white hole, there are some significant similarities which lead us to view this model as a specific realization of quantum gravity generating a non-singular transition from a black hole to a 'white hole', as proposed in [67–69], with this general picture also found in [46, 47, 50, 71, 72]. Also, since the effective equations in this case are known for both the interior and exterior regions, as well as at the discontinuity at the surface of the star, it is now possible to properly include the edge effects that become large after the bounce.

The dynamics of the LQG Oppenheimer-Snyder space-time can be split in two main phases: the black hole collapse and the white hole shock wave. First, the star collapses until its surface $L(t)$ reaches $x_{\rm outer} \sim R_S$, at which point an apparent horizon appears and the star forms a black hole. Then, quantum gravity effects become important

when L nears $x_{\rm min} \sim (\ell_{\rm Pl}^2 R_S)^{1/3}$. The quantum gravity effects are sufficiently strong to stop the collapse of the star and cause a bounce. Note that the region inside $x_{\rm min}$ is never trapped as there is an interior horizon at $x = x_{\rm inner} \sim x_{\rm min} + (\gamma^4 \Delta^2 / 27 R_S)^{1/3}$. Then, after the bounce, edge effects become important and slow the expansion of the star. These edge effects can be understood qualitatively to arise from the surface L being caught between an anti-trapped region lying within part of the interior of the star, and the trapped region outside the star for $L < x < x_{\rm outer}$. As the surface of the star L slowly moves outwards, the trapped region becomes smaller, until $L = x_{\rm outer}$ and the apparent horizon vanishes; at this point the solution no longer corresponds to a black hole. We estimate that due to these edge effects, the lifetime of the black hole (as measured by a distant observer detecting light signals emitted from the surface of the star) is $T \sim R_S^2 / \ell_{\rm Pl}$. Note that matter plays an important role in this context, giving a much shorter lifetime than what spin foam calculations have found for vacuum space-times [49, 51]. After the surface L of the star has once more passed $x = x_{\rm outer}$, high-energy photons could be emitted by the expanding star, producing a potentially observable astronomical signature.

There are two results that show a remarkable unity between LQG holonomy corrections applied to different families of space-times. First, the equation of motion for the Oppenheimer-Snyder (flat FLRW) interior is identical to the LQC effective Friedmann equation for flat FLRW space-times in the limit that edge effects are neglected. Although the derivation of the two equations is quite different, they describe the same physics, so it is reassuring that both procedures give the same dynamics. Second, the vacuum spherically symmetric solution for a black hole of mass M is only valid to a minimal radius $x_{\rm min} \sim (R_S \ell_{\rm Pl}^2)^{1/3}$ [33, 34]. This vacuum solution corresponds to the exterior of the Oppenheimer-Snyder solution, and it turns out that the minimal radius of the interior is exactly $x_{\rm min}$: to generate a Schwarzschild-like exterior of mass M, there must be a matter field extending to at least the radius $x_{\rm min}$.

Once again, the consistency between LQG results in vacuum and LTB space-times is remarkable.

There remain a number of important open problems that we leave for future work. First, a better understanding of the physics of the white hole shock wave could be used to calculate the lifetime of a black hole more accurately, and could also give predictions concerning the light emitted by a white hole that could be seen by distant observers. It would also be interesting to study more realistic black hole collapse models by including matter fields with pressure and/or a radially-varying density, and also to determine the stability of the solution to further infalling matter. We point out that since the expanding solution that we obtain is not exactly a white hole (although it does share some qualitative similarities), the instability results for white holes [73, 74] are not directly applicable here. Nonetheless, despite their differences, it does seem likely that at least some of the phenomenology of this model could be similar to what has been found for transitions from a black hole to a white hole [75–77]. Finally, it will also be important to include other quantum effects, most notably Hawking radiation, to obtain a complete picture of quantum gravity effects in black hole space-times.

Bibliography

[1] G. Lemaître, "The expanding universe," Ann. Soc. Sci. Bruxelles **A53** (1933) 51. Republished in Gen. Rel. Grav. **29** (1997) 641.

[2] R. C. Tolman, "Effect of inhomogeneity on cosmological models," Proc. Nat. Acad. Sci. **20** (1934) 169–176. Republished in Gen. Rel. Grav. **29** (1997) 935.

[3] H. Bondi, "Spherically symmetrical models in general relativity," Mon. Not. Roy. Astron. Soc. **107** (1947) 410–425.

[4] T. Thiemann, *Modern Canonical Quantum General Relativity*. Cambridge Monographs on Mathematical Physics. Cambridge University Press, 2007.

[5] C. Vaz, L. Witten and T. Singh, "Toward a midisuperspace quantization of Lemaitre-Tolman-Bondi collapse models," Phys. Rev. D **63** (2001) 104020, arXiv:gr-qc/0012053.

[6] C. Kiefer, J. Muller-Hill and C. Vaz, "Classical and quantum LTB model for the non-marginal case," Phys. Rev. D **73** (2006) 044025, arXiv:gr-qc/0512047.

[7] C. Kiefer and T. Schmitz, "Singularity avoidance for collapsing quantum dust in the Lemaître-Tolman-Bondi model," Phys. Rev. D **99** (2019) 126010, arXiv:1904.13220.

[8] A. Ashtekar and P. Singh, "Loop Quantum Cosmology: A Status Report," Class. Quant. Grav. **28** (2011) 213001, arXiv:1108.0893.

[9] A. Ashtekar, T. Pawlowski, and P. Singh, "Quantum Nature of the Big Bang: Improved dynamics," Phys. Rev. D **74** (2006) 084003, arXiv:gr-qc/0607039.

[10] L. Modesto, "Disappearance of black hole singularity in quantum gravity," Phys. Rev. D **70** (2004) 124009, arXiv:gr-qc/0407097.

[11] A. Ashtekar and M. Bojowald, "Quantum geometry and the Schwarzschild singularity," Class. Quant. Grav. **23** (2006) 391–411, arXiv:gr-qc/0509075.

[12] C. G. Boehmer and K. Vandersloot, "Loop Quantum Dynamics of the Schwarzschild Interior," Phys. Rev. D **76** (2007) 104030, arXiv:0709.2129.

[13] M. Campiglia, R. Gambini, and J. Pullin, "Loop quantization of spherically symmetric midi-superspaces: The Interior problem," AIP Conf. Proc. **977** (2008) 52–63, arXiv:0712.0817.

[14] D.-W. Chiou, "Phenomenological loop quantum geometry of the Schwarzschild black hole," Phys. Rev. D **78** (2008) 064040, arXiv:0807.0665.

[15] J. Brannlund, S. Kloster, and A. DeBenedictis, "The Evolution of Lambda Black Holes in the Mini-Superspace Approximation of Loop Quantum Gravity," Phys. Rev. D **79** (2009) 084023, arXiv:0901.0010.

[16] A. Joe and P. Singh, "Kantowski-Sachs spacetime in loop quantum cosmology: bounds on expansion and shear scalars and the viability of quantization prescriptions," Class. Quant. Grav. **32** (2015) 015009, arXiv:1407.2428.

[17] A. Corichi and P. Singh, "Loop quantization of the Schwarzschild interior revisited," Class. Quant. Grav. **33** (2016) 055006, arXiv:1506.08015.

[18] J. Cortez, W. Cuervo, H. A. Morales-Técotl, and J. C. Ruelas, "Effective loop quantum geometry of Schwarzschild interior," Phys. Rev. D **95** (2017) 064041, arXiv:1704.03362.

[19] J. Olmedo, S. Saini, and P. Singh, "From black holes to white holes: a quantum gravitational, symmetric bounce," Class. Quant. Grav. **34** (2017) 225011, arXiv:1707.07333.

[20] J. Ben Achour, F. Lamy, H. Liu, and K. Noui, "Polymer Schwarzschild black hole: An effective metric," EPL **123** (2018) 20006, arXiv:1803.01152.

[21] A. Ashtekar, J. Olmedo, and P. Singh, "Quantum Transfiguration of Kruskal Black Holes," Phys. Rev. Lett. **121** (2018) 241301, arXiv:1806.00648.

[22] N. Bodendorfer, F. M. Mele, and J. Münch, "Effective Quantum Extended Spacetime of Polymer Schwarzschild Black Hole," Class. Quant. Grav. **36** (2019) 195015, arXiv:1902.04542.

[23] E. Alesci, S. Bahrami, and D. Pranzetti, "Quantum gravity predictions for black hole interior geometry," Phys. Lett. **B797** (2019) 134908, arXiv:1904.12412.

[24] M. Assanioussi, A. Dapor, and K. Liegener, "Perspectives on the dynamics in a loop quantum gravity effective description of black hole interiors," Phys. Rev. D **101** (2020) 026002, arXiv:1908.05756.

[25] M. Bojowald and R. Swiderski, "Spherically symmetric quantum geometry: Hamiltonian constraint," Class. Quant. Grav. **23** (2006) 2129–2154, arXiv:gr-qc/0511108.

[26] R. Gambini and J. Pullin, "Black holes in loop quantum gravity: The Complete space-time," Phys. Rev. Lett. **101** (2008) 161301, arXiv:0805.1187.

[27] J. D. Reyes, "Spherically Symmetric Loop Quantum Gravity: Connection to Two-Dimensional Models and Applications to Gravitational Collapse,". PhD thesis, The Pennsylvania State University, 2009. Available online at https://etda.libraries.psu.edu/catalog/10349.

[28] R. Gambini and J. Pullin, "Loop quantization of the Schwarzschild black hole," Phys. Rev. Lett. **110** (2013) 211301, arXiv:1302.5265.

[29] R. Gambini, J. Olmedo, and J. Pullin, "Quantum black holes in Loop Quantum Gravity," Class. Quant. Grav. **31** (2014) 095009, arXiv:1310.5996.

[30] J. Ben Achour, S. Brahma, and A. Marciano, "Spherically symmetric sector of self dual Ashtekar gravity coupled to matter: Anomaly-free algebra of constraints with holonomy corrections," Phys. Rev. D **96** (2017) 026002, arXiv:1608.07314.

[31] M. Bojowald, S. Brahma, and D.-h. Yeom, "Effective line elements and black-hole models in canonical loop quantum gravity," Phys. Rev. D **98** (2018) 046015, arXiv:1803.01119.

[32] D.-W. Chiou, W.-T. Ni, and A. Tang, "Loop quantization of spherically symmetric midisuperspaces and loop quantum geometry of the maximally extended Schwarzschild spacetime," arXiv:1212.1265.

[33] R. Gambini, J. Olmedo and J. Pullin, "Spherically symmetric loop quantum gravity: analysis of improved dynamics," Class. Quant. Grav. **37** (2020) 205012, arXiv:2006.01513.

[34] J. G. Kelly, R. Santacruz and E. Wilson-Ewing, "Effective loop quantum gravity framework for vacuum spherically symmetric spacetimes," Phys. Rev. D **102** (2020) 106024, arXiv:2006.09302.

[35] R. Gambini, J. Pullin, and S. Rastgoo, "Quantum scalar field in quantum gravity: The vacuum in the spherically symmetric case," Class. Quant. Grav. **26** (2009) 215011, arXiv:0906.1774.

[36] R. Gambini, E. M. Capurro, and J. Pullin, "Quantum spacetime of a charged black hole," Phys. Rev. D **91** (2015) 084006, arXiv:1412.6055.

[37] M. Bojowald, S. Brahma, and J. D. Reyes, "Covariance in models of loop quantum gravity: Spherical symmetry," Phys. Rev. D **92** (2015) 045043, arXiv:1507.00329.

[38] M. Campiglia, R. Gambini, J. Olmedo, and J. Pullin, "Quantum self-gravitating collapsing matter in a quantum geometry," Class. Quant. Grav. **33** (2016) 18LT01, arXiv:1601.05688.

[39] V. Husain and O. Winkler, "Quantum Hamiltonian for gravitational collapse," Phys. Rev. D **73** (2006) 124007, arXiv:gr-qc/0601082.

[40] V. Husain, "Critical behaviour in quantum gravitational collapse," Adv. Sci. Lett. **2** (2009) 214, arXiv:0808.0949.

[41] S. Hossenfelder, L. Modesto, and I. Premont-Schwarz, "A Model for non-singular black hole collapse and evaporation," Phys. Rev. D **81** (2010) 044036, arXiv:0912.1823.

[42] F. Benitez, R. Gambini, L. Lehner, S. Liebling, and J. Pullin, "Critical collapse of a scalar field in semiclassical loop quantum gravity," Phys. Rev. Lett. **124** (2020) 071301, arXiv:2002.04044.

[43] A. Ashtekar, V. Taveras, and M. Varadarajan, "Information is Not Lost in the Evaporation of 2-dimensional Black Holes," Phys. Rev. Lett. **100** (2008) 211302, arXiv:0801.1811.

[44] A. Ashtekar, F. Pretorius, and F. M. Ramazanoglu, "Evaporation of 2-Dimensional Black Holes," Phys. Rev. D **83** (2011) 044040, arXiv:1012.0077.

[45] Y. Tavakoli, J. Marto, and A. Dapor, "Semiclassical dynamics of horizons in spherically symmetric collapse," Int. J. Mod. Phys. D **23** (2014) 1450061, arXiv:1303.6157.

[46] C. Bambi, D. Malafarina and L. Modesto, "Non-singular quantum-inspired gravitational collapse," Phys. Rev. D **88** (2013), 044009, arXiv:1305.4790.

[47] Y. Liu, D. Malafarina, L. Modesto and C. Bambi, "Singularity avoidance in quantum-inspired inhomogeneous dust collapse," Phys. Rev. D **90** (2014) 044040, arXiv:1405.7249.

[48] M. Christodoulou, C. Rovelli, S. Speziale, and I. Vilensky, "Planck star tunneling time: An astrophysically relevant observable from background-free quantum gravity," Phys. Rev. D **94** (2016) 084035, arXiv:1605.05268.

[49] M. Christodoulou and F. D'Ambrosio, "Characteristic Time Scales for the Geometry Transition of a Black Hole to a White Hole from Spinfoams," arXiv:1801.03027.

[50] J. Ben Achour, S. Brahma, S. Mukohyama and J. P. Uzan, "Towards consistent black-to-white hole bounces from matter collapse," JCAP **09**, 020 (2020), arXiv:2004.12977.

[51] E. Bianchi, M. Christodoulou, F. D'Ambrosio, H. Haggard, C. Rovelli, "White Holes as Remnants: A Surprising Scenario for the End of a Black Hole," Class. Quant. Grav. **35** (2018) 225003, arXiv:1802.04264.

[52] V. Husain and O. Winkler, "Quantum resolution of black hole singularities," Class. Quant. Grav. **22** (2005) L127–L134, arXiv:gr-qc/0410125.

[53] J. Ziprick and G. Kunstatter, "Dynamical Singularity Resolution in Spherically Symmetric Black Hole Formation," Phys. Rev. D **80** (2009) 024032, arXiv:0902.3224.

[54] M. Bojowald, J. D. Reyes, and R. Tibrewala, "Non-marginal LTB-like models with inverse triad corrections from loop quantum gravity," Phys. Rev. D **80** (2009) 084002, arXiv:0906.4767.

[55] A. Kreienbuehl, V. Husain, and S. S. Seahra, "Modified general relativity as a model for quantum gravitational collapse," Class. Quant. Grav. **29** (2012) 095008, arXiv:1011.2381.

[56] M. Bojowald, G. M. Paily, J. D. Reyes, and R. Tibrewala, "Black-hole horizons in modified space-time structures arising from canonical quantum gravity," Class. Quant. Grav. **28** (2011) 185006, arXiv:1105.1340.

[57] V. Husain and T. Pawlowski, "Time and a physical Hamiltonian for quantum gravity," Phys. Rev. Lett. **108** (2012) 141301, arXiv:1108.1145.

[58] D. Arruga, J. Ben Achour and K. Noui, "Deformed General Relativity and Quantum Black Holes Interior," Universe **6** (2020) 39, arXiv:1912.02459.

[59] P. D. Lasky, A. W. Lun, and R. B. Burston, "Initial value formalism for dust collapse," ANZIAM Journal **49** (2007) 205, arXiv:gr-qc/0606003.

[60] K. Giesel, J. Tambornino, and T. Thiemann, "LTB spacetimes in terms of Dirac observables," Class. Quant. Grav. **27** (2010) 105013, arXiv:0906.0569.

[61] V. Taveras, "Corrections to the Friedmann Equations from LQG for a Universe with a Free Scalar Field," Phys. Rev. D **78** (2008) 064072, arXiv:0807.3325.

[62] C. Rovelli and E. Wilson-Ewing, "Why are the effective equations of loop quantum cosmology so accurate?," Phys. Rev. D **90** (2014) 023538, arXiv:1310.8654.

[63] K. Vandersloot, "Loop quantum cosmology and the k = - 1 RW model," Phys. Rev. D **75** (2007) 023523, arXiv:gr-qc/0612070.

[64] P. Singh and E. Wilson-Ewing, "Quantization ambiguities and bounds on geometric scalars in anisotropic loop quantum cosmology," Class. Quant. Grav. **31** (2014) 035010, arXiv:1310.6728.

[65] A. Ashtekar and E. Wilson-Ewing, "Loop quantum cosmology of Bianchi type II models," Phys. Rev. D **80** (2009) 123532, arXiv:0910.1278.

[66] J. R. Oppenheimer and H. Snyder, "On Continued gravitational contraction," Phys. Rev. **56** (1939) 455–459.

[67] C. Rovelli and F. Vidotto, "Planck stars," Int. J. Mod. Phys. **D23** (2014) 1442026, arXiv:1401.6562.

[68] H. M. Haggard and C. Rovelli, "Quantum-gravity effects outside the horizon spark black to white hole tunneling," Phys. Rev. D **92** (2015) 104020, arXiv:1407.0989.

[69] C. Barcelo, R. Carballo-Rubio, L. J. Garay and G. Jannes, "The lifetime problem of evaporating black holes: mutiny or resignation," Class. Quant. Grav. **32** (2015) 035012, arXiv:1409.1501.

[70] D. N. Page, "Average entropy of a subsystem," Phys. Rev. Lett. **71** (1993) 1291–1294, arXiv:gr-qc/9305007.

[71] T. Schmitz, "Towards a quantum Oppenheimer-Snyder model," Phys. Rev. D **101** (2020) 026016, arXiv:1912.08175.

[72] W. Piechocki and T. Schmitz, "Quantum Oppenheimer-Snyder model," Phys. Rev. D **102** (2020) 046004, arXiv:2004.02939.

[73] D. M. Eardley, "Death of White Holes in the Early Universe," Phys. Rev. Lett. **33** (1974) 442–444.

[74] C. Barceló, R. Carballo-Rubio, and L. J. Garay, "Black holes turn white fast, otherwise stay black: no half measures," JHEP **01** (2016) 157, arXiv:1511.00633.

[75] A. Barrau, B. Bolliet, F. Vidotto and C. Weimer, "Phenomenology of bouncing black holes in quantum gravity: a closer look," JCAP **02** (2016) 022, arXiv:1507.05424.

[76] F. Vidotto, "Measuring the last burst of non-singular black holes," Found. Phys. **48** (2018) 1380, arXiv:1803.02755.

[77] R. Carballo-Rubio, F. Di Filippo, S. Liberati and M. Visser, "Phenomenological aspects of black holes beyond general relativity," Phys. Rev. D **98** (2018) 124009, arXiv:1809.08238.

Chapter 4

On the fate of quantum black holes

4.1 Introduction

In general relativity, collapsing matter may form a black hole depending on the initial conditions [1, 2]. The simplest black hole in classical general relativity is spherically symmetric, singular, and stable. In the semiclassical theory where quantum fields propagate on classical space-times, black holes are unstable due to Hawking radiation [3]. The endpoint of the process of Hawking evaporation remains unknown—it is expected that a theory of quantum gravity will answer this question by resolving the singularity and providing dynamics past the classically singular region.

One approach to quantum gravity is loop quantum gravity (LQG), a non-perturbative attempt to quantize general relativity using a background-independent Hilbert space where the inner product does not utilize the space-time metric [4–6]. Solving the full quantum dynamics in LQG currently remains out of reach, but there is a substantial body of work on symmetry-reduced models, including applications to homogeneous cosmological space-times known as loop quantum cosmology (LQC) [7], and to inhomogeneous spherically symmetric models including black hole space-times [8].

There are two main inputs from LQG in studying these simpler systems, the holonomy and inverse triad operators. These arise due to the quantization procedure used: (i) the connection and its curvature do not exist as operators and must be defined using the holonomy operators, and (ii) a well-defined inverse triad operator is required for constructing the constraint operators. These two features lead to what are respectively called "holonomy" and "inverse triad" corrections.

In symmetry-reduced models these features arise through polymer quantization. Denoting the phase space configuration variables q_j (corresponding to the connection) and p_j (corresponding to spatial metric degrees of freedom), the polymer quantization prescription is based on elementary operators corresponding to the (non-differentiable) complex exponential $\hat{U}_\mu(q_j) = \widehat{\exp(i\mu q_j)}$ and the operator $\hat{p}_j$; (the inverse momentum operators $\widehat{p_j^{-1}}$ corresponding to the inverse triad operator of LQG is defined using these elementray operators). The parameter μ in the operator $\hat{U}_\mu(q_j)$ corresponds to the coordinate length of a holonomy segment. This parameter is chosen by requiring that the holonomies appearing in curvature operators must have a physical length of the order of the Planck length $\ell_{\rm Pl}$. This requirement is implemented by relating the coordinate length μ to a physical length using the spatial metric. Since the spatial metric can be reconstructed from p_j it follows that $\mu = \mu(p_j)$; this prescription is known in the literature (for historical reasons) as the $\bar{\mu}$ scheme or "improved dynamics".

In LQC, these methods have successfully led to the resolution of the big-bang singularity in classical general relativity, replacing it with a non-singular bounce in homogeneous cosmological space-times [7, 9].

The application of LQG techniques to black hole space-times falls into three main categories. Works in the first category use the classical isometry between the black hole interior and the Kantowski-Sachs homogeneous space-time. This suggests a description of the black hole interior where LQC methods can be applied directly [10–28]. Although simple, this approach has several drawbacks: the isometry between

the Schwarzschild interior and the Kantowski-Sachs space-time may not hold in full quantum gravity (it is known to fail for some modified gravity theories [29]); the isometry requires the presence of an outer horizon and assumes there is no inner horizon; and the standard improved dynamics scheme as applied in [12] fails near the horizon (likely due to the spatial coordinates becoming null).

In the second category are works that use coordinates in spherical symmetry where the radial coordinate remains spacelike throughout the entire space-time, making it is possible to treat the interior and exterior of the black hole on an equal footing for quantization [30–38]. Building on earlier works [12, 39], the improved dynamics scheme was recently applied to vacuum spherically symmetric space-times [40–42]. These works provide a framework that can be used to study the entire black hole space-time (not just the interior). It has the advantage that the correct classical limit is recovered where the space-time curvature is small compared to the Planck scale.

There is also work in a third category which aims for a full LQG treatment of states potentially corresponding to black holes in canonical LQG [43–45], in the covariant spin foam approach [46–51], and in the group field theory reformulation of LQG [52]. Although it is challenging to include inhomogeneous matter fields and make contact with semiclassical physics, these works provide some guidance for recovering low curvature classical black hole space-times from full quantum gravity.

To determine the fate of a black hole in quantum gravity, it is important to include matter so that the entire process from gravitational collapse to black hole formation to its entire subsequent evolution is captured. Initial steps in this direction used Oppenheimer-Snyder type models where the interior is an FRLW cosmology [53–58], and thin shells [59–61]. Beyond this there is work on inhomogeneous models including a scalar field with holonomy corrections [62] or with inverse triad corrections [63–65], a dust field with inverse triad corrections [66, 67], and Wheeler-DeWitt canonical quantization [68].

A generic feature of these works is that, as in cosmology, the singularity is resolved and matter bounces when space-time curvature reaches the Planck scale. This is seen in LQG [53–58] and in other approaches [69–74, 93]; a model-independent view is studied in [75], and a recent review is [76].

It may also be possible to understand the bounce generated by quantum gravity effects as a transition from a black hole to a white hole [77, 78], with potential observational consequences [79–81]. However, since white holes are known to be unstable [82, 83] this scenario requires further study. An additional feature of non-singular black holes in classical gravity is mass inflation at inner horizons [84–86]. We will see that the model we consider here is free of these two problems.

Building on earlier work on the vacuum Schwarzschild space-time [41], the improved dynamics scheme was applied to the entire space-time of a spherically symmetric inhomogeneous dust model, and used to study the quantization of the Oppenheimer-Snyder model [87]. It was found that quantum gravity effects halt the collapse, resolve the singularity and cause a bounce; the dust then expands outwards until the outer horizon disappears. This led to an estimate of $M^2/m_{\rm Pl}$ for the lifetime of this quantum black hole.

In this paper, and the companion letter [88], we revisit this inhomogeneous dust model to define the quantum theory in full. We then derive the effective equations with quantum corrections for the theory; these are two coupled partial differential equations. We numerically solve the effective equations to a high degree of accuracy for a variety of initial conditions. Our solutions extend all previous works by describing evolution from initial collapse to the formation of apparent horizons, to their subsequent disappearance following a bounce and re-expansion of matter. This provides a complete lifetime scenario of black holes with matter. As further developments to the companion letter [88], this paper contains (i) significant calculations concerning the quantum theory and the derivation of the effective dynamics, (ii) analytic results for Oppenheimer-Snyder

and thin shell solutions, (iii) an in-depth description of the main features in the conformal diagram, and (iv) a discussion on some implications for the information loss problem and possible astrophysical consequences.

An important feature and common point of concern for dust collapse models in classical gravity is the formation of caustics, also referred to as "shell-crossing singularities." This feature is often viewed as undesirable; it can be avoided in the classical theory by restricting the initial data so the central singularity is reached before caustic formation [89–92]. The same restriction may also be imposed in quantized models [61]; however, such restrictions are undesirable as they limit the exploration of possible solutions.

In a quantized theory that has the potential to resolve singularities, caustics are unavoidable: ingoing matter trajectories will inevitably cross outgoing ones during matter evolution past a bounce. For this reason it is essential to avoid excising potential caustics "by hand" and instead permit so-called "weak solutions" [94, 95]. Such solutions are an essential part of non-linear wave dynamics. A common feature of weak solutions is a shock wave, corresponding to a discontinuity in the field. In the gravitational case, the shock wave corresponds to a discontinuity in the metric, and therefore in the geometry of space-time.

The effective equation we derive and solve numerically is a non-linear $1 + 1$ dimensional continuity equation. We solve this equation numerically using the well-known Godunov method [96]; this is one of a class of so-called "finite volume" methods for solving non-linear continuity equations. This method generates weak numerical solutions past the points of characteristic crossing, resulting in shock wave formation. Using this scheme we simulate the collapse of initial matter configurations where no horizon is initially present. We find generically that as the dust profile falls inward, a pair of apparent horizons form when the Schwarzschild radius is reached. The collapse continues until the space-time curvature reaches the Planck scale, and matter bounces

outward as a shock wave; the shock is a discontinuity in the metric. The shock wave moves outward together with the inner apparent horizon until they reach the outer horizon located at the Schwarzschild radius; at this point both apparent horizons merge and disappear. To an outside observer this would appear as a spherical shock wave emanating from a horizon.

Our numerical procedure allows a calculation of the black hole lifetime, defined as the time between the formation and disappearance of the outermost apparent horizon as measured by a distant observer. After evolutions spanning two orders of magnitude in data mass M, we find that this lifetime is $T \sim M^2/m_{\rm Pl}$. This extends and reinforces the estimate obtained for Oppenheimer-Snyder collapse that yielded the same result [87]. Furthermore, from the evolution of a double peaked Gaussian data, we demonstrate that a collapsing pulse followed by another does not result in recollapse, and does not cause mass inflation at the inner horizons; in all cases the final state is a single outgoing shock wave.

The structure of the paper is as follows: in Sec. 4.2 we review the classical theory of Lemaître-Tolman-Bondi space-times; in Sec. 4.3 we define the quantum theory; in Sec. 4.4 we derive the effective dynamics from the quantum theory, consider some simple cases and determine the conformal diagram for dust collapse in this model; in Sec. 4.5 we summarize the numerical method we use and present our results; in Sec. 4.6 we discuss potential implications of our work including some consequences for the information loss problem; and we conclude in Sec. 4.7 with a summary and outlook.

4.2 Classical theory

In this section we review the class of Lemaître-Tolman-Bondi (LTB) metrics and its Hamiltonian theory in the connection-triad variables as a prelude to studying the

quantum theory.

4.2.1 Hamiltonian Lemaître-Tolman-Bondi dynamics

LTB space-times are spherically symmetric solutions of Einstein gravity with a pressureless dust field that provide simple models for stellar collapse and non-linear cosmological perturbations. The metric is often written in the diagonal form [97]

$$\mathrm{d}s^2 = -\mathrm{d}t^2 + \frac{(\partial_r R(r,t))^2}{1+\mathcal{E}(r)}\mathrm{d}r^2 + R(r,t)^2\mathrm{d}\Omega^2, \tag{4.1}$$

where $\mathrm{d}\Omega^2 = \mathrm{d}\theta^2 + \sin^2\theta\,\mathrm{d}\phi^2$. The dust stress energy tensor is $T_{\mu\nu} = \rho(x,t)\,u_\mu u_\nu$, where $u_\mu = \partial_\mu T$ is the 4-velocity of the dust field and T is the dust field variable.

Although the coordinate system (4.1) is commonly used, a different set of coordinates based on a generalization of the Painlevé-Gullstrand coordinates of the Schwarzschild space-time is better suited for a Hamiltonian description of the dynamics [95]. Introducing the coordinate $x = R(r,t)$, the metric becomes

$$\mathrm{d}s^2 = -\mathrm{d}t^2 + \frac{1}{1+\mathcal{E}(x,t)}\left(\mathrm{d}x + N^x\mathrm{d}t\right)^2 + x^2\mathrm{d}\Omega^2, \tag{4.2}$$

with $N^x = -\partial_t R$. The Schwarzschild solution in Painlevé-Gullstrand coordinates is recovered in the vacuum $T_{\mu\nu} = 0$ case [95].

For the quantum theory it is convenient to use the connection-triad Hamiltonian formulation minimally coupled to dust. In spherical symmetry, the densitized triads have two independent components corresponding to the radial and angular directions,

$$E^x_1 = E^a\sin\theta, \qquad E^\theta_2 = E^b\sin\theta, \qquad E^\phi_3 = E^b. \tag{4.3}$$

The canonically conjugate Ashtekar-Barbero connection $A^i_a = \Gamma^i_a + \gamma K^i_a$ is defined in terms of the spin-connection Γ^i_a and the extrinsic curvature K^i_a, and γ is the Barbero-

Immirzi parameter [98, 99] (note that the classical theory is independent of the value of γ, but not the quantum theory). In spherical symmetry, the Ashtekar-Barbero connection can be parametrized as

$$A_a^i \tau_i dx^a = a\,\tau_1\,dx + \left(b\,\tau_2 - \frac{\partial_x E^a}{2E^b}\,\tau_3\right) d\theta + \left(-\cot\theta\tau_1 + \frac{\partial_x E^a}{2E^b}\tau_2 + b\,\tau_3\right)\sin\theta\,d\phi. \quad (4.4)$$

As a function of densitized triads, the spherically symmetric metrics take the form

$$\mathrm{d}s^2 = -N^2\mathrm{d}\tau^2 + \frac{(E^b)^2}{E^a}(\mathrm{d}x + N^x\mathrm{d}t)^2 + E^a\mathrm{d}\Omega^2, \quad (4.5)$$

where $N(x,t)$ and $N^x(x,t)$ are the lapse function and radial shift vector.

In the general case E^a, E^b, a, b, N and N^x, as well as T and its momentum p_T, are all functions of x and t. To make contact with the metric (4.2) we impose the radial gauge fixing $E^a = x^2$, which sets $N^x = -b/\gamma$ to ensure the gauge is preserved by the dynamics [41]. Additionally it is convenient to fix the dust time gauge $T = t$ which requires $N = 1$ as the gauge-fixing condition [100]. With these gauge choices that fix a, E^a, T, p_T, there remains only a two-dimensional phase space parametrized by (b, E^b), and the metric (4.5) exactly matches the form given in (4.2),

$$\mathrm{d}s^2 = -\mathrm{d}t^2 + \frac{(E^b)^2}{x^2}\left(\mathrm{d}x - \frac{b}{\gamma}\,\mathrm{d}t\right)^2 + x^2\mathrm{d}\Omega^2, \quad (4.6)$$

with $(E^b)^2/x^2 = 1/(1+\mathcal{E})$.

Since all gauge freedom is fixed at this stage, the constraints have been solved and there only remains the physical canonical action [41, 87]

$$S_{GF} = \int \mathrm{d}t \int \mathrm{d}x \left(\frac{\dot{b}E^b}{G\gamma} - \mathcal{H}_{\mathrm{phys}}\right), \quad (4.7)$$

where

$$\mathcal{H}_{\mathrm{phys}} = -\frac{1}{2G\gamma}\left[\frac{|E^b|}{\gamma x}\partial_x(xb^2) + \frac{\gamma\,|E^b|}{x} + \frac{2\gamma x^2}{(E^b)^2}\partial_x\,|E^b| - \frac{3\gamma x}{|E^b|}\right] \quad (4.8)$$

is the physical Hamiltonian that generates evolution with respect to physical time T (which has been gauge-fixed to $T = t$). The third and fourth terms can be combined by integrating by parts the third term, keeping the total derivative the result is

$$\mathcal{H}_{\rm phys} = -\frac{1}{2G\gamma}\left[\frac{\left|E^b\right|}{\gamma x}\partial_x(xb^2) + \frac{\gamma\left|E^b\right|}{x} + \frac{\gamma x}{|E^b|} - 2\gamma\,\partial_x\left(\frac{x^2}{|E^b|}\right)\right]. \tag{4.9}$$

The total derivative does not affect the equations of motion, but it is important when calculating the energy density of the dust through $\mathcal{H}_{\rm phys}$, see below.

The gauge-fixed action (4.7) also determines the symplectic structure for the remaining phase space variables,

$$\{b(x_1), E^b(x_2)\} = G\gamma\ \delta(x_1 - x_2). \tag{4.10}$$

The dust energy density is related to the physical Hamiltonian by [87]

$$\rho = -\ \frac{\mathcal{H}_{\rm phys}}{4\pi x\ |E^b|}, \tag{4.11}$$

and the total mass contained within a radius x is

$$m(x,t) = 4\pi\int_0^x \mathrm{d}\tilde{x}\ \tilde{x}\ \left|E^b\right|\rho(\tilde{x},t) = -\int_0^x \mathrm{d}\tilde{x}\,\mathcal{H}_{\rm phys}(\tilde{x},t). \tag{4.12}$$

The equations of motion follow from $\dot{f} = \{f, \int dx\ \mathcal{H}_{\rm phys}\}$, assuming $E^b > 0$ they are

$$\dot{E^b} = \frac{bE^b}{\gamma x} - \frac{b}{\gamma}\,\partial_x E^b, \tag{4.13}$$

$$\dot{b} = \frac{\gamma x}{2(E^b)^2} - \frac{1}{2\gamma x}\Big(2xb\partial_x b + b^2 + \gamma^2\Big). \tag{4.14}$$

4.2.2 Marginally bound solutions

A particularly simple family of LTB metrics are those with $\mathcal{E} = 0$ in the metric (4.2), referred to in the literature as marginally bound solutions. Physically these correspond to solutions where the energy of all dust particles is zero (with their positive kinetic energy cancelled by their negative gravitational potential energy, and both going to zero at infinity). There are many other interesting families of LTB metrics with $\mathcal{E} \neq 0$, but as a first step in studying LTB space-times in effective LQG we focus here on the marginally bound class of solutions. In triad variables these correspond to $E^b = x$, which is readily seen as a solution to the E^b equation of motion, and the remaining canonical equation for $b(x,t)$ simplifies to

$$\dot{b} + \frac{1}{2\gamma x}\partial_x(xb^2) = 0. \tag{4.15}$$

The dust energy density for this class of solutions is

$$\rho(x,t) = \frac{1}{8\pi G\gamma^2 x^2}\partial_x\left(xb^2\right), \tag{4.16}$$

and the mass function is

$$m(x,t) = 4\pi\int_0^x \mathrm{d}\tilde{x}\ \tilde{x}^2\rho(\tilde{x},t). \tag{4.17}$$

As an aside, note that the equation of motion for b may also be rewritten in terms of the mass function [95]

$$\dot{m} + \sqrt{\frac{2Gm}{x}}\ \partial_x m = 0. \tag{4.18}$$

The dynamics for this system can be solved by the method of characteristics by writing $b = b(x(\lambda), t(\lambda))$ to transform (4.15) into the equations

$$\frac{\mathrm{d}t}{\mathrm{d}\lambda} = 1, \qquad \frac{\mathrm{d}x}{\mathrm{d}\lambda} = \frac{b(\lambda)}{\gamma}, \qquad \frac{\mathrm{d}b}{\mathrm{d}\lambda} = -\frac{b^2(\lambda)}{2\gamma x(\lambda)}. \tag{4.19}$$

The first two equations determine the characteristic curves in the (x, t) plane, while the third gives the value of b along these curves. These may be solved with the initial conditions

$$t(\lambda = 0) = 0, \qquad x(\lambda = 0) = x_0, \qquad b(\lambda = 0) = b_0(x_0), \tag{4.20}$$

where $b_0(x) = b(x, 0)$ is the initial data for b; it may be determined from an initial profile for the dust energy density $\rho_0(x)$ by inverting (4.16).

It is straightforward to solve these coupled ODEs: the first gives $\lambda = t$, while the equation for $\mathrm{d}(x^{-1}b)/\mathrm{d}\lambda$ is separable, leaving a final ODE which is also separable once b/x is known. The solution for $x(\lambda)$ and $b(\lambda)$ is

$$x(\lambda) = x_0 \left(1 + \frac{3b_0(x_0)}{2\gamma x_0}\lambda\right)^{2/3}, \qquad b(\lambda) = \frac{b_0(x_0)}{\left(1 + \frac{3b_0(x_0)}{2\gamma x_0}\lambda\right)^{1/3}}. \tag{4.21}$$

By following different characteristic curves (each curve labeled by its initial radial position x_0), it is possible to determine $b(x, t)$ by inverting $x(\lambda, x_0)$—for this system inverting $t(\lambda, x_0)$ is trivial.

Depending on the initial conditions, characteristic curves starting at different radial points x_0 can intersect; if this happens the solution for b becomes multivalued at these points since the value of b on different curves will typically differ. The space-time points where characteristic curves intersect are known as shell-crossings. Shell-crossings are characterized by the condition $\partial_{x_0} x(\lambda, x_0) = 0$, these are points where the determinant of the Jacobian associated to the transformation $(\lambda, x_0) \to (t, x)$ becomes zero, and $x(\lambda, x_0)$ ceases to be invertible.

The time it takes before a shell-crossing develops depends on the initial profile $b_0(x)$, and is given by

$$t_S = \frac{-2\gamma x_0}{b_0 + 2x_0 \partial_{x_0} b_0}. \tag{4.22}$$

It is possible to choose initial conditions to ensure shell-crossings never occur [90], but another approach is to extend the equations of motion to allow for weak solutions [94]. This is commonly required for non-linear wave equations like (4.15) and leads to the observable phenomena of shock waves. For this system, the shock wave will form in the gravitational field, i.e., the metric.

4.2.3 Weak solutions and shock waves

Weak solutions arise in many contexts, and consist of solutions to an integrated form of the equations of motion that cannot satisfy the original n^{th}-order differential equations since they are not n times differentiable. Some examples in general relativity are the Israel junction conditions for distributional matter sources such as thin shells [101], and the Dray-'t Hooft shock wave [102].

In general, for systems described by flow equations with velocities that depend on the field, it is common for characteristic curves to intersect, leading to a breakdown of the evolution generated by the differential equations beyond the intersection point. The solution to this problem is to seek "weak solutions" that solve an integrated form of the differential equation.

It can often happen that a weak solution is discontinuous, and then the discontinuity is known as a shock wave. Typically, shock waves propagate dynamically; a simple example is a sonic boom. Many physical phenomena exhibit shock waves, which commonly arise as weak solutions to non-linear wave equations.

To review and illustrate the basic idea, consider the non-linear conservation equation

$$\dot{u} + \partial_x f(u, x) = 0, \tag{4.23}$$

where $f(u, x)$ is a non-linear function of u, and potentially depends on x as well.

If $u(x,t)$ satisfies the integral equation

$$\int_0^\infty \mathrm{d}t \int_{-\infty}^\infty \mathrm{d}x \Big[(\partial_t \varphi)u + (\partial_x \varphi) f(u,x)\Big] = -\int_{-\infty}^\infty \mathrm{d}x\ \varphi(x,0)u(x,0) \tag{4.24}$$

for any test function $\varphi(x,t)$ of compact support that is continuously differentiable, then u is called a weak solution of this conservation equation. If discontinuities in u only arise along the x-axis (as would be expected for a physical system with a well-posed initial value problem), it is sufficient to consider the integral equation

$$\frac{\mathrm{d}}{\mathrm{d}t}\int_{x_1}^{x_2} \mathrm{d}x\ u + \int_{x_1}^{x_2} \mathrm{d}x\ \partial_x f(u,x) = \frac{\mathrm{d}}{\mathrm{d}t}\int_{x_1}^{x_2} \mathrm{d}x\ u + f(u(x_2),x_2) - f(u(x_1),x_1) = 0, \tag{4.25}$$

for any interval $[x_1, x_2]$ of interest.

A discontinuity in $u(x)$ propagates as a shock wave with a speed determined by the integral equation. To see this, consider (4.25) when there is a discontinuity at $x = L(t)$ in the interval $[x_1, x_2]$. Then the integral splits into two parts to give

$$\frac{\mathrm{d}}{\mathrm{d}t}\int_{x_1}^{L} \mathrm{d}x\ u + \frac{\mathrm{d}}{\mathrm{d}t}\int_{L}^{x_2} \mathrm{d}x\ u + f(u(x_2),x_2) - f(u(x_1),x_1) = 0; \tag{4.26}$$

expanding the first term gives

$$\frac{\mathrm{d}L}{\mathrm{d}t}\cdot \lim_{x\to L^-} u + \int_{x_1}^{L} \mathrm{d}x\ \partial_t u + \frac{\mathrm{d}L}{\mathrm{d}t}\cdot \lim_{x\to L^+} u + \int_{L}^{x_2} \mathrm{d}x\ \partial_t u + f(u(x_2),x_2) - f(u(x_1),x_1) = 0, \tag{4.27}$$

where $x \to L^+$ and $x \to L^-$ denote the limits from above and below the discontinuity at $x = L$ respectively. Taking the limits $x_1 \to L^-$ and $x_2 \to L^+$, the contributions from the integrals go to 0, and solving for $\mathrm{d}L/\mathrm{d}t$ gives the Rankine-Hugoniot condition

$$\frac{\mathrm{d}L}{\mathrm{d}t} = \frac{[f(u,x)]}{[u]}, \tag{4.28}$$

where $[g] = \lim_{x\to L^+} g(x) - \lim_{x\to L^-} g(x)$ denotes the amplitude of the discontinuity

in the function $g(x)$ at $x = L$.

Returning now to LTB space-times, we are interested in weak solutions that permit discontinuities in the metric due to shell-crossings [94, 95]. The equation of motion (4.15) can be rewritten in the form of a conservation equation with $u = xb$ and $f(u, x) = u^2/2\gamma x$. It gives the integral equation

$$\frac{\mathrm{d}}{\mathrm{d}t}\int_{x_1}^{x_2} \mathrm{d}x\ xb(x,t) + \frac{x_2 b(x_2,t)^2}{2\gamma} - \frac{x_1 b(x_1,t)^2}{2\gamma} = 0, \tag{4.29}$$

and the Rankine-Hugoniot condition gives the propagation speed of a dust shock wave:

$$\frac{\mathrm{d}L}{\mathrm{d}t} = \frac{L[b^2]}{2\gamma L[b]} = \frac{b(L^+) + b(L^-)}{2\gamma}. \tag{4.30}$$

In general, numerics are necessary to solve the dynamics of a non-linear wave equation of the general form (4.23); we discuss the Godunov numerical scheme in Sec. 4.5.

Finally, we note that different prescriptions to find weak solutions are not guaranteed to be equivalent, since there are (for functions with discontinuities) many inequivalent integral forms for any given differential equation that can be obtained by non-linear field redefinitions. In particular, the weak solutions derived from (4.29) are inequivalent to the Israel junction conditions—although in both cases the induced three-dimensional metric across the discontinuous surface will be continuous, the Israel junction conditions impose an additional relation on the trace-free extrinsic curvature, while on the other hand it is a relation on b that is implicitly imposed by (4.29). We leave a more detailed exploration of weak solutions in classical general relativity for future work; in the remainder of this paper we consider weak solutions to (4.29) (and its equivalent for the LQC effective equations).

4.2.4 Discretization

To pass to the quantum theory, it is convenient to start from a discretization of the classical theory. There are of course many discretizations that are possible and equivalent in the limit that the discretization parameter becomes infinitesimally small. Here, for the sake of simplicity we will choose a rather direct discretization.

First, we introduce a lattice in the radial direction denoted by x_n, with $x_0 = 0$ and the width of each interval given by $w_n = x_{n+1} - x_n > 0$. It is possible to set w_n to be the same for all n, but that is not necessary here; we will however assume that w_n is fixed for each n and does not evolve dynamically.

Given this discretization, we further assume that all fields are constant in each interval $[x_n, x_{n+1})$, and approximate derivatives by

$$\partial_x f(x) \to \frac{f(x_{n+1}) - f(x_n)}{w_n}. \tag{4.31}$$

With these choices, the action for the discretized theory becomes

$$S_{GF}^{\rm disc} = \int {\rm d}t \sum_n \left(w_n \frac{\dot{b}_n E^b_n}{G\gamma} - \mathcal{H}_n^{\rm disc} \right), \tag{4.32}$$

where $b_n = b(x_n), E^b_n = E^b(x_n)$ and (for $n \neq 0$)

$$\mathcal{H}_n^{\rm disc} = -\frac{w_n}{2G\gamma} \left[\frac{\left|E^b_n\right|}{\gamma x_n} \cdot \frac{x_{n+1} b^2_{n+1} - x_n b^2_n}{w_n} + \frac{\gamma \left|E^b_n\right|}{x_n} + \frac{\gamma x_n}{\left|E^b_n\right|} \right], \tag{4.33}$$

dropping the boundary term.

Note that the same general expression cannot be used for $\mathcal{H}_0^{\rm disc}$ due to the presence of $x_0 = 0$ in some denominators. Various regularizations to address this difficulty are possible; looking ahead to the quantum theory where there are inverse triad operators, we simply set $\mathcal{H}_0^{\rm disc} = 0$.

The Poisson brackets for the discretized variables are now

$$\{b_m, E^b_n\} = \frac{G\gamma}{w_n}\,\delta_{mn}, \tag{4.34}$$

and the equations of motion (for $n \geq 2$ and assuming $E^b > 0$) are

$$\dot{E}^b_n = -\frac{x_n b_n}{\gamma} \cdot \left(\frac{E^b_n}{w_n x_n} - \frac{E^b_{n-1}}{w_{n-1} x_{n-1}} \right), \tag{4.35}$$

$$\dot{b}_n = -\frac{x_{n+1} b^2_{n+1} - x_n b^2_n}{2\gamma w_n x_n} - \frac{\gamma}{2x_n} + \frac{\gamma x_n}{2(E^b_n)^2}. \tag{4.36}$$

In the equations of motion for $n = 1$, there are no contributions from $n = 0$, while the equations of motion for $n = 0$ are trivial, $\dot{E}^b_0 = 0$ and $\dot{b}_0 = 0$, at least for the choice $\mathcal{H}^{\rm disc}_0 = 0$.

Finally, the energy density is given by

$$\rho_n = -\frac{\mathcal{H}^{\rm disc}_n}{4\pi w_n x_n |E^b_n|} - \frac{1}{4\pi w_n x_n |E^b_n|} \cdot \frac{1}{G w_n} \left(\frac{x^2_{n+1}}{|E^b_{n+1}|} - \frac{x^2_n}{|E^b_n|} \right), \tag{4.37}$$

(the second term is the total derivative that was dropped in (4.33) but is necessary to calculate ρ_n), while the total mass within a radius x_n is

$$m_n = 4\pi \sum_{p=0}^{n} w_p x_p |E^b_p| \rho_p. \tag{4.38}$$

4.3 Quantum theory

The quantum theory for LTB space-times defined here is based upon the methods of loop quantum cosmology (LQC). Starting from the discretized classical theory given in Sec. 4.2.4, an LQC Hilbert space is defined at each point x_n in the radial lattice; the total Hilbert space for LTB space-times is given by their tensor product. (Note that due to the gauge-fixing which gives a physical Hamiltonian, there is no distinction

between a kinematical and physical Hilbert space in this case.) Then, the dynamics are generated by the Hamiltonian operator.

4.3.1 Hilbert space

LQC techniques were first developed for cosmological space-times that are homogeneous and therefore have a finite number of degrees of freedom. This is not the case for LTB space-times, which allow fields that can depend on the radial coordinate. This adds a certain degree of complexity that is not present in the treatment of Friedman-Lemaître-Robertson-Walker (FLRW), Bianchi, or Kantowski-Sachs space-times.

To address this problem, we introduce an arbitrary discretization of the radial coordinate x as explained in Sec. 4.2.4. At each node n, we can define a Hilbert space $\mathbb{H}_n$ following the standard methods of LQC, and then the full Hilbert space $\mathbb{H}$ for LTB space-times will be given by the tensor product $\mathbb{H} = \otimes\mathbb{H}_n$.

As usual in LQC, the elementary operators for each Hilbert space $\mathbb{H}_n$ correspond to densitized triads and complex exponentials of components of the Ashtekar-Barbero connection, from which it is possible to construct holonomies along coordinate edges.

To understand the relation between complex exponentials of b and holonomies, recall that after the gauge-fixing imposed on the classical theory, it is the angular component of A^i_a that has not been gauge-fixed and therefore we are interested in holonomies along paths tangent to, for example, $(\partial/\partial\theta)^a$ along the equator $\phi = \pi/2$; in general the paths of interest are portions of a great circle at different radii x_n. We use the 'K' loop quantization [103, 104] that is based on the 'extrinsic curvature holonomy',

$$\begin{aligned} h_{n,\theta}(\mu) &= \exp\left(\int_0^\mu \gamma K^i_\theta(x_n)\tau_i \, d\theta\right) \\ &= \exp\left(\int_0^\mu b_n \tau_2 \, d\theta\right) = \cos\left(\frac{\mu b_n}{2}\right)\mathbb{I} + 2\sin\left(\frac{\mu b_n}{2}\right)\tau_2, \end{aligned} \tag{4.39}$$

where μ is the coordinate length of the holonomy's path (in this case μ is the angle covered by the portion of the great circle). To be concrete, here we consider the great circle $\phi = \pi/2$, but the result would be similar for any other path along a portion of a great circle. The τ^i are a basis in the fundamental representation of the $\mathfrak{su}(2)$ Lie algebra with $\tau^i\tau^j = \frac{1}{2}\epsilon^{ij}{}_k\tau^k - \frac{1}{4}\delta^{ij}\mathbb{I}$, and $\mathbb{I}$ is the 2×2 identity matrix. Importantly, due to spherical symmetry the path integral along θ is trivial and easily evaluated—this would not be true for paths in the radial direction, but these are not needed in this case due to the gauge-fixing that has been imposed before quantization.

This defintion of the holonomy operator uses the fundamental representation of $\mathfrak{su}(2)$, also commonly utilized in LQC. Other choices are in principle possible and have been explored in LQC [105–107]. But the key physical feature of singularity avoidance that is central to our results is not affected by this choice: the curvature operator constructed from the holonomy is a bounded operator regardless of the representation of $\mathfrak{su}(2)$.

The non-trivial dependence on b_n in (4.39) is fully captured by the complex exponentials

$$\mathcal{N}_n(\mu) = \exp(i\mu b_n) \tag{4.40}$$

of the component b of the Ashtekar-Barbero connection. Given this result, we can choose the fundamental operators (at each node n) in the quantum theory to correspond to the densitized triad E^b and complex exponentials of b.

It is convenient to express the Hilbert space $\mathbb{H}_n$ using the E^b-representation where the states $|E^b\rangle$ form an orthonormal basis

$${}_n\langle E^b|\tilde{E^b}\rangle_n = \delta_{E^b\tilde{E^b}}, \tag{4.41}$$

and are eigenkets of the triad operator

$$\hat{E}^b_n|E^b\rangle_n = E^b|E^b\rangle_n. \tag{4.42}$$

As usual in LQC, the operators corresponding to $\mathcal{N}_n(\mu)$ act as shift operators in this representation,

$$\hat{\mathcal{N}}_n(\mu)|E^b\rangle_n = |E^b + \frac{1}{w_n}\,\hbar G\gamma\mu\rangle_n, \tag{4.43}$$

a direct calculation confirms that the commutator of these elementary operators matches the Poisson bracket of the equivalent observables on the classical phase space, up to the required factor of $i\hbar$,

$$\{\mathcal{N}_n(\mu), E^b_n\} = \frac{iG\gamma\mu}{w_n}\mathcal{N}_n(\mu) \qquad \rightarrow \qquad [\hat{\mathcal{N}}_n(\mu), \hat{E}^b_n] = -\frac{\hbar G\gamma\mu}{w_n}\hat{\mathcal{N}}_n(\mu). \tag{4.44}$$

Since $\hat{E}^b_n$ has a discrete spectrum, it is also necessary to define an inverse triad operator for each $\mathbb{H}_n$. There is considerable ambiguity in the possible choices here (see [104] for a discussion); we take the simplest choice possible [108]:

$$\widehat{\frac{1}{E^b_n}}|E^b\rangle_n = \begin{cases} 0 & \text{if } \hat{E}^b_n|E^b\rangle_n = 0, \\ \left(E^b_n\right)^{-1}|E^b\rangle_n & \text{otherwise.} \end{cases} \tag{4.45}$$

In addition, note that x_n^{-1} appears in the Hamiltonian, a term which could be problematic at the origin. Since these terms appear due to the gauge-fixing of $E^a = x^2$, there would normally be an inverse triad operator for $(E^a)^{-1}$ that vanishes for $E^a = 0$, so we add the requirement that all terms in the Hamiltonian containing x_n^{-1} vanish when $x_n = 0$.

Any state $|\Psi\rangle_n \in \mathbb{H}_n$ has the general form of a countable sum

$$|\Psi\rangle_n = \sum_{E^b} \psi(E^b)\,|E^b\rangle_n, \tag{4.46}$$

with finite norm

$$ {}_n\langle\Psi|\Psi\rangle_n = \sum_{E^b} \left|\psi(E^b)\right|^2 . \tag{4.47} $$

As already mentioned, the full Hilbert space $\mathbb{H}$ is given by the tensor product of the Hilbert spaces $\mathbb{H}_n$ located at each node, $\mathbb{H} = \otimes\mathbb{H}_n$, and the elementary operators $E^b_n, \mathcal{N}_{n,\mu}$ acting at different nodes $n \neq m$ commute.

Finally, if the orientation of the densitized triad E^b_i is flipped, $E^b_i(x) \to -E^b_i(x)$ (and also $b \to -b$), the space-time geometry remains the same. Therefore, we require that the parity transformation

$$ \hat{\Pi}\Psi(E^b_0, E^b_1, \ldots, E^b_n, \ldots) = \Psi(-E^b_0, -E^b_1, \ldots, -E^b_n, \ldots) \tag{4.48} $$

leaves the wave function invariant, namely

$$ \hat{\Pi}\Psi = \Psi. \tag{4.49} $$

As an aside, we note that it is possible to define a parity transformation at a given node which changes the sign of the E^b_n argument of Ψ. However, this is not natural from a physical point of view since parity transformations are global operations and cannot act locally, therefore we do not introduce such an operator.

4.3.2 Quantum dynamics

In order to define an operator corresponding to the physical Hamiltonian in LQC, it is first necessary to construct a non-local operator corresponding to $\hat{b}_n$, which captures one of the components of the field strength through

$$ \hat{F}_{\theta\phi}{}^1(x_n) = \hat{b}^2_n \sin\theta. \tag{4.50} $$

Note that this operator is non-local since it is constructed from holonomies along edges of finite, not infinitesimal, length. Following the usual LQC procedure for the 'K' quantization [103, 104], we use a holonomy of minimal physical length $\sim \ell_{\mathrm{Pl}}$,

$$\hat{b}_n = -2\,\mathrm{Tr}\left(\frac{\hat{h}_{n,\theta}(2\bar{\mu}_n) - \hat{h}_{n,\theta}(-2\bar{\mu}_n)}{2\bar{\mu}_n}\tau_2\right) = \frac{\sin\bar{\mu}_n b_n}{\bar{\mu}_n}, \tag{4.51}$$

where $\bar{\mu}_n$ is a coordinate length chosen so that the physical length of the path is $\sqrt{\Delta}$, where $\Delta \sim \ell_{\mathrm{Pl}}^2$ is the smallest non-zero eigenvalue of the area operator in LQG. Of course, $\sin\bar{\mu}_n b_n$ can be expressed in terms of $\hat{\mathcal{N}}_n(\bar{\mu})$ and $\hat{\mathcal{N}}_n(-\bar{\mu}) = \hat{\mathcal{N}}_n(\bar{\mu})^\dagger$.

As the holonomy (4.39) follows a path where only the coordinate θ varies, it is straightforward to relate the coordinate length in the θ direction to the physical length through the metric (4.6), $|\mathrm{d}s| = x|\mathrm{d}\theta|$. Requiring that the physical length be given by $\sqrt{\Delta}$ sets

$$\bar{\mu}_n = \frac{\sqrt{\Delta}}{x_n}, \tag{4.52}$$

which implies that the operator $\hat{b}_n$ acts on basis states as

$$\hat{b}_n|E^b\rangle_n = \frac{x_n}{\sqrt{\Delta}}\Big(|E^b + \frac{1}{w_n x_n}G\hbar\gamma\sqrt{\Delta}\rangle - |E^b - \frac{1}{w_n x_n}G\hbar\gamma\sqrt{\Delta}\rangle\Big). \tag{4.53}$$

Interestingly, in this case $\bar{\mu}_n$ is independent of phase-space variables, unlike in the LQC of homogeneous space-times. This is ultimately due to the gauge-fixing of $E^a = x^2$ in Sec. 4.2.1.

With this definition, it is now possible to express the operator for the (discretized) physical Hamiltonian (4.33) in terms of the elementary operators. As in the classical theory, the total physical Hamiltonian operator is given by a sum of operators, each corresponding to the physical Hamiltonian on one node of the lattice,

$$\hat{\mathcal{H}} = \sum_n \hat{\mathcal{H}}_n, \tag{4.54}$$

and using the elementary operators defined above, together with the definition for $\hat{b}_n$ that captures the non-local curvature along angular directions, gives

$$\hat{\mathcal{H}}_n = -\frac{w_n}{2G\gamma}\left[\frac{1}{\gamma x_n}\widehat{\sqrt{|E^b_n|}}\frac{1}{w_n}\left[\frac{x^3_{n+1}}{\Delta}\sin^2\left(\frac{\sqrt{\Delta}b_{n+1}}{x_{n+1}}\right) - \frac{x^3_n}{\Delta}\sin^2\left(\frac{\sqrt{\Delta}b_n}{x_n}\right)\right]\widehat{\sqrt{|E^b_n|}} + \gamma x_n\left|\widehat{\frac{1}{E^b_n}}\right| + \frac{\gamma}{x_n}|\hat{E}^b_n|\right]. \tag{4.55}$$

The only factor-ordering choice to be made is in the first term, where we chose a symmetric factor-ordering between $\hat{E}^b_n$ and $\hat{b}^2_n$.

Note that given the definition of the inverse triad operators and the requirement that terms in the Hamiltonian containing x_n^{-1} also vanish for $n = 0$ (due to inverse triad corrections for E^a which has been gauge-fixed to x^2_n, see the discussion following the definition of the inverse triad operator in Sec. 4.3.1), it follows that $\hat{\mathcal{H}}_0 = 0$. So although $\hat{\mathcal{H}}_0$ is well-defined, it is trivial. For all other n, $\hat{\mathcal{H}}_n$ is non-trivial and acts on $\mathbb{H}_n \otimes \mathbb{H}_{n+1}$, given the discretization scheme we chose for derivatives in Sec. 4.2.4. Assuming $E^b_n \neq 0$, the inverse triad operators give the second line in (4.45) and the action of $\hat{\mathcal{H}}_n$ (for $n \geq 1$) on basis states $|E^b\rangle_n \otimes |E^b\rangle_{n+1} = |E^b_n, E^b_{n+1}\rangle$ is:

$$\begin{aligned}\hat{\mathcal{H}}_n|E^b_n,E^b_{n+1}\rangle = {} & \frac{x^3_{n+1}\left|E^b_n\right|}{8G\gamma^2\Delta x_n}\left(|E^b_n, E^b_{n+1}+\ell_{n+1}\rangle + |E^b_n, E^b_{n+1}-\ell_{n+1}\rangle\right) \\ & - \frac{x^2_n\sqrt{|E^b_n|}}{8G\gamma^2\Delta}\left(\sqrt{|E^b_n+\ell_n|}\,|E^b_n+\ell_n, E^b_{n+1}\rangle + \sqrt{|E^b_n-\ell_n|}\,|E^b_n-\ell_n, E^b_{n+1}\rangle\right) \\ & - \left[\frac{(x^3_{n+1}-x^3_n)\left|E^b_n\right|}{4G\gamma^2\Delta x_n} + \frac{w_n\left|E^b_n\right|}{2Gx_n} + \frac{w_n x_n}{2G|E^b_n|}\right]|E^b_n, E^b_{n+1}\rangle,\end{aligned} \tag{4.56}$$

where

$$\ell_n = \frac{2G\hbar\gamma\sqrt{\Delta}}{w_n x_n}. \tag{4.57}$$

Note that if $E^b_n = 0$, then all terms vanish exactly (the last term is zero due to the inverse triad operator).

Also, recall that $\hat{\mathcal{H}}$ is a true Hamiltonian (not a constraint) due to the dust-time

gauge-fixing, and the Hamiltonian operator is related to the dust energy density operator,

$$\hat{\rho}_n = -\frac{1}{4\pi w_n x_n}\left|\widehat{\frac{1}{E^b_n}}\right|^{1/2}\left[\hat{\mathcal{H}}_n + \frac{1}{G w_n}\left(x^2_{n+1}\left|\widehat{\frac{1}{E^b_{n+1}}}\right| - x^2_n\left|\widehat{\frac{1}{E^b_n}}\right|\right)\right]\left|\widehat{\frac{1}{E^b_n}}\right|^{1/2}, \quad (4.58)$$

while the mass operator is given by

$$\hat{m}_n = 4\pi\sum_{p=0}^{n} w_p x_p \sqrt{\left|\hat{E}^b_p\right|}\hat{\rho}_p\sqrt{\left|\hat{E}^b_p\right|}, \quad (4.59)$$

where we have again used a symmetric factor-ordering for both operators.

Finally, to reconstruct all of the components in the metric (4.6), it is also necessary to define an operator corresponding to N^x. Recall that the flat FLRW space-time (minimally coupled to dust) is a particular solution of the LTB space-time; starting from the standard flat FLRW line element in spherical coordinates $\mathrm{d}s^2 = -\mathrm{d}t^2 + a(t)^2(\mathrm{d}r^2 + r^2\mathrm{d}\Omega^2)$ where $a(t)$ is the scale factor, the coordinate transformation $x = a(t)\cdot r$ gives a line element that has precisely the form (4.6) with $E^b = x$ and $N^x = -xH$, where H is the Hubble rate. In LQC the Hubble rate in terms of the phase space variables is $H = (\gamma\sqrt{\Delta})^{-1}\sin(\bar{\mu}b)\cos(\bar{\mu}b)$, see, e.g., [109] (where we have simplified the notation by removing hats, and denoted the non-zero component of the Ashtekar-Barbero connection for the flat FLRW space-time by b). This suggests that the appropriate operator for N^x in LTB space-times is

$$\hat{N}^x_n = -\frac{x_n}{\gamma\sqrt{\Delta}}\sin\left(\frac{\sqrt{\Delta}b_n}{x_n}\right)\cos\left(\frac{\sqrt{\Delta}b_n}{x_n}\right). \quad (4.60)$$

This choice has the correct classical limit, and it also agrees with earlier work [40, 41] (although it differs from the choice proposed in [110]). This operator is not obtained by simply replacing the classical b_n in N^x by the operator $\hat{b}_n$ defined in (4.51); nonetheless, this is a natural choice for the operator as it ensures that the homogeneous sector of

(marginally bound) LTB space-times agrees with earlier results obtained for flat FLRW space-times in LQC. (Note that there is a priori no guarantee that $(N^x)^2 \sim b^2$ and the field strength ${F_{\theta\phi}}^1 \sim b^2$ will be represented by the same operator in the quantum theory; it is possible for $\hbar$ corrections to modify these terms differently.)

As an aside, we mention two points concerning the operator $\hat{N}^x_n$. First, even though as argued above we find (4.60) to be the most strongly motivated definition for $\hat{N}^x_n$, it is nonetheless possible to make other choices, see, e.g., [110] for an alternate choice in vacuum space-times. A different choice affects quantitative results, but our numerical evidence suggests that the key qualitative properties of the (effective) LQC dynamics for LTB space-times, such as the non-singular bounce, shock wave formation, and black hole lifetime are not significantly modified by different choices for N^x—this is due in large part to fact that the evolution of b and E^b does not depend on the reconstruction of the metric via (4.60). A second technical point is the following. Although this has so far not been done, it should be possible to define a consistent quantum theory for LTB space-times without first imposing any gauges before quantization, and instead impose appropriate gauges only after the theory has been quantized. Gauge fixing after quantization would require introducing operators corresponding to gauge-fixing conditions that ensure the gauge choices are preserved dynamically, and these gauge-fixing conditions will fix the Lagrange multipliers, here corresponding to the lapse and shift. The classical gauge-fixing conditions for the dust-time and areal gauges in LTB space-times are known, and it would be interesting to determine their form as operators in LQC; in particular, it will be necessary to express the components of the Ashtekar-Barbero connection in terms of holonomies. Although deriving the specific form of such gauge-fixing conditions for LQC lies beyond the scope of this paper, it can be shown that since the operator for N^x is not related to the classical one by a simple 'polymerization' where each b_n term is replaced by $\hat{b}_n$, similarly the LQC gauge-fixing conditions cannot be obtained simply by taking

the classical expressions and performing a direct polymerization [111]. This is not surprising for two reasons: first, the LQC shift vector is not given by the direct polymerization of the classical expression, and second, the non-gauge-fixed LQC scalar and diffeomorphism constraints for the LTB space-times are not related to the classical expressions through a direct polymerization, since this would result in a quantum constraint algebra which does not close and hence would give an inconsistent theory. A more careful and sophisticated treatment is needed to construct the non-gauge-fixed LQC theory for LTB space-times; this presumably requires following LQG more closely and avoiding shortcuts like polymerization which appear to work only in the simplest contexts.

This completes the definition of the loop quantization of LTB space-times. We next derive effective equations which capture important quantum gravity effects, and are significantly easier to solve than the full quantum dynamics.

4.4 Effective Theory

Loop quantum cosmology effective equations are functions on the classical phase space that include some quantum corrections in the form of terms containing $\hbar$ that arise from, e.g., holonomy corrections. It would of course be preferable to solve the full quantum dynamics, but this is a technically challenging problem—deriving semiclassical physics would require constructing the unitary evolution operator for the Hamiltonian and calculating its action on semiclassical states. Instead, as a first step, we extract and solve the effective equations with holonomy corrections from the LTB quantum theory defined in Sec. 4.3.

For homogeneous cosmological space-times, it has been shown that the quantum dynamics of sharply-peaked states is well-approximated by a set of effective equations, and that these effective equations remain a good approximation to the quantum

dynamics for sharply peaked states even when the space-time curvature becomes Planckian, so long as the relevant length scales remain large compared to $\ell_{\rm Pl}$ [9, 109, 112, 113]. The main approximation underlying the effective equations is that they assume quantum fluctuations are negligible, but include important effects like the fundamental quantum discreteness encoded by the non-local curvature operator in the Hamiltonian.

In addition to results in cosmology, some early work on black holes suggests that effective dynamics are also reliable for black hole space-times with a large mass, at least for (i) states that are sharply peaked and (ii) so long as one only probes length scales $\ell \gg \ell_{\rm Pl}$ [114]. If these two conditions are satisfied, then the effective dynamics are expected to provide a good approximation to the full quantum dynamics, even when the curvature is Planckian.

In this section, we define the LQC effective Hamiltonian for LTB space-times in the dust-time and areal gauges, derive the LQC effective dynamics, and find analytic weak solutions for some simple configurations.

4.4.1 Effective Dynamics

The effective equations for LTB space-times can be derived from the quantum theory by expressing the Hamiltonian operator (4.55) as a function on the classical phase space. For the LTB space-time, this gives an effective Hamiltonian (for the discretized theory) composed of the sum over n of

$$\mathcal{H}_n^{\rm eff} = -\frac{1}{2G\gamma}\left[\frac{E_n^b}{\gamma w_n x_n}\left(\frac{x_{n+1}^3}{\Delta}\,\sin^2\frac{\sqrt{\Delta}b_{n+1}}{x_{n+1}} - \frac{x_n^3}{\Delta}\,\sin^2\frac{\sqrt{\Delta}b_n}{x_n}\right) + \frac{\gamma x_n}{E_n^b} + \frac{\gamma E_n^b}{x_n}\right], \tag{4.61}$$

assuming $E^b > 0$ for the sake of simplicity. The continuum limit is easily taken; the resulting Hamiltonian is

$$\int \mathrm{d}x\, \mathcal{H}^{\mathrm{eff}}_{\mathrm{phys}} = -\frac{1}{2G\gamma}\int \mathrm{d}x \left[\frac{E^b}{\gamma\Delta x}\partial_x\left(x^3 \sin^2\frac{\sqrt{\Delta}b}{x}\right) + \frac{\gamma x}{E^b} + \frac{\gamma E^b}{x}\right]. \tag{4.62}$$

The transition from the Hamiltonian operator to this effective expression requires taking the expectation of the former in a semiclassical Gaussian state peaked on a phase space point (see, e.g., [115]), and then taking the continuum limit. This is the same process used to obtain the effective LQC dynamics, where the Hamiltonian operator with matter is also unbounded. A shortcut that is known to work in LQC, and one we use here, is to replace the quantum operators with the appropriate phase space functions. Note that the effective dynamics do not take into account dispersion effects of the Hamiltonian operator captured by expressions as such $\Delta(\mathcal{H}_n)^2 \equiv \langle\hat{\mathcal{H}}_n^2\rangle - \langle\hat{\mathcal{H}}_n\rangle^2$ for expectation values in semiclassical states, which are of higher order in $\hbar$.

The Poisson bracket is the same as in the classical theory,

$$\{b(x_1), E^b(x_2)\} = G\gamma\,\delta(x_1 - x_2), \tag{4.63}$$

and the effective equations of motion are generated, as usual, by taking the Poisson brackets of the dynamical variables with the effective Hamiltonian, $\int \mathrm{d}x\, \mathcal{H}^{\mathrm{eff}}_{\mathrm{phys}}$, giving

$$\dot{b} = \frac{\gamma x}{2(E^b)^2} - \frac{\gamma}{2x} - \frac{x}{\gamma\Delta}\sin\frac{\sqrt{\Delta}}{x}b\left[\frac{3}{2}\sin\frac{\sqrt{\Delta}}{x}b + x\,\partial_x \sin\frac{\sqrt{\Delta}}{x}b\right], \tag{4.64}$$

$$\dot{E}^b = -\frac{x^2}{\gamma\sqrt{\Delta}}\,\partial_x\left(\frac{E_b}{x}\right)\sin\frac{\sqrt{\Delta}}{x}b\,\cos\frac{\sqrt{\Delta}}{x}b. \tag{4.65}$$

As in the classical theory, b and E^b determine the metric,

$$\mathrm{d}s^2 = -\mathrm{d}t^2 + \frac{E_b^2}{x^2}(\mathrm{d}x + N^x\mathrm{d}t)^2 + x^2\mathrm{d}\Omega^2, \tag{4.66}$$

where the shift vector is related to b by

$$N^x = -\frac{x}{\gamma\sqrt{\Delta}} \sin\frac{\sqrt{\Delta}}{x} b \ \cos\frac{\sqrt{\Delta}}{x} b, \tag{4.67}$$

taking the prescription (4.60) used for the quantum theory.

Finally, the energy density in the effective theory follows from (4.58),

$$\rho = \frac{1}{8\pi G\gamma\, x E^b}\left[\frac{E^b}{\gamma\Delta x}\partial_x\left(x^3\sin^2\frac{\sqrt{\Delta}b}{x}\right) + \frac{\gamma x}{E^b} + \frac{\gamma E^b}{x} - 2\gamma\,\partial_x\left(\frac{x^2}{E^b}\right)\right]. \tag{4.68}$$

We note that the area gap Δ and the Barbero-Immirzi parameter γ often combine in the form $\gamma^2\Delta$, and many observables of physical interest depend only on this combination. This also occurs in LQC and seems to be a general feature of loop quantized symmetry-reduced systems. In contrast, in LQG the quantities γ and Δ are distinct (although related, since Δ is proportional to γ), and can be distinguished for example by measuring the spectrum of the LQG area operator.

4.4.2 Marginally bound solutions

As in the classical theory, $E^b = x$ corresponds to the effective version of the marginally bound solutions. For this family of solutions, b is the only dynamical degree of freedom left, satisfying the equation of motion

$$\dot{b} + \frac{1}{2\gamma\Delta x}\partial_x\left(x^3\sin^2\frac{\sqrt{\Delta}\,b}{x}\right) = 0. \tag{4.69}$$

The energy density is closely related to b through

$$\rho = \frac{1}{8\pi G\gamma^2\Delta\, x^2}\,\partial_x\left(x^3\sin^2\frac{\sqrt{\Delta}\,b}{x}\right), \tag{4.70}$$

which can also be expressed in terms of $\dot{b}$, although this relation will not be necessary for us here. Expanding the derivative,

$$\rho = \frac{1}{8\pi G\gamma^2\Delta}\left(3\sin^2\frac{\sqrt{\Delta}\,b}{x} + 2\sqrt{\Delta}\sin\frac{\sqrt{\Delta}\,b}{x}\cos\frac{\sqrt{\Delta}\,b}{x}\left(\partial_x b - \frac{b}{x}\right)\right). \tag{4.71}$$

In the homogeneous limit of $\partial_x b = 0$, the energy density is bounded above by $\rho_c = 3/8\pi G\gamma^2\Delta$, the critical energy density for spatially flat FLRW space-times in LQC.

It is simpler and more intuitive to give initial conditions in terms of the density $\rho(x, t_0)$; these can be translated into initial conditions for b through

$$b(x, t_0) = -\frac{x}{\sqrt{\Delta}}\arcsin\left(\sqrt{\frac{8\pi G\gamma^2\Delta}{x^3}\int_0^x \mathrm{d}\tilde{x}\ \tilde{x}^2\rho(\tilde{x}, t_0)}\right)\ . \tag{4.72}$$

When taking the square root, we chose an overall negative sign; this choice means that the initial data corresponds to a collapse scenario. On the other hand, taking the positive root would correspond to an LTB space-time with dust initially moving outwards.

For collapse models, an important quantity is the outgoing null expansion θ_+, which is used to locate marginal apparent horizons via $\theta_+ = 0$. For the LTB metric (4.66), with $E^b = x$, the outgoing null expansion is

$$\theta_+ = \frac{2}{x}(1 - N^x) = \frac{2}{x} + \frac{1}{\gamma\sqrt{\Delta}}\sin\frac{2\sqrt{\Delta}\,b}{x}. \tag{4.73}$$

Similarly, the in-going null expansion is $\theta_- = -(2/x)\cdot(1 + N^x)$.

It is possible to find implicit solutions for b by using the method of characteristics, namely by finding curves in the (x, t) plane parametrized by λ such that along these curves the partial differential equation (4.69) becomes a set of coupled ordinary differential equations. Solving the set of coupled ordinary differential equations along

each of these curves gives the full solution, although in implicit form in terms of the parameter λ.

It is convenient to first introduce the variable $\beta = \sqrt{\Delta}\, b/x$, in which case the equation of motion becomes

$$\dot{\beta} + \frac{1}{2\gamma\sqrt{\Delta}x^2}\partial_x\left(x^3 \sin^2\beta\right) = 0. \tag{4.74}$$

As an aside, note that this equation can be rewritten as

$$\dot{\beta} = -4\pi G\gamma\sqrt{\Delta}\,\rho, \tag{4.75}$$

and since $\rho \geq 0$, it follows that β is monotonically decreasing.

Taking a parametrized curve $(x(\lambda), t(\lambda))$ and evaluating $\beta(\lambda)$ at points along this curve gives

$$\frac{\mathrm{d}\beta}{\mathrm{d}\lambda} = \frac{\partial\beta}{\partial t}\frac{\mathrm{d}t}{\mathrm{d}\lambda} + \frac{\partial\beta}{\partial x}\frac{\mathrm{d}x}{\mathrm{d}\lambda}. \tag{4.76}$$

By choosing a curve such that

$$\frac{\mathrm{d}\beta}{\mathrm{d}\lambda} = -\frac{3}{2}\sin^2\beta, \tag{4.77}$$

the equation of motion for β implies that

$$\frac{\mathrm{d}x}{\mathrm{d}\lambda} = x\sin\beta\cos\beta, \qquad \frac{\mathrm{d}t}{\mathrm{d}\lambda} = \gamma\sqrt{\Delta}. \tag{4.78}$$

Solving these ODEs first gives $\lambda = t/\gamma\sqrt{\Delta}$ (setting $\lambda(t=0) = 0$), and

$$\cot\left(\beta(\lambda)\right) = \cot\beta_0 + \frac{3\lambda}{2}, \qquad \left(\frac{x}{x_0}\right)^3 = \frac{\sin^2\beta_0}{\sin^2\beta}. \tag{4.79}$$

For each curve, the initial conditions are $t(\lambda = 0) = 0$ and $x(\lambda = 0) = x_0$. For such a curve, $\beta(\lambda = 0) = \beta_0(x_0)$, and we have the exact implicit solutions for $\beta(x, t)$.

These can be inverted numerically everywhere, except where characteristics cross—at these points the method of characteristics fails, and it is necessary to search for weak solutions to the equation of motion. As mentioned previously, it is always possible in the classical theory to restrict initial data such that caustics do not form [90, 91, 94], but as we explain next this is not possible in the effective quantum theory due to the singularity avoidance and bounce: shock waves are a general feature of quantum dust collapse.

As in the classical case, shock formation occurs when the Jacobian for the transformation $(\lambda, x_0) \to (t, x)$ vanishes. Since $\partial_\lambda t = \gamma\sqrt{\Delta}$ and $\partial_{x_0} t = 0$, the Jacobian vanishes if and only if $\partial_{x_0} x = 0$. Rewriting

$$x = \left(x_0^3 \sin^2\beta_0 \left[1 + (\cot\beta_0 + \tfrac{3}{2}\lambda)^2\right]\right)^{1/3}, \tag{4.80}$$

a numerical investigation finds that the derivative

$$\partial_{x_0} x = \frac{1}{3}\left(\frac{\sin^2\beta_0}{\sin^2\beta}\right)^{1/3}\left[3 + 2x_0\beta_0'\left(\cot\beta_0 - \frac{1}{\sin^2\beta_0}\cdot\frac{\frac{3}{2}\lambda + \cot\beta_0}{1 + \left(\frac{3}{2}\lambda + \cot\beta_0\right)^2}\right)\right] \tag{4.81}$$

generically vanishes for initial data with in-falling dust that satisfies the two following properties: the initial density ρ_0 is not zero everywhere, and there is an exterior vacuum region $x \geq x_e$ where $\rho_0 = 0$. Physically, this can be understood by following characteristics in the interior and exterior regions. In the interior, the characteristics for dust particles will eventually bounce due to LQC effects and move outwards, while in the vacuum exterior region characteristic curves will always move inwards. As a result, these two families of characteristic curves must eventually cross; see also the discussion in [93]. (Note that characteristic curves where $\rho \neq 0$ may also cross, but this depends quite sensitively on the initial configuration of ρ_0 and will not always occur, while characteristic curves for the interior matter region and the exterior vacuum region will cross after the bounce.) Therefore, for this large class of initial data,

characteristics will cross, showing that it is necessary to allow for weak solutions to the effective dynamics.

4.4.3 Weak solutions

As characteristic curves will cross, weak solutions to the dynamics must be considered. As reviewed in Sec. 4.2.3, it is helpful to write the dynamics in the form of a conservation law $\dot{u} + \partial_x[f(u,x)] = 0$, which can in turn be expressed as an integral equation. Then, the speed of a shock wave located at $x = L(t)$ is given by $\mathrm{d}L/\mathrm{d}t = [f(u,x)]/[u]$, where $[g(x)] = \lim_{x\to L^+} g(x) - \lim_{x\to L^-} g(x)$.

To rewrite the equation of motion (4.69) as a conservation law, it is useful to introduce the variable $B = \sqrt{\Delta}\, x\, b$, whose dynamics are given by

$$\dot{B} + \partial_x \left(\frac{x^3}{2\gamma\sqrt{\Delta}} \sin^2 \frac{B}{x^2} \right) = 0. \tag{4.82}$$

Then, the speed of any shock waves that may form is given by

$$\frac{\mathrm{d}L}{\mathrm{d}t} = \frac{L^3}{2\gamma\sqrt{\Delta}} \cdot \frac{[\sin^2 \frac{B}{x^2}]}{[B]} = \frac{L}{2\gamma\sqrt{\Delta}} \cdot \frac{[\sin^2 \beta]}{[\beta]}. \tag{4.83}$$

Here we give the expression in terms of both of the variables B and $\beta = B/x^2$; depending on the calculation, one variable may be more convenient than the other.

The Oppenheimer-Snyder model and the thin shell solution can be solved analytically; the general case for arbitrary initial data profiles requires a numerical solution.

4.4.3.1 Oppenheimer-Snyder solution

The Oppenheimer-Snyder collapse model has two regions: a 'star' interior region $x < L(t)$ where the energy density ρ is radially constant (but grows with time as the

star collapses and becomes denser), and a vacuum exterior region $x > L(t)$ where $\rho = 0$. We will denote the interior region with the index i and the exterior region with the index e.

The solution for the $\rho_e = 0$ vacuum exterior region follows from (4.70),

$$\sin \beta_e = -\sqrt{\frac{\gamma^2 \Delta R_S}{x^3}}, \tag{4.84}$$

where the minus sign is due to the attractive nature of the gravitational field generated by the dust field in the interior, and the constant of integration is chosen to match the classical solution. As usual, $R_S = 2GM$ is the classical Schwarzschild radius and M is the total mass of the star (which is a constant of the motion). Also, note that $\dot{\beta}_e = 0$.

Similarly, for the interior region (4.70) shows that if $\partial_x \rho = 0$, then $\partial_x \beta = 0$ also, and (4.74) becomes

$$\dot{\beta}_i = -\frac{3 \sin^2 \beta_i}{2\gamma\sqrt{\Delta}}, \tag{4.85}$$

with the solution

$$-\cot \beta_i = \frac{3(t - t_0)}{2\gamma\sqrt{\Delta}} \qquad \Rightarrow \qquad \sin \beta_i = \frac{-1}{\sqrt{1 + 9t^2/4\gamma^2\Delta}}. \tag{4.86}$$

The minus sign indicates that the Oppenheimer-Snyder star is collapsing, rather than expanding, and in the second relation we have fixed the constant of integration $t_0 = 0$. Since β_i is monotonically decreasing, as seen in (4.75), it follows that for $t < 0$, then $-\pi/2 < \beta_i < 0$, while $-\pi < \beta_i < -\pi/2$ for $t > 0$. As a result, β_i itself is given by

$$\beta_i = \begin{cases} -\arcsin \frac{1}{\sqrt{1+9t^2/4\gamma^2\Delta}}, & \text{for } t < 0, \\ -\pi + \arcsin \frac{1}{\sqrt{1+9t^2/4\gamma^2\Delta}}, & \text{for } t > 0, \end{cases} \tag{4.87}$$

keeping in mind that $-\pi/2 < \arcsin x < \pi/2$.

In terms of the gauge-fixed metric (4.66), the interior is a flat FLRW space-time

with a dust field whose energy density evolves as

$$\rho_i = \frac{3}{2\pi G\left(9t^2 + 4\gamma^2\Delta\right)}. \tag{4.88}$$

During the $t < 0$ contracting phase of the star, β is continuous across the boundary between the interior and exterior solutions (although not differentiable), so there is no shock wave and the location of the boundary $x = L(t)$ can be determined by requiring that β be continuous across the boundary, giving [87]

$$L = \left(\frac{9R_S t^2}{4} + \gamma^2\Delta R_S\right)^{1/3}. \tag{4.89}$$

Using this expression to rewrite the energy density of the interior, it is clear that $L(t)$ plays the role of the scale factor for the FLRW-like interior, with

$$\rho_i = \frac{3M}{4\pi L^3}, \tag{4.90}$$

and the effective Friedman equation that L satisfies during the collapse phase is

$$\left(\frac{\dot{L}}{L}\right)^2 = \frac{8\pi G}{3}\rho\left(1 - \frac{\rho}{\rho_c}\right), \tag{4.91}$$

which is exactly identical to the LQC effective Friedman equation for flat FLRW space-times.

A bounce occurs at $t = 0$ when $\beta_i = -\pi/2$. The bounce occurs both in the radius L of the collapsing star, which reaches a minimum and begins to increase, and also in the energy density ρ, which reaches a maximum precisely equal to $\rho_c = 3/8\pi G\gamma^2\Delta$, the critical energy density in LQC, and then decreases after the bounce.

The post-bounce dynamics are significantly different from the collapse, because after the bounce $\beta_i < -\pi/2$ while $\beta_e > -\pi/2$, showing that a discontinuity in β has formed: there is now a shock in the gravitational field. Since there is a shock, L no

longer follows the dynamics given by (4.91) which holds only when the solution is continuous; instead the motion of the front of the shock wave during the expanding phase is determined by the Rankine-Hugoniot condition (4.83),

$$\frac{\mathrm{d}L}{\mathrm{d}t} = \frac{\gamma\sqrt{\Delta}/2}{\pi - \arcsin\sqrt{\frac{\gamma^2\Delta R_S}{L^3}} - \arcsin\sqrt{\frac{\gamma^2\Delta}{\frac{9}{4}t^2+\gamma^2\Delta}}} \cdot \left(\frac{R_S}{L^2} - \frac{L}{\frac{9}{4}t^2+\gamma^2\Delta}\right). \tag{4.92}$$

In the interior, away from the shock, the energy density after the bounce decreases following (4.88), but L moves more slowly after the bounce, as compared to before, and the outside region remains vacuum. The combination of these effects implies that a growing fraction of the dust field becomes trapped at the boundary $x = L(t)$ in the expanding phase,

$$\rho_{\mathrm{int}} = \frac{3}{2\pi G\,(9t^2+4\gamma^2\Delta)}\Theta\Big(L(t)-x\Big) + \left(M - \frac{2L^3}{G\,(9t^2+4\gamma^2\Delta)}\right)\delta\Big(L(t)-x\Big), \tag{4.93}$$

where $\Theta(x)$ is the Heaviside function.

Since the energy density of dust in the interior quickly decays, soon after the bounce it is reasonable to approximate the interior by a flat Minkowski space-time where $\beta = -\pi$ and $\sin\beta = 0$. Further, soon after the bounce $L \gg L_{\mathrm{bounce}} = (\gamma^2\Delta R_S)^{1/3}$ and it is possible to neglect terms of the order L_{bounce}/L. With these two approximations, the speed of the shock (4.92) reduces to

$$\frac{\mathrm{d}L}{\mathrm{d}t} \approx \frac{\gamma\sqrt{\Delta}R_S}{2\pi L^2}, \tag{4.94}$$

which can be solved to give

$$L(t) \approx \left(\frac{3\gamma\sqrt{\Delta}R_S\,t}{2\pi}\right)^{1/3}, \tag{4.95}$$

although this result is a good approximation only for $t \gg t_{\mathrm{Pl}}$. At the bounce $L(0)$

does not vanish, rather $L(0) = L_{\text{bounce}} = \gamma^2 \Delta R_S$.

With these results, it is straightforward to determine the space-time metric; putting $E^b = x$ into (4.66),

$$\mathrm{d}s^2 = -\mathrm{d}t^2 + \Big(\mathrm{d}x + N^x \mathrm{d}t\Big)^2 + x^2 \mathrm{d}\Omega^2, \tag{4.96}$$

the lapse $N^x = -(x/\gamma\sqrt{\Delta}) \cdot \sin\beta \cos\beta$ is [87]

$$N^x = \begin{cases} -\dfrac{6xt}{9t^2 + 4\gamma^2\Delta} & \text{if } x \leq L(t), \\ \sqrt{\dfrac{R_S}{x}\left(1 - \dfrac{\gamma^2 \Delta R_S}{x^3}\right)} & \text{if } x > L(t); \end{cases} \tag{4.97}$$

where $L(t)$ is given by (4.89) for the collapse $t < 0$ portion of the space-time, while L expands more slowly following (4.92) for $t > 0$ after the bounce. For more details on the exterior vacuum solution see [41], and for the interior solution see [87].

In addition, it is possible to calculate the lifetime of an Oppenheimer-Snyder black hole solution, defined as the (proper) time interval between the formation of the outer apparent horizon, and its eventual disappearance when the outgoing shock wave reaches it, as measured by a distant observer. Assuming the distant observer detects lightlike signals emitted from the surface L just before the formation of the black hole and just after the emergence of the shock from the outer apparent horizon, this observer's proper time interval is simply given by the coordinate interval $T = t_2 - t_1$ between these two events [87]. For this calculation, we make the approximation that the apparent horizon is located at R_S, neglecting corrections to the location of the horizon of the order $\sim \ell_{\text{Pl}}^2/R_S$ that are negligible for black holes with $M \gg m_{\text{Pl}}$.

The black hole forms at $t = t_1$ when $L = R_S$ during the collapse phase, so by inverting (4.89) we find

$$t_1 = -\frac{2}{3}\sqrt{R_S^2 - \gamma^2\Delta} \approx -\frac{2R_S}{3}, \tag{4.98}$$

showing that the collapse time of the Oppenheimer-Snyder star is of the order of $\sim M$.

On the other hand, the apparent horizon vanishes once the outgoing shock wave reaches $L = R_S$, and the solution (4.95) gives

$$t_2 \approx \frac{2\pi R_S^2}{3\gamma\sqrt{\Delta}}. \tag{4.99}$$

As an aside, we mention that it is also possible to numerically integrate the exact equation

$$t_2 = \int_{L_{\rm bounce}}^{R_S} \left(\frac{{\rm d}L}{{\rm d}t}\right)^{-1} {\rm d}L, \tag{4.100}$$

with ${\rm d}L/{\rm d}t$ given by (4.92), and the result of this calculation is in excellent agreement with the approximate solution (4.99). This shows that the time between the bounce and the disappearance of the outer apparent horizon scales as $\sim M^2/m_{\rm Pl}$, in agreement with an earlier estimate [87].

Combining these two results and keeping only the dominant term (assuming $M \gg m_{\rm Pl}$), the lifetime of an Oppenheimer-Snyder black hole is predicted to be

$$T \approx \frac{2\pi R_S^2}{3\gamma\sqrt{\Delta}}. \tag{4.101}$$

As we shall discuss in more detail in Sec. 4.6, this prediction for the lifetime of a black hole is shorter than the Page time and has important implications for the information loss problem.

4.4.3.2 Thin shell solution

Another interesting solution to consider is a thin shell, where the interior is Minkowski with $\sin\beta_i = 0$, and the exterior is Schwarzschild with $\sin\beta_e = -\sqrt{\gamma^2\Delta R_S/x^3}$;

these two solutions are separated by a thin shell of total mass M located at $x = L(t)$,

$$\rho = \frac{M}{4\pi x^2}\,\delta\Big(x - L(t)\Big). \tag{4.102}$$

There are two cases of interest, the contracting case when $\beta_i = 0$, and the expanding case $\beta_i = -\pi$.

Before studying the dynamics, it is important to note that although there is a bounce, a contracting thin shell solution does not immediately become an expanding thin shell solution when the bounce occurs. The key point is that a thin shell of mass M can reach a minimal radius $L_{\min} = (\gamma^2 \Delta R_S)^{1/3}$. When the shell reaches this minimal radius, the thin shell splits, with a portion continuing to fall inwards and another portion being scattered outwards. The scattering process is continuous, with a broad distribution of dust being scattered backwards until there is a bounce at the origin (the total mass remains M throughout). This process can be seen in more detail using the numerical methods described in Sec. 4.5. For this reason, the ingoing and outgoing shell solutions must be treated separately. (Another way to see that the ingoing thin shell does not immediately become an outgoing shell after reaching $L_{\min}$ is that an ingoing shell has $\beta_i = 0$, while an outgoing shell has $\beta_i = -\pi$, so the first cannot just bounce at $L_{\min}$ and become the second without any changes to the interior.)

For the case of an ingoing thin shell, the shock speed relation (4.83) gives

$$\frac{\mathrm{d}L}{\mathrm{d}t} = -\frac{2\gamma\sqrt{\Delta}R_S}{L^2 \arcsin\sqrt{\gamma^2 \Delta R_S / L^3}}, \tag{4.103}$$

this can be integrated to give an analytic implicit solution for $L(t)$, although it is not especially transparent or useful. Instead, the collapse time t_{in} can be obtained by integrating $(\mathrm{d}L/\mathrm{d}t)^{-1}$ from $L = R_S$ (again neglecting small Planckian corrections to

the location of the outer apparent horizon) to $L_{\min} = (\gamma^2 \Delta R_S)^{1/3}$; the result is

$$t_{\text{in}} = -\int_{R_S}^{L_{\min}} \frac{2L^2}{\gamma\sqrt{\Delta}R_S} \arcsin\sqrt{\frac{\gamma^2\Delta R_S}{L^3}}\, \mathrm{d}L \approx \frac{2R_S}{3}, \tag{4.104}$$

dropping subleading corrections of order $\hbar$. As expected, the time for collapse is $t_{\text{in}} \sim M$, as is the case for the Oppenheimer-Snyder collapse (in this particular case, even the prefactors of the leading order term match for the thin shell and Oppenheimer-Snyder solutions).

Switching now to the outgoing case, the shock speed (4.83) becomes

$$\frac{\mathrm{d}L}{\mathrm{d}t} = \frac{\gamma\sqrt{\Delta}R_S}{2L^2(\pi - \arcsin\sqrt{\gamma^2\Delta R_S/L^3})}, \tag{4.105}$$

so the time for the shell to travel from $L_{\min}$ to R_S is

$$t_{\text{out}} = \int_{L_{\min}}^{R_S} \frac{2L^2}{\gamma\sqrt{\Delta}R_S}\left(\pi - \arcsin\sqrt{\frac{\gamma^2\Delta R_S}{L^3}}\right) \mathrm{d}L \approx \frac{2\pi R_S^2}{3\gamma\sqrt{\Delta}}, \tag{4.106}$$

again only keeping the leading order term when evaluating the integral.

In general, the lifetime of a black hole can be split into three parts: a collapse time, a bounce time, and an outgoing time. (The bounce time may be zero in some cases where the bounce occurs simultaneously everywhere, like in the Oppenheimer-Snyder model, but this will not necessarily always be true.) The lifetime of a black hole will be dominated by the outgoing time t_{out},

$$T \approx t_{\text{out}} \approx \frac{2\pi R_S^2}{3\gamma\sqrt{\Delta}}. \tag{4.107}$$

Note that the leading order contribution to T is identical for the thin shell and Oppenheimer-Snyder solutions. This is not surprising because after the bounce, the dust energy density ρ in the Oppenheimer-Snyder interior rapidly decays to the point where the interior is well approximated by Minkowski space and all of the matter is

located at the shock. In other words, soon after the bounce the Oppenheimer-Snyder solution becomes (to an excellent approximation) an outgoing thin shell. Further, as shall be seen in Sec. 4.5, numerics show that this occurs quite generally: for a large class of initial density profiles for the collapse, after the bounce the outgoing shock wave rapidly tends to the outgoing thin shell solution. For this reason, the lifetime of a black hole appears to be universal to leading order with $T = 2\pi R_S^2/(3\gamma\sqrt{\Delta}) + \mathcal{O}(M)$.

4.4.3.3 Conformal diagram

The conformal diagram for the effective vacuum solution has already been studied in considerable detail [116], but there are some important differences in the conformal diagram once matter (in this case dust) is included. For concreteness, we will sketch the conformal diagram for the Oppenheimer-Snyder collapse model derived in Sec. 4.4.3.1, but we expect a qualitatively similar diagram for most of the main features for other solutions to the LQC effective dynamics for LTB space-times that start from a collapse that leads to the formation of a black hole—this expectation is met for the numerical solutions we obtain in Sec. 4.5.

In the Oppenheimer-Snyder model, during collapse the radius $L(t)$ of the dust sphere is given by (4.89), while after the bounce the shock wave moves outwards following (4.92), whose solution is approximated by (4.95) for times $t \gg t_{\rm Pl}$.

In broad strokes, the conformal diagram shows the following events and processes. First, a pair of apparent horizons appears when $L = R_S$ during the collapse, the outer horizon is null and remains at the radius $x = R_S$, while the inner horizon lies inside L for almost all of the collapse. Second, the inner horizon crosses outside L only a short (Planckian) time before the bounce, at this point the inner horizon becomes null and remains at the same radius $x_{\rm inner}$ until the fourth stage. Third, after the inner horizon stops at $x_{\rm inner}$ the entire spherical region bounded by L no longer lies within a trapped region and the dust sphere bounces (this meets general expectations described in

[75]). Fourth, a shock wave forms after the bounce, the shock-wave front briefly moves beyond the inner horizon and then the inner horizon rapidly moves outwards and catches up, at which point the shock and the inner horizon move outwards together. Finally, the shock wave eventually reaches the outer apparent horizon located at $x = R_S$, at this time the inner and outer horizons meet and annihilate, and the black hole disappears.

An important point is that due to the gravitational shock wave that forms after the bounce, there is a discontinuity in the gravitational field, namely in the space-time metric. This means that the $x = L$ surface has different properties with respect to the inner and outer metrics. In particular, during most of the fourth stage mentioned above, the $x = L$ surface is timelike according to the inner space-time metric, but spacelike according to the outer metric. Further, when constructing the conformal diagram, different coordinate transformations will be required for the interior and exterior regions for stages four and five after the bounce (and these are discontinuous across the boundary); as a result the location of the boundary surface $x = L$ in the conformal diagram will not be the same with respect to the interior and exterior metrics. Due to this, we identify the two locations of the boundary surface and excise the region in the conformal diagram that lies between the location of the boundary with respect to the inner and outer metrics.

With the overview complete, we now revisit each of the stages described above in more detail, first determining the location of the apparent horizons, and then describing the trajectory of $L(t)$. We do not construct the conformal diagram rigourously through coordinate transformations of the metric, but rather provide a sketch by determining which horizons and trajectories are null, spacelike, or timelike.

In spherical symmetry, the location of the apparent horizons is given by the zeros of $\Theta_+ = |\nabla x|^2$ [117], which for the Painlevé-Gullstrand form of the metric (with $E^b = x$)

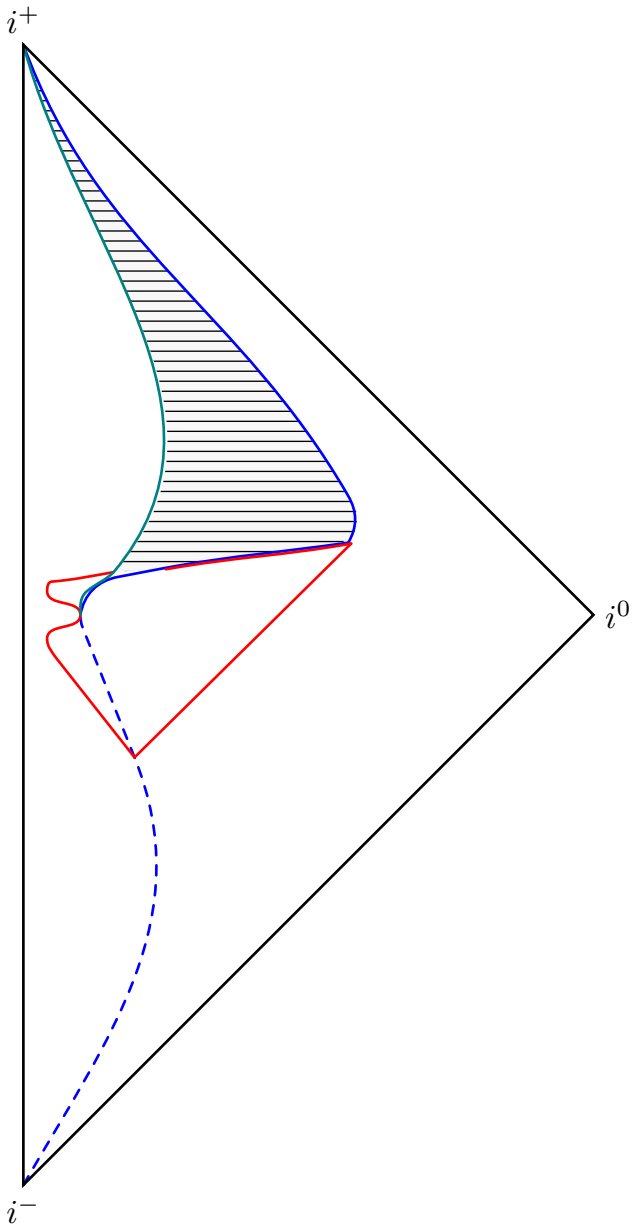

Figure 4.1: Conformal diagram for the Oppenheimer-Snyder model showing the radius of the collapsing dust sphere (dashed line), the inner and outer apparent horizons (red lines) and the outgoing shock wave as seen from the exterior (dark blue line) and as seen from the interior (light blue line). The outgoing trajectories of the shock wave are identified, and the region in between (horizontal hatching) is excised from the conformal diagram.

gives

$$\Theta_+ = |\nabla x|^2 = 1 - (N^x)^2, \tag{4.108}$$

and recall that in the effective theory $N^x = -(x/\gamma\sqrt{\Delta}) \cdot \sin\beta\cos\beta$.

During collapse, the shift vector in the interior ($x \leq L$) is given by the upper relation in (4.97), so for the interior region the zeros $x_{h,i}$ of Θ_+ are located at

$$x_{h,i}(t) = \frac{3|t|}{2} + \frac{2\gamma^2\Delta}{3|t|}. \tag{4.109}$$

Of course, there is only an apparent horizon in the interior if the location of this $x_{h,i}$ lies within $L = (\frac{9}{4}R_S t^2 + \gamma^2\Delta R_S)^{1/3}$. Neglecting quantum gravity corrections, it is easy to verify that an apparent horizon appears at $t = -2R_S/3$ at the location $x_{h,i} = R_S$, and then moves inwards as $x_{h,i} = -3t/2$, this is a faster rate than L.

Once quantum gravity corrections become important close to the bounce time $t = 0$, the apparent horizon in the interior will cross over $x_{h,i} = L$ and enter the exterior region. The time this occurs can be approximated by assuming the quantum gravity corrections dominate, so the location of the apparent horizon is $x_{h,i} \approx 2\gamma^2\Delta/(6t)$ while $L \approx L_{\text{bounce}} = (\gamma^2\Delta R_S)^{1/3}$, implying a crossover time of $t_c \approx -(8\gamma^4\Delta^2/27R_S)^{1/3}$. Substituting this back into $L(t)$ gives $L(t_c) \approx L_{\text{bounce}} + (\gamma^4\Delta^2/27R_S)^{1/3}$.

Also note that the minimum radius of the apparent horizon in the interior is $x_{h,i} = 2\gamma\sqrt{\Delta}$, which is reached at $t = -2\gamma\sqrt{\Delta}\,/3$.

To recap, there is an apparent horizon inside the dust sphere during the collapse, between the times when L reaches the radii $L \approx R_S$ and $L \approx L_{\text{bounce}} + (\gamma^4\Delta^2/27R_S)^{1/3}$. Importantly, note that $\Theta_+ > 0$ for $x < x_{h,i}(t)$, so it is the region $x > x_{h,i}$ that is trapped, while the region $x < x_{h,i}(t)$ is not trapped; this shows that this apparent horizon is an inner horizon.

For the exterior, the shift vector during collapse is given by the lower relation in (4.97), so the zeros of Θ_+ for the vacuum exterior region are located at the solutions

of the following implicit equation for $x_{h,e}$,

$$x_{h,e} = R_S \left(1 - \frac{\gamma^2 \Delta R_S}{x_{h,e}^3}\right). \tag{4.110}$$

Once again, these apparent horizons are only present if $x_{h,e} > L(t)$. It is immediately clear that there will be an apparent horizon at $x_{\text{outer}} = R_S$, neglecting quantum gravity corrections, once $L(t)$ passes the Schwarzschild radius. As expected, this is an outer horizon since $\Theta_+ < 0$ for $x < R_S$.

There is another solution to (4.110) that gives a second apparent horizon at $x_{\text{inner}} \approx L_{\text{bounce}} + (\gamma^4 \Delta^2 / 27 R_S)^{1/3}$, whose location matches the radius where the interior horizon $x_{h,i}$ exits the surface L of the dust sphere as described above. This is an inner horizon where $\Theta_+ > 0$ for $x < x_{\text{inner}}$, again as expected.

In summary, during the collapse phase a pair of apparent horizons forms when L reaches the radius $x \approx R_S$ (up to small Planckian corrections), with the outer horizon remaining at R_S in the vacuum exterior, while the radius of the inner horizon decreases faster than L (staying within the dust sphere) until it reaches x_{inner}, at which time the inner horizon crosses outside the trajectory of L, enters the vacuum exterior region and stays at x_{inner}.

After the bounce, a shock wave forms and moves outwards, as described in Sec. 4.4.3.1. The outer horizon at R_S will stay there until the outgoing shock L reaches it a time $\sim M^2/m_{\text{Pl}}$ later, at which point it will disappear. On the other hand, the inner horizon will follow (4.109) and contract back to its minimum radius of $x_{h,i} = 2\gamma\sqrt{\Delta}$ at $t = 2\gamma\sqrt{\Delta}/3$ before expanding once more. For the short period of time that $L > x_{h,i}$, the dust located inside this region is moving outwards in a trapped region—this does not indicate a violation of the dominant energy condition, but rather is due to quantum gravity effects being large and significantly modifying the dynamics from what could be expected from classical general relativity. After

$t = 2\gamma\sqrt{\Delta}/3$, the inner apparent horizon will rapidly move outward until it reaches the shock, at which point it will move in lockstep with the shock until they reach the outer apparent horizon (a time $\sim M^2/m_{\rm Pl}$ later) and then the two apparent horizons will disappear. After this, even though the black hole is now gone the shock will continue to move outwards forever.

We note also that the dust is not superluminal as it emerges from the horizon. This may be seen by recalling that for the Oppenheimer-Snyder collapse model considered here, the dust ball is isomorphic to (a portion of) the FLRW space-time. As in the FLRW space-time, the dust is not superluminal—it is just co-moving with the region of space-time that is rapidly expanding after the bounce.

The trajectory of the two (outer and inner) apparent horizons, as described, is shown in the conformal diagram in Fig. 4.1, the two apparent horizons are shown as red lines.

The other trajectory of interest in the conformal diagram is the path followed by $L(t)$, denoting the surface of the dust sphere during collapse, and the location of the shock wave after the bounce. The normal vector to the surface $x = L(t)$ is

$$n_\mu = -\left(\frac{\mathrm{d}L}{\mathrm{d}t}\right)(\mathrm{d}t)_\mu + (\mathrm{d}x)_\mu, \tag{4.111}$$

and the sign of

$$g^{\mu\nu}n_\mu n_\nu = 1 - \left(\frac{\mathrm{d}L}{\mathrm{d}t}\right)^2 - 2N^x\left(\frac{\mathrm{d}L}{\mathrm{d}t}\right) - (N^x)^2 \tag{4.112}$$

will determine whether the trajectory of L is timelike or spacelike.

During the collapse, using the solution (4.89) for $L(t)$ and the metric (4.66) with the shift vector (4.97) evaluated at $x = L$, a direct calculation gives $n^\mu n_\mu = 1$ at all times—independently of whether the interior or exterior metric is used—showing that $L(t)$ follows a timelike trajectory during the collapse.

After the bounce, the norm of n_μ will depend on the metric that is used; due to the discontinuity in the gravitational field, using the interior metric or the exterior metric will give a different answer.

With respect to the interior metric,

$$(n^\mu n_\mu)_i = 1 - \left(\frac{\mathrm{d}L}{\mathrm{d}t}\right)^2 + \frac{12\,t\,L(t)}{9t^2+4\gamma^2\Delta}\cdot\left(\frac{\mathrm{d}L}{\mathrm{d}t}\right) - \frac{36\,t^2\,L(t)^2}{(9t^2+4\gamma^2\Delta)^2}, \tag{4.113}$$

while with respect to the exterior metric,

$$(n^\mu n_\mu)_e = 1 - \left(\frac{\mathrm{d}L}{\mathrm{d}t}\right)^2 - 2\sqrt{\frac{R_S}{L(t)} - \frac{\gamma^2\Delta R_S^2}{L(t)^4}}\cdot\left(\frac{\mathrm{d}L}{\mathrm{d}t}\right) - \frac{R_S}{L(t)} + \frac{\gamma^2\Delta R_S^2}{L(t)^4}. \tag{4.114}$$

Note that in both cases $L(t)$ is given by the same solution to the differential equation (4.92). Clearly, if $n^\mu n_\mu > 0$, then the trajectory of $L(t)$ is timelike, while if $n^\mu n_\mu < 0$, then $L(t)$ is moving in a spacelike manner.

By numerically solving (4.92) for $L(t)$, it can be verified that, according to the interior metric, $L(t)$ follows a trajectory that is almost always timelike, except for the brief interval after the bounce when $L > x_{h,i}$. On the other hand, the post-bounce trajectory of L with respect to the outer metric is spacelike until L reaches the outer apparent horizon at $x = R_S$, at which instant it is null and then immediately after becomes timelike.

This is shown in the conformal diagram in Fig. 4.1, where the trajectory of $L(t)$ during collapse is given by the dashed blue line, while after the bounce the trajectory of $L(t)$ with respect to the interior and exterior metrics is shown in pale blue and dark blue respectively. As discussed above, there are two trajectories for $L(t)$ in the conformal diagram after the bounce, this is due to the discontinuity in the metric across the shock wave located at $L(t)$ after the bounce: different coordinate transformations are required for the interior and exterior regions to construct the conformal diagram, so the common boundary of the interior and exterior does not have the same location

in the conformal diagram. The conformal diagram is made whole by identifying the two locations of the boundary, and excising the portion of the conformal diagram in between (marked with a horizontal hatching).

To understand this identification in the conformal diagram, consider an infalling particle that reaches the dark blue solid line in Fig. 4.1 corresponding to the location of the shock as seen from the exterior. When the particle reaches a point on the dark blue line, it also lies on a point on the light blue line since these lines are physically the same and therefore identified (recall that the hatched region is excised from the conformal diagram). The particle would then continue to move inwards, above the light blue line in the region inside the shock wave.

In summary, the qualitative picture combining the locations of the apparent horizons and also $L(t)$ is depicted in the conformal diagram shown in Fig. 4.1: the star surface collapses to form a black hole with the formation of an outer null horizon at $x = R_S$ (neglecting tiny Planckian corrections to the location of the outer apparent horizon), together with an inner dynamical horizon; a bounce occurs when $L(t) = L_{\rm bounce} = (\gamma^2 \Delta R_S)^{1/3}$ and an outgoing gravitational shock wave forms; the shock wave slowly moves outward, and when the inner and outer horizons meet and annihilate the black hole ceases to exist.

We note that the conformal diagram constructed here is specifically for the Oppenheimer-Snyder collapse. In Sec. 4.5, we present the conformal diagram inferred from numerical solutions for a different family of initial data corresponding to the collapse of dust with a Gaussian radial density profile, see Fig. 4.6. Although the conformal diagrams have some differences, the important qualitative features are similar: there is a non-singular bounce, a gravitational shock wave, and the eventual disappearance of the black hole when the inner and outer apparent horizons meet and annihilate after a time $\sim M^2/m_{\rm Pl}$.

4.5 Numerical solutions

As discussed in the previous section, shell crossings are a feature of the effective dynamics, and evolution beyond the point where characteristic curves cross requires finding weak solutions; a numerical approach is generally needed for this. In this section we review and apply the well-known Godunov method to this problem, this is one of a family of numerical techniques available for solving non-linear flow equations.

4.5.1 Godunov method

The Godunov method is a numerical approach for solving differential equations that are non-linear conservation laws of the form $\partial_t \rho(x,t) + \partial_x j(\rho) = 0$; see, e.g., [96] for an in-depth discussion of this and related algorithms.

To use this method we first write the evolution equation (4.69) by defining

$$B(x,t) = x\, b(x,t) \quad \text{and} \quad m(x,B) = \frac{x^3}{2\gamma^2\Delta} \sin^2\left(\frac{B}{x^2}\right). \tag{4.115}$$

This gives the desired form of a conservation law

$$\partial_t B(x,t) + \partial_x m(x,B) = 0\ ; \tag{4.116}$$

the current in this equation is the mass function $m(x,t)$, which is related to the dust density (4.70):

$$m(x,t) = 4\pi \int_0^x \mathrm{d}\tilde{x}\ \tilde{x}^2 \rho(\tilde{x},t). \tag{4.117}$$

It is also evident from (4.115) that the current has an explicit x dependence.

Integrating (4.116) over a spatial interval $x_L \leq x \leq x_R$ and time interval $t_1 \leq t \leq t_2$

gives the integral form of the conservation equation (4.116),

$$\int_{x_L}^{x_R} \mathrm{d}x\ B(t_2,x) = \int_{x_L}^{x_R} \mathrm{d}x\ B(t_1,x) - \int_{t_1}^{t_2} \mathrm{d}t\ \Big[m(x,B)\Big]_{x_L}^{x_R}. \tag{4.118}$$

In either form the conservation equation is non-linear and cannot be solved analytically (except for a few especially simple configurations like thin shells and the Oppenheimer-Snyder model). Finite-volume methods like the Godunov scheme are based on the approximation that at each time step, the field is piecewise constant in every spatial cell j of width δx; that is, the field at the point (x, t_n) is defined by the spatial average over the cell

$$B_j^n = \frac{1}{\delta x} \int_{x_j - \frac{1}{2}\delta x}^{x_j + \frac{1}{2}\delta x} \mathrm{d}x\ B(x,t_n), \tag{4.119}$$

and this average value is then assigned to each point in the interval,

$$B(x,t_n) = B_j^n, \qquad x \in (x_j - \tfrac{1}{2}\delta x, x_j + \tfrac{1}{2}\delta x). \tag{4.120}$$

In this way, the field $B(x,t)$ is taken to be piecewise constant.

This discretization makes a numerical integration of the equation (4.118) possible on a space-time lattice of spacings δt and δx,

$$B_j^{n+1} = B_j^n - \frac{1}{\delta x} \int_{t_n}^{t_{n+1}} \mathrm{d}t\ \Big[m(x,B)\Big]_{x_j - \frac{1}{2}\delta x}^{x_j + \frac{1}{2}\delta x}. \tag{4.121}$$

This form of the equation shows that B_j^{n+1} can be calculated by adding the flux $m(x,B)$ across the boundaries $x_j + \frac{1}{2}\delta x$ and $x_j - \frac{1}{2}\delta x$ to the initial value B_j^n. However the fact that the time integral is from t_n to t_{n+1} means that the method is implicit and the net flux in the integrand requires careful construction. This is accomplished by the Godunov method.

The key insight underlying the Godunov method is that, given the initial conditions

of a piecewise constant field B, it is possible to solve exactly for the flux functions $m(x_j + \frac{1}{2}\delta x, B)$ and $m(x_j - \frac{1}{2}\delta x, B)$, at least for a short period of time.

The basic idea is illustrated by focusing on the flux through the boundary $x_{bd} = x_j + \frac{1}{2}\delta x$: if B is moving outwards, the flux across the boundary is given by $m(x_{bd}, B_j^n)$; if the field is moving inwards the flux is given by $m(x_{bd}, B_{j+1}^n)$. These simple forms are due to the piecewise constant prescription for B within the cell $[x_j - \frac{1}{2}\delta x, x_j + \frac{1}{2}\delta x]$. A similar consideration applies to the cell boundary at $x_j - \frac{1}{2}\delta x$.

It remains to determine the direction in which the flux moves. This requires the velocity of B, given by the derivative of the current function m in (4.116) with respect to B,

$$v = \partial_B m = \frac{x}{\gamma^2 \Delta} \sin\left(\frac{B}{x^2}\right) \cos\left(\frac{B}{x^2}\right); \tag{4.122}$$

v depends on both the position x and the value of the field B.

There are four possible types of B-field velocity configurations at each boundary x_{bd} between two lattice cells. Denoting quantities on the left and right of the boundary by the subscripts L and R respectively, the possibilities are:

(i) $v_L \geq 0$ and $v_R \geq 0$: field moving right/outwards;

(ii) $v_L \leq 0$ and $v_R \leq 0$: field moving left/inwards;

(iii) $v_L \geq 0 \geq v_R$: shock wave;

(iv) $v_L < 0 < v_R$: rarefaction wave.

The first two cases are simple as they have velocities in the same direction. The third case corresponds to a shock wave with speed $v_s = [m]/[B]$ (4.28), with its sign determining whether the shock moves outwards (positive v_s) or inwards (negative v_s), and flux $m(x_{bd}, B_j^n)$ or $m(x_{bd}, B_{j+1}^n)$ respectively. The fourth case is a rarefaction wave, the corresponding flux is obtained by taking $m(x_{bd}, B_s)$ where B_s is the stationary

value of B where $v = 0$. From (4.116) and (4.122), $v = 0$ for $B = \pi x^2/2$, for which $m(x_{bd}, B_s) = x_{bd}^3/(2\gamma^2\Delta)$.

By looking at the explicit forms in terms of B of the current $m(x, B)$ in (4.115) and the velocity $v(x, B)$ in (4.122), the flux for these four cases are summarized by

$$F(B_j^n, B_{j+1}^n, x_{bd}) = \begin{cases} \min_{B_j^n \le B \le B_{j+1}^n} \Big(m(x_{bd}, B) \Big) & \text{for } B_j^n \le B_{j+1}^n, \\ \max_{B_{j+1}^n \le B \le B_j^n} \Big(m(x_{bd}, B) \Big) & \text{for } B_j^n > B_{j+1}^n. \end{cases} \tag{4.123}$$

The min and max refer the minimum/maximum value attained by $m(x_{bd}, B)$ for B in the given interval. This is the general Godunov scheme for the flux; it holds also for a non-convex flux function (m in this case); i.e., for either sign of $\partial_B^2 m$. Here, due to the relatively simple (although non-convex) form of m, for the interval $B \in [-\pi x_{bd}^2, 0]$ the minimum is always one of the two endpoints, while the maximum is either one of the two endpoints or the stationary point $m(x_{bd}, B_s) = x_{bd}^3/(2\gamma^2\Delta)$ if the stationary point B_s lies between B_L and B_R.

With this prescription of the flux function, discrete evolution equation takes the explicit form

$$B_j^{n+1} = B_j^n - \frac{\delta t}{\delta x} \Big[F(B_{j+1}^n, B_j^n, x_j + \tfrac{1}{2}\delta x) - F(B_j^n, B_{j-1}^n, x_j - \tfrac{1}{2}\delta x) \Big], \tag{4.124}$$

For boundary conditions, since $B = xb$ we impose that $B(x = 0) = 0$, and we also assume that there is no infalling matter coming from beyond the outermost lattice point x_{last} by assuming that $\dot{B}(x_{\text{last}}) = 0$, recall that $\dot{B} = 0$ in vacuum as seen in (4.75).

Lastly, the discrete evolution scheme is stable provided δt is chosen small enough to satisfy the Courant-Friedrich-Lewy condition that $\delta t < \delta x/|v_{\max}|$ where $|v_{\max}|$ is the maximal speed v at any boundary x_{bd} for the given time step. In the numerical code, we determine δt dynamically by finding the maximum characteristic speed $v_{\max}$

at each time step and using this to fix δt to an appropriate value.

The MATLAB code we used is available online [118].

4.5.2 Results

We used the algorithm described above to generate numerical solutions for Gaussian and hyperbolic tangent initial density profiles given by

$$\rho_0^G(x) = \exp\Big(-(x-x_0)^2/\sigma^2\Big), \tag{4.125}$$

$$\rho_0^T(x) = 1+\tanh\Big(-(x-x_0)/\sigma\Big), \tag{4.126}$$

that we use to construct an initial mass function

$$m(x,t=0) = M\,\frac{\int_0^x \mathrm{d}\tilde{x}\ \rho_0(\tilde{x})}{\int_0^\infty \mathrm{d}\tilde{x}\ \rho_0(\tilde{x})}, \tag{4.127}$$

where M denotes the total mass. We considered M ranging from $5m_{\rm Pl}$ to $\sim 200m_{\rm Pl}$. Inverting (4.115) gives the initial profile for B,

$$B(x,t=0) = -x^2\arcsin\left(\sqrt{\frac{2\gamma^2\Delta\, m(x,t=0)}{x^3}}\right), \tag{4.128}$$

and we evolve B using the Godunov method described above. The negative sign of the square root corresponds to a density profile that is initially contracting, this is the case of interest for gravitational collapse.

Time frames from a typical simulation of Gaussian data for $M = 5\ m_{\rm Pl}$ are shown in Fig. 4.2. The left column displays the evolving density profile at the displayed times, and the right column is the function

$$\Theta_+(x,t) = |\nabla x|^2 = 1-(N^x)^2 = 1-\frac{x^2}{4}\sin^2\left(\frac{2B}{x^2}\right), \tag{4.129}$$

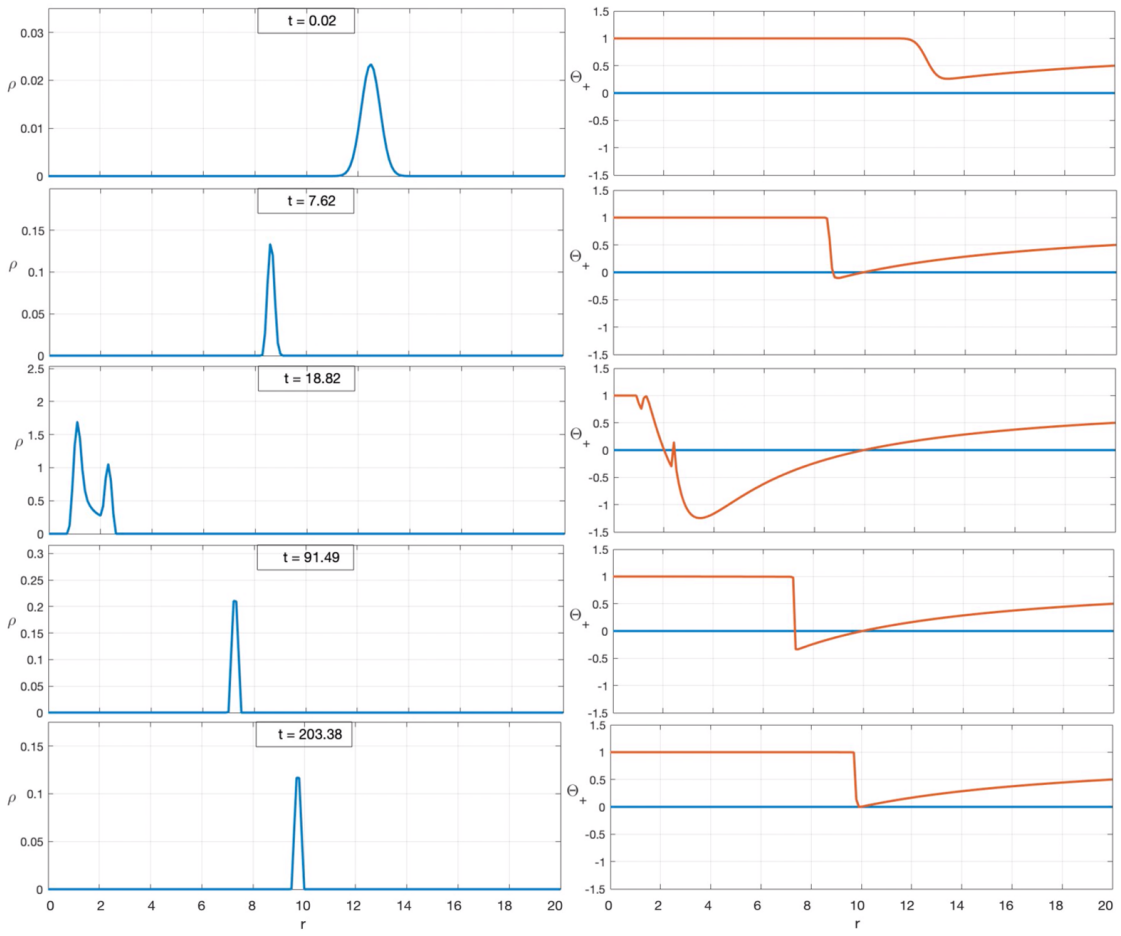

Figure 4.2: Frames from a numerical simulation of black hole formation and evolution for the Gaussian initial density profile with $M = 5m_{\rm Pl}$; the left column is the energy density ρ; the right column is the function Θ_+; its zeros give the locations of apparent horizons. The middle frame shows part of the bounce. Axes are in Planck units and $\gamma^2\Delta = 1$.

the roots of Θ_+ give the locations of the evolving apparent horizons [117]. A number of features are apparent in Fig. 4.2: as the density profile moves inward, it compresses to become a sharp pulse; the outer horizon forms at the Schwarzschild radius $R_S = 2GM = 10\ell_{\rm Pl}$ as the pulse crosses this radial location; the inner horizon moves inward until the matter bounces, and then moves outward; finally in the last frame the inner and outer horizons merge and disappear as the outgoing shock wave exits the horizon. These general features can be seen for all choices of M (except very small $M < 8\gamma\sqrt{\Delta}/\sqrt{27}G$ for which a horizon never forms [41], although the bounce and

shock formation still occur).

The collapse for hyperbolic tangent initial data is somewhat different, but there is also a bounce and an outgoing shock, this is shown in Fig. 4.3. The outgoing evolution is quite similar to that for Gaussian initial data: the density becomes sharply peaked at the shock, and the inner horizon moves outwards until it meets the outer horizon. These general features occur for all hyperbolic tangent initial data with $M > 8\gamma\sqrt{\Delta}/\sqrt{27}G$.

The evolution of two Gaussian profiles is shown in Fig. 4.4. Again the main features are qualitatively similar: horizon formation, non-singular bounce, shock formation, and eventual disappearance of the horizons. There are two notable points for the double pulse results: the second ingoing profile does not cause the outgoing shock wave to recollapse, and the mass function remains bounded at the inner horizon. These features show a robustness of the results to perturbations.

We also calculated the black hole lifetime T from numerical simulations. This is the time between the formation and disappearance of its outer apparent horizon. It is natural to calculate this using the proper time of a distant observer who observes a light ray emitted shortly before the collapse forming the black hole (for example, from a supernova of a collapsing star), and another light ray emitted by the shock wave once it has exited the outer apparent horizon. A short calculation shows that this proper time interval, as measured by a distant observer, equals the Painlevé-Gullstrand coordinate time between the formation and disappearance of the outer apparent horizon [87].

In our simulations, we numerically record the times at which the outer horizon appears and disappears, the results are shown in Fig. 4.5. The best fit is shown in each of the plots, in both cases the leading order behaviour is

$$T \approx \frac{8\pi}{3}M^2 + \mathcal{O}(M), \tag{4.130}$$

in units where $G = \hbar = c = 1$, and having set $\gamma^2\Delta = 1$ for the numerics.

This result is in good agreement with the expectation from analytic calculations in the Oppenheimer-Snyder and thin shell models (4.101) and (4.107). This not surprising: numerical simulations show that soon after the bounce, the dust density can be approximated by a thin shell, so the thin shell calculation gives the correct leading order contribution to T.

The predicted black hole lifetime $T \sim M^2/m_{\rm Pl}$ is very long in astrophysical terms, but short compared to the lifetime of a black hole as predicted by standard Hawking evaporation calculations. We comment below in Sec. 4.6 on the implications of this result for the information loss problem.

This completes our description of numerical results. We now provide several comments and describe the conformal diagram suggested by our simulations.

The outgoing shock wave may be viewed in some ways as "white hole." Indeed, it has been argued that quantum gravity might generate a transition from a black hole to a white hole [78]. But white holes are known to be unstable to infalling matter in general relativity; under small perturbations they recollapse and subsequently form a black hole [82, 83]. Our results are similar in spirit in that a singularity is replaced by a bounce, but different in the important detail that a shock wave is not a white hole. Our simulation of the double Gaussian provides numerical evidence that the outgoing shock wave is stable to an ingoing perturbation. This distinguishes our result from the black to white hole transition ideas.

Another instability in classical general relativity is mass inflation [84–86]. This is the observation that the mass function grows without bound at an inner Cauchy horizon under time-dependent perturbations. On this horizon, infalling radiation is infinitely blueshifted. Therefore, in generic collapse the expectation is that backreaction would produce a curvature singularity at an inner horizon. This effect has also been observed in some non-singular black hole models in loop quantum gravity [119].

There is no mass inflation evident in our simulations. While the curvature is not well-defined at the shock due to the jump discontinuity, the density remains finite at all times and the total mass in the space-time is dynamically conserved.

To summarize these points, our numerical simulations show that there is no recollapse of the shock wave, and there is no mass inflation.

Our last observation is the determination of a conformal diagram. The diagram corresponding to our numerical solutions is qualitatively similar to that for the effective Oppenheimer-Snyder model described in Sec. 4.4.3.3. The main difference is during the collapse phase, where some features of the conformal diagram depend on the initial density profile. For the hyperbolic tangent data, the conformal diagram is essentially identical to the one derived analytically for the Oppenheimer-Snyder collapse model shown in Fig. 4.1.

For Gaussian initial data, the conformal diagram is shown in Fig. 4.6. It is slightly different in two ways. Firstly, the trajectory of the star surface is replaced by a packet of dust trajectories, and there may be multiple dynamical inner horizons depending on the type of initial data chosen (for example, if there are multiple Gaussian packets in the initial dust profile). Secondly, the inner horizon moves differently during the collapse phase: it moves inwards more slowly, following the Gaussian dust density. Despite these two points of difference, the main features remain the same: a collapse during which inner and outer horizons are formed, a non-singular bounce, formation and outward evolution of a shock wave, and the eventual disappearance of the inner and outer horizons when they meet.

As for the conformal diagram for the Oppenheimer-Snyder model, the trajectory of the shock wave can be calculated with respect to the inner space-time metric, or the outer one, with different results. This is why two trajectories are shown for the shock wave; these curves are identified in the conformal diagram and the hatched region in between is excised.

4.6 Implications for black hole physics

We discuss here potential consequences of shock wave formation, and the implications of the predicted black hole lifetime for the information loss problem.

4.6.1 Shock wave formation and quantum geometry domain walls

All our simulations show shock wave formation, this appears to be a generic feature of any initial data profile. For some initial profiles, a shock wave may form during the collapse phase; these are the cases that may be artificially avoided by imposing restrictions on initial data as in [61, 89–92]. No matter the initial conditions, characteristic curves from the $\rho \neq 0$ region and the exterior vacuum region cross after the bounce.

Thus, in every case, including the double-peaked Gaussian profiles, an outgoing shock wave eventually emerges from the Schwarzschild radius signaling the end of the black hole phase. Although our simulations were limited to masses up to $\sim 200\ m_{\rm Pl}$, the shock wave is expected to emerge from the outer horizon for data of any mass since there is no mechanism in the effective equation for the current to change sign during the outgoing phase. (Although the shock wave solutions we find may be viewed in some respects to be similar to a white hole solution, their properties are quite different: the shock wave solution is stable to infalling matter whereas a white hole solution is not [82].)

The occurrence of a shock wave has not been noticed in previous work, likely because many of the earlier studies focused on vacuum solutions or only included simple models for matter with a finite number of degrees of freedom (as opposed to a field theory with local degrees of freedom like the LTB space-time). Still, it is important to ask whether the shock wave is a robust prediction, or merely the

consequence of some restriction, for example a gauge choice that may fail. As such, it would be useful to extend this work by relaxing the gauge conditions (namely the areal and dust-time gauges), but this generalization lies beyond the scope of this paper and is left for future work. Instead, we present some general arguments supporting the formation of a shock wave in a non-singular bouncing black hole in LQG.

Firstly, the bounce of the dust ball is not surprising—the region inside the collapsing dust sphere is locally similar to a contracting cosmological space-time (in fact, for the Oppenheimer-Snyder model this is an exact isomorphism), and these are known to bounce in loop quantum cosmology [7]. Secondly, the vacuum region outside the dust sphere has no local degrees of freedom (at least in the spherically symmetric case we consider here) and therefore cannot evolve in the absence of matter; for example, in the marginally bound LTB space-times we consider here, by combining (4.69) and (4.70) it is easy to show that $\dot{b} = 0$ when $\rho = 0$. With these two ingredients, we expect a bounce inside the collapsing dust ball, but not outside. This causes a discontinuity to form, and it is the source of the shock wave.

Another way to see this is to consider an initial configuration with a dense core and a more dilute outer region; the core will bounce first and collide with the outer region which is still collapsing; this causes a shell-crossing and thereby the formation of a shock wave. More generally, if there is an effective description of the space-time, it will presumably be governed by a wave equation that can reasonably be expected to be non-linear; solutions to non-linear wave equations are typically weak solutions, often including shock waves (especially solutions corresponding to highly energetic phenomena). Given this general expectation, it has been argued that it is necessary to allow weak solutions for LTB space-times even in classical general relativity [94, 95]. It is therefore not surprising that weak solutions are important also for effective metrics with quantum gravity corrections, as we find here. These arguments suggest that shock waves are a robust feature of quantum black holes formed from matter collapse,

at least in LQG and possibly in other approaches to quantum gravity that resolve the black hole singularity.

There are different perspectives one can take when studying the shock waves found here. The simplest is to view the shock as a weak solution of the non-linear wave equation, as we have done. Another complementary perspective that may be valuable is to view the shock wave as a domain wall in space-time.

The late-time post-bounce effective solution has two regions, the inside region (lying within the shock wave), and the outside region. Since the shock wave is slowly moving outwards, the boundary between the two regions is also dynamical. Each region is separately well described by an effective line element, with a discontinuity across the shock. Taking seriously the perspective of LQG that a classical geometry should emerge from the coarse-grained description of many microscopic Planck-scale quanta of geometry, we propose the interpretation that the two regions are in different phases of the underlying quanta of geometry, with the shock wave being a domain wall separating the two (and carrying a non-zero energy density). From this perspective, the effective dynamics may have a thermodynamic interpretation, and the bounce can be understood as creating a domain wall separating two geometric phases.

At late times after the bounce, nearly all the dust accumulates on the shock wave, with the result that the interior region is nearly Minkowski and the exterior is nearly classical Schwarzschild. These are two vacuum solutions of classical general relativity, presumably corresponding to different microscopic configurations of the fundamental quanta of geometry. As the shock wave (or domain wall) moves outwards, the outside Schwarzschild vacuum geometry slowly relaxes to the Minkowski vacuum geometry. From a quantum geometry perspective, the shock wave is a domain wall that separates two different phases of vacuum quantum gravity.

4.6.2 Observable consequences

It is natural to expect that a shock wave emerging from what was a black hole could have significant observational consequences. The black hole lifetime result $T \sim M^2/m_{\rm Pl}$ suggests that (dust) black holes of $\sim 10^{-8}$ solar masses have a lifetime of approximately the current age of the universe. If formed in the very early universe, such black holes would be on the verge of disappearing via shock wave emission at the present time.

A more realistic collapse model will include several matter fields, not just dust. If the general picture obtained here continues to be applicable, then photons (for example) would be part of the shock wave, and be unable at first to move outward any faster due to the outer apparent horizon. After the shock wave exits the horizon, photons would no longer be trapped and could move outwards faster than the shock, and ultimately be detected by distant observers. The same scenario holds for other types of particles, so a shock wave would release a variety of astroparticles. For a discussion of possible observational consequences in a related (but not identical) scenario, see [79–81].

Another possibility that we mention is that the shock wave might also generate significant gravitationally induced particle production that might be detectable.

However, the prospect for such potential phenomenological consequences could be suppressed (perhaps significantly) by the gravitational redshift of the exterior Schwarzschild geometry: if a photon escapes from the shock wave after the shock has emerged a short distance δ outside its Schwarzschild radius R_S, the photon's frequency would be red-shifted by a factor $\sim \delta/R_S$ (assuming $\delta \ll R_S$); this redshift could make observations challenging even if the photon is initially highly energetic.

4.6.3 Information loss problem

The prediction that the black hole lifetime is of the order $T \sim M^2/m_{\rm Pl}$ has important implications for the black hole information loss problem.

It is well known that a black hole emits thermal radiation at the Hawking temperature $T_H = \hbar/8\pi G k_B M$. Assuming a quasi-static evaporation process, if black hole evaporation is the only quantum effect, its lifetime would be $\sim M^3/m_{\rm Pl}^2$ [3]. This leads to the black hole information loss problem: an initially pure state of matter on a black hole background evolves into a thermal state with non-zero entropy.

This problem with unitarity arises well before a black hole has completely evaporated. Assuming that the entropy of black hole thermodynamics $S = A/4G\hbar$ represents (the logarithm of) the number of microscopic degrees of freedom constituting a black hole, if the initial state is pure and the evolution is unitary, then any Hawking radiation (although it may appear to be thermal) must be entangled with geometric degrees of freedom in the black hole. As the black hole evaporates, the number of Hawking quanta increases while the number of black hole geometric degrees of freedom decreases. The increase in the number of Hawking quanta indicates that the required entanglement between Hawking radiation and the black hole degrees of freedom must also increase. But this is in tension with the decreasing number of black hole degrees of freedom. The Page time is when $\exp(A/4G\hbar)$, the number of degrees of freedom in the (evaporating) black hole, is no longer sufficient for the Hawking quanta to be entangled with the black hole [120, 121]. It is at the Page time that the information loss problem truly denotes a potential loss of unitarity in the dynamics; before the Page time it is (at least in principle) possible for all Hawking radiation to be entangled with the black hole and for the total system (black hole and Hawking radiation) to remain in a pure state. The Page time is approximately half the evaporation lifetime of a black hole, and therefore is of order $\sim M^3/m_{\rm Pl}^2$.

There are several differences between the features derived here as compared to the standard treatment. Two particularly important differences are the absence of a singularity and the absence of an eternal event horizon. In the standard semi-classical treatment of Hawking evaporation, the background space-time is assumed to be the classical Schwarzschild geometry, with a singularity and event horizon. These features make it difficult to see how information could escape a black hole: firstly, any information inside the horizon would eventually hit the singularity and be destroyed there, and (assuming energy conditions hold) information would not be able to travel in a spacelike fashion to escape the event horizon. In contrast, in the scenario we study, quantum gravity effects resolve the singularity and replace the eternal event horizon by a long-lived but temporary apparent horizon. As a result, the two obvious obstructions to information recovery are removed by quantum gravity effects, which also significantly change the causal structure of the space-time. This is exhibited in the conformal diagram in Fig. 4.6.

This result is in agreement with earlier work in LQG, which similarly suggests that quantum gravity effects will resolve the singularity, thereby enlarging the space-time and also replacing the event horizon by an apparent horizon which eventually vanishes [8, 11, 50, 122]. However, there are some important differences in the specific way this occurs in comparison to earlier proposals, in large part due to the presence of matter. During the collapse process, an inner horizon forms inside the dust ball, and eventually exits the dust ball just before the bounce. (As a concrete example, in the Oppenheimer-Snyder collapse model the location of the inner horizon is at its 'Hubble radius' $r_H = L/\dot{L}$, and it exits the star when $r_H = L$.) Continuity requires that this inner horizon extend into the vacuum region outside the dust ball, and this modifies in some important aspects the general scenario proposed in Refs. [11, 50, 122].

Specifically, with an inner horizon, the radial coordinate x (of the areal gauge) is space-like (and therefore $x =$ constant surfaces are timelike) in the region between the

origin and the inner horizon, including a neighbourhood outside the dust sphere at the bounce. Due to this fact, it is impossible to glue a white hole solution to the future of a black hole solution, a scenario that requires $x =$ constant surfaces be spacelike. Hence, instead of a black hole to white hole transition, the future of the black hole in this scenario is an outgoing shock wave, as described in detail here with the conformal diagram in Fig. 4.1.

In addition to the absence of a singularity and the absence of an eternal event horizon, Hawking radiation can continue only while the black hole outer horizon exists—this is the black hole lifetime $T \sim M^2/m_{\rm Pl}$ before the shock wave reaches this horizon. (This feature is another important difference with earlier studies of black holes in LQG, which typically assume that the black hole will eventually fully evaporate after a lifetime of $T \sim M^3/m_{\rm Pl}^2$ [11, 50, 122], although see [77, 78] for a discussion on different possible lifetimes, including $T \sim M^2/m_{\rm Pl}$.) Due to the shorter lifetime of the outer horizon that we find, Hawking evaporation would end well before the Page time (assuming the initial black hole mass satisfies $M \gg m_{\rm Pl}$). As a result, the amount of Hawking radiation would be relatively small (compared to what is predicted by the standard semiclassical calculations based on the assumption that the black hole completely evaporates due to Hawking radiation). Therefore, this limited amount of Hawking radiation could remain entangled with the degrees of freedom of the black hole without loss of unitarity, and information could escape with the shock wave, in gravitational and matter degrees of freedom, as the shock wave exits the horizon.

To summarize, quantum gravity effects captured by our model (i) remove the singularity, (ii) remove the event horizon, and (iii) predict the lifetime of a quantum black hole to be $\sim M^2/m_{\rm Pl}$. The combination of these three ingredients suggests that Hawking radiation lasts for the duration of the black hole's lifetime $T \sim M^2/m_{\rm Pl}$. As a consequence, Hawking radiation can remain entangled with black hole degrees of

freedom (or perhaps with Planckian geometric or pre-geometric degrees of freedom [122]), and information can be recovered (at least in principle) by an outside observer once the shock wave exits the outer apparent horizon at the end of the black hole's lifetime.

We leave for future work an extension of this model to include Hawking radiation, and develop further the resolution of the information loss problem suggested here.

4.7 Summary

This work provides a model for black hole formation and subsequent evolution based on a loop quantization of Lemaître-Tolman-Bondi space-times. Using the effective equations derived from the quantum theory, the singularity is replaced by a non-singular bounce, and a shock forms after the bounce in the gravitational field, with a discontinuity in the metric. We find weak solutions to the effective dynamics, these include analytic solutions for the Oppenheimer-Snyder and thin shell models, and numerical solutions for a variety of initial dust energy density profiles. The black hole lifetime, predicted to be $T \sim M^2/m_{\rm Pl}$, together with the absence of a singularity or an event horizon, suggests that the information loss problem is avoided; Hawking radiation remains entangled with the black hole degrees of freedom, and ends as the shock wave exits the outer apparent horizon in a time much less than the Page time.

Our results provide a step towards providing an all-encompassing view of black hole physics—an effective quantum dynamics problem in a field theoretic setting that describes gravitational collapse to black hole formation to post-bounce dynamics. This field-theoretic description goes beyond "quantizing the Schwarzschild metric" or the Oppenheimer-Snyder model, which are both systems with only a finite number of degrees of freedom.

Spherically symmetric systems with matter provide useful field theory models, and dust is the simplest form of matter. A next step would be to extend this model to include other types of matter that have non-vanishing pressure; for example, it would be interesting to consider a massless scalar field in spherical symmetry, a system that has been well studied classically—for some recent work in this direction (although it does not use the improved dynamics), see [62].

There remain a number of questions within the dust model. First, it would also be interesting to revisit the model without imposing any gauges before quantization.

Second, the weak solutions we described are for the subset of LTB space-times with $E^b = x$; it would be interesting to see whether the main features we report here remain unaltered for the more general case without this condition. The physical argument that characteristics inevitably cross when a bounce occurs suggests that an outgoing shock wave will remain.

Another question concerns the effective equations themselves. The quantum gravity corrections they contain capture the fundamental discreteness that comes from the discrete spectrum of the area operator in loop quantum gravity, but they neglect quantum fluctuations. It would be interesting to look for solutions to the quantum dynamics that include quantum fluctuations as well, especially in the high-curvature regime.

Beyond the specific model proposed here, our results suggest a new perspective that a shock wave following a bounce may be a ubiquitous feature of singularity avoidance in black holes for any approach to quantum gravity, and raise the possibility that a lifetime of the order of $\sim M^2/m_{\rm Pl}$ provides a means for solving the black hole information loss problem.

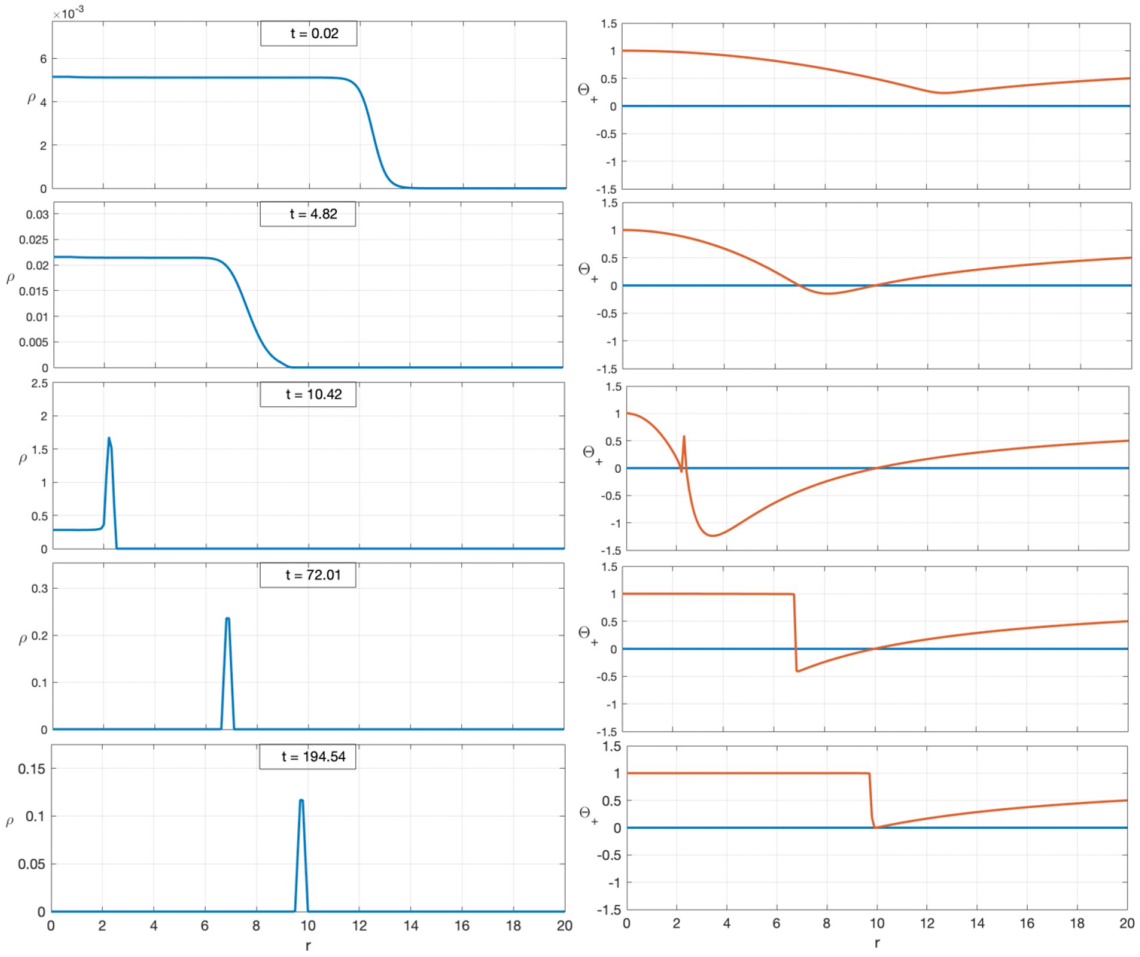

Figure 4.3: Frames from a numerical simulation of black hole formation and evolution for the Gaussian initial density profile with $M = 5m_{\rm Pl}$; the left column is the energy density ρ; the right column is the function Θ_+; its zeros give the locations of apparent horizons. The middle frame shows part of the bounce. Axes are in Planck units and $\gamma^2\Delta = 1$.

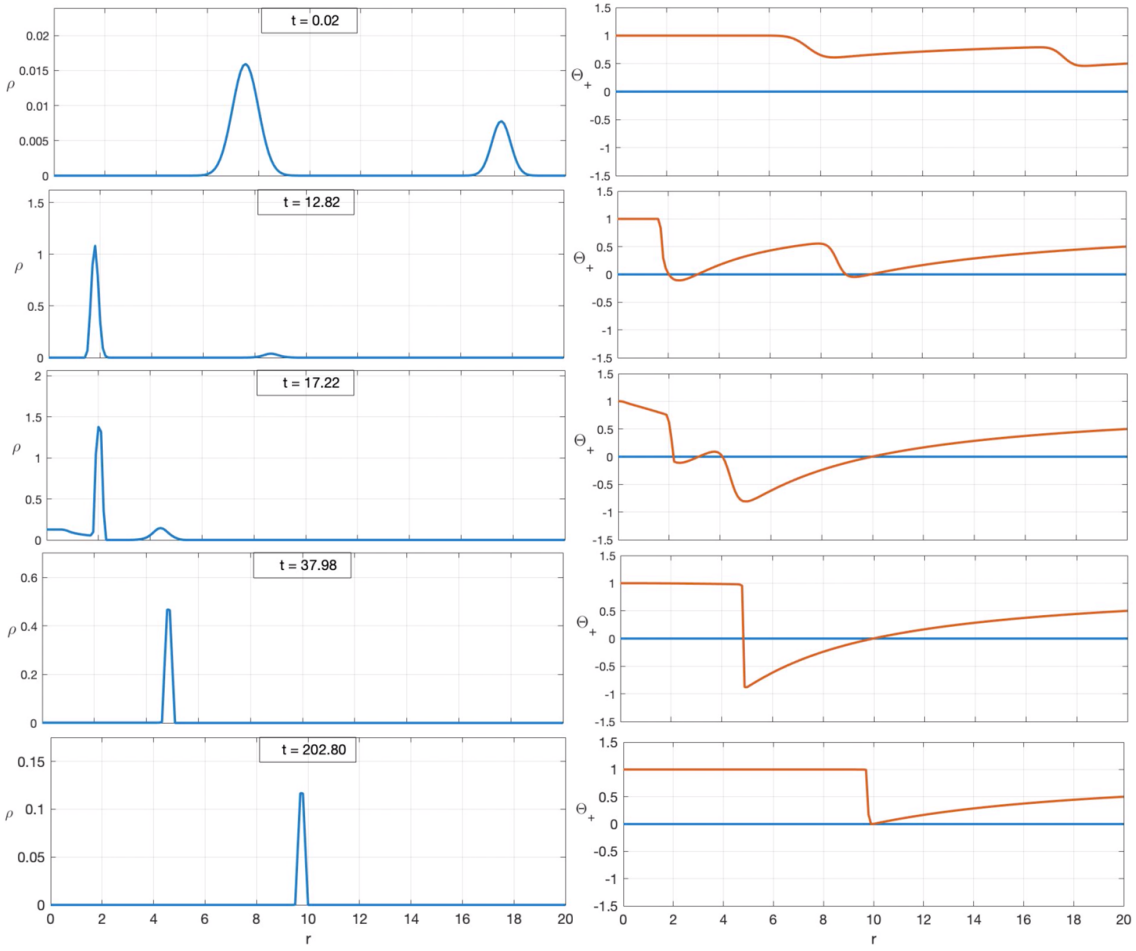

Figure 4.4: Frames from a numerical simulation of black hole formation and evolution for the initial density profile $\rho_0(x) = \exp[-2(x-7.5)^2]/5 + \exp[-4(x-17.5)^2]/10$ in (4.127) with $M = 5\ m_{\rm Pl}$; the left column is the energy density ρ; the right column is the function Θ_+; its zeros give the locations of apparent horizons. The middle frame shows part of the bounce. Axes are in Planck units and $\gamma^2\Delta = 1$. These frames are also shown in the companion letter [88].

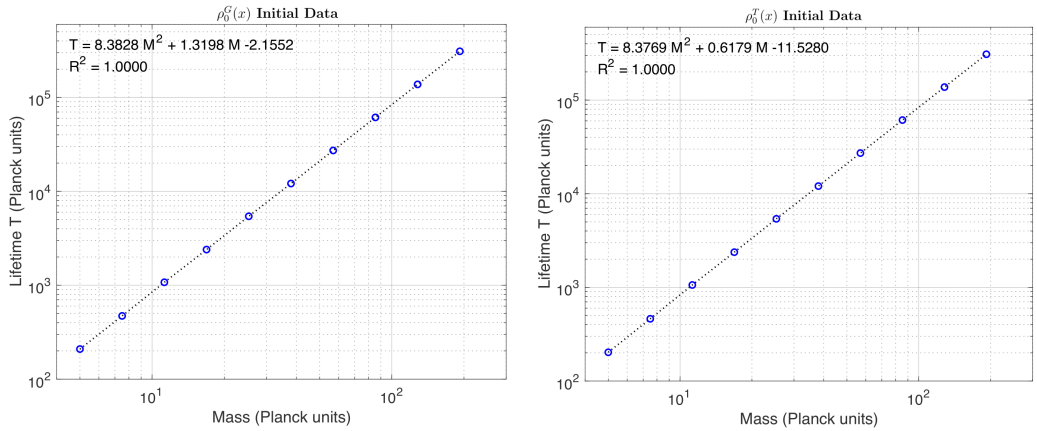

Figure 4.5: Black hole lifetime T as a function of data mass M for Gaussian (left) and hyperbolic tangent (right) initial density profiles. The leading order dependence is $T = 8\pi M^2/3 + \mathcal{O}(M)$ to an excellent approximation. Axes are in Planck units with $\gamma^2\Delta = 1$. These plots are also shown in the companion letter [88].

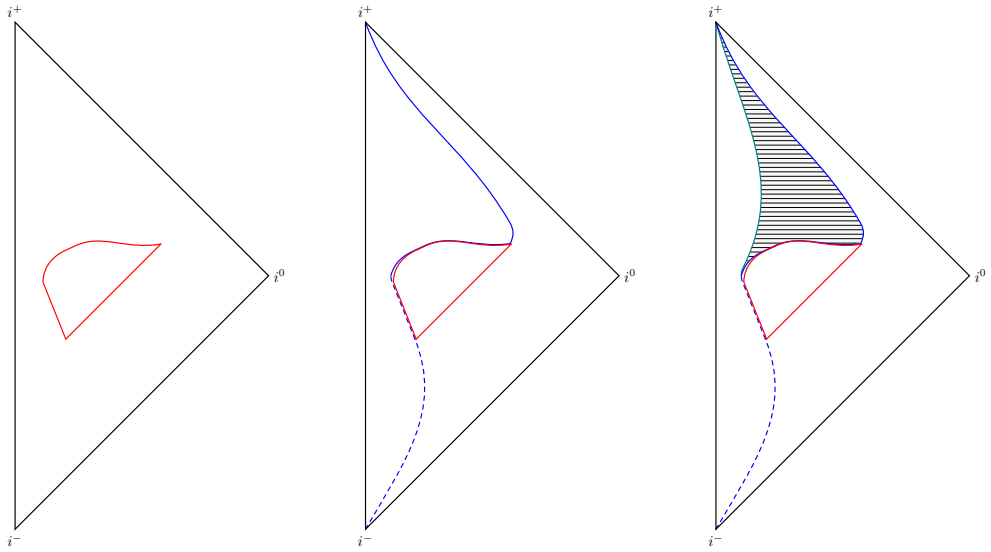

Figure 4.6: The conformal diagram is shown in three frames. The left frame shows the apparent horizons in red; the outer horizon is null. The middle frame also includes the location of the collapsing Gaussian wave packet with the dashed blue line, and the solid blue gives the outgoing shock wave as seen by an outside observer, the shock wave exits at the point where the inner and outer horizons meet. The third frame illustrates the discontinuity in the metric at the shock wave—its trajectory is timelike from the perspective of the interior (shown in cyan), while it is spacelike with respect to the exterior metric until it exits the outer horizon at which time it becomes timelike; the hatched region is excised and the inner and outer shock wave trajectories are identified. The rightmost conformal diagram is also shown in the companion letter [88].

Bibliography

[1] D. Christodoulou, "The Structure and Uniqueness of Generalized Solutions of the Spherically Symmetric Einstein Scalar Equations," Commun. Math. Phys. **109** (1987) 591–611.

[2] M. W. Choptuik, "Universality and scaling in gravitational collapse of a massless scalar field," Phys. Rev. Lett. **70** (1993) 9–12.

[3] S. W. Hawking, "Particle Creation by Black Holes," Commun. Math. Phys. **43** (1975) 199–220. [Erratum: Commun.Math.Phys. 46, 206 (1976)].

[4] A. Ashtekar and J. Lewandowski, "Background independent quantum gravity: A Status report," Class. Quant. Grav. **21** (2004) R53, `arXiv:gr-qc/0404018`.

[5] C. Rovelli, *Quantum Gravity*. Cambridge University Press, 2004.

[6] T. Thiemann, *Modern Canonical Quantum General Relativity*. Cambridge University Press, 2007.

[7] A. Ashtekar and P. Singh, "Loop Quantum Cosmology: A Status Report," Class. Quant. Grav. **28** (2011) 213001, `arXiv:1108.0893`.

[8] A. Perez, "Black Holes in Loop Quantum Gravity," Rept. Prog. Phys. **80** (2017) 126901, `arXiv:1703.09149`.

[9] A. Ashtekar, T. Pawlowski, and P. Singh, "Quantum Nature of the Big Bang: Improved dynamics," Phys. Rev. D **74** (2006) 084003, `arXiv:gr-qc/0607039`.

[10] L. Modesto, "Disappearance of black hole singularity in quantum gravity," Phys. Rev. D **70** (2004) 124009, arXiv:gr-qc/0407097.

[11] A. Ashtekar and M. Bojowald, "Quantum geometry and the Schwarzschild singularity," Class. Quant. Grav. **23** (2006) 391–411, arXiv:gr-qc/0509075.

[12] C. G. Boehmer and K. Vandersloot, "Loop Quantum Dynamics of the Schwarzschild Interior," Phys. Rev. D **76** (2007) 104030, arXiv:0709.2129.

[13] M. Campiglia, R. Gambini, and J. Pullin, "Loop quantization of spherically symmetric midi-superspaces : The Interior problem," AIP Conf. Proc. **977** (2008) 52–63, arXiv:0712.0817.

[14] D.-W. Chiou, "Phenomenological loop quantum geometry of the Schwarzschild black hole," Phys. Rev. D **78** (2008) 064040, arXiv:0807.0665.

[15] J. Brannlund, S. Kloster, and A. DeBenedictis, "The Evolution of Lambda Black Holes in the Mini-Superspace Approximation of Loop Quantum Gravity," Phys. Rev. D **79** (2009) 084023, arXiv:0901.0010.

[16] A. Joe and P. Singh, "Kantowski-Sachs spacetime in loop quantum cosmology: bounds on expansion and shear scalars and the viability of quantization prescriptions," Class. Quant. Grav. **32** (2015) 015009, arXiv:1407.2428.

[17] A. Corichi and P. Singh, "Loop quantization of the Schwarzschild interior revisited," Class. Quant. Grav. **33** (2016) 055006, arXiv:1506.08015.

[18] J. Cortez, W. Cuervo, H. A. Morales-Tecotl, and J. C. Ruelas, "Effective loop quantum geometry of Schwarzschild interior," Phys. Rev. D **95** (2017) 064041, arXiv:1704.03362.

[19] J. Olmedo, S. Saini, and P. Singh, "From black holes to white holes: a quantum gravitational, symmetric bounce," Class. Quant. Grav. **34** (2017) 225011, arXiv:1707.07333.

[20] J. Ben Achour, F. Lamy, H. Liu, and K. Noui, "Polymer Schwarzschild black hole: An effective metric," EPL **123** (2018) 20006, arXiv:1803.01152.

[21] A. Ashtekar, J. Olmedo, and P. Singh, "Quantum extension of the Kruskal spacetime," Phys. Rev. D **98** (2018) 126003, arXiv:1806.02406.

[22] N. Bodendorfer, F. M. Mele, and J. Münch, "Effective Quantum Extended Spacetime of Polymer Schwarzschild Black Hole," Class. Quant. Grav. **36** (2019) 195015, arXiv:1902.04542.

[23] M. Assanioussi, A. Dapor, and K. Liegener, "Perspectives on the dynamics in a loop quantum gravity effective description of black hole interiors," Phys. Rev. D **101** (2020) 026002, arXiv:1908.05756.

[24] N. Bodendorfer, F. M. Mele, and J. Münch, "(b,v)-type variables for black to white hole transitions in effective loop quantum gravity," Phys. Lett. B **819** (2021) 136390, arXiv:1911.12646.

[25] C. Zhang, Y. Ma, S. Song, and X. Zhang, "Loop quantum Schwarzschild interior and black hole remnant," Phys. Rev. D **102** (2020) 041502, arXiv:2006.08313.

[26] F. Sartini and M. Geiller, "Quantum dynamics of the black hole interior in loop quantum cosmology," Phys. Rev. D **103** (2021) 066014, arXiv:2010.07056.

[27] M. Geiller, E. R. Livine, and F. Sartini, "Symmetries of the black hole interior and singularity regularization," SciPost Phys. **10** (2021) 022, arXiv:2010.07059.

[28] K. Blanchette, S. Das, S. Hergott, and S. Rastgoo, "Black hole singularity

resolution via the modified Raychaudhuri equation in loop quantum gravity," Phys. Rev. D **103** (2021) 084038, arXiv:2011.11815.

[29] M. de Cesare, S. S. Seahra, and E. Wilson-Ewing, "The singularity in mimetic Kantowski-Sachs cosmology," JCAP **07** (2020) 018, arXiv:2002.11658.

[30] M. Bojowald and R. Swiderski, "Spherically symmetric quantum geometry: Hamiltonian constraint," Class. Quant. Grav. **23** (2006) 2129–2154, arXiv:gr-qc/0511108.

[31] M. Campiglia, R. Gambini, and J. Pullin, "Loop quantization of spherically symmetric midi-superspaces," Class. Quant. Grav. **24** (2007) 3649–3672, arXiv:gr-qc/0703135.

[32] R. Gambini and J. Pullin, "Black holes in loop quantum gravity: The Complete space-time," Phys. Rev. Lett. **101** (2008) 161301, arXiv:0805.1187.

[33] J. D. Reyes, "Spherically Symmetric Loop Quantum Gravity: Connection to Two-Dimensional Models and Applications to Gravitational Collapse,". PhD thesis, The Pennsylvania State University, 2009. Available online at https://etda.libraries.psu.edu/catalog/10349.

[34] M. Bojowald, G. M. Paily, J. D. Reyes, and R. Tibrewala, "Black-hole horizons in modified space-time structures arising from canonical quantum gravity," Class. Quant. Grav. **28** (2011) 185006, arXiv:1105.1340.

[35] R. Gambini, J. Olmedo, and J. Pullin, "Quantum black holes in Loop Quantum Gravity," Class. Quant. Grav. **31** (2014) 095009, arXiv:1310.5996.

[36] J. Ben Achour, S. Brahma, and A. Marciano, "Spherically symmetric sector of self dual Ashtekar gravity coupled to matter: Anomaly-free algebra of constraints with holonomy corrections," Phys. Rev. D **96** (2017) 026002, arXiv:1608.07314.

[37] M. Bojowald, S. Brahma, and D.-h. Yeom, "Effective line elements and black-hole models in canonical loop quantum gravity," Phys. Rev. **D98** (2018) 046015, arXiv:1803.01119.

[38] A. Alonso-Bardaji and D. Brizuela, "Anomaly-free deformations of spherical general relativity coupled to matter," Phys. Rev. D **104** (2021) 084064, arXiv:2106.07595.

[39] D.-W. Chiou, W.-T. Ni, and A. Tang, "Loop quantization of spherically symmetric midisuperspaces and loop quantum geometry of the maximally extended Schwarzschild spacetime," arXiv:1212.1265.

[40] R. Gambini, J. Olmedo, and J. Pullin, "Spherically symmetric loop quantum gravity: analysis of improved dynamics," Class. Quant. Grav. **37** (2020) 205012, arXiv:2006.01513.

[41] J. G. Kelly, R. Santacruz, and E. Wilson-Ewing, "Effective loop quantum gravity framework for vacuum spherically symmetric spacetimes," Phys. Rev. D **102** (2020) 106024, arXiv:2006.09302.

[42] M. Han and H. Liu, "Improved effective dynamics of loop-quantum-gravity black hole and Nariai limit," Class. Quant. Grav. **39** (2022) 035011, arXiv:2012.05729.

[43] T. Thiemann and H. A. Kastrup, "Canonical quantization of spherically symmetric gravity in Ashtekar's selfdual representation," Nucl. Phys. B **399** (1993) 211–258, arXiv:gr-qc/9310012.

[44] E. Alesci, S. Bahrami, and D. Pranzetti, "Quantum gravity predictions for black hole interior geometry," Phys. Lett. B **797** (2019) 134908, arXiv:1904.12412.

[45] E. Alesci, S. Bahrami, and D. Pranzetti, "Asymptotically de Sitter universe inside a Schwarzschild black hole," Phys. Rev. D **102** (2020) 066010, arXiv:2007.06664.

[46] M. Christodoulou, C. Rovelli, S. Speziale, and I. Vilensky, "Planck star tunneling time: An astrophysically relevant observable from background-free quantum gravity," Phys. Rev. D **94** (2016) 084035, arXiv:1605.05268.

[47] M. Christodoulou and F. D'Ambrosio, "Characteristic Time Scales for the Geometry Transition of a Black Hole to a White Hole from Spinfoams," arXiv:1801.03027.

[48] E. Bianchi, M. Christodoulou, F. D'Ambrosio, H. M. Haggard, and C. Rovelli, "White Holes as Remnants: A Surprising Scenario for the End of a Black Hole," Class. Quant. Grav. **35** (2018) 225003, arXiv:1802.04264.

[49] P. Martin-Dussaud and C. Rovelli, "Evaporating black-to-white hole," Class. Quant. Grav. **36** (2019) 245002, arXiv:1905.07251.

[50] F. D'Ambrosio, M. Christodoulou, P. Martin-Dussaud, C. Rovelli, and F. Soltani, "End of a black hole's evaporation," Phys. Rev. D **103** (2021) 106014, arXiv:2009.05016.

[51] F. Soltani, C. Rovelli, and P. Martin-Dussaud, "End of a black hole's evaporation. II.," Phys. Rev. D **104** (2021) 066015, arXiv:2105.06876.

[52] D. Oriti, D. Pranzetti, and L. Sindoni, "Black Holes as Quantum Gravity Condensates," Phys. Rev. D **97** (2018) 066017, arXiv:1801.01479.

[53] L. Modesto, "Gravitational collapse in loop quantum gravity," Int. J. Theor. Phys. **47** (2008) 357–373, arXiv:gr-qc/0610074.

[54] S. Hossenfelder, L. Modesto, and I. Premont-Schwarz, "A Model for non-singular black hole collapse and evaporation," Phys. Rev. D **81** (2010) 044036, arXiv:0912.1823.

[55] Y. Tavakoli, J. Marto, and A. Dapor, "Semiclassical dynamics of horizons in spherically symmetric collapse," Int. J. Mod. Phys. D **23** (2014) 1450061, arXiv:1303.6157.

[56] C. Bambi, D. Malafarina, and L. Modesto, "Non-singular quantum-inspired gravitational collapse," Phys. Rev. D **88** (2013) 044009, arXiv:1305.4790.

[57] Y. Liu, D. Malafarina, L. Modesto, and C. Bambi, "Singularity avoidance in quantum-inspired inhomogeneous dust collapse," Phys. Rev. D **90** (2014) 044040, arXiv:1405.7249.

[58] J. Ben Achour, S. Brahma, and J.-P. Uzan, "Bouncing compact objects I: Quantum extension of the Oppenheimer-Snyder collapse," JCAP **2003** (2020) 041, arXiv:2001.06148.

[59] M. Campiglia, R. Gambini, J. Olmedo, and J. Pullin, "Quantum self-gravitating collapsing matter in a quantum geometry," Class. Quant. Grav. **33** (2016) 18LT01, arXiv:1601.05688.

[60] J. Ziprick, J. Gegenberg, and G. Kunstatter, "Polymer Quantization of a Self-Gravitating Thin Shell," Phys. Rev. D **94** (2016) 104076, arXiv:1609.06665.

[61] K. Giesel, B.-F. Li, and P. Singh, "Nonsingular quantum gravitational dynamics of an Lemaître-Tolman-Bondi dust shell model: The role of quantization prescriptions," Phys. Rev. D **104** (2021) 106017, arXiv:2107.05797.

[62] F. Benitez, R. Gambini, L. Lehner, S. Liebling, and J. Pullin, "Critical collapse of a scalar field in semiclassical loop quantum gravity," Phys. Rev. Lett. **124** (2020) 071301, arXiv:2002.04044.

[63] V. Husain and O. Winkler, "Quantum resolution of black hole singularities," Class. Quant. Grav. **22** (2005) L127–L134, arXiv:gr-qc/0410125.

[64] J. Ziprick and G. Kunstatter, "Dynamical Singularity Resolution in Spherically Symmetric Black Hole Formation," Phys. Rev. D **80** (2009) 024032, arXiv:0902.3224.

[65] A. Kreienbuehl, V. Husain, and S. S. Seahra, "Modified general relativity as a model for quantum gravitational collapse," Class. Quant. Grav. **29** (2012) 095008, arXiv:1011.2381.

[66] M. Bojowald, T. Harada, and R. Tibrewala, "Lemaitre-Tolman-Bondi collapse from the perspective of loop quantum gravity," Phys. Rev. D **78** (2008) 064057, arXiv:0806.2593.

[67] M. Bojowald, J. D. Reyes, and R. Tibrewala, "Non-marginal LTB-like models with inverse triad corrections from loop quantum gravity," Phys. Rev. D **80** (2009) 084002, arXiv:0906.4767.

[68] C. Vaz and L. Witten, "Canonical quantization of spherically symmetric dust collapse," Gen. Rel. Grav. **43** (2011) 3429–3449, arXiv:1111.6821.

[69] C. Barceló, R. Carballo-Rubio, and L. J. Garay, "Mutiny at the white-hole district," Int. J. Mod. Phys. D **23** (2014) 1442022, arXiv:1407.1391.

[70] C. Barcelo, R. Carballo-Rubio, L. J. Garay, and G. Jannes, "The lifetime problem of evaporating black holes: mutiny or resignation," Class. Quant. Grav. **32** (2015) 035012, arXiv:1409.1501.

[71] C. Kiefer and T. Schmitz, "Singularity avoidance for collapsing quantum dust in the Lemaître-Tolman-Bondi model," Phys. Rev. D **99** (2019) 126010, arXiv:1904.13220.

[72] W. Piechocki and T. Schmitz, "Quantum Oppenheimer-Snyder model," Phys. Rev. D **102** (2020) 046004, arXiv:2004.02939.

[73] T. Schmitz, "Exteriors to bouncing collapse models," Phys. Rev. D **103** (2021) 064074, arXiv:2012.04383.

[74] J. Münch, "Effective quantum dust collapse via surface matching," Class. Quant. Grav. **38** (2021) 175015, arXiv:2010.13480.

[75] J. Ben Achour, S. Brahma, S. Mukohyama, and J. P. Uzan, "Towards consistent black-to-white hole bounces from matter collapse," JCAP **09** (2020) 020, arXiv:2004.12977.

[76] D. Malafarina, "Classical collapse to black holes and quantum bounces: A review," Universe **3** (2017) 48, arXiv:1703.04138.

[77] C. Rovelli and F. Vidotto, "Planck stars," Int. J. Mod. Phys. D **23** (2014) 1442026, arXiv:1401.6562.

[78] H. M. Haggard and C. Rovelli, "Quantum-gravity effects outside the horizon spark black to white hole tunneling," Phys. Rev. D **92** (2015) 104020, arXiv:1407.0989.

[79] A. Barrau and C. Rovelli, "Planck star phenomenology," Phys. Lett. B **739** (2014) 405–409, arXiv:1404.5821.

[80] A. Barrau, C. Rovelli, and F. Vidotto, "Fast Radio Bursts and White Hole Signals," Phys. Rev. D **90** (2014) 127503, arXiv:1409.4031.

[81] A. Barrau, B. Bolliet, F. Vidotto, and C. Weimer, "Phenomenology of bouncing black holes in quantum gravity: a closer look," JCAP **02** (2016) 022, arXiv:1507.05424.

[82] D. M. Eardley, "Death of White Holes in the Early Universe," Phys. Rev. Lett. **33** (1974) 442–444.

[83] C. Barceló, R. Carballo-Rubio, and L. J. Garay, "Black holes turn white fast, otherwise stay black: no half measures," JHEP **01** (2016) 157, arXiv:1511.00633.

[84] E. Poisson and W. Israel, "Inner-horizon instability and mass inflation in black holes," Phys. Rev. Lett. **63** (1989) 1663–1666.

[85] A. Ori, "Inner structure of a charged black hole: An exact mass-inflation solution," Phys. Rev. Lett. **67** (1991) 789–792.

[86] V. Husain, "Radiation collapse and gravitational waves in three-dimensions," Phys. Rev. D **50** (1994) R2361–R2363, arXiv:gr-qc/9404047.

[87] J. G. Kelly, R. Santacruz, and E. Wilson-Ewing, "Black hole collapse and bounce in effective loop quantum gravity," Class. Quant. Grav. **38** (2021) 04LT01, arXiv:2006.09325.

[88] V. Husain, J. G. Kelly, R. Santacruz, and E. Wilson-Ewing, "Quantum gravity of dust collapse: Shock waves from black holes," Phys. Rev. Lett. **128**, (2022) 121301, arXiv:2109.08667.

[89] P. Szekeres and A. Lun, "What is a shell crossing singularity?," J. Austral. Math. Soc. B **41** (1999) 167–179.

[90] C. Hellaby and K. Lake, "Shell crossings and the Tolman model," Astrophys. J. **290** (1985) 381.

[91] I. Booth, L. Brits, J. A. Gonzalez, and C. Van Den Broeck, "Marginally trapped tubes and dynamical horizons," Class. Quant. Grav. **23** (2006) 413–440, arXiv:gr-qc/0506119.

[92] K. Giesel, J. Tambornino, and T. Thiemann, "LTB spacetimes in terms of Dirac observables," Class. Quant. Grav. **27** (2010) 105013, arXiv:0906.0569.

[93] T. Schmitz, "Towards a quantum Oppenheimer-Snyder model," Phys. Rev. D **101** (2020) 026016, arXiv:1912.08175.

[94] B. C. Nolan, "Dynamical extensions for shell crossing singularities," Class. Quant. Grav. **20** (2003) 575–586, arXiv:gr-qc/0301028.

[95] P. D. Lasky, A. W. C. Lun, and R. B. Burston, "Initial value formalism for dust collapse," ANZIAM Journal **49** (6, 2007) arXiv:gr-qc/0606003.

[96] R. J. LeVeque, *Finite Volume Methods for Hyperbolic Problems*. Cambridge University Press, 2002.

[97] K. Bolejko, M.-N. Celerier, and A. Krasinski, "Inhomogeneous cosmological models: Exact solutions and their applications," Class. Quant. Grav. **28** (2011) 164002, arXiv:1102.1449.

[98] J. F. Barbero G., "Real Ashtekar variables for Lorentzian signature space times," Phys. Rev. D **51** (1995) 5507, arXiv:gr-qc/9410014.

[99] G. Immirzi, "Quantum gravity and Regge calculus," Nucl. Phys. B Proc. Suppl. **57** (1997) 65, arXiv:gr-qc/9701052.

[100] V. Husain and T. Pawlowski, "Time and a physical Hamiltonian for quantum gravity," Phys. Rev. Lett. **108** (2012) 141301, arXiv:1108.1145.

[101] W. Israel, "Singular hypersurfaces and thin shells in general relativity," Il Nuovo Cimento B (1965-1970) **44** (1966) 1–14.

[102] T. Dray and G. 't Hooft, "The Gravitational Shock Wave of a Massless Particle," Nucl. Phys. B **253** (1985) 173–188.

[103] K. Vandersloot, "Loop quantum cosmology and the k = - 1 RW model," Phys. Rev. D **75** (2007) 023523, arXiv:gr-qc/0612070.

[104] P. Singh and E. Wilson-Ewing, "Quantization ambiguities and bounds on geometric scalars in anisotropic loop quantum cosmology," Class. Quant. Grav. **31** (2014) 035010, arXiv:1310.6728.

[105] K. Vandersloot, "On the Hamiltonian constraint of loop quantum cosmology," Phys. Rev. D **71** (2005) 103506, arXiv:gr-qc/0502082.

[106] J. Ben Achour, S. Brahma, and M. Geiller, "New Hamiltonians for loop quantum cosmology with arbitrary spin representations," Phys. Rev. D **95** (2017) 086015, arXiv:1612.07615.

[107] L. Amadei, A. Perez and S. Ribisi, "Landscape of polymer quantum cosmology," Phys. Rev. D **107** (2023) 086007, arXiv:2203.07044.

[108] E. Wilson-Ewing, "Lattice loop quantum cosmology: scalar perturbations," Class. Quant. Grav. **29** (2012) 215013, arXiv:1205.3370.

[109] C. Rovelli and E. Wilson-Ewing, "Why are the effective equations of loop quantum cosmology so accurate?," Phys. Rev. D **90** (2014) 023538, arXiv:1310.8654.

[110] R. Gambini, J. Olmedo, and J. Pullin, "Loop Quantum Black Hole Extensions Within the Improved Dynamics," Front. Astron. Space Sci. **8** (2021) 74, arXiv:2012.14212.

[111] K. Giesel, B. F. Li, P. Singh and S. A. Weigl, "Consistent gauge-fixing conditions in polymerized gravitational systems," Phys. Rev. D **105** (2022) 066023, arXiv:2112.13860.

[112] V. Taveras, "Corrections to the Friedmann Equations from LQG for a Universe with a Free Scalar Field," Phys. Rev. D **78** (2008) 064072, arXiv:0807.3325.

[113] M. Bojowald and S. Brahma, "Minisuperspace models as infrared contributions," Phys. Rev. D **93** (2016) 125001, arXiv:1509.00640.

[114] C. Zhang, "Reduced phase space quantization of black holes: Path integrals and effective dynamics," Phys. Rev. D **104** (2021) 126003, arXiv:2106.08202.

[115] V. Husain and O. Winkler, "Semiclassical states for quantum cosmology," Phys. Rev. D **75** (2007) 024014, arXiv:gr-qc/0607097.

[116] J. Münch, "Causal structure of a recent loop quantum gravity black hole collapse model," Phys. Rev. D **104** (2021) 046019, arXiv:2103.17112.

[117] V. Faraoni, G. F. R. Ellis, J. T. Firouzjaee, A. Helou, and I. Musco, "Foliation dependence of black hole apparent horizons in spherical symmetry," Phys. Rev. D **95** (2017) 024008, arXiv:1610.05822.

[118] The code is available with the source files on the arXiv.org page.

[119] E. G. Brown, R. B. Mann, and L. Modesto, "Mass Inflation in the Loop Black Hole," Phys. Rev. D **84** (2011) 104041, arXiv:1104.3126.

[120] D. N. Page, "Average entropy of a subsystem," Phys. Rev. Lett. **71** (1993) 1291–1294, arXiv:gr-qc/9305007.

[121] D. N. Page, "Time Dependence of Hawking Radiation Entropy," JCAP **09** (2013) 028, arXiv:1301.4995.

[122] A. Perez, "No firewalls in quantum gravity: the role of discreteness of quantum geometry in resolving the information loss paradox," Class. Quant. Grav. **32** (2015) 084001, arXiv:1410.7062.

Chapter 5

Discussion

5.1 Discussion

The work in this thesis developed a model of black hole formation due to matter collapse within the framework of effective LQG and presented a new way to tackle the spherically symmetric black hole problem. Unlike many previous studies, the framework presented allows one to model the full space-time without unnaturally splitting the interior and exterior portions and "gluing" along the horizon. Moreover, there are no issues with the semi-classical limit of the effective theory presented, as we found that quantum corrections near the singularity die off sufficiently quickly as we move to larger radii, reducing to the classical theory where one would expect; this resolves an issue found in some of the earlier works on this subject [1]. This represents a crucial first step in the direction of a complete understanding of black hole space-times and matter collapse in effective LQG.

By first studying the vacuum space-time, we found that in order to understand the region surrounding the classical singularity, it was imperative that matter be included in our framework. The extension to include matter from the start is one of the few early works that consider a matter collapse scenario in effective LQG. This allows us

to glean insight into the properties of more realistic black holes that invariably form due to gravitational collapse[1]. Our work suggests that dust collapse in an effective model of quantum gravity will indeed produce a black hole — just as in the classical case — but won't remain static, even in spherical symmetry. The quantum "pressure" will eventually stop the collapse when the density of the ball reaches its maximum allowed by the Planck length, and explode outwardly producing a shock wave. As the shock wave reaches the horizon, the space-time around this region is distorted allowing it to travel beyond the horizon, a classically forbidden phenomenon. This result, should it be physical, would have huge implications for the information loss problem that has plagued physics for decades after Hawkings discovery that black holes radiate energy, eventually evaporating completely. The lifetime estimate we find implies that the evaporation process would end prior to the Page time, when the shockwave exits the outer horizon, avoiding the non-unitary evolution that is implied by the Hawking result.

Although there is still some debate as to whether the shock wave results we have presented are indeed physical [2], there is strong evidence to suggest this is the case generically [3]. We will discuss this in more detail below, but in [2] the authors argue that the shock in the Oppenheimer-Snyder (OS) model can be removed through a coordinate transformation. Shell-crossing singularities on the other hand cannot be removed through coordinate changes. They arise very generically and signal the formation of a shock [3], as we have seen in this thesis. We note that although shocks arise generically in our model, their specific dynamics still needs to be better understood. Since weak solutions to partial differential equations are not unique, we still need some input from quantum gravity to select the correct physical solution. We make a specific proposal (based on the use of the Ashtekar–Barbero variables), but other choices are possible, and could lead to important differences in the evolution of

[1]This is still not the whole story, however, since real black holes have angular momentum, while this work is in spherical symmetry.

the shock, a point that remains to be studied.

5.2 Vacuum Construction

The first step in our construction was a reduction to spherically symmetric space-times which are the simplest space-times for which a black hole solution exists classically. To encompass the entirety of space-time at once, we introduced a distinct set of coordinates — specifically, Painlevé-Gullstrand coordinates. The reason for this choice is quite simple as explained in the introduction: in order to properly implement the holonomy corrections, a required step in deriving the effective theory, we needed to compare the length of the path along which we compute holonomies to the physical Planck length which requires the use of the metric. In the standard Schwarzschild coordinates, this leads to issues at the event horizon where coordinates become null (and hence physical lengths in the direction of that coordinate become 0) making it impossible to make a comparison to the Planck length. To facilitate such a comparison, a new coordinate system was chosen that was horizon penetrating. The necessary coordinates cannot become null as we reach the event horizon, or switch character anywhere in space-time for that matter, making PG coordinates a very natural choice.

After rewriting the symmetry reduced theory in terms of connection and triad variables, the next step was to derive the effective theory by incorporating holonomy corrections à la LQC. It proved difficult to implement the holonomy corrections even after the reduction to spherical symmetry for several reasons. The first of these is simply the fact that it is difficult to calculate holonomies in the radial direction due to the path ordering in its definition, in conjunction with the fact that general spherically symmetric metrics are inhomogeneous. Another difficulty was a constraint algebra that would not close. This second difficulty arises if we abandon trying to capture the holonomy (by its explicit calculation) and simply try to polymerize the

system instead, which in general is not equivalent [4]. Recall that in GR closure of the constraint algebra is one of the requirements of a consistent theory since this ensures the invariance of the theory under different choices of coordinates[2] — a very natural requirement for any physical theory and one of the main ingredients in the Hamiltonian theory of GR.

Even though it proves difficult to compute holonomies in the radial direction, we can take a quick-and-dirty approach by simply replacing connection variables by their trigonometric counterparts in the scalar and diffeomorphism constraints, similar to what happens by carrying out the full calculation (when it is possible), and study this theory. Indeed this method is often implemented when studying effective theories in LQC and has proven to be quite effective (no pun intended) in capturing the leading order quantum corrections to the classical theory implied by LQG. The difficulty here lies in the fact that the inhomogeneity of spherically symmetric metrics makes the algebra non-trivial[3] and when a polymerization of the type described above is carried out, it is not so easy to retain the algebra closure. This type of problem has been studied before, albeit for different sectors, and one resolution was to add counter terms as in [5]. Here however, we could not find a solution using this method in the case of spherical symmetry.

Another possibility is that it is necessary to work with the full holonomy. This approach, however, would significantly increase the mathematical complexity of the problem making it somewhat infeasible for an initial investigation into the spherically symmetric sector. In the framework discussed, the requirement of algebra closure, coupled with the fact that holonomies could not be calculated in a straightforward manner, led us to a further reduction in the form of a gauge fixing (to the areal gauge),

[2]Put another way, constraint algebra closure ensures diffeomorphim invariance. In addition to this, having constraints that Poisson commute with the Hamiltonian is also required to have consistent dynamics.

[3]By non-trivial here we mean that the algebra does not simply vanish. If this were so, as is the case for homogeneous cosmologies, any polymerization function can be chosen and not affect the algebra.

although this is by no means the only way forward.

In [6, 7], the authors choose instead to abelianize the algebra by a change of variables. This means that algebra closure holds regardless of the polymerization chosen and we are again free to choose any polymerization we see fit. Interestingly, we found that the solution the authors study in [7], although arising from a completely different construction, turns out to be a solution of our vacuum EOMs as well, which speaks to the robustness of our vacuum results.

Another alternative to the areal gauge may be to impose the so-called "LTB condition". This amounts to a relationship between triads of the form $E^b \sim \partial_x E^a$ (in our notation), while leaving the diffeomorphism constraint unpolymerized — an interesting possibility discussed in [8]. We note that imposing the LTB condition also leads to results that are consistent with what we obtained. Classically, this type of relationship exists between the triad variables in spherical symmetry (see for example the PG solution given by (2.26) in Chapter 2) and imposing this kind of relationship can be viewed as a generalization of the areal gauge chosen here. Such a generalization may also have important implications on the formation or absence of shock waves during gravitational collapse [3, 14].

This possibility was considered in our vacuum work early on since it significantly simplifies the Hamiltonian constraint, but abandoned since the LTB condition is not (always) a second-class constraint[4]. We instead decided to avoid this issue by choosing a different gauge, i.e., the areal gauge. We note that in [8] and [14], the authors show how to properly impose the LTB condition in effective LTB space-times. Furthermore, in [14] it is shown that by leaving the diffeomorphism constraint unpolymerized, algebra closure in this setting can be achieved. This is a possible route forward in order to avoid the areal gauge fixing that we have imposed and to extend the model.

[4]The LTB condition being second-class is not a requirement, but if it's not second-class then the procedure is more complicated [10].

Imposition of the areal gauge allowed us to implement a 'K' loop quantization[5], a well known procedure in LQC. A more common type of quantization known as the 'A' loop quantization[6], was not available here since their holonomies give functions that are not trigonometric functions of the connection variables — a requirement for promoting them to operators in the quantum theory. This further reduction (after symmetry reduction) and quantization ensured generic[7] algebra closure and a theory that is free from anomalies [12]. From this modified theory, the effective EOMs were derived the same way as in the classical case, namely by taking the Poisson brackets of our phase space variables with the modified Hamiltonian. After deriving the EOMs, we were able to find multiple solutions including the quantum counterpart to the PG metric, the main solution that was studied in the remainder of Chapter 2.

We found several interesting properties of the effective vacuum space-time that were a deviation from the classical spherically symmetric black hole from general relativity, as well as earlier models of effective LQG black holes where the interior was quantized in isolation via the Kantowski-Sachs isometry. First, the space-time we found may include 0, 1 or 2 horizons depending on the mass of the black hole. Furthermore, there exists a minimum mass required to form a black hole that is related to several parameters of the quantum model via the relation $M_\star = 8\gamma\sqrt{\Delta}/\sqrt{27}G$. Interestingly this mass is larger than the mass of elementary particles such as electrons which thus cannot create black holes alone. We also touched on the thermodynamics of this space-time and it was shown that there is a maximum surface gravity, a deviation from the thermodynamics of classical black holes. Finally, as discussed in Chapter 2, although multiple solutions were found, with the modified algebra it is not exactly clear how coordinate transformations work in this setting. For example, by taking

[5]With this type of quantization, one computes holonomies of the extrinsic curvature, hence 'K' loop.

[6]With this type of quantization, one computes holonomies of the Ashtekar–Barbero connection, hence 'A' loop. See [11] for more details on the application of both quantization methods in LQC.

[7]Generic in the sense that we are free to choose any polymerization function and the algebra will still close regardless of this choice, just as in cosmology.

our solution and performing a coordinate transformation by the usual procedure to Swarzschild-like coordinates[8], it can be shown that the new metric does not solve the modified EOMs. As discussed in the introduction, this could mean one of two things: either the model needs to be corrected to recover covariance, for example perhaps the Hamiltonian we derive only holds in a specific gauge, and modifications are required so it can hold more generally [13–17], or there is a quantum deformation to diffeomorphism invariance. This is currently an open problem that will need to be better understood moving forward if we want to develop a more robust framework for spherically symmetric LQG.

Although the original aim of the vacuum work was to describe the entire space-time in an effective framework, we found a ball of radius $x_{\min} = (\gamma\Delta R_S)^{1/3}$ that could not be studied in the vacuum space-time. As we reach this radius from above, the space-time metric reduces to the classical Minkowski space-time; we can think of this as the radius where quantum gravity "pressure" exactly cancels gravity. As we continue to move to smaller radii, the metric components become imaginary and we can no longer study the structure of space-time in this region. As a consequence of this, curvature scalars remain bounded everywhere space-time is well defined, reaching their (mass independent) maximum value at the surface of the forbidden region.

The existence of a forbidden region in the vacuum space-time, which seems like a surprising result at first glance, becomes quite intuitive upon further inspection. In Chapter 2, we argued that the reason for this region in our space-time is a consequence of: 1) there being no gravitational waves in spherical symmetry, thus requiring a matter field to introduce curvature into the space-time and 2) the existence of a maximal energy density when incorporating holonomy corrections à la LQC. This implies that the matter core must extend out to a minimum radius of $x_{\min}$. This was

[8]By "Schwarzschild-like" here we mean coordinates where there are no off-diagonal terms in the metric and the g_{tt} and g_{xx} components of the metric are related by $g_{xx} = 1/g_{tt}$, which is the case for the classical Schwarzschild metric.

our motivation for including a matter field in Chapter 3, allowing us to both extend the framework studied in Chapter 2 to this region, while at the same time developing a more comprehensive picture of what the life of black holes in our universe may look like.

5.3 Adding Matter

In Chapter 3, a matter field was included in the framework constructed and studied extensively in Chapter 2. Dust was the matter field of choice since it is an idealized type of matter where the individual particles that make it up do not interact with each other. It is also well known in the literature that this type of matter is a convenient choice of clock in the Hamiltonian formulation of quantum gravity [18, 19]. These facts made it particularly attractive to use as an extension of the vacuum model since we were able to include a matter field with minimal complications and get a Hamiltonian that takes nearly the same form as the vacuum case.

The addition of matter allowed us to study a more realistic scenario where black holes are formed due to collapsing matter rather than the simple, yet unrealistic, case of an eternal black hole studied in the second chapter. Indeed, this addition allowed us to study the entire evolution of matter in the effective setting from the initial collapse, to a point of maximum density, to the death of the black hole via an outwardly travelling shock wave that is able to exit the horizon. This latter finding is particularly interesting since it is impossible for matter to escape a black hole after falling within the event horizon in the classical space-time.

The inclusion of matter followed the same procedure as the vacuum framework, where the theory was cast in Hamiltonian form using Ashtekar variables as the canonical variables, with the same areal gauge fixing. The (dust) matter field was added and the theory was further gauge fixed by using the dust field as our reference

clock — this left us with a fully gauge fixed theory and a physical Hamiltonian. Moreover, we no longer had to worry ourselves with constraint algebra closure, which we recall proved to be difficult to impose in the vacuum case prior to gauge fixing. Since we gauge fixed away the diffeomorphism constraint by imposing the areal gauge, and now gauge fixed the Hamiltonian constraint by choosing the dust field as a clock, we were left with a constraint free model. This means we had a free hand in modifying the theory without needing to check if the modifications broke the constraint algebra. Note that although we had this free hand, we again used exactly the same corrections as in the vacuum case, since this procedure is well motivated by LQC. This fact made the matter theory simpler to deal with than the vacuum theory in some sense, which is sensible considering the theory has been gauge fixed further after the introduction of matter. Moreover, the Hamiltonian took the same form as before and thus the EOMs were the same as in the vacuum setting. Indeed we can even recover the vacuum space-time from this theory by taking $\mathcal{H}_{\text{phys}} = 0$.

The evolution of the dust field naturally depends in its initial distribution. Since black holes are typically formed due to stellar collapse, an obvious first pass was to study what star-like evolution may look like in this model. We studied star-like collapse by studying an idealized initial distribution where dust homogeneously fills space out to a finite radius and is surrounded by vacuum beyond this radius — classically known as the Oppenheimer-Snyder model. In this scenario, we found that the ball initially collapses, falling inward towards the center, and reaches a point of maximum density (minimum radius) before starting to expand outwardly — a bounce.

It is quite striking to see the cohesive picture that emerges here, where the EOMs give exactly the LQC effective Friedmann equation for spatially flat FLRW space-times. That is, we found agreement between LQC and the seemingly very different system we are studying here. This agreement carries over to the maximum density reached by the collapsing matter, which which we found agrees exactly with the LQC critical density

where the bounce occurs in cosmological space-times. This correspondence is what is found in the classical setting when studying dust collapse as well, where we have an FLRW solution in the stars' interior, but it is not obvious that this should remain the case in the effective setting, so this came as a pleasant surprise. Furthermore, we found the minimum radius of the ball of dust is exactly the radius of the forbidden region of the vacuum space-time, making very concrete the argument that matter is required to have a picture of the full space-time.

For the Oppenheimer-Snyder model, when edge effects were neglected at the boundary of the dust filled region and vacuum space-time, the collapse and bounce is completely symmetric and the lifetime of the black hole is on the order of M, the black hole mass. Of course, this would make black holes in our universe unrealistically short-lived were this the case. To get a more realistic estimate of the lifetime, we considered what happens at the edge of our star, which acts as a barrier between the exterior and interior. Moreover, after the bounce the metric components (corresponding to the shift vector) become discontinuous at the boundary between the interior and exterior — a phenomenon known as a shock wave. Thus, we found that although strong singularities were absent in the effective theory, being replaced by a quantum gravitational bounce, weak singularities persist. Our previous assumptions leading to the effective Friedmann equation no longer hold, and we were forced to include edge effects due to the discontinuity in the gravitational field to get a realistic picture of the evolution of the outgoing phase.

The effect of such a shock wave is that it allows matter to travel outward past the outer horizon, an impossible feat in the classical setting where no matter can travel outwardly after falling within the event horizon. Physically, the matter moves outwardly until reaching the inner horizon. Matter piles up here forming a kind of thin-shell until enough has piled up to distort the space-time locally. Once distorted, the horizon has a chance to move outward. The matter then piles up at the new inner

horizon location and the process repeats, allowing the shock wave to move radially outward indefinitely. Eventually, the inner horizon reaches the outer horizon, at which point they both disappear, marking the death of our black hole after which the shock wave will continue its outward march. The picture that develops in this scenario is in striking contrast to the classical, spherically symmetric scenario where once matter collapses beyond its Schwarzschild radius, it is doomed to fall to the singularity and remain static for the entirety of its life.

The formation of the shock wave also has the effect of making the bounce asymmetric — the expansion phase is now much longer than the collapse phase. This is due to the fact that the matter now has to "wait" at the inner horizon for enough matter to pile up until the space-time is sufficiently distorted and the matter can move further outward. Interestingly, we found an estimate of the lifetime of the black hole when including these edge effects to be on the order of M^2. This is a much more plausible lifetime than the M estimate prior to their inclusion, and in agreement with some earlier proposals arguing that black-white hole transition should have a similar lifetime [20]. A major difference between our work here and other works is that our lifetime estimate is the result of a solution to the equations of motion of our model, rather than the qualitative arguments used to arrive at this estimate in, for e.g., [20].

5.4 Further Investigation

Chapter 4 was dedicated to a more complete study of the system of PDEs that was derived in the previous chapter. Transforming the system of PDEs into a system of ODEs using the method of characteristics, although generally possible, led to issues that are somewhat delicate to deal with in the form of shell-crossing singularities, which make evolution beyond them non-unique. Classically, it is possible to avoid these types of singularities by fine-tuning initial conditions so that shell crossings

won't occur before matter reaches the central singularity [21, 22]. We saw however that this is no longer possible in the effective quantum theory due to the singularity avoidance and bounce — shock waves are a general feature of quantum dust collapse.

In our model, where shock waves seem to be a ubiquitous feature of our EOMs, we dealt with discontinuities that show up in the evolution by considering the EOMs in integral form, rather than their more familiar differential counterpart. In this form, we were able to study two models analytically — namely the Oppenheimer-Snyder model and thin shell collapse, both very well studied in the classical setting. An encouraging result of these solutions was that the shock wave exits the black hole (reaches the outer horizon) in a time of $T \approx \frac{2\pi R_S^2}{3\gamma\sqrt{\Delta}}$, to leading order. The agreement between leading order lifetimes was an expected result. In the case of OS collapse, after the bounce matter piles up at the horizon relatively quickly (in a time on the order of M), leaving Minkowski space-time inside and a thin shell at the shock wave. Since the outgoing phase is the dominant phase when computing the black hole lifetime, it is quite sensible that both of these models would have the same lifetime to leading order. This estimate corroborates the estimate for black hole lifetimes that was made when including edge effects from the previous chapter. The analytic OS case also allowed us to sketch the conformal diagram, giving insight into the structure that such a space-time should have.

In the remainder of the chapter, the well known Gudonov numerical method [23] was used to solve the EOMs for general initial matter configurations, giving a comprehensive picture of the collapse and bounce of matter in the spherically symmetric sector of effective LQG. Numerical studies of several initial distributions were carried out including a single and double Guassian pulse and a star-like distribution of matter where the density dies off smoothly as we move outward from the stars' center. In each of these situations, a lifetime of approximately $T \sim 8\pi M^2/3$ was found, giving further credence to the earlier estimate. Unlike the classical collapse scenario, in all

cases tested, we found no evidence of mass inflation or the re-collapse of matter into a black hole as more matter is introduced into the system — a phenomenon exhibited by white holes in classical GR. We found that once the shock wave inevitibly forms, it seems to move outwardly ad infinitum. We note here that in a recent paper studying a generalization of the marginally bound LTB space-times studied in this work, the authors show that this is not always the case. If the initial configuration is bound, the shock will asymptote to a maximal radius rather than escaping to infinity [24].

5.5 Conclusion

Our study of black hole evolution illuminated the quantum structure of space-time that arises from effective LQG and how this may affect physics in a non-trivial way. The quantum structure not only affects the dynamics of space-time itself, but the dynamics of fields and particles on these space-times as well. This research, although relying on several simplifying assumptions including a spherically symmetric space-time and the use of the areal and dust time gauges, leads to important insights into the structure of our universe beyond its classical description, and gives a glimpse into some new effects that a discrete space-time structure may lead to — a structure that is indeed motivated by quantum gravity.

The vacuum model that was developed acted as a stepping stone to understanding a more complete matter collapse scenario and allowed us to make contact with earlier work in this direction. This framework was also useful for the fact that it allowed us to fairly straightforwardly add matter to the system, while maintaining essentially the same formalism as in vacuum. Although we were able to use the vacuum framework to make contact with previous work, this work is distinct in it use of the areal gauge for implementing the effective framework, the fact that we study the entire space-time without splitting it into interior and exterior segments and the inclusion of matter.

This represents a step forward for the effective theory of black holes in LQG.

One of the main strengths of the results presented here is the inhomogeneous description of the space-time we started with — a direct consequence of the fact that we did not study the interior space-time as a cosmology as in many early works on this subject. Indeed, the conservation equation derived from the EOMs has a spatially dependent flux; when LQC techniques are applied to the Schwarzschild interior only, the EOMs have no radial dependence (they are ODEs) and miss shock wave type solutions from developing altogether.

In addition to this, older studies typically considered only vacuum solutions, completely ignoring the collapse process which is another key ingredient for shock wave formation[9]. As a consequence, we found black holes with lifetimes on the order of M^2, which is different than the lifetimes found in studies considering only vacuum solutions or that break up space-time (unnaturally) into interior and exterior portions. This lifetime result, if it is indeed realized by black holes in our universe, would have huge implications for the information loss problem, one of the most important open problems in quantum gravity today.

The shock wave is not only the most interesting and unexpected result we find, but perhaps also the least understood aspect of the model currently, although there has been some recent work attempting to understand shock waves and their consequences in this setting [2, 3]. The shock wave essentially constitutes a domain wall separating two portions of the space-time — an interior (nearly) Minkowski space-time from the exterior Schwarzschild. It effectively acts as thin shell bringing quantum corrections to external observers. It is quite different from the white hole solutions that have been proposed in other works such as [20, 25, 26], and does not exhibit some of the undesirable characteristics of white holes from classical GR such as instablity under the accretion of matter. Indeed, our simulations showed that the outgoing shock wave

[9]Recall that the shock wave arises as a metric discontinuity in our solutions when studying the evolution of matter.

will absorb any additional matter it comes into contact with, rather than recollapsing to form another black hole.

Aside from purely theoretical implications, the shock wave could potentially carry with it observable consequences. If, for example, the shock wave carries a signature of the quantum structure of space-time, this may be measurable in some capacity by an external observer after the shock wave exits the horizon. This brings up a very interesting possibility of testing some kind of prediction of the current model and may present an opportunity to test the effects of quantum gravity in an observational setting, although more work would need to be done to precisely define what kind of effect would be expected. There are of course additional challenges of such an endeavor, such as the extremely long lifetime of astrophysical black holes due to their large mass, but the observable consequence possibility is nonetheless valid.

In saying this, there is still an interesting debate as to whether the shock wave is in fact physical, or if it is simply a coordinate singularity due to the use of PG coordinates in our construction. Recall that in Schwarzschild space-time in the standard coordinates, there is a singularity at the horizon. This singularity can be removed however by an alternative choice of coordinates, such as PG coordinates. The ability to remove this singularity by a coordinate transformation means that it is a "coordinate singularity" rather than a physical singularity (such as the singularity at the center of the Schwarzschild black hole). Physical singularities are present in all coordinate systems and cannot be removed via a simple coordinate transformation.

In [2], the authors argue that something similar may be happening in the model presented here, at least for the case of the Oppenheimer-Snyder dust profile. Specifically, they show that the discontinuity in the gravitational field (the shock) can be removed by performing different coordinate transformations on either side of the surface of the OS star after the bounce. This allows the dust field (used as a relational clock) to evolve at different rates in the interior and exterior regions, but comes at

the cost of introducing a new discontinuity in the dust field itself. We emphasize that the arguments presented however only apply to the OS space-time.

In more general (and realistic) cases, if we start with a continuous density profile of compact support for the dust, it can be shown that, in the marginally bound case (which we studied in Chapter 4), shell-crossing singularities necessarily occur, even for initial density profiles that are arbitrarily close to OS [3]. This result suggests that the shock is indeed physical, in contrast to several recent papers claiming otherwise that focus on the OS configuration, which escapes the theorem presented in [3] as the density profile is not continuous [2, 14]. More recent work generalizing our model beyond the marginally bound configuration also has evidence in support of shock wave formation [24]. We conclude this section by emphasizing that it is possible that a less restrictive[10] extension of our model may be necessary in order to definitively answer this question.

5.5.1 Future Work

Rather than an end point, this work should be thought of as a starting point where we've introduced a new direction of study for the spherically symmetric sector of LQG (of which LTB space-times and dust collapse are a subset). While this work presented many new results, it also introduced a lot of questions and opened many avenues for future work.

One pressing question, that is of fundamental importance, is the relationship between solutions of the effective theory. As we have already discussed, the algebra of our effective theory is closed suggesting that diffeomorphism invariance has been maintained, but since the constraint algebra has changed, although the symmetries are preserved, they have been deformed. This is to say, there are quantum deformations to the symmetry, in this case the diffeomorphisms. This means that it is currently

[10]Less restrictive in our use of the areal gauge and our choice of PG coordinates.

not clear how different solutions of the modified theory are related to one another, something that will need to be better understood moving forward.

Another important result that needs to be investigated further is to determine if the shock wave is physical or not. If the shock wave is not observable, then why is it showing up as a seemingly generic feature of this work? Is it the gauge fixing we chose? Is it the coordinates? Is it related to the polymerization prescription? All of these questions will need to be understood in more depth moving forward. If, on the other hand, the shock wave is observable, then new questions arise such as what exactly are we observing or what observable consequences does the shock wave have and what are the implications for observing the Planck scale physics that these phenomena are the result of?

A somewhat less pressing but still interesting path for investigation is whether we can reconstruct the initial matter configurations given the lifetime of the black hole. Recall that different matter configurations led to different estimated black hole lifetimes (although the leading order term is the same). Perhaps unrealistic, but it would be interesting to determine if there is some kind of one-to-one map between black hole lifetimes and initial matter distributions of the model presented here. This would allow us to reconstruct the initial matter configuration from the lifetime alone. In saying this, the estimated lifetime was always of order M^2 (with the same prefactor) for all marginally bound configurations we looked at, and it was only (comparatively small) subleading corrections of order M that were different for different configurations. If this is the case then it would be very difficult to look for such an effect observationally, meaning this is likely solely a theoretical endeavour.

Aside from the above, which are more or less directly related to the model studied in this thesis, where do we go from here? Beyond simply extending our model to the non-marginally bound case, which has been studied in [24], a completely general effective framework for spherical symmetry is desirable, although currently out of

reach. If there is a way to perform polymer quantization without gauge fixing, while maintaining algebra closure, such a model may give insights into the vacuum space-time beyond the results presented here. We note that work along these lines has been done in [14], under the assumption that the radial component of the connection is not polymerized, and that the diffeomorphism constraint is not deformed. Ideally however, it would be nice to polymerize (or even better include holonomies) along the radial direction as well.

Recall that alternative methods such as adding counter terms as in [5, 12] don't seem to reliably fix the algebra closure issue in the framework presented here. Furthermore, in addition to the algebra closure issue, recall that the areal gauge was chosen to avoid having to compute holonomies in the radial direction. If we wish to avoid gauge fixing, rather than choose some ad hoc polymerization, the proper polymerization functions should be calculated through explicit calculation of the holonomy, so that the effective theory is motivated by LQG. Obviously difficult, but a method for calculating holonomies in non-trivial directions without resorting to gauge fixing or abelianizations of the type studied in [7] would be ideal.

Moving beyond the current framework entirely, the next step in this picture would be first to study the evolution of more realistic matter fields, such as a scalar field, in order to determine how this would affect the quantum dynamics or causal structure of the space-time developed here. Steps in this direction have been taken in effective LQG [27–33], but not in the exact framework that we have developed. Initial attempts to include a scalar field were taken early in our work, but again the algebra closure issue was non-trivial, so it is not currently clear how scalar fields can be incorporated into our model (at least without a further gauge fixing such as the dust time gauge).

Secondly, since real black holes that exist in our universe invariably have angular momentum, a similar framework to describe Kerr black holes (which possess angular momentum) should be developed and steps in this direction have already been taken

in effective LQG at large [34–42]. Finally, although quantization of the spherically symmetric sector can be developed, the dynamics of the quantum theory is difficult to tackle. The ultimate goal would really be to find quantum states from the full theory that correspond to spherically symmetric space-times and compare the quantum dynamics of such states to the effective models such as those developed here. Only then would we have a truly definitive answer as to whether or not our effective model is capturing the pertinent features of the quantum dynamics of such states. This kind of analysis remains quite a way off, with this work representing a small step in this direction.

Bibliography

[1] M. Bouhmadi-López, S. Brahma, C. Y. Chen, P. Chen and D. h. Yeom, "Asymptotic non-flatness of an effective black hole model based on loop quantum gravity," Phys. Dark Univ. **30**, 100701 (2020), arXiv:1902.07874.

[2] F. Fazzini, C. Rovelli and F. Soltani, "Painlevé-Gullstrand coordinates discontinuity in the quantum Oppenheimer-Snyder model," Phys. Rev. D **108**, 044009 (2023), arXiv:2307.07797.

[3] F. Fazzini, V. Husain and E. Wilson-Ewing,"Shell-crossings and shock formation during gravitational collapse in effective loop quantum gravity," Phys. Rev. D **109**, 084052 (2024), arXiv:2312.02032.

[4] J. Münch, A. Perez, S. Speziale and S. Viollet, "Generic features of a polymer quantum black hole," Class. Quant. Grav. **40**, 135003 (2023), arXiv:2212.06708.

[5] T. Cailleteau, J. Mielczarek, A. Barrau and J. Grain, "Anomaly-free scalar perturbations with holonomy corrections in loop quantum cosmology," Class. Quant. Grav. **29**, 095010 (2012), arXiv:1111.3535.

[6] R. Gambini and J. Pullin, "Loop quantization of the Schwarzschild black hole," Phys. Rev. Lett. **110**, 211301 (2013), arXiv:1302.5265.

[7] R. Gambini, J. Olmedo and J. Pullin,"Spherically symmetric loop quantum

gravity: analysis of improved dynamics," Class. Quant. Grav. **37**, 205012 (2020), arXiv:2006.01513.

[8] K. Giesel, H. Liu, E. Rullit, P. Singh and S. A. Weigl, "Embedding generalized LTB models in polymerized spherically symmetric spacetimes," arXiv:2308.10949.

[9] K. Giesel, H. Liu, P. Singh and S. A. Weigl,"Generalized analysis of a dust collapse in effective loop quantum gravity: fate of shocks and covariance," arXiv:2308.10953.

[10] P. Dirac, *Lectures On Quantum Mechanics*, Belfer Graduate School of Science, monograph series (Dover Publications, 2001).

[11] P. Singh and E. Wilson-Ewing,"Quantization ambiguities and bounds on geometric scalars in anisotropic loop quantum cosmology," Class. Quant. Grav. **31**, 035010 (2014), arXiv:1310.6728.

[12] M. Bojowald, G. M. Hossain, M. Kagan and S. Shankaranarayanan, "Anomaly freedom in perturbative loop quantum gravity," Phys. Rev. D **78**, 063547 (2008), arXiv:0806.3929.

[13] A. Alonso-Bardaji, D. Brizuela and R. Vera, "An effective model for the quantum Schwarzschild black hole," Phys. Lett. B **829**, 137075 (2022), arXiv:2112.12110.

[14] K. Giesel, H. Liu, P. Singh and S. A. Weigl,"Generalized analysis of a dust collapse in effective loop quantum gravity: fate of shocks and covariance," arXiv:2308.10953.

[15] M. Bojowald and E. I. Duque, "Emergent modified gravity: Covariance regained," Phys. Rev. D **108**, 084066 (2023), arXiv:2310.06798.

[16] C. Zhang, J. Lewandowski, Y. Ma and J. Yang, "Black Holes and Covariance in Effective Quantum Gravity," arXiv:2407.10168.

[17] I. H. Belfaqih, M. Bojowald, S. Brahma and E. I. Duque, "Black holes in effective loop quantum gravity: Covariant holonomy modifications," arXiv:2407.12087.

[18] V. Husain and T. Pawlowski, "Time and a physical Hamiltonian for quantum gravity," Phys. Rev. Lett. **108**, 141301 (2012), arXiv:1108.1145.

[19] V. Husain and T. Pawlowski,"Dust reference frame in quantum cosmology," Class. Quant. Grav. **28**, 225014 (2011), arXiv:1108.1147.

[20] H. M. Haggard and C. Rovelli,"Quantum-gravity effects outside the horizon spark black to white hole tunneling," Phys. Rev. D **92**, 104020 (2015), arXiv:1407.0989.

[21] C. Hellaby and K. Lake, "Shell crossings and the Tolman model," Astrophys. J. **290**, 381 (1985).

[22] P. S. Joshi and R. V. Saraykar, "Shell-crossings in Gravitational Collapse," Int. J. Mod. Phys. D **22**, 1350027 (2013), arXiv:1205.3263.

[23] R. J. LeVeque, *Finite Volume Methods for Hyperbolic Problems*. Cambridge University Press, 2002.

[24] L. Cipriani, F. Fazzini and E. Wilson-Ewing, "Gravitational collapse in effective loop quantum gravity: beyond marginally bound configurations," Phys. Rev. D **110**, 066004 (2024), arXiv:2404.04192.

[25] N. Bodendorfer, F. M. Mele and J. Münch,"(b,v)-type variables for black to white hole transitions in effective loop quantum gravity," Phys. Lett. B **819**, 136390 (2021), arXiv:1911.12646.

[26] M. Han, C. Rovelli and F. Soltani, "Geometry of the black-to-white hole transition within a single asymptotic region," Phys. Rev. D **107**, 064011 (2023), arXiv:2302.03872.

[27] F. Benitez, R. Gambini, L. Lehner, S. Liebling and J. Pullin,"Critical collapse of a scalar field in semiclassical loop quantum gravity," Phys. Rev. Lett. **124**, 071301 (2020), arXiv:2002.04044.

[28] R. Gambini, F. Benítez and J. Pullin,"A Covariant Polymerized Scalar Field in Semi-Classical Loop Quantum Gravity," Universe **8**, no.10, 526 (2022), arXiv:2102.09501.

[29] F. Benítez, R. Gambini, S. L. Liebling and J. Pullin,"Criticality in the collapse of spherically symmetric massless scalar fields in semiclassical loop quantum gravity," Phys. Rev. D **104**, 024008 (2021), arXiv:2106.00674.

[30] R. Gambini and J. Pullin, "Loop quantum gravity of a spherically symmetric scalar field coupled to gravity with a clock," Class. Quant. Grav. **40**, 085016 (2023), arXiv:2303.09392.

[31] C. Y. Shao, C. Zhang, W. Zhang and C. G. Shao, "Scalar fields around a loop quantum gravity black hole in de Sitter spacetime: Quasinormal modes, late-time tails and strong cosmic censorship," Phys. Rev. D **109**, 064012 (2024), arXiv:2309.04962.

[32] R. Gambini and J. Pullin, "Quantization of spherically symmetric loop quantum gravity coupled to a scalar field and a clock: the asymptotic limit," Class. Quant. Grav. **40**, 245009 (2023), arXiv:2311.05766.

[33] R. Gambini and J. Pullin, "Quantum Scalar Fields Interacting with Quantum Black Hole Asymptotic Regions," Universe **10**, no.2, 77 (2024), arXiv:2402.02587.

[34] F. Caravelli and L. Modesto, "Spinning Loop Black Holes," Class. Quant. Grav. **27**, 245022 (2010), arXiv:1006.0232.

[35] S. Brahma, C. Y. Chen and D. H. Yeom,"Testing Loop Quantum Gravity from Observational Consequences of Nonsingular Rotating Black Holes," Phys. Rev. Lett. **126**, 181301 (2021),arXiv:2012.08785.

[36] J. Kumar, S. U. Islam and S. G. Ghosh, "Loop Quantum Gravity motivated multihorizon rotating black holes," JCAP **11**, 032 (2022), arXiv:2209.13562.

[37] S. U. Islam, J. Kumar, R. Kumar Walia and S. G. Ghosh,"Investigating Loop Quantum Gravity with Event Horizon Telescope Observations of the Effects of Rotating Black Holes," Astrophys. J. **943**, no.1, 22 (2023), arXiv:2211.06653.

[38] H. X. Jiang, C. Liu, I. K. Dihingia, Y. Mizuno, H. Xu, T. Zhu and Q. Wu, "Shadows of loop quantum black holes: semi-analytical simulations of loop quantum gravity effects on Sagittarius A* and M87*," JCAP **01**, 059 (2024), arXiv:2312.04288.

[39] J. Kumar, S. U. Islam and S. G. Ghosh, "Strong gravitational lensing by loop quantum gravity motivated rotating black holes and EHT observations," Eur. Phys. J. C **83**, no.11, 1014 (2023), arXiv:2305.04336.

[40] Z. Li, Y. Li and J. Jiang, "Loop quantum gravity and quasinormal mode of Kerr–Newman black hole," Mod. Phys. Lett. B **37**, 2350095 (2023).

[41] C. Liu, H. Siew, T. Zhu, Q. Wu, Y. Sun, Y. Zhao and H. Xu, "Constraints on the rotating self-dual black hole with quasi-periodic oscillations," JCAP **11**, 096 (2023), arXiv:2305.12323.

[42] Z. W. Xia, H. Yang and Y. G. Miao, "Scalar fields around a rotating loop quantum gravity black hole: Waveform, quasi-normal modes and superradiance," Class. Quant. Grav. **41**, 165010 (2024), arXiv:2310.00253.

Appendix A

Lifetime of a Quantum Black Hole

The lifetime of the black hole is of course observer-dependent. Here we consider the lifetime as measured by a distant observer (located at a fixed radius $x = R \gg R_S$), who measures the proper time elapsed between receiving two light signals; the first sent during the collapse of the star just before the black hole forms, and the second sent shortly after the surface of the star L exits the apparent horizon after the bounce.

Here, for the sake of concreteness we assume that the two light signals are emitted from the $x = L$ surface of the Oppenheimer-Snyder star when $L = 3GM$, but other choices will give similar results. Explicitly, the first light signal is emitted when $L = 3GM$ during the contracting phase, and the second light signal is emitted when $L = 3GM$ after the bounce.

Using the coordinate system (3.19) for the vacuum exterior of the star, null radial geodesics satisfy

$$0 = -\dot{t}^2 + 2N^x \dot{t}\dot{x} + \dot{x}^2, \tag{A.1}$$

with dots denoting a derivative with respect to an affine parameter. Note that the explicit form of N^x is not necessary here, all that matters is that N^x depends only the radial coordinate x but not on the time coordinate t; this condition will always be

satisfied for the exterior of the Oppenheimer-Snyder star in spherical symmetry, even without assuming the Einstein equations (in classical general relativity, $N^x = \sqrt{R_S/x}$).

By solving for $\dot{t}/\dot{x} = dt/dx$ and integrating, it follows that the t and x coordinates for outgoing null radial geodesics (passing through $x = x_o > R_S$ at the coordinate time $t = t_o$) satisfy

$$t(x) = t_o + f(x) - f(x_o), \tag{A.2}$$

with $f(x) = \int dx \, [N^x + \sqrt{(N^x)^2 + 1}\,]$.

Therefore, if two light signals are emitted at $x = 3GM$ at times $t_1(3GM) = 0$ and $t_2(3GM) = \Delta t_L$, then the elapsed time (as measured by a distant observer located at $x = R \gg R_S$) will be, using (A.2),

$$\begin{aligned} \Delta t_{\rm d} &= t_2(R) - t_1(R) \\ &= t_2(3GM) + f(R) - f(3GM) \\ &\qquad - [t_1(3GM) + f(R) - f(3GM)] \\ &= \Delta t_L. \end{aligned} \tag{A.3}$$

Finally, the elapsed proper time for an observer at constant radius $x = R \gg R_S$ is $\Delta\tau_{\rm d} \approx \Delta t_{\rm d}$ for the metric (3.19) (up to small corrections of the order R_S/R that can safely be neglected), therefore

$$\Delta\tau_{\rm d} \approx \Delta t_{\rm d} = \Delta t_L. \tag{A.4}$$

So the lifetime of a quantum black hole is simply given by the difference in coordinate time, in terms of the metric (3.19), between the times the first and second light signals were emitted for some $x_{\rm emission} > R_S$, respectively from the collapse and from the shock wave after the bounce.

Appendix B

Publication Rights

This appendix contains reuse and permissions licenses for permission to reuse articles published by APS© that make up chapters 2 and 4 of this thesis. Note that such a license is not required for chapter 3 of this thesis, which was published by IOP Publishing© in 2020. Please see Author Rights on the IOP Publishing© website for further details.

American Physical Society
Reuse and Permissions License

15-Apr-2024

This license agreement between the American Physical Society ("APS") and Jarod Kelly ("You") consists of your license details and the terms and conditions provided by the American Physical Society and SciPris.

Licensed Content Information

License Number:	**RNP/24/APR/078012**
License date:	15-Apr-2024
DOI:	10.1103/PhysRevD.102.106024
Title:	Effective loop quantum gravity framework for vacuum spherically symmetric spacetimes
Author:	Jarod George Kelly, Robert Santacruz, and Edward Wilson-Ewing
Publication:	Physical Review D
Publisher:	American Physical Society
Cost:	USD $ 0.00

Request Details

Does your reuse require significant modifications: No

Specify intended distribution locations:	Canada
Reuse Category:	Reuse in a thesis/dissertation
Requestor Type:	Author of requested content
Items for Reuse:	Whole Article
Format for Reuse:	Electronic

Information about New Publication:

University/Publisher:	University of New Brunswick
Title of dissertation/thesis:	Spherically Symmetric Space-times in Effective LQG
Author(s):	Jarod George Kelly
Expected completion date:	Jun. 2024

License Requestor Information

Name:	Jarod Kelly
Affiliation:	Individual
Email Id:	jarod.kelly@unb.ca
Country:	Canada

American Physical Society
Reuse and Permissions License

TERMS AND CONDITIONS

The American Physical Society (APS) is pleased to grant the Requestor of this license a non-exclusive, non-transferable permission, limited to Electronic format, provided all criteria outlined below are followed.

1. You must also obtain permission from at least one of the lead authors for each separate work, if you haven't done so already. The author's name and affiliation can be found on the first page of the published Article.
2. For electronic format permissions, Requestor agrees to provide a hyperlink from the reprinted APS material using the source material's DOI on the web page where the work appears. The hyperlink should use the standard DOI resolution URL, http://dx.doi.org/{DOI}. The hyperlink may be embedded in the copyright credit line.
3. For print format permissions, Requestor agrees to print the required copyright credit line on the first page where the material appears: "Reprinted (abstract/excerpt/figure) with permission from [(FULL REFERENCE CITATION) as follows: Author's Names, APS Journal Title, Volume Number, Page Number and Year of Publication.] Copyright (YEAR) by the American Physical Society."
4. Permission granted in this license is for a one-time use and does not include permission for any future editions, updates, databases, formats or other matters. Permission must be sought for any additional use.
5. Use of the material does not and must not imply any endorsement by APS.
6. APS does not imply, purport or intend to grant permission to reuse materials to which it does not hold copyright. It is the requestor's sole responsibility to ensure the licensed material is original to APS and does not contain the copyright of another entity, and that the copyright notice of the figure, photograph, cover or table does not indicate it was reprinted by APS with permission from another source.
7. The permission granted herein is personal to the Requestor for the use specified and is not transferable or assignable without express written permission of APS. This license may not be amended except in writing by APS.
8. You may not alter, edit or modify the material in any manner.
9. You may translate the materials only when translation rights have been granted.
10. APS is not responsible for any errors or omissions due to translation.
11. You may not use the material for promotional, sales, advertising or marketing purposes.
12. The foregoing license shall not take effect unless and until APS or its agent, Aptara, receives payment in full in accordance with Aptara Billing and Payment Terms and Conditions, which are incorporated herein by reference.
13. Should the terms of this license be violated at any time, APS or Aptara may revoke the license with no refund to you and seek relief to the fullest extent of the laws of the USA. Official written notice will be made using the contact information provided with the permission request. Failure to receive such notice will not nullify revocation of the permission.
14. APS reserves all rights not specifically granted herein.
15. This document, including the Aptara Billing and Payment Terms and Conditions, shall be the entire agreement between the parties relating to the subject matter hereof.

American Physical Society
Reuse and Permissions License

15-Apr-2024

This license agreement between the American Physical Society ("APS") and Jarod Kelly ("You") consists of your license details and the terms and conditions provided by the American Physical Society and SciPris.

Licensed Content Information

License Number:	**RNP/24/APR/078013**
License date:	15-Apr-2024
DOI:	10.1103/PhysRevD.106.024014
Title:	Fate of quantum black holes
Author:	Viqar Husain et al.
Publication:	Physical Review D
Publisher:	American Physical Society
Cost:	USD $ 0.00

Request Details

Does your reuse require significant modifications: No

Specify intended distribution locations:	Canada
Reuse Category:	Reuse in a thesis/dissertation
Requestor Type:	Author of requested content
Items for Reuse:	Whole Article
Format for Reuse:	Electronic

Information about New Publication:

University/Publisher:	University of New Brunswick
Title of dissertation/thesis:	Spherically Symmetric Space-times in Effective LQG
Author(s):	Jarod George Kelly
Expected completion date:	Jun. 2024

License Requestor Information

Name:	Jarod Kelly
Affiliation:	Individual
Email Id:	jarod.kelly@unb.ca
Country:	Canada

American Physical Society
Reuse and Permissions License

TERMS AND CONDITIONS

The American Physical Society (APS) is pleased to grant the Requestor of this license a non-exclusive, non-transferable permission, limited to Electronic format, provided all criteria outlined below are followed.

1. You must also obtain permission from at least one of the lead authors for each separate work, if you haven't done so already. The author's name and affiliation can be found on the first page of the published Article.
2. For electronic format permissions, Requestor agrees to provide a hyperlink from the reprinted APS material using the source material's DOI on the web page where the work appears. The hyperlink should use the standard DOI resolution URL, http://dx.doi.org/{DOI}. The hyperlink may be embedded in the copyright credit line.
3. For print format permissions, Requestor agrees to print the required copyright credit line on the first page where the material appears: "Reprinted (abstract/excerpt/figure) with permission from [(FULL REFERENCE CITATION) as follows: Author's Names, APS Journal Title, Volume Number, Page Number and Year of Publication.] Copyright (YEAR) by the American Physical Society."
4. Permission granted in this license is for a one-time use and does not include permission for any future editions, updates, databases, formats or other matters. Permission must be sought for any additional use.
5. Use of the material does not and must not imply any endorsement by APS.
6. APS does not imply, purport or intend to grant permission to reuse materials to which it does not hold copyright. It is the requestor's sole responsibility to ensure the licensed material is original to APS and does not contain the copyright of another entity, and that the copyright notice of the figure, photograph, cover or table does not indicate it was reprinted by APS with permission from another source.
7. The permission granted herein is personal to the Requestor for the use specified and is not transferable or assignable without express written permission of APS. This license may not be amended except in writing by APS.
8. You may not alter, edit or modify the material in any manner.
9. You may translate the materials only when translation rights have been granted.
10. APS is not responsible for any errors or omissions due to translation.
11. You may not use the material for promotional, sales, advertising or marketing purposes.
12. The foregoing license shall not take effect unless and until APS or its agent, Aptara, receives payment in full in accordance with Aptara Billing and Payment Terms and Conditions, which are incorporated herein by reference.
13. Should the terms of this license be violated at any time, APS or Aptara may revoke the license with no refund to you and seek relief to the fullest extent of the laws of the USA. Official written notice will be made using the contact information provided with the permission request. Failure to receive such notice will not nullify revocation of the permission.
14. APS reserves all rights not specifically granted herein.
15. This document, including the Aptara Billing and Payment Terms and Conditions, shall be the entire agreement between the parties relating to the subject matter hereof.

Vita

Candidate's full name:

- Jarod George Kelly

University attended:

- Ph.D. candidate, University of New Brunswick Fredericton, Canada, 2016-2024
- B.Sc. Mechanical Engineering, University of New Brunswick Fredericton, Canada, 2011-2015

Publications:

- Husain, V., Kelly, J., Santacruz, R. & Wilson-Ewing, E. Fate of quantum black holes. Phys. Rev. D. **106**, 024014 (2022)
- Husain, V., Kelly, J., Santacruz, R. & Wilson-Ewing, E. Quantum Gravity of Dust Collapse: Shock Waves from Black Holes. Phys. Rev. Lett.. **128**, 121301 (2022)
- Kelly, J., Santacruz, R. & Wilson-Ewing, E. Black hole collapse and bounce in effective loop quantum gravity. Class. Quant. Grav.. **38**, 04LT01 (2021)
- Kelly, J., Santacruz, R. & Wilson-Ewing, E. Effective loop quantum gravity framework for vacuum spherically symmetric spacetimes. Phys. Rev. D. **102**, 106024 (2020)

- Kelly, J. & Seahra, S. Velocity-dependent deformations of the energy spectrum of a quantum cavity from Lorentz symmetry violations. Phys. Rev. D **100**, 064002 (2019)

Conference Presentations:

- Quantum gravity of dust collapse
  Atlantic GR, Online, 2022
- Effective loop quantum gravity framework for vacuum spherically symmetric space-times
  CAP Virtual Congress, Online, 2021
- Effective loop quantum gravity framework for vacuum spherically symmetric space-times
  Atlantic GR, Online, 2021
- Detecting Lorentz Symmetry Violations with a Quantum Cavity
  Inter-Campus Seminar Day, University of New Brunswick, 2019
- Detecting Lorentz Violations with a Quantum Cavity
  Atlantic GR, St. Francis Xavier University, 2018

Projects:

- New Brunswick Innovation Foundation (NBIF) Project: "Artificial Intelligence for Stock Price Valuations", Stockcalc, 2022-2023
- Department of National Defence IDEaS Project: "Short-Cycle Contagion Modelling Toolkit", The Black Arcs, 2022-2023
- Natural Sciences and Engineering Research Council (NSERC) Engage Grant Project: "Mathematical Optimization of Heat Conduction Algorithms", C-Therm Technologies Ltd., 2019-2020